COMBINING ACTIVE SITE AND ALLOSTERIC INHIBITORS TO STUDY PROTEIN TYROSINE KINASES

by

Taylor Kathryn Johnson

A dissertation submitted in partial fulfillment
of the requirements for the degree of
Doctor of Philosophy
(Medicinal Chemistry)
in the University of Michigan
2017

Doctoral Committee:

Assistant Professor Matthew B. Soellner, Chair
Professor Carol A. Fierke
Professor George A. Garcia
Professor Anna K. Mapp
Assistant Professor Brent R. Martin

ACKNOWLEDGEMENTS

Graduate school is not a solitary endeavor, and I certainly could not have done it alone. There are so many people that I need to recognize for helping me get where I am today. I would first like to thank my advisor Dr. Matthew Soellner for the guidance he has provided for last five years. Matt, you have really helped me grow as scientist through your constant support. For me, you achieved the perfect balance of providing scientific help when I needed it and giving me freedom when I was ready for it. Looking back, I realized that you have helped me learn so much throughout grad school, not only about my specific projects, but also how think about and approach science. I am also incredibly grateful for all the help you provided me during my postdoc application process. I certainly could not have navigated that process without your help.

I also need to thank the members of my committee: Dr. Carol Fierke, Dr. George Garcia, Dr. Anna Mapp, and Dr. Brent Martin for being a truly helpful committee. You always provided valuable suggestions at my committee meetings, and you helped me appropriately prioritize projects that I needed to complete to graduate.

I would also like to thank everyone that I interacted with in the Soellner lab. Thank you to all the past members: Dr. Kristin Ko, Dr. Frank Kwarcinski, Dr. Meghan Breen, Dr. Kristoffer Brandvold, Dr. Shana Santos, Dr. Steve Bremmer, Michael Steffey, and Christel Fox. You were all very helpful to me when I was a new member joining the lab. Thank you for being willing to talk through difficult problems with me and teach me all the techniques I learned in lab. Thank you also to the current members: Dr. Sameer Phadke, Michael Agius, and Eric Lachacz. Not only are you excellent scientific sounding boards, but you all also keep lab fun every day.

Over the past five years, I have become good friends with my fellow Soellner lab mates, but I have a few more friends I want to thank for helping me make it through grad school. To all my Med Chem, Jurassic Puck teammates, David, Joe, Will, and Nate, I have really enjoyed playing with you for the last few years. It was a much needed way to let off a little steam at the end of the week. I hope the team stays strong after I stop managing. To all the other friends I made during grad school and the ones from undergrad who still give me constant support, Helen,

Max, Melissa, Laura, Jenna, Ella, and Izzy, thank you so much for always being there and letting me know I could count on you if I ever needed help.

Finally, I would like to thank my family for their love and support. Mom, Dad, Shelby, and Trent, thank you for always being there for me. I really cannot put into words how fortunate I have been in my life to have a support network like the four of you. I am going to miss seeing you every Sunday for dinner, when I move.

TABLE OF CONTENTS

LIST OF TABLES

TABLE

LIST OF FIGURES

FIGURE

LIST OF SCHEMES

SCHEME

LIST OF APPENDICES

APPENDIX

ABSTRACT

Kinases play a crucial role in a variety of cell signaling pathways that control processes such as: growth, motility, and angiogenesis. Not surprisingly, dysregulation of proper kinase signaling often leads to cancer. Since the introduction of imatinib, a small molecule kinase inhibitor for the treatment of chronic myelogenous leukemia (CML), kinase inhibitors have become a popular drug class with 28 approved as drugs. All of these inhibitors bind in the conserved ATP-binding pocket, and as a result, many are promiscuous and bind off-target kinases. This dissertation describes our work to target kinases through mechanisms other than the ATP-binding pocket. Through targeting pockets other than the ATP-binding pocket, we also demonstrate the importance of understanding kinase global conformation.

We created bivalent inhibitors (inhibitors that can bind two sites within their target simultaneously) for two protein tyrosine kinases: c-Src and c-Abl. In both, the bivalent inhibitors were synthesized by linking an ATP-competitive inhibitor to an allosteric inhibitor of the kinase using azide-alkyne click chemistry. In doing so, we created inhibitors that were both more potent and selective than the separate binding pieces alone. Our c-Src bivalent inhibitor was the first c-Src inhibitor that was selective for the active form of the kinase over the inactive form. Additionally, the bivalent inhibitor of c-Abl was cell permeable and had a cellular therapeutic index of 14.

We also discovered an allosteric modulator of c-Src *via* a screen of 1,000 compounds. We determined that this small molecule stabilizes the open conformation of c-Src and, accordingly, is an activator of c-Src. Finally, we investigated the interplay between an allosteric inhibitor of c-Abl (GNF-2) and various ATP-competitive inhibitors. None of the FDA approved, ATP-competitive inhibitors tested showed synergy with GNF-2 because they stabilized different global conformations in c-Abl. Only one ATP-competitive inhibitor stabilized the same conformation as GNF-2, and gratifyingly, this was the only combination that showed synergy. Additionally, this combination was capable of overcoming an imatinib resistant mutant in CML. These findings will play a crucial role in understanding drug combinations. This dissertation

provides novel findings about the important role that global conformation plays in kinase inhibition.

CHAPTER I

Exploiting Small Molecules that Bind Outside the ATP-Pocket of Protein Tyrosine Kinases

Abstract

Kinases are a highly abundant and important protein in cells. Within the last 15 years, kinase inhibitors have become important drugs. Due to the conserved nature of the ATP-binding pocket and the fact that most kinase inhibitors bind in this pocket, they are often promiscuous and are not always the best tools to study kinases in the cell. As complex, regulator enzymes, however, kinases often have other less conserved pockets that can be exploited to create selective inhibitors and learn more about the roles these important enzymes play in cellular signaling. The work introduced here describes several attempts to design and use small molecules that bind outside the ATP-binding pocket to study protein tyrosine kinases.

Kinases Play an Important Role in Cell Signaling

Cellular processes are regulated by complex signaling pathways where protein kinases often play important regulatory roles. There are 518 known human protein kinases that make up almost 2% of the entire human genome (referred to as the kinome).[1] Protein kinases transfer the gamma phosphate of ATP to a hydroxyl containing amino acid (serine, threonine, or tyrosine) on their protein substrate. It is estimated that about one-third of proteins are phosphorylated by kinases providing as many as 20,000 unique phosphoproteins.[2] These phosphoproteins, in turn, propagate a cellular signal.[3] This can be achieved in a variety of ways: the phosphorylation event can activate the protein substrate,[4] inactivate the protein substrate,[5] or provide a docking site for other signaling molecules.[6] These signaling cascades control complex cellular processes such as: metabolism, transcription, cell cycle progression, motility, apoptosis, and differentiation.[1] Not surprisingly, dysregulation of the kinase signaling involved in these processes often leads to disease states such as cancer.[7,8] The first discovered proto-oncogene was, in fact, a protein kinase, c-Src.[9]

Despite the breadth and diversity of the kinome, there are many conserved features within the catalytic, kinase domain (**Figure 1.1**). The kinase domain is composed of an N-lobe mostly made up of β-sheets and the C-lobe which is comprised primarily of α-helices.[10] These two lobes are connected via a linker region referred to as the hinge. ATP binds in the pocket formed at the interface of these two lobes. Furthermore, there are several features within this pocket that are necessary for transfer of the gamma phosphate on ATP to the hydroxyl containing amino acid substrate.

i. A magnesium cofactor and the three conserved catalytic residues: Lys, Asp, and Glu.
ii. The glycine-rich loop that forms the ceiling of the ATP binding site. It is often termed the phosphate-binding loop (P-loop) due to the role it plays in enabling catalysis by clamping down on the phosphates of ATP.[11]
iii. The activation loop, containing the catalytic Asp, as well as a hydroxyl containing amino acid (Ser/Thr/Tyr) that serves as a phosphorylation site, playing a role in regulating the enzyme.[11]

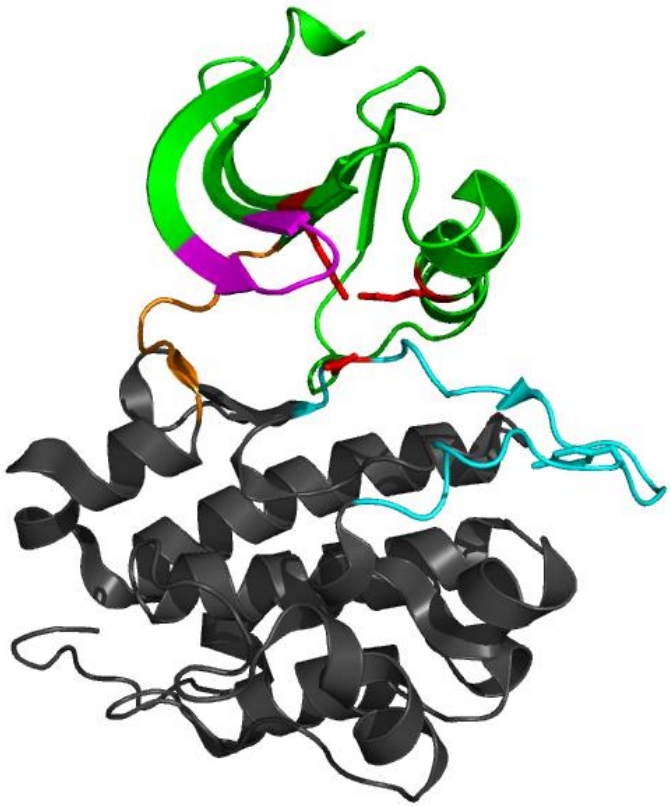

Figure 1.1. Conserved features of the kinase domain (PDB: 1Y57). The N-lobe is colored green and the C-lobe is colored gray with the hinge connecting the two highlighted in orange. The conserved catalytic residues are shown in stick form (red). The P-loop is highlighted in magenta and the activation loop in cyan with the phosphorylated tyrosine shown in stick form.

The Importance of Kinase Inhibitors

As early as the 1960s, with the discovery of a shortened chromosome, termed the Philadelphia chromosome, present in some leukemias,[12] scientists have slowly been gaining information that there are specific molecular causes to some cancers. As such, targeted therapy that eliminates the molecular cause, and subsequently the cancer, has become the desired path for cancer treatment. In 2001, imatinib (**Figure 1.2**) became one of the first approved small molecule targeted therapies. The first two examples of specific targeted therapies before imatinib were both antibodies: rituximab for B-cell non-Hodgkin lymphoma and trastuzumab for HER2-positive breast cancer.[13,14] Imatinib treats chronic myelogenous leukemia (CML), which is caused by the aforementioned shortened, Philadelphia chromosome. CML is an adult leukemia that makes up approximately 15 to 20 percent of all adult leukemias.[15] The Philadelphia chromosome is caused by the translocation of chromosomes 9 and 22 creating a fusion protein BCR-Abl between a portion of *Abl1* on chromosome 9 and *Bcr* on chromosome 22.[16] The fusion protein BCR-Abl causes cancer through several mechanisms. Firstly, the point of fusion between BCR and Abl cuts off the regulatory tail of Abl, which leads to a constitutively active Abl and aberrant Abl signaling.[17] Additionally, BCR has a coiled-coil domain, which promotes dimerization of BCR-Abl. Dimerization of Abl facilitates Abl autophosphorylation and further increases Abl activity.[17]

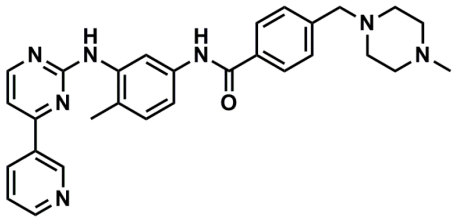

Figure 1.2. Structure of imatinib

Imatinib is an ATP-competitive inhibitor of the kinase c-Abl. It was highly successful in CML treatment. Before the development of imatinib treatment, the median survival time for a patient with CML was 3-5 years. Now with imatinib treatment, the 7-10 year survival rate is approximately 85 percent.[15,18,19] c-Abl is not the only kinase that imatinib inhibits; another target of imatinib is the kinase c-KIT. [20] Hirota *et al*. discovered in the late 1990s that c-KIT contains several gain-of-function mutations in gastrointestinal stromal tumors (GIST).[21] Imatinib was then re-purposed successfully as a treatment for GIST.[20] Due to the success of imatinib, more kinase-

targeted therapies have emerged. There are now 28 approved kinase inhibitors.[22] Of the 28 approved kinase inhibitors, only four are specific for serine/threonine kinases. Almost all of these drugs target protein tyrosine kinases (PTKs). For this reason, the work in this dissertation focuses on two tyrosine kinases, c-Src and c-Abl.

The importance of c-Abl in cancer has already been described. c-Src is the other kinase studied in this dissertation due to the important role it also plays in cancer. In healthy tissues, c-Src regulates cell division, motility, adhesion, angiogenesis, and survival.[9,23] Not surprisingly, c-Src is often overexpressed in cancer; however, it is increased c-Src activity, not overexpression, that most often correlates with malignant potential.[9,23] Furthermore, c-Src contributes to trastuzumab (mentioned earlier) resistance in Her2-postitive breast cancer.[24] Some of the cancers in which c-Src is implicated include colon, lung, and breast.[25] Recent work from our lab has developed an inhibitor of c-Src that has been effective at shrinking triple negative breast cancer (TNBC) tumors in mice.[26] TNBC is more difficult to treat than other breast cancers and could really benefit from a targeted therapy.[27,28]

All FDA approved kinase inhibitors bind to one of three unique conformations within the ATP-binding pocket.[22,29,30] Most of these inhibitors (19 of 30) are classified as Type I inhibitors meaning that they bind the active kinase conformation. The active conformation is the conformation that binds ATP and is shown in **Figure 1.1**. Seven approved inhibitors are known as Type II inhibitors, and they bind the inactive, DFG-out conformation. The DFG-out conformation is characterized by an outward flip of the activation loop causing the catalytically important residues Asp-Phe-Gly (DFG) to flip out of the ATP-binding pocket.[31] The third ATP-binding pocket conformation is an addition inactive conformation referred to as αC-helix-out. This conformation is characterized by outward movement of the αC-helix which disrupts a salt bridge between the catalytic lysine and glutamate.[32,33] Four ATP-competitive inhibitors are known to bind this conformation. Imatinib is relatively selective for c-Abl and binds the DFG-out conformation of c-Abl. It was hypothesized that the selectivity of imatinib was due to the inability of most kinases to adopt the DFG-out. It was previously thought that c-Src could not adopt DFG-out; however, this has since been shown to be incorrect.[34,35] Recently, using a "matched set" of conformation-selective kinase inhibitors, our lab has shown that DFG-out inhibitors and Type I inhibitors are equally selective while αC-helix-out inhibitors are slightly more selective.[36]

c-Src and c-Abl are Multi-Domain Kinases

All FDA-approved kinase inhibitors bind the ATP pocket.[37] This is not surprising due to the fact that the ATP binding pocket is well-defined, hydrophobic pocket.[37] Often, these compounds lack specificity due to the highly conserved nature of the ATP binding pocket. Furthermore, high cellular levels of ATP greatly diminishes the cellular potency of kinase inhibitors *in vitro*.[37] There are several strategies for creating more selective kinase inhibitors. Most of these strategies involve interacting with elements outside the ATP-binding pocket.[38,39] In order to bind regions outside the ATP-pocket, it is important to consider the global conformation of a kinase.

Earlier, we highlighted the conserved features of the kinase domain (**Figure 1.1**). Almost all kinases, including the PTKs c-Src and c-Abl, however, have other domains important for protein-protein interactions and autoregulation. The conformation that all the domains adopt in relation to each other is referred to as the global conformation. The global conformation of c-Src is shown in **Figure 1.3**. Both c-Src and c-Abl contain Src Homology 2 (SH2) and Src Homology 3 (SH3) domains in addition to the catalytic, kinase domain. SH2 domains are small, 100 residue domains that recognize and bind phosphotyrosine residues.[40] SH3 domains bind proline-rich sequences that form a polyproline type II helix.[40] The SH2 and SH3 domains provide substrate docking sites and autoregulation for both kinases.[41,32,42] Most commercial assays or kinase inhibitor studies only use the kinase domain;[43–45] however, it is now known that inhibitors that bind within the ATP-binding pocket can cause global changes to the kinase.[33] Described below are several methods for binding outside the ATP-binding pocket and interacting with the global kinase structure.

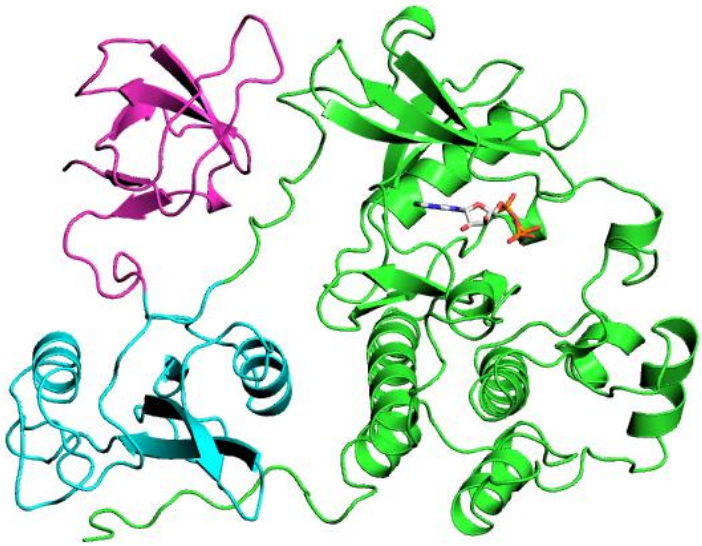

Figure 1.3. Three domain structure of the PTK c-Src. The kinase (catalytic) domain is colored in green with the SH3 domain in magenta and the SH2 domain in cyan. An analog of ATP is shown in white in the ATP-binding pocket.

Allosteric Kinase Modulators

Allosteric modulators bind in a site other than the active-site but have an impact upon the activity of the enzyme. Allosteric modulators are often unique to a particular kinase because they generally exploit more unique pockets within the kinase.[46] For this reason, however, they are often more difficult to identify. There are several well studied allosteric inhibitors in Ser/Thr kinases. For example, the allosteric kinase inhibitor CI-1040 (**Figure 1.4**) inhibits the Ser/Thr kinases MEK1 and MEK2 by occupying a pocket adjacent to the ATP binding site.[47,48] The Ser/Thr kinase Akt also has several allosteric inhibitors (**Figure 1.4**). These allosteric inhibitors of Akt only bind to the full length construct of Akt and not the kinase domain due to the unique mechanism of activation of Akt.[49] These allosteric inhibitors of Akt demonstrate the importance of kinase global conformation and not just kinase catalytic activity.

In tyrosine kinases, one of the best examples of an allosteric inhibitor is GNF-2. GNF-2 is a small molecule that binds in the myristate pocket of c-Abl (**Figure 1.4**).[50] This pocket in c-Abl provides a docking site for the autoregulatory myristate tail of c-Abl. This method of autoregulation in c-Abl is unique rendering GNF-2 highly selective.[42] Furthermore, GNF-2 only demonstrates inhibitory effect with constructs of c-Abl that contain the SH2 and SH3 domains despite the fact that the myristate pocket resides in the kinase domain.[51] Like many of the other allosteric inhibitors discussed, the binding of GNF-2 depends on the global structure of c-Abl.

This dissertation focuses on the PTKs c-Src and c-Abl, and since c-Abl already has a well established allosteric pocket, we wanted to focus on allosteric modulators of c-Src. **Chapter III** details our efforts to identify an allosteric inhibitor of c-Src that would modulate its global conformation. There are no examples of a allosteric inhibitors of c-Src; however, there is an example of a small molecule inhibitor of c-Src that is peptide substrate-competitive and not ATP-competitive.[52]

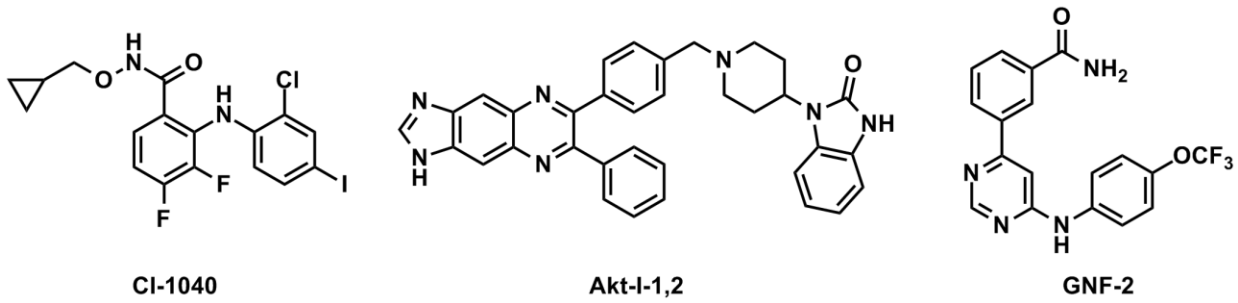

Figure 1.4. Examples of allosteric inhibitors of protein kinases.

Bivalent Kinase Inhibitors

Bivalent inhibitors are inhibitors capable of binding two sites of a protein simultaneously. This leads to a significant increase in potency due to the addition of the free energy of binding.[53] Furthermore, due to the ability to bind two unique sites, bivalent inhibitors have the potential to be highly selective. While the ATP-binding pocket of kinases is highly conserved, other pockets in kinases are more specialized to the unique substrates and function of a kinase.[52] As such, a bivalent inhibitor that exploits these other binding sites has the potential for selectivity. There have been many examples of bivalent kinase inhibitors. Generally, these bivalent inhibitors can be broken into two classes: bisubstrate and generic bivalent inhibitors.[54] Bisubstrate kinase inhibitors gain their name due to the fact that they bind in the binding pockets of both substrates of the kinase, ATP and the peptide/protein substrate. There are several examples in the literature as well as several that our lab has developed (**Figure 1.5a**).[54–56]

Generic bivalent inhibitors do not have as specific binding sites as bisubstrate inhibitors. **Chapters II** and **IV** detail our efforts to develop bivalent inhibitors for c-Src and c-Abl, respectively. There are already several accounts of bivalent inhibitors for these PTKs. In the early 2000s, Lawrence and coworkers developed a series of bivalent inhibitors of c-Src that linked an SH2 domain peptide to a substrate-binding peptide.[57–59] Additionally, Maly and coworkers developed several bivalent inhibitors of c-Src and c-Abl that utilize a O^6-

alkylguanine-DNA alkyltransferase (AGT) linker expressed in cells (Figure **1.5b**).[60,61] Furthermore, our lab has developed bivalent inhibitors of c-Src using enzyme-templated fragment elaboration.[62] With the work in **Chapters II** and **IV**, we hoped to improve upon the current bivalent inhibitors of c-Src and c-Abl by creating inhibitors that were specific to distinct global conformations of the kinase. The bivalent inhibitor of c-Abl utilizes and ATP-competitive inhibitor linked to GNF-2. The c-Src bivalent inhibitor targets the ATP-binding pocket and the SH2 domain.

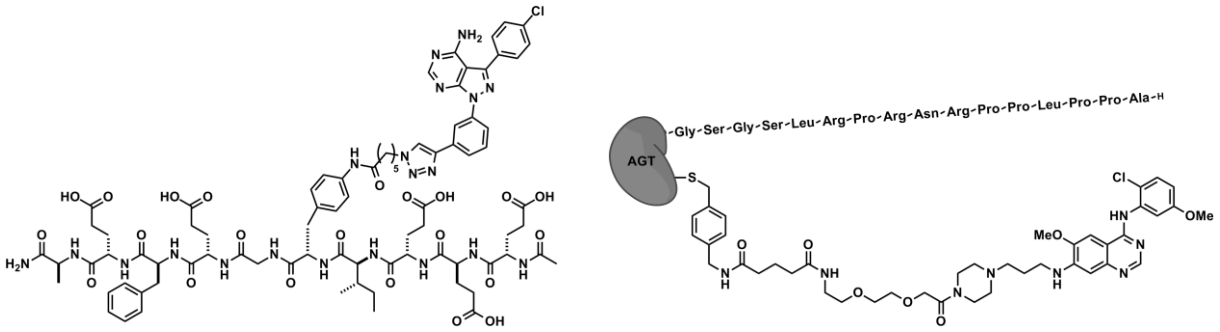

a **b**

Figure 1.5. Examples of (**a**) bisubstrate and (**b**) generic bivalent inhibitors of protein kinases.

As mentioned earlier, SH2 domains bind phosphotyrosine (pY) containing peptide sequences. Of the 32 non-receptor tyrosine kinases, most of which contain an SH2 domain, most are specific for the peptide sequences that they bind.[63] The Src family kinases (c-Src, Hck, Yes, Fyn, Lyn, Blk, Yrk, Fgr, and Lck)[25] all bind an optimal sequence of pYEEI[64] while c-Abl binds an optimal sequence of pYENP.[65] The peptide specificity results from the amino acids three residues c-terminal to the phosphotyrosine.[65] There has been some work to develop small molecules that bind SH2 domains.[66] There are several reported small molecules that bind the SH2 domain of c-Src.[67,68] Furthermore, by replacing the phosphotyrosine with 4′-(difluorophosphonomethyl)phenylalanine (F_2Pmp), it was possible to create phosphatase-resistant SH2 domain binding ligands; however, they are likely not cell permeable.[66]

Drug Combination Therapy

Before the early 1960s, the idea of combining chemotherapy drugs seemed unthinkable, but now it is considered the standard treatment. One of the first combination therapies for cancer was "VAMP" used for child leukemias.[69] "VAMP" was an acronym for the combination of **v**incristine, **a**methopterin, 6-**m**ercaptopurine, and **p**rednisone, and it was the first of many

combination treatment programs that drastically increased the rate and duration of remission.[69] After VAMP, combination therapy boomed with the creation of MOMP which combined nitrogen mustard, vincristine, methotrexate, and prednisone for Hodgkins lymphoma and cyclophosphamide, methotrexate, and 5-fluorouracil for breast cancer.[69] Combination therapies are successful because they can target different pathways involved in the cancer. Additionally, combining drugs can lower the dose of drug required to achieve an effect, which then can lower the negative side effects. Furthermore, drug combinations can sometimes work together to create an even better effect than one would expect from a simple addition of two agents, a phenomenon referred to as synergy.[70] Synergistic combinations can further lessen the negative side effects by requiring even less drug.

Combination therapy can also be used with kinase inhibitors. Generally, kinase inhibitor combinations involve kinase inhibitors that target different pathways; however, it could be feasible to target a single kinase with combinations of allosteric and ATP-competitive inhibitors. As mentioned earlier, allosteric modulators of kinases are excellent tools. Furthermore, since they bind in sites distinct from the conserved ATP-binding pocket, one could imagine that combining allosteric with ATP-competitive inhibitors could have far reaching implications for the treatment of kinase driven diseases. Already, there have been results that show combining allosteric and ATP-competitive inhibitors can overcome clinical resistance mutations. Gray and coworkers demonstrated that GNF-2 can be combined with nilotinib (an approved c-Abl inhibitor for CML) to overcome a clinical mutation that neither inhibitor can target (T315I).[71] In fact, Novartis is currently developing GNF-2 analogs for combination therapy with Nilotinib to treat the T315I mutation.[72] Our research described in **Chapter V**, further investigates combinations of ATP-competitive inhibitors and GNF-2.

Conclusions

Kinases play an important role in regulating a variety of cellular processes. When these pathways are dysregulated, they often lead to disease states such as cancer. Targeted therapies such as kinase inhibitors have proven successful drugs. They are also important probes to continue to study kinase function in cells. Unfortunately, all approved kinase inhibitors bind in the conserved ATP-binding pocket, which causes some of them to be promiscuous and bind off-target kinases. To establish selective and valuable tools to study kinases biochemically and

incellulo, we looked to create and utilize inhibitors that bind outside the conserved ATP-binding pocket. We used several different strategies that all yielded a wealth of information about kinase global conformation and biology.

References

(1) Manning, G.; Whyte, D. B.; Martinez, R.; Hunter, T.; Sudarsanam, S. The Protein Kinase Complement of the Human Genome. *Science.* **2002**, *298* (5600), 1912–1934.

(2) Johnson, S. A.; Hunter, T. Kinomics: Methods for Deciphering the Kinome. *Nat. Methods* **2005**, *2* (1), 17–25.

(3) Cohen, P. The Origins of Protein Phosphorylation. *Nat. Cell Biol.* **2002**, *4* (5), E127–E130.

(4) Nolen, B.; Taylor, S.; Ghosh, G. Regulation of Protein Kinases: Controlling Activity through Activation Segment Conformation. *Mol. Cell* **2004**, *15* (5), 661–675.

(5) Ayrapetov, M. K.; Wang, Y.-H.; Lin, X.; Gu, X.; Parang, K.; Sun, G. Conformational Basis for SH2-Tyr(P)527 Binding in Src Inactivation. *J. Biol. Chem.* **2006**, *281* (33), 23776–23784.

(6) Batzer, A. G.; Rotin, D.; Ureña, J. M.; Skolnik, E. Y.; Schlessinger, J. Hierarchy of Binding Sites for Grb2 and Shc on the Epidermal Growth Factor Receptor. *Mol. Cell Biol.* **1994**, *14* (8), 5192–5201.

(7) Cohen, P. Protein Kinases--the Major Drug Targets of the Twenty-First Century? *Nat. Rev. Drug Discov.* **2002**, *1* (4), 309–315.

(8) Blume-Jensen, P.; Hunter, T. Oncogenic Kinase Signalling. *Nature* **2001**, *411* (6835), 355–365.

(9) Martin, G. S. The Hunting of the Src. *Nat. Rev. Mol. Cell Biol.* **2001**, *2* (6), 467–475.

(10) Knighton, D. R.; Zheng, J. H.; Ten Eyck, L. F.; Ashford, V. A.; Xuong, N. H.; Taylor, S. S.; Sowadski, J. M. Crystal Structure of the Catalytic Subunit of Cyclic Adenosine Monophosphate-Dependent Protein Kinase. *Science.* **1991**, *253* (5018), 407 LP-414.

(11) Huse, M.; Kuriyan, J. The Conformational Plasticity of Protein Kinases. *Cell* **2002**, *109* (3), 275–282.

(12) Nowell, P. C.; Hungerford, D. A. Chromosome Studies on Normal and Leukemic Human Leukocytes. *J. Natl. Cancer Inst.* **1960**, *25* (1), 85–109.

(13) McLaughlin, P.; Grillo-López, A. J.; Link, B. K.; Levy, R.; Czuczman, M. S.; Williams, M. E.; Heyman, M. R.; Bence-Bruckler, I.; White, C. A.; Cabanillas, F.; Jain, V.; Ho, A. D.; Lister, J.; Wey, K.; Shen, D.; Dallaire, B. K. Rituximab Chimeric Anti-CD20 Monoclonal Antibody Therapy for Relapsed Indolent Lymphoma: Half of Patients Respond to a Four-Dose Treatment Program. *J. Clin. Oncol.* **1998**, *16* (8), 2825–2833.

(14) Slamon, D. J.; Leyland-Jones, B.; Shak, S.; Fuchs, H.; Paton, V.; Bajamonde, A.; Fleming, T.; Eiermann, W.; Wolter, J.; Pegram, M.; Baselga, J.; Norton, L. Use of Chemotherapy plus a Monoclonal Antibody against HER2 for Metastatic Breast Cancer That Overexpresses HER2. *N. Engl. J. Med.* **2001**, *344* (11), 783–792.

(15) Druker, B. J.; Tamura, S.; Buchdunger, E.; Ohno, S.; Segal, G. M.; Fanning, S.; Zimmermann, J.; Lydon, N. B. Effects of a Selective Inhibitor of the Abl Tyrosine Kinase on the Growth of Bcr-Abl Positive Cells. *Nat. Med.* **1996**, *2* (5), 561–566.

(16) Kurzrock, R.; Gutterman, J. U.; Talpaz, M. The Molecular Genetics of Philadelphia

Chromosome–Positive Leukemias. *N. Engl. J. Med.* **1988**, *319* (15), 990–998.
(17) Cilloni, D.; Saglio, G. Molecular Pathways: BCR-ABL. *Clin. Cancer Res.* **2012**, *18* (4), 930–937.
(18) Druker, B. J.; Guilhot, F.; O'Brien, S. G.; Gathmann, I.; Kantarjian, H.; Gattermann, N.; Deininger, M. W. N.; Silver, R. T.; Goldman, J. M.; Stone, R. M.; Cervantes, F.; Hochhaus, A.; Powell, B. L.; Gabrilove, J. L.; Rousselot, P.; Reiffers, J.; Cornelissen, J. J.; Hughes, T.; Agis, H.; Fischer, T.; Verhoef, G.; Shepherd, J.; Saglio, G.; Gratwohl, A.; Nielsen, J. L.; Radich, J. P.; Simonsson, B.; Taylor, K.; Baccarani, M.; So, C.; Letvak, L.; Larson, R. A. Five-Year Follow-up of Patients Receiving Imatinib for Chronic Myeloid Leukemia. *N. Engl. J. Med.* **2006**, *355* (23), 2408–2417.
(19) Hochhaus, A.; O'Brien, S. G.; Guilhot, F.; Druker, B. J.; Branford, S.; Foroni, L.; Goldman, J. M.; Müller, M. C.; Radich, J. P.; Rudoltz, M.; Mone, M.; Gathmann, I.; Hughes, T. P.; Larson, R. A. Six-Year Follow-up of Patients Receiving Imatinib for the First-Line Treatment of Chronic Myeloid Leukemia. *Leukemia* **2009**, *23* (6), 1054–1061.
(20) Capdeville, R.; Buchdunger, E.; Zimmermann, J.; Matter, A. Glivec (STI571, Imatinib), a Rationally Developed, Targeted Anticancer Drug. *Nat. Rev. Drug Discov.* **2002**, *1* (7), 493–502.
(21) Hirota, S.; Isozaki, K.; Moriyama, Y.; Hashimoto, K.; Nishida, T.; Ishiguro, S.; Kawano, K.; Hanada, M.; Kurata, A.; Takeda, M.; Muhammad Tunio, G.; Matsuzawa, Y.; Kanakura, Y.; Shinomura, Y.; Kitamura, Y. Gain-of-Function Mutations of c-Kit in Human Gastrointestinal Stromal Tumors. *Science.* **1998**, *279* (5350), 577–580.
(22) Wu, P.; Nielsen, T. E.; Clausen, M. H. Small-Molecule Kinase Inhibitors: An Analysis of FDA-Approved Drugs. *Drug Discov. Today* **2016**, *21* (1), 5–10.
(23) Thomas, S. M.; Brugge, J. S. Cellular Functions Regulated by Src Family Kinases. *Annu. Rev. Cell Dev. Biol.* **1997**, *13*, 513–609.
(24) Zhang, S.; Huang, W.-C.; Li, P.; Guo, H.; Poh, S.-B.; Brady, S. W.; Xiong, Y.; Tseng, L.-M.; Li, S.-H.; Ding, Z.; Sahin, A. A.; Esteva, F. J.; Hortobagyi, G. N.; Yu, D. Combating Trastuzumab Resistance by Targeting SRC, a Common Node Downstream of Multiple Resistance Pathways. *Nat. Med.* **2011**, *17* (4), 461–469.
(25) Yeatman, T. J. A Renaissance for SRC. *Nat. Rev. Cancer* **2004**, *4* (6), 470–480.
(26) Gilani, R.; Phadke, S.; Bao, L. W.; Lachacz, E.; Dziubinski, M.; Brandvold, K.; Steffey, M.; Kwarcinski, F.; Graveel, C. R.; Kidwell, K. M.; Merajver, S. D.; Soellner, M. B. UM-164: A Potent c-Src/p38 Kinase Inhibitor with in Vivo Activity against Triple Negative Breast Cancer. *Clin. Cancer Res.* **2016**, *22* (20), 5087–5096.
(27) Dent, R.; Trudeau, M.; Pritchard, K. I.; Hanna, W. M.; Kahn, H. K.; Sawka, C. A.; Lickley, L. A.; Rawlinson, E.; Sun, P.; Narod, S. A. Triple-Negative Breast Cancer: Clinical Features and Patterns of Recurrence. *Clin. Cancer Res.* **2007**, *13* (15 Pt 1), 4429–4434.
(28) Foulkes, W.; Smith, I.; Reis-Filho, J. Triple-Negative Breast Cancer. *N. Engl. J. Med.* **2010**, *363*, 1938–1948.
(29) Wang, Q.; Zorn, J. A.; Kuriyan, J. A Structural Atlas of Kinases Inhibited by Clinically Approved Drugs. *Methods Enzym.* **2014**, *548*, 23–67.
(30) USFDA Approved Protein Kinase Inhibitors. *Blue Ridge Inst. Med. Res. Horse Shoe, NC* **2015**, http://www.Brimr.Org/PKI/PKIs.htm.
(31) Zhao, Z.; Wu, H.; Wang, L.; Liu, Y.; Knapp, S.; Liu, Q.; Gray, N. S. Exploration of Type II Binding Mode: A Privileged Approach for Kinase Inhibitor Focused Drug Discovery?

ACS Chem. Biol. **2014**, *9* (6), 1230–1241.
(32) Wenqing, X.; Harrison, S.; Eck, M. Three-Dimensional Structure of the Tyrosine Kinase c-Src. *Nature* **1997**, *385*, 595–602.
(33) Krishnamurty, R.; Brigham, J. L.; Leonard, S. E.; Ranjitkar, P.; Larson, E. T.; Dale, E. J.; Merritt, E. A.; Maly, D. J. Active Site Profiling Reveals Coupling between Domains in SRC-Family Kinases. *Nat. Chem. Biol.* **2013**, *9* (1), 43–50.
(34) Dar, A. C.; Lopez, M. S.; Shokat, K. M. Small Molecule Recognition of c-Src via the Imatinib-Binding Conformation. *Chem. Biol.* **2008**, *15* (10), 1015–1022.
(35) Seeliger, M. A.; Ranjitkar, P.; Kasap, C.; Shan, Y.; Shaw, D. E.; Shah, N. P.; Kuriyan, J.; Maly, D. J. Equally Potent Inhibition of c-Src and Abl by Compounds That Recognize Inactive Kinase Conformations. *Cancer Res.* **2009**, *69* (6), 2384–2392.
(36) Kwarcinski, F. E.; Brandvold, K. R.; Phadke, S.; Beleh, O. M.; Johnson, T. K.; Meagher, J. L.; Seeliger, M. A.; Stuckey, J. A.; Soellner, M. B. Conformation-Selective Analogues of Dasatinib Reveal Insight into Kinase Inhibitor Binding and Selectivity. *ACS Chem. Biol.* **2016**, *11* (5), 1296–1304.
(37) Knight, Z. A.; Shokat, K. M. Features of Selective Kinase Inhibitors. *Chem. Biol.* **2005**, *12* (6), 621–637.
(38) Brandvold, K. R.; Steffey, M. E.; Fox, C. C.; Soellner, M. B. Development of a Highly Selective c-Src Kinase Inhibitor. *ACS Chem. Biol.* **2012**, *7* (8), 1393–1398.
(39) Kwarcinski, F. E.; Fox, C. C.; Steffey, M. E.; Soellner, M. B. Irreversible Inhibitors of c-Src Kinase That Target a Nonconserved Cysteine. *ACS Chem. Biol.* **2012**, *7* (11), 1910–1917.
(40) Boggon, T. J.; Eck, M. J. Structure and Regulation of Src Family Kinases. *Oncogene* **2004**, *23* (48), 7918–7927.
(41) Thomas, J. W.; Ellis, B.; Renee, J.; Knight, W. B.; White, G. C.; Schaller, M. D.; Boerner, R. J.; Ii, C. W. SH2- and SH3-Mediated Interactions between Focal Adhesion Kinase and Src. *J. Biol. Chem.* **1998**, *273* (1), 577–583.
(42) Nagar, B.; Hantschel, O.; Young, M. A.; Scheffzek, K.; Veach, D.; Bornmann, W.; Clarkson, B.; Superti-Furga, G.; Kuriyan, J. Structural Basis for the Autoinhibition of c-Abl Tyrosine Kinase. *Cell* **2003**, *112* (6), 859–871.
(43) Fabian, M. A.; Biggs, W. H.; Treiber, D. K.; Atteridge, C. E.; Azimioara, M. D.; Benedetti, M. G.; Carter, T. A.; Ciceri, P.; Edeen, P. T.; Floyd, M.; Ford, J. M.; Galvin, M.; Gerlach, J. L.; Grotzfeld, R. M.; Herrgard, S.; Insko, D. E.; Insko, M. A.; Lai, A. G.; Lélias, J.-M.; Mehta, S. A.; Milanov, Z. V; Velasco, A. M.; Wodicka, L. M.; Patel, H. K.; Zarrinkar, P. P.; Lockhart, D. J. A Small Molecule-Kinase Interaction Map for Clinical Kinase Inhibitors. *Nat. Biotechnol.* **2005**, *23* (3), 329–336.
(44) Karaman, M. W.; Herrgard, S.; Treiber, D. K.; Gallant, P.; Atteridge, C. E.; Campbell, B. T.; Chan, K. W.; Ciceri, P.; Davis, M. I.; Edeen, P. T.; Faraoni, R.; Floyd, M.; Hunt, J. P.; Lockhart, D. J.; Milanov, Z. V; Morrison, M. J.; Pallares, G.; Patel, H. K.; Pritchard, S.; Wodicka, L. M.; Zarrinkar, P. P. A Quantitative Analysis of Kinase Inhibitor Selectivity. *Nat. Biotechnol.* **2008**, *26* (1), 127–132.
(45) Anastassiadis, T.; Deacon, S. W.; Devarajan, K.; Ma, H.; Peterson, J. R. Comprehensive Assay of Kinase Catalytic Activity Reveals Features of Kinase Inhibitor Selectivity. *Nat. Biotechnol.* **2011**, *29* (11), 1039–1045.
(46) Fang, Z.; Grütter, C.; Rauh, D. Strategies for the Selective Regulation of Kinases with Allosteric Modulators: Exploiting Exclusive Structural Features. *ACS Chem. Biol.* **2013**, *8*

(1), 58–70.
(47) Zhang, J.; Yang, P. L.; Gray, N. S. Targeting Cancer with Small Molecule Kinase Inhibitors. *Nat. Rev. Cancer* **2009**, *9* (1), 28–39.
(48) Ohren, J. F.; Chen, H.; Pavlovsky, A.; Whitehead, C.; Zhang, E.; Kuffa, P.; Yan, C.; McConnell, P.; Spessard, C.; Banotai, C.; Mueller, W. T.; Delaney, A.; Omer, C.; Sebolt-Leopold, J.; Dudley, D. T.; Leung, I. K.; Flamme, C.; Warmus, J.; Kaufman, M.; Barrett, S.; Tecle, H.; Hasemann, C. a. Structures of Human MAP Kinase Kinase 1 (MEK1) and MEK2 Describe Novel Noncompetitive Kinase Inhibition. *Nat. Struct. Mol. Biol.* **2004**, *11* (12), 1192–1197.
(49) Lindsley, C. W.; Zhao, Z.; Leister, W. H.; Robinson, R. G.; Barnett, S. F.; Defeo-Jones, D.; Jones, R. E.; Hartman, G. D.; Huff, J. R.; Huber, H. E.; Duggan, M. E. Allosteric Akt (PKB) Inhibitors: Discovery and SAR of Isozyme Selective Inhibitors. *Bioorg. Med. Chem. Lett.* **2005**, *15* (3), 761–764.
(50) Adrián, F. J.; Ding, Q.; Sim, T.; Velentza, A.; Sloan, C.; Liu, Y.; Zhang, G.; Hur, W.; Ding, S.; Manley, P.; Mestan, J.; Fabbro, D.; Gray, N. S. Allosteric Inhibitors of Bcr-Abl-Dependent Cell Proliferation. *Nat. Chem. Biol.* **2006**, *2* (2), 95–102.
(51) Choi, Y.; Seeliger, M. a; Panjarian, S. B.; Kim, H.; Deng, X.; Sim, T.; Couch, B.; Koleske, A. J.; Smithgall, T. E.; Gray, N. S. N-Myristoylated c-Abl Tyrosine Kinase Localizes to the Endoplasmic Reticulum upon Binding to an Allosteric Inhibitor. *J. Biol. Chem.* **2009**, *284* (42), 29005–29014.
(52) Breen, M. E.; Steffey, M. E.; Lachacz, E. J.; Kwarcinski, F. E.; Fox, C. C.; Soellner, M. B. Substrate Activity Screening with Kinases: Discovery of Small-Molecule Substrate-Competitive c-Src Inhibitors. *Angew. Chem. Int. Ed.* **2014**, *53* (27), 7010–7013.
(53) Jencks, W. P. On the Attribution and Additivity of Binding Energies. *Proc. Natl. Acad. Sci.* **1981**, *78* (7), 4046–4050.
(54) Cox, K. J.; Shomin, C. D.; Ghosh, I. Tinkering Outside the Kinase ATP Box: Allosteric (Type IV) and Bivalent (Type V) Inhibitors of Protein Kinases. *Futur. Med. Chem.* **2011**, *3* (1), 29–43.
(55) Lamba, V.; Ghosh, I. New Directions in Targeting Protein Kinases: Focusing upon True Allosteric and Bivalent Inhibitors. *Curr. Pharm. Des.* **2012**, *18* (20), 2936–2945.
(56) Brandvold, K. R.; Santos, S. M.; Breen, M. E.; Lachacz, E. J.; Steffey, M. E.; Soellner, M. B. Exquisitely Specific Bisubstrate Inhibitors of c-Src Kinase. *ACS Chem. Biol.* **2015**, *10*, 1387–1391.
(57) Profit, A.; Lee, T.; Lawrence, D. Bivalent Inhibitors of Protein Tyrosine Kinases. *J. Am. Chem. Soc.* **1999**, *121* (2), 280–283.
(58) Profit, A. A.; Lee, T. R.; Niu, J.; Lawrence, D. S. Molecular Rulers: An Assessment of Distance and Spatial Relationships of Src Tyrosine Kinase Sh2 and Active Site Regions. *J. Biol. Chem.* **2001**, *276* (12), 9446–9451.
(59) Hah, J.-M.; Sharma, V.; Li, H.; Lawrence, D. S. Acquisition of a "Group A"-Selective Src Kinase Inhibitor via a Global Targeting Strategy. *J. Am. Chem. Soc.* **2006**, *128* (18), 5996–5997.
(60) Hill, Z. B.; Perera, B. G. K.; Maly, D. J. A Chemical Genetic Method for Generating Bivalent Inhibitors of Protein Kinases. *J. Am. Chem. Soc.* **2009**, *131* (19), 6686–6688.
(61) Hill, Z. B.; Perera, B. G. K.; Maly, D. J. Bivalent Inhibitors of the Tyrosine Kinases ABL and SRC: Determinants of Potency and Selectivity. *Mol. BioSyst.* **2011**, *7* (2), 447–456.
(62) Kwarcinski, F. E.; Steffey, M. E.; Fox, C. C.; Soellner, M. B. Discovery of Bivalent

Kinase Inhibitors via Enzyme-Templated Fragment Elaboration. *ACS Med. Chem. Lett.* **2015**, *6*, 898–901.
(63) Filippakopoulos, P.; Müller, S.; Knapp, S. SH2 Domains: Modulators of Nonreceptor Tyrosine Kinase Activity. *Curr. Opin. Struct. Biol.* **2009**, *19* (6), 643–649.
(64) Liu, B. A.; Jablonowski, K.; Shah, E. E.; Engelmann, B. W.; Jones, R. B.; Nash, P. D. SH2 Domains Recognize Contextual Peptide Sequence Information to Determine Selectivity. *Mol. Cell. Proteomics* **2010**, *9*, 2391–2404.
(65) Zhou, S.; Shoelson, S.; Chaudhuri, M.; Gish, G.; Pawson, T.; Haser, W.; King, F.; Roberts, T.; Ratnofsky, S.; Lechleider, R.; Neel, B.; Birge, R.; Fajardo, J.; Chou, M.; Hanafusa, H.; Schaffhausen, B.; Cantley, L. SH2 Domains Recognize Specific Phosphopeptide Sequences. *Cell* **1993**, *72* (5), 767–778.
(66) Shakespeare, W. SH2 Domain Inhibition: A Problem Solved? *Curr. Opin. Chem. Biol.* **2001**, *5* (4), 409–415.
(67) Lunney, E.; Para, K. Structure-Based Design of a Novel Series of Nonpeptide Ligands That Bind to the pp60src SH2 Domain. *J. Am. Chem. Soc.* **1997**, *7863* (20), 12471–12476.
(68) Lunney, E.; Para, K.; Plummer, M.; Prasad, J.; Saltiel, A.; Sawyer, T.; Shahripour, A.; Stankovic, C. Compounds, Compositions and Methods for Inhibiting the Binding of Proteins Containing an SH2 Domain to Cognate Phosphorylated Proteins, 1997.
(69) DeVita, V. T.; Chu, E. A History of Cancer Chemotherapy. *Cancer Res.* **2008**, *68* (21), 8643 LP-8653.
(70) Chou, T.-C. Drug Combination Studies and Their Synergy Quantification Using the Chou-Talalay Method. *Cancer Res.* **2010**, *70* (2), 440–446.
(71) Zhang, J.; Adrián, F. J.; Jahnke, W.; Cowan-Jacob, S. W.; Li, A. G.; Iacob, R. E.; Sim, T.; Powers, J.; Dierks, C.; Sun, F.; Guo, G.-R.; Ding, Q.; Okram, B.; Choi, Y.; Wojciechowski, A.; Deng, X.; Liu, G.; Fendrich, G.; Strauss, A.; Vajpai, N.; Grzesiek, S.; Tuntland, T.; Liu, Y.; Bursulaya, B.; Azam, M.; Manley, P. W.; Engen, J. R.; Daley, G. Q.; Warmuth, M.; Gray, N. S. Targeting Bcr-Abl by Combining Allosteric with ATP-Binding-Site Inhibitors. *Nature* **2010**, *463* (7280), 501–506.
(72) Furet, P.; Grotzfeld, R. M.; Jones, D. B.; Manley, P.; Marzinzik, A.; Pelle, X. F. A.; Salem, B.; Schoepfer, J. Preparation of Benzamide Derivatives for Inhibiting the Activity of ABL1, ABL2 and BCR-ABL1 for Treating Cancer and Viral Infections. WO 2013/171642 A1, 2013.

CHAPTER II

Bivalent Inhibitors of c-Src Tyrosine Kinase That Bind a Regulatory Domain[a]

Abstract

We have developed a general methodology to produce bivalent kinase inhibitors for c-Src that interact with the SH2 and ATP binding pockets. Our approach led to a highly selective bivalent inhibitor of c-Src. We demonstrate impressive selectivity for c-Src over homologous kinases. Exploration of the unexpected high level of selectivity yielded insight into the inherent flexibility of homologous kinases. Finally, we demonstrate that our methodology is modular and both the ATP-competitive fragment and conjugation chemistry can be swapped.

Introduction

Protein kinases are key regulatory enzymes in human cell signaling, both in healthy and diseased tissue. Efforts to pharmacologically elucidate kinase signaling have been hampered by a lack of selective kinase inhibitors.[1–3] The vast majority of reported kinase inhibitors bind to the conserved ATP-site.[4] Owing to the conserved nature of the ATP pocket, nearly all ATP-competitive kinase inhibitors are promiscuous and bind to undesired off-targets.[4–6] One strategy to improve the selectivity of kinase inhibitors is to interact with elements outside the conserved ATP pocket.[7–9]

We previously reported bisubstrate inhibitors of c-Src in which an ATP-competitive inhibitor was tethered to a substrate phosphorylation site peptide.[10] Here, we explore the conversion of a promiscuous ATP-competitive kinase inhibitor into a bivalent inhibitor of c-Src that interacts with the SH2 domain of c-Src (in addition to the ATP-binding pocket). Our strategy involves conjugation of the two binding elements with "click chemistry" to enable a modular

[a] The work in this chapter contains a few small additions to the published work presented in Johnson, T. K.; Soellner, M. B. Bivalent Inhibitors of c-Src Tyrosine Kinase That Bind a Regulatory Domain. *Bioconjug. Chem.* **2016**, *27* (7), 1745–1749.

design.[11] We demonstrate that both copper-catalyzed and catalyst-free strain-release click reactions[12] can readily be employed to construct bivalent inhibitors. The modularity of our design is showcased by the synthesis of two distinct bivalent inhibitors starting from two different ATP-competitive inhibitor fragments.

Bivalent kinase inhibitors that target two distinct domains have been reported,[8,9] however, there are no reports of such bivalent inhibitors purely constructed of small molecule—peptide hybrids. In addition, little is known about the selectivity changes transitioning from a promiscuous ATP-competitive inhibitor to a bivalent inhibitor also targeting a regulatory domain (here SH2 domain).[13] Lawrence and co-workers reported fully peptidic bivalent inhibitors that link a substrate-phosphorylation site peptide to a SH2 domain interacting peptide.[14,15] Maly and co-workers have reported linking ATP-competitive small molecules to SH2 domain binding peptides using a large, protein-based linker.[16] In contrast, our design provides a significantly lower molecular weight bivalent inhibitor than either method previously described.

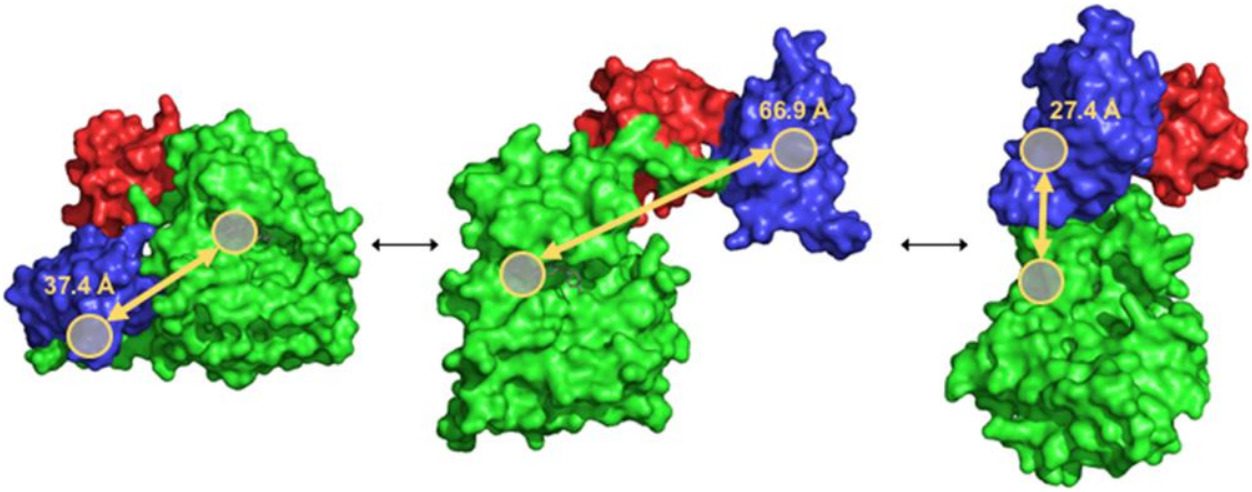

Figure 2.1. Conformational equilibrium of c-Src. c-Src exists in equilibrium between "open" and "closed" conformations. The closed, autoinhibited conformation (left, PDB: 2SRC), and open, active conformations (middle, PDB: 1Y57, and right, PDB: 1OPL). The kinase catalytic domains are colored green, SH2 domains colored blue, and SH3 domains colored red. For each conformation, distances between the ATP-binding pocket and the SH2 phosphotyrosine binding pockets are displayed and colored gold.

c-Src is known to exist in two distinct global conformations, open and closed (**Figure 1.1**).[17,18] The open conformation is the conformation that exists associated with the plasma membrane and is known to correlate with disease progression.[19] In contrast to the open conformation, the closed conformation is highly rigid.[20] Crystal structures of the closed conformation reveal that the distance between the ATP-pocket and the phospho-Tyr binding pocket of the SH2 domain is 37 Å (**Figure 1.1** and **Appendix A**, **Figure A.1**) Due to the inherent

rigidity of the inactive conformation, we hypothesized that we could selectively inhibit the open conformation using a bivalent inhibitor constructed with a linker shorter than 37 Å. We predicted that a bivalent inhibitor with a linker too short to interact with the closed, rigid conformation could still bind to the open, flexible conformation. To our knowledge, there has been no report of a c-Src inhibitor that can selectively inhibit the active conformation over the inactive conformation.

Bivalent Inhibitor Design

Our design strategy involves ATP-competitive inhibitors with a pendant alkyne and a SH2 domain binding phospho-peptide containing a PEG linker and pendant azide (**Scheme 2.1**).[21,22] We hypothesized that a linker shorter than 37 Å could provide an inhibitor that selectively inhibits the active conformation of c-Src. Thus, we elected to use a 33-atom PEG linker with a calculated maximal length of 25 Å (**Appendix A**, **Figure A.2**). For an ATP-competitive inhibitor, we selected an aminopyrazole fragment that is a promiscuous kinase inhibitor.[23] We previously profiled an aminopyrazole fragment and found that it potently binds 117 of 200 kinases in that panel.[24] To enable conjugation to a peptide, we synthesized **2.1**, an aminopyrazole fragment with a pendant alkyne. We found **2.1** to be a competent inhibitor of 3-domain c-Src (IC_{50} = 2.9 μM). For the SH2 domain interacting peptide, we selected a previously reported pentapeptide, H_2N-Q-pY-E-E-I-$CONH_2$.[25] Solid phase peptide synthesis was employed to synthesize **2.2**, the SH2 interacting peptide with an N-terminal azido linker.[26] Copper-mediated click chemistry was then used to construct bivalent inhibitor **2.3**.

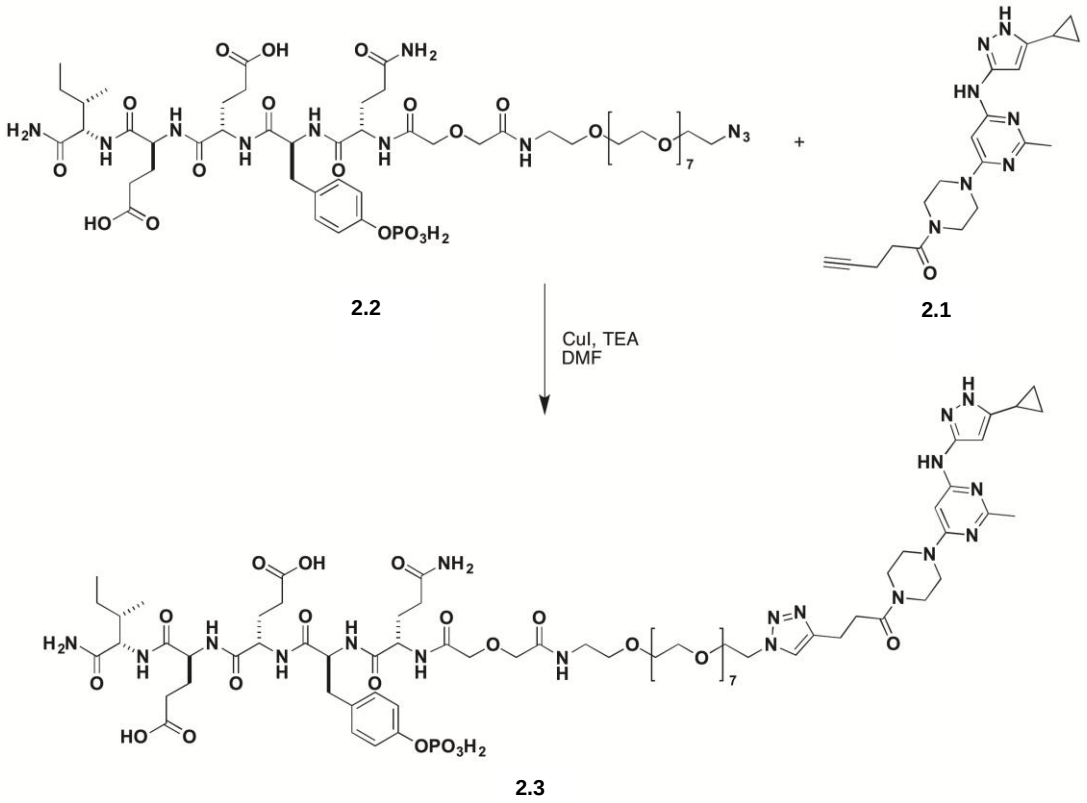

Scheme 2.1. Copper catalyzed click cycloaddition of ATP-competitive alkyne **2.1** and azido-SH2-peptide **2.2** afford triazole-linked bivalent inhibitor **2.3**.

Biochemical Evaluation of Bivalent Inhibitor

We evaluated bivalent inhibitor **2.3** in a continuous activity assay[27] with 3-domain c-Src[28] and found **2.3** was a potent inhibitor (**Table 2.1**, IC_{50} = 0.16 μM). Relative to ATP-competitive fragment **2.1**, this represents a 18-fold improvement in binding affinity. We next tested **2.3** against a kinase domain only construct of c-Src and found that bivalent inhibitor **2.3** has similar affinity to the ATP-competitive inhibitor alone (**2.3**, IC_{50} = 2.1 μM; **2.1**, IC_{50} = 1.3 μM). These results are consistent with bivalent inhibitor **2.3** requiring both the catalytic and SH2 domains to achieve optimal binding. Comparing kinase domain to 3-domain c-Src constructs, bivalent inhibitor **2.3** binds 13-fold tighter to the c-Src construct with an SH2 domain (**Table 2.1**).

Table 2.1. IC_{50} values for **2.1** and **2.3** with various c-Src kinase constructs.

c-Src construct	2.1 IC_{50} (μM)	2.3 IC_{50} (μM)
kinase domain	1.3 ± 0.5	2.1 ± 0.3
3-domain (3D)	2.9 ± 0.6	0.16 ± 0.01
pY416 3D	2.4 ± 0.6	0.24 ± 0.1
pY527 3D	1.4 ± 0.1	1.8 ± 0.1
SH2-eng 3D	2.7 ± 0.6	2.2 ± 0.8

We hypothesized that using a linker shorter than the distance from the ATP-site to the SH2-domain found in the crystal structure for inactive/closed conformation of c-Src (PDB: 2SRC) we could selectively target the more flexible active conformation of c-Src. To test this hypothesis, we utilized constructs of 3-domain c-Src that are active (pY416)[29] and conformations known to be inactive and rigid (pY527 and SH2-engaged).[17,30] Gratifyingly, we found that bivalent inhibitor **2.3** is a selective inhibitor of pY416 c-Src over the pY527 and SH2-engaged constructs (**Table 2.1**: pY416 IC_{50} = 0.24 μM, pY527 IC_{50} = 1.8 μM, SH2-engaged IC_{50} = 2.3 μM). In contrast, ATP-competitive inhibitor **2.1** has no preference for open vs closed c-Src constructs (see **Appendix A** for additional data). To our knowledge, there are no reports for any kinase inhibitor with this level of selectivity for the active kinase conformation.

Table 2.2. IC_{50} values for **2.1** and **2.3** with various c-Src homologous kinases.

kinase	2.1 IC_{50} (μM)	2.3 IC_{50} (μM)
Hck	8.9	2.8 ± 0.7
Lck	9.3	5.3 ± 0.6
Blk	21.8	5.3 ± 0.7
Frk	9.6	5.6 ± 0.4
Fgr	4.6	3.1 ± 0.9
Lyn	10.8	2.5 ± 0.2
Abl	15.0	4.0 ± 0.4
Fyn1	2.8	0.27 ± 0.02

Next, we wanted to determine whether bivalent inhibitor **2.3** is selective for c-Src over homologous kinases. Thus, we tested both ATP-competitive inhibitor **2.1** and bivalent inhibitor **2.3** for inhibition against a panel of 8 homologous kinases,[31] including 7 members of the Src family (**Table 2.2**). ATP-competitive inhibition **2.1** could only be tested with n=1 IC_{50} curves due to a limited amount of protein. Importantly, each of these kinases includes a SH2

domain.[32,33] The average IC_{50} for bivalent inhibitor **2.3** was 3.5 μM, with the exception of Fyn1. From these data, we observe that **2.3** is highly selective (average of 22-fold selective) for c-Src across this panel of homologous kinases. In addition, we observed only a modest increase in potency for bivalent inhibitor **2.3** compared to ATP-competitive inhibitor **2.1**.

The level of selectivity we observed across homologous kinases is very impressive, however, it was unexpected given that the ATP-competitive inhibitor inhibits each kinase similarly and the SH2 binding element is known to interact with many Src family kinases.[25,34] We wanted to study the surprising selectivity using c-Src and Hck kinases. The ATP-competitive fragment binds with similar potency to both c-Src and Hck (c-Src IC_{50} = 2.9 ± 0.6 μM; Hck IC_{50} = 8.9 ± 0.5 μM) and cannot explain the selectivity observed for bivalent inhibitor **2.3**. Next, to probe the affinity of the SH2 interacting peptide with both c-Src and Hck, we measured the affinity of a related SH2 peptide containing a N-terminal fluorophore and the same core residues as our bivalent inhibitor (FITC-E-P-**Q-pY-E-E-I**-P-I-Y-L-NH_2, bold corresponds to the core SH2 binding residues found in bivalent inhibitor **2.3**). We found the SH2 peptide binds to both c-Src and Hck with equal affinity (c-Src EC_{50} = 0.72 ± 0.1 μM, Hck EC_{50} = 1.0 ± 0.3 μM). From these data, we conclude that the selectivity is not arising from either the ATP-competitive fragment or the SH2-binding element.

We hypothesized that the inter-domain flexibility for homologous kinases might be different – and thus responsible for the selectivity observed. To explore this hypothesis, we measured the binding of our bivalent inhibitor **2.3** to 3-domain Hck constructs with varied open/closed (flexible/rigid) conformations (in order of most open and flexible to most closed and rigid: wild-type, SH2-engaged, and SH3-engaged).[35,36] We found that bivalent inhibitor **2.3** binds tighter to SH3-engaged compared to wild-type 3-domain Hck (IC_{50} = 0.6 and 2.8 μM, respectively). These data suggest that activated Hck is less flexible than c-Src. Furthermore, engagement of the SH3 domain of Hck likely brings the SH2 and catalytic domains closer in proximity. Interestingly, Fyn1 is the only Src family kinase (SFK) other than c-Src for which **3** binds potently (Fyn1 IC_{50} = 0.27 μM). A recent study of SFKs indicated that Fyn1 was significantly more flexible than other SFKs.[37] Together, our findings reveal that homologous kinases have varied conformational flexibility, and that this flexibility can be selectively targeted using bivalent kinase inhibitors.

We have previously shown that bisubstrate kinase inhibitors are less susceptible to mutations within a single binding pocket.[10] We wanted to determine whether bivalent inhibitor **2.3** could inhibit c-Src with a clinically relevant gatekeeper mutation (T338M).[38] The T338M mutation renders c-Src resistant to nearly all ATP-competitive inhibitors, including all FDA-approved inhibitors of c-Src.[39,40] We found that bivalent inhibitor **2.3** is also potent inhibitor of 3-domain T338M c-Src (IC_{50} = 0.19 μM). These data suggest that bivalent inhibition of kinases is indeed an effective strategy to inhibit drug-resistant kinase mutants.

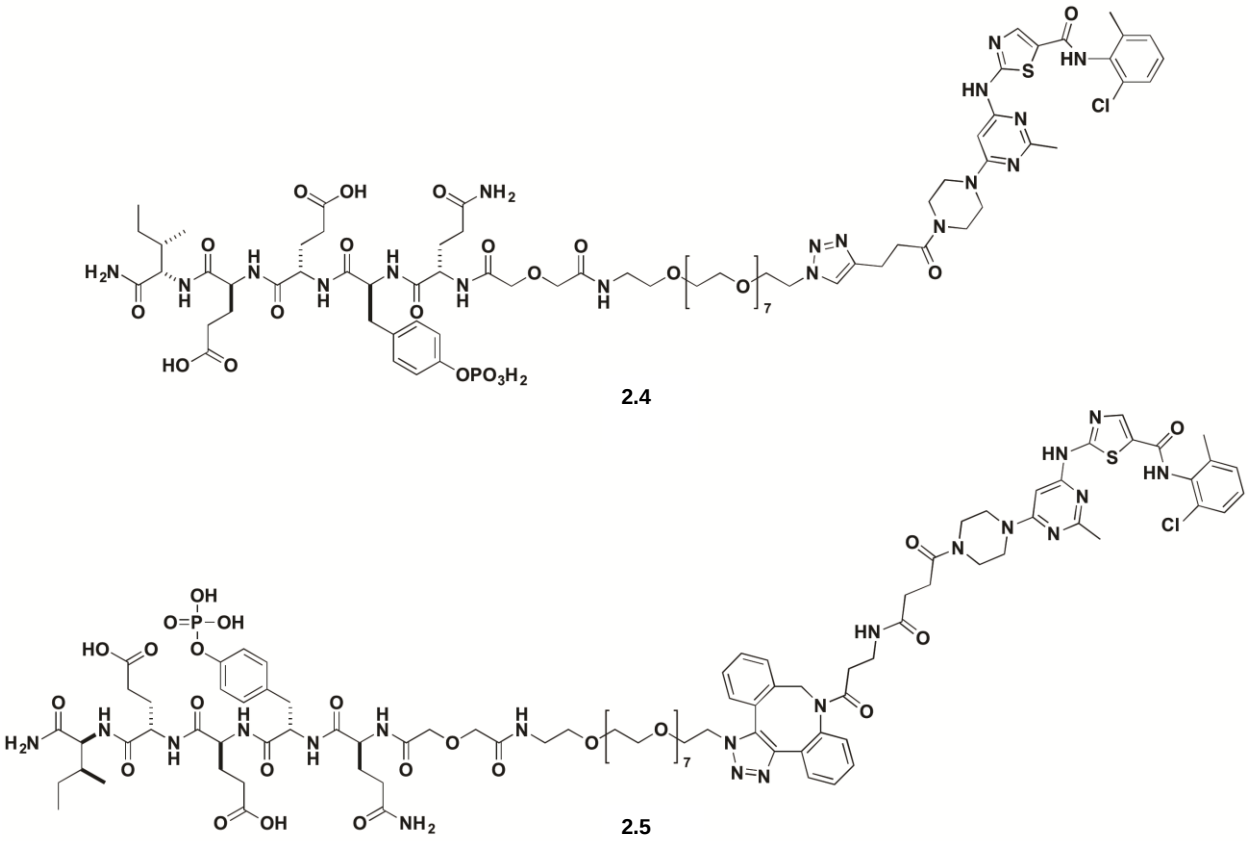

Figure 2.2. Copper catalyzed dasatinib bivalent **2.4** and catalyst-free bivalent **2.5**.

Modular Design

Our conjugation strategy, utilizing azide-alkyne click chemistry, was designed to be modular in nature. To showcase the modularity, we synthesized an analog of dasatinib (an FDA-approved dual c-Src/Abl inhibitor) with a pendant alkyne (see **Materials and Methods** for details).[41] Conjugation to the azido SH2 peptide **2.2** to dasatinib~alkyne (**2.15**) yielded bivalent inhibitor **2.4** (**Figure 2.2**). This inhibitor was too potent to evaluate in our enzymatic activity

assays (due to titration of the lowest enzyme concentrations accessible to our activity assay). Thus, we utilized a commercial binding assay that is performed in reticulocyte lysate containing ~5 mM ATP (Luceome Biotechnologies, Tucson, AZ)[42,43] to measure the affinity of **2.4** with full-length c-Src. In this assay, compound **2.4** has an IC_{50} = 1 nM for full length Src, while the ATP-competitive fragment (dasatinib) has an IC_{50} of 18 nM. This represents an 18-fold improvement in binding affinity upon conversion of the ATP-competitive fragment to bivalent inhibitor **2.4**. Notably, an 18-fold improvement is identical to the binding affinity increase found with the aminopyrazole-based system. These data demonstrate that the ATP-competitive inhibitor can be swapped for a different ligand in a straightforward manner. Thus, one could modulate selectivity (or other properties) by selecting from a multitude of known ATP-competitive kinase inhibitors.

Finally, we wanted to explore whether we could replace the copper-catalyzed click conjugation chemistry with a strain-release click chemistry. To enable catalyst-free conjugations, we synthesized dasatinib with a pendant cyclooctyne (**Scheme 2.5**). Incubation of azido peptide **2.2** with dasatinib~cyclooctyne provided bivalent inhibitor **2.5** (**Figure 2.2**). In our enzymatic activity assay, this bivalent inhibitor titrates enzyme (K_i < 10 nM), having similar activity to the copper catalyzed version (**2.4**). One advantage of catalyst-free cycloadditions is the ability to perform on-enzyme conjugation in situations where copper might be toxic.[12,44] This could enable rapid *in situ* generation of bivalent kinase inhibitors from starting fragments.

Conclusions

We have developed a platform to generate bivalent inhibitors that interact both with the ATP-binding site and a regulatory domain, here a SH2 domain. While the ATP pocket is conserved across the kinome,[4] interaction with a SH2 domain can provide instant selectivity because the vast majority of kinases do not possess a SH2 domain.[45] Furthermore, we found that our ATP-to-SH2 bivalent kinase inhibitors possess high selectivity across homologous kinases. We found that selectivity can be obtained even for kinases which share optimal SH2-peptide binding sequences. Using model kinases with varied flexibility, we demonstrated that flexibility of the kinase (in particular inter-domain flexibility) is responsible for the high level of selectivity obtained.

To demonstrate the modularity of our bivalent inhibitor design, we swapped the ATP-competitive fragment to a dasatinib analog and obtained a bivalent inhibitor with single digit nanomolar potency. The conjugation chemistry can also be changed, here we used both copper-catalyzed and strain-promoted click reactions to synthesize bivalent inhibitors.

While outside the scope of this chapter, we have previously demonstrated that peptide-based kinase inhibitors can be used in cellular assays after appending a cell-penetrating peptide.[10] In addition, one could envision using small molecule SH2 ligands to construct fully non-peptide bivalent inhibitors that might have inherent cell permeability. These studies are ongoing in our laboratory.

Materials and Methods

General Synthetic Methods

Unless otherwise noted, all reagents were obtained via commercial sources and used without further purification. All ^{1}H NMR spectra were measured with a Varian MR400 or Inova 500 spectrometer. Mass Spectrometry (HRMS) was carried out by the University of Michigan Mass Spectrometry Facility (J. Windak, director).

Synthetic Protocols

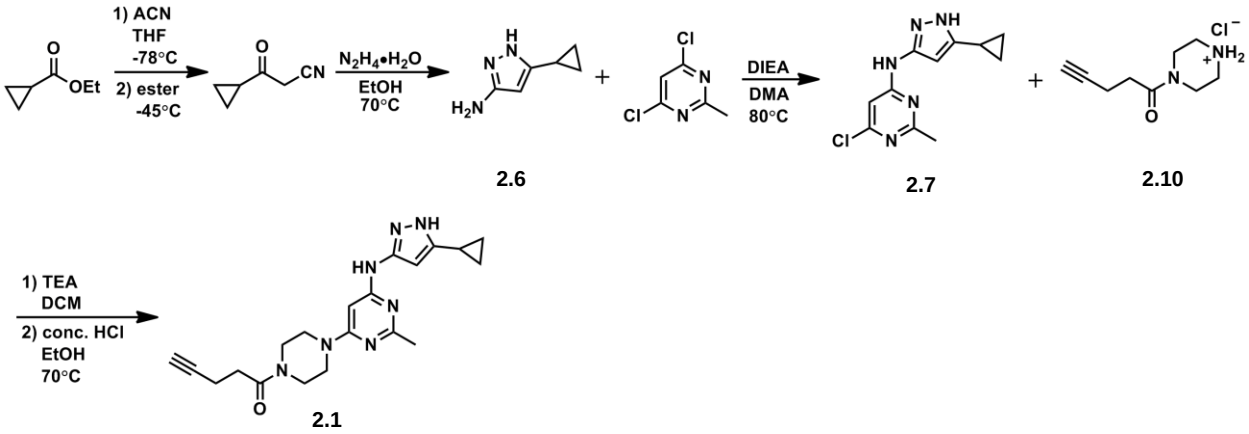

Scheme 2.2: Synthetic Scheme for Compound 2.1

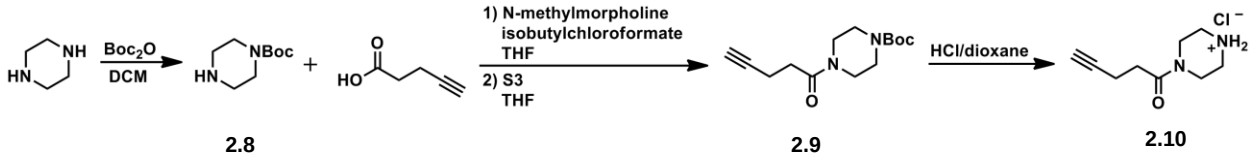

Scheme 2.3: Synthetic Scheme for Compound 2.10

Synthesis of 2.6: This compound was prepared as previously reported.[21]

Synthesis of 2.7: Compound **2.6** (997.4 mg, 8.10 mmol) was combined with 2,6-dichloro-4-methylpyrimidine (1.3216 g, 8.11mmol) in an oven-dried round bottom flask. DMA (20.0 mL) was added followed by DIEA (2.10 mL, 12.02 mmol) and the reaction was stirred at 80°C overnight. The reaction was then brought up in EtOAc and washed 3 times with sat. NH_4Cl. After drying over Na_2SO_4, the product was purified by silica gel chromatography using a Biotage Isolera One (linear gradient 40 → 90% EtOAc in hexanes). The pure fractions were combined and the solvent was removed under reduced pressure to yield **2.7** as a yellow solid (690 mg, 34% yield). **Spectral data.** ^{1}H NMR (500 MHz, Chloroform-*d*) δ 9.82 (s, 1H), 7.50 (s, 1H), 7.08 (s, 1H), 5.84 (s, 1H), 2.56 (s, 3H), 1.87 (tt, *J* = 8.4, 5.0 Hz, 1H), 1.04 – 0.99 (m, 2H), 0.76 (dt, *J* = 6.6, 4.8 Hz, 2H); ^{13}C NMR (100 MHz, dmso) δ 167.81, 160.80, 148.28, 146.32, 101.48, 92.70, 25.69, 8.18, 7.13; HRMS-ESI (m/z): $[M + H]^+$ calcd for $C_{11}H_{12}ClN_5$ 250.0854; found 250.0853.

Synthesis of 2.8: This compound was prepared as previously reported.[22]

Synthesis of 2.9: 4-pentynoic acid (392.9 mg, 4.01 mmol) was added to an oven-dried flask. Anhydrous THF (2.70 mL) was then added to the flask followed by N-methylmorpholine (0.44 mL, 4.03 mmol). Isobutyl chloroformate (0.52 mL, 4.03 mmol) was then added dropwise and the reaction was stirred for 30 minutes. The reaction was then filtered and washed with THF. The filtrate was then added to a solution of **2.8** (481.6 mg, 2.59 mmol) in anhydrous THF (2.7 mmol), and the reaction was stirred for 2 hrs. Upon completion, the solvent was removed under reduced pressure. The resulting residue was brought up in EtOAc and washed one time each with sat. bicarb, 10% citrate, and brine. After drying over Na_2SO_4, the product was purified by silica gel chromatography using a Biotage Isolera One (linear gradient 30 → 80% EtOAc in hexanes). The pure fractions were combined and the solvent was removed under reduced pressure to yield **2.9**

as a white solid (690 mg, 97% yield). **Spectral data.** ^{1}H NMR (500 MHz, Chloroform-*d*) δ 3.60 (t, *J* = 5.4 Hz, 2H), 3.43 (d, *J* = 22.3 Hz, 6H), 2.60 – 2.53 (m, 4H), 1.98 (q, *J* = 2.5 Hz, 1H), 1.47 (s, 9H); ^{13}C NMR (126 MHz, cdcl$_3$) δ 188.00, 169.54, 83.30, 80.36, 68.87, 45.21, 41.51, 32.18, 28.36, 14.49; HRMS-ESI (m/z): $[M + H]^+$ calcd for $C_{14}H_{22}N_2O_3$ 267.1703; found 267.1705, $[M + Na]^+$ calcd for $C_{14}H_{22}N_2O_3$ 289.1523; found 289.1522.

Synthesis of 2.10: **2.9** (266.2 mg, 0.98 mmol) was added to an oven-dried flask. Anhydrous 1,4-dioxane (0.62 mL) was added followed by 4 N HCl in dioxane (2.30 mL, 9.2 mmol). The resulting solution was stirred for 1.5 hrs. The solvent was then removed under reduced pressure. The resulting residue was carried forward crude without purification assuming theoretical yield.

Synthesis of 2.1: **2.10** (199.5 mg, 0.98 mmol) was added to an oven-dried flask. DCM (10.0 mL) was added followed by TEA (0.15 mL, 1.08 mmol). The resulting mixture was stirred for 0.5 hrs and then washed once with 10% K_2CO_3. The solvent was then removed under reduced pressure. **2.7** was added to the flask containing the resulting residue and brought up in EtOH (3.0 mL). Concentrated HCl was added and the reaction was refluxed overnight. Upon completion, the EtOH was removed under reduced pressure. The resulting residue was brought up in EtOAc and washed 3 times each with bicarb and brine. After drying over Na_2SO_4, the product was purified by silica gel chromatography using a Biotage Isolera One (linear gradient 0 → 5% MeOH in EtOAc). The pure fractions were combined and the solvent was removed under reduced pressure to yield **2.1** as a white solid (100 mg, 54% yield). **Spectral data.** ^{1}H NMR (500 MHz, DMSO-d_6) δ 12.02 (s, 1H), 9.26 (s, 1H), 6.55 (s, 1H), 5.76 (s, 1H), 3.54 (s, 8H), 2.77 (t, *J* = 2.6 Hz, 1H), 2.59 (t, *J* = 7.4 Hz, 2H), 2.38 (td, *J* = 7.5, 7.0, 2.6 Hz, 2H), 2.28 (s, 3H), 1.88 – 1.80 (m, 1H), 0.89 (dt, *J* = 8.7, 3.2 Hz, 2H), 0.68 – 0.63 (m, 2H); ^{13}C NMR (100 MHz, dmso) δ 169.62, 165.13, 162.91, 92.01, 84.53, 81.54, 71.66, 44.53, 43.96, 43.68, 41.12, 31.75, 25.83, 14.28, 8.18, 7.29; HRMS-ESI (m/z): $[M + H]^+$ calcd for $C_{20}H_{25}N_7O$ 380.2193; found 380.2191.

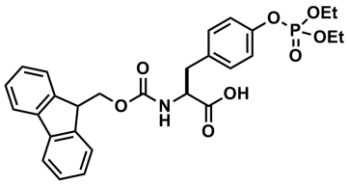

Synthesis of 2.11: This compound was prepared as previously reported.[26]

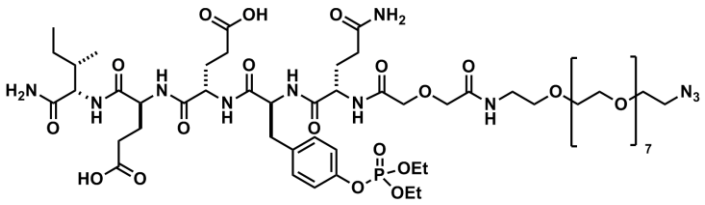

Synthesis of 2.2: Compound **2.2** was synthesized on 0.2 mmol scale on Rink Amide AM resin (0.47 mmol/g) using standard Fmoc solid-phase peptide synthesis. Couplings were performed using DIEA and HBTU in NMP and were allowed to proceed for 30 minutes at room temperature with the exception of **2.11**, which was coupled using PyBOP. Fmoc deprotections were performed using piperidine in NMP and were allowed to proceed for 15 min at room temperature. The completeness of each coupling and deprotection was monitored by the Kaiser test. After deprotection of the final amino acid in the sequence, the peptide was capped by coupling on N_3-PEG_7-CO_2H using PyBOP and DIEA in NMP. Cleavage of the peptide from the resin with concomitant removal of all side chain-protecting groups was accomplished with 2 mL of a 95% TFA, 2.5% H_2O, and 2.5% TIPS solution for 45 minutes twice. The TFA was mostly removed under reduced pressure. The product was precipitated in ether and carried forward crude without purification assuming theoretical yield.

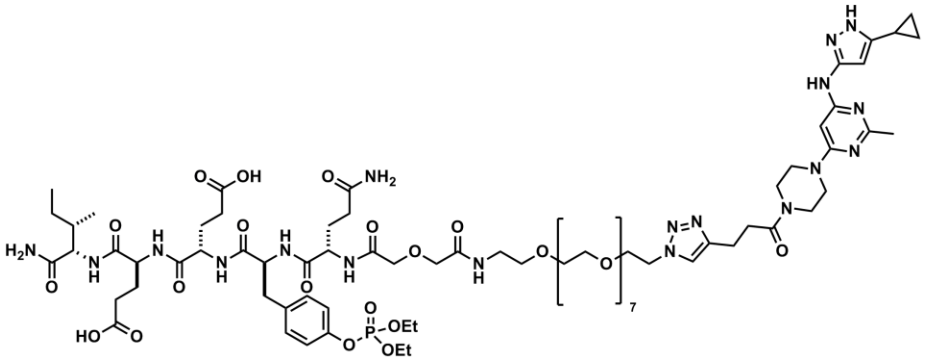

Synthesis of 2.12: **2.2** (135.2 mg, 0.1 mmol), CuI (19.1 mg, 0.1 mmol) and **2.1** (55.0 mg, 0.14 mmol) were added to an oven-dried flask. DMF (1.0 mL) was added followed by TEA (0.05 mL, 0.36 mmol). The reaction mixture was stirred at 60°C overnight. The reaction was purified by reverse-phase HPLC using a linear 5→95% acetonitrile + 0.1% TFA in water gradient. Lyophilization afforded **2.12** as a white solid (48.5 mg, 28% yield). **Spectral data.** MS-ESI (m/z): $[M + 2H]^+$ calcd for $C_{76}H_{119}N_{18}O_{26}P$, 866.42; found 866.59.

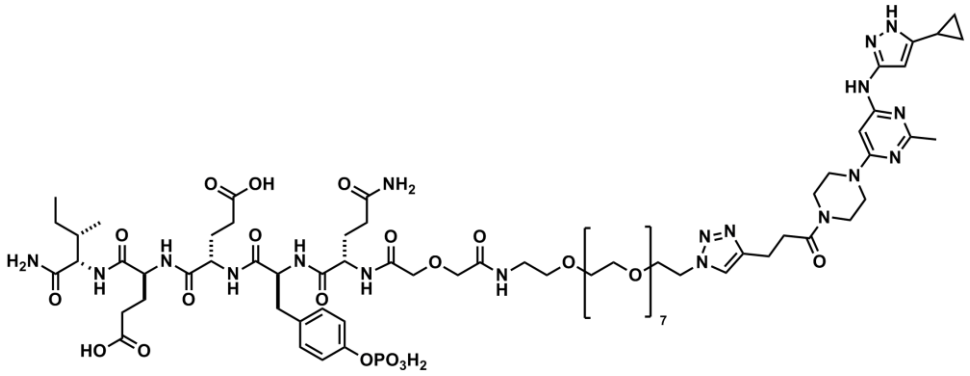

Synthesis of 2.3: **2.12** (48.5 mg, 0.028 mmol) was added to an oven-dried flask. DCM (0.5 mL) was then added followed by TMS-Br (0.5 mL) and the reaction mixture was stirred overnight. The solvent was then removed under reduced pressure. The reaction mixture was then suspended in water (0.5 mL) and stirred for 2 hrs. The reaction was purified by reverse-phase HPLC using a linear 5→95% acetonitrile + 0.1% TFA in water gradient. Lyophilization afforded **2.3** as a white powder (5.5 mg, 12% yield). **Spectral data.** HRMS-ESI (m/z): [M] calcd for $C_{72}H_{111}N_{18}O_{26}P$ 1674.7649; found after resolved isotope deconvolution 1674.7648.

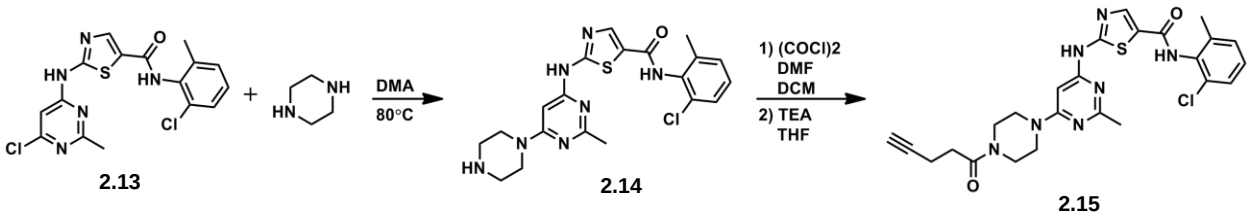

2.13 2.14 2.15

Scheme 2.4: Synthetic Scheme for Compound 2.15.

Synthesis of 2.13: This compound was prepared as previously reported.[41]

Synthesis of 2.14: 2.13 (76.1 mg, 0.19 mmol) was added to an oven-dried flask. Anhydrous DMA (0.38 mL) was added followed by piperazine (112.8 mg, 0.95 mmol). The resulting solution was stirred at 80°C for 2.5 hrs. After completion, the reaction was cooled to room temperature and water was added to precipitate the product. The resulting residue was filtered and carried forward crude without purification.

Synthesis of 2.15: $(COCl)_2$ (0.02 mL, 0.23 mmol) was added to a stirred solution of 4-pentynoic acid (15.1 mg, 0.075 mmol) in anhydrous DCM (0.23 mL). Catalytic DMF (1 drop) was added and the reaction was allowed to stir for 2 hrs. The solvent was then removed under reduced pressure. The resulting residue was then dissolved in anhydrous THF (0.5 mL). **2.14** (41.8 mg, 0.09 mmmol) and TEA (0.02 mL, 0.14 mmol) were added and the reaction was allowed to stir overnight. The solvent was then removed under reduced pressure. The resulting residue was brought up in EtOAc and washed with 10% citrate, sat. bicarb, and brine. After drying over Na_2SO_4, the product was purified by silica gel chromatography using a Biotage Isolera One (linear gradient 50 → 100% EtOAc in Hexanes). The peak fractions were combined and the solvent was removed under reduced pressure. The product was not pure and was further purified by reverse-phase HPLC using a linear 30→90% acetonitrile + 0.1% TFA in water gradient. Lyophilization afforded **2.15** as a white solid (3.2 mg, 8.1% yield). **Spectral Data.** ^{1}H NMR (500 MHz, DMSO-d_6) δ 11.53 (s, 1H), 9.89 (s, 1H), 8.22 (s, 1H), 7.40 (d, J = 7.7 Hz, 1H), 7.27 (dt, J = 15.4, 7.5 Hz, 2H), 6.06 (s, 1H), 3.56 (d, J = 6.5 Hz, 8H), 2.78 (t, J = 2.7 Hz, 1H), 2.59 (t, J = 7.4 Hz, 2H), 2.42 (s, 3H), 2.38 (td, J = 7.5, 7.1, 2.6 Hz, 2H), 2.23 (s, 3H); ^{13}C NMR (176 MHz, dmso) δ 169.58, 165.61, 162.94, 162.59, 160.36, 157.40, 141.24, 139.25, 133.94, 132.86,

129.46, 128.62, 127.44, 84.53, 83.21, 71.71, 44.48, 43.91, 43.66, 42.55, 31.82, 25.99, 18.74, 14.30; HRMS-ESI (m/z): $[M + H]^+$ calcd for $C_{25}H_{26}ClN_7O_2S$ 524.1630; found 524.1625.

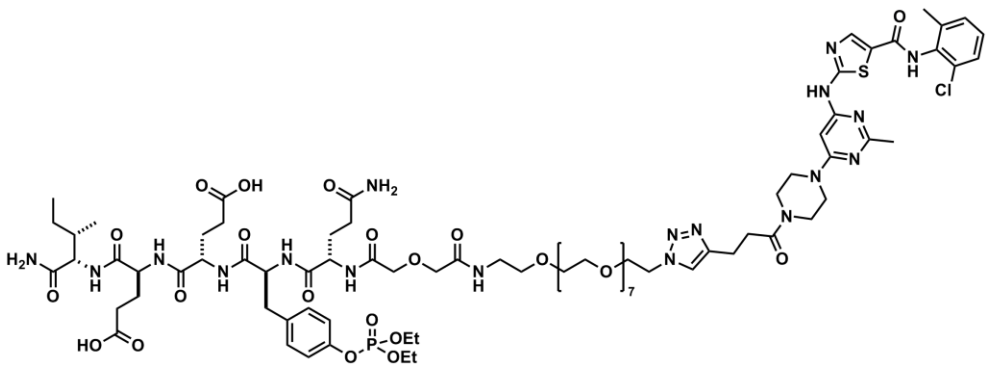

Synthesis of 2.16: **2.2** (20.3 mg, 0.015mmol), CuI (5.8 mg, 0.03 mmol) and **2.15** (6.3 mg, 0.012 mmol) were added to an oven-dried flask. DMF (0.24 mL) was added followed by TEA (0.01 mL, 0.07 mmol). The reaction mixture was stirred at 45°C overnight. The reaction was purified by reverse-phase HPLC using a linear 20→80% acetonitrile + 0.1% TFA in water gradient. Lyophilization afforded **2.16** as a white solid (4.0 mg, 18% yield). **Spectral data.** MS-ESI (m/z): $[M + 2H]^+$ calcd for $C_{81}H_{120}ClN_{18}O_{27}PS$, 938.39; found 938.08.

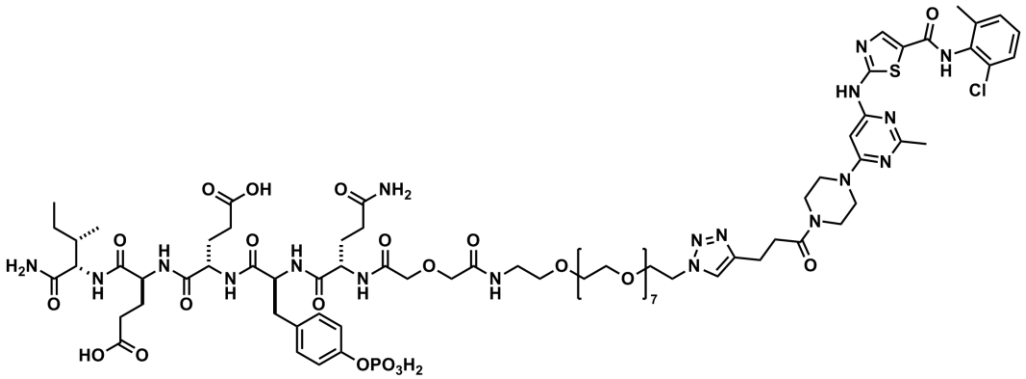

Synthesis of 2.4: **2.16** (4.0 mg, 0.002 mmol) was added to an oven-dried flask. ACN (0.5 mL) was then added followed by TMS-Br (0.5 mL) and reaction mixture was stirred overnight. Water (0.5 mL) was then added and the reaction was again stirred overnight. The solvent was then removed under reduced pressure. The reaction was purified by reverse-phase HPLC using a linear 20→80% acetonitrile + 0.1% TFA in water gradient. Lyophilization afforded **2.4** as a

white powder (0.5 mg, 14% yield). Spectral data. HRMS-ESI (m/z): [M] calcd for $C_{77}H_{112}ClN_{18}O_{27}PS$ 1818.7091; found after resolved isotope deconvolution 1818.7093.

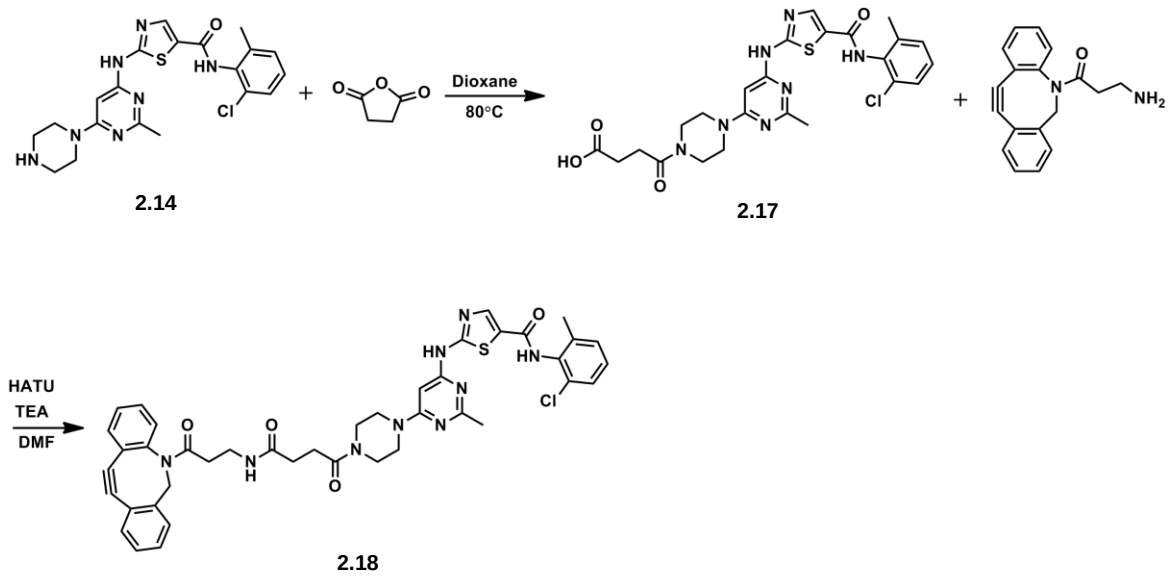

Scheme 2.5: Synthetic Scheme for Compound 2.18

Synthesis of 2.17: 2.14 (95.2 mg, 0.21 mmol) was added to an oven-dried flask. Dioxane (1.0 mL) was added followed by succinic anhydride (21.0 mg, 0.21 mmol). The resulting solution was stirred at 80°C overnight. After completion, the reaction was cooled to room temperature. The resulting residue was filtered to afford **2.17** as a tan solid (83.0 mg, 73% yield). **Spectral Data.** ^{1}H NMR (500 MHz, DMSO-*d6*) δ 11.95 (s, 1H), 11.53 (s, 1H), 9.89 (s, 1H), 8.23 (s, 1H), 7.40 (d, *J* = 7.6 Hz, 1H), 7.27 (dt, *J* = 15.3, 7.5 Hz, 2H), 6.06 (s, 1H). 3.56 (dd, *J* = 17.6, 11.5 Hz, 8H), 2.58 (t, *J* = 6.6 Hz, 2H), 2.45 (t, *J* = 6.7 Hz, 2H), 2.42 (s, 3H), 2.24 (s, 3H). ^{13}C NMR (100 MHz, dmso) δ 174.36, 170.24, 165.62, 162.93, 162.63, 160.32, 157.37, 141.25, 139.24, 133.93, 132.85, 129.45, 128.30, 127.43, 126.17, 83.17, 66.77, 44.39, 43.82, 43.62, 29.33, 27.92, 26.01, 18.73. MS-ESI (m/z): $[M + H]^+$ calcd for $C_{24}H_{26}ClN_7O_4S$ 544.1528; found 544.1522.

Synthesis of 2.18: 2.17 (49.0 mg, 0.09 mmmol) and HATU (45.5 mg, 0.12 mmol) were added to an oven-dried flask. DMF (0.92 mL) and TEA (0.04 mL, 0.28 mmol) were added and the reaction was allowed to stir for 10 min. After pre-activation of the acid, DBCO-amine (23.7 mg, 0.09 mmol) was added and the reaction was stirred overnight. After completion, the reaction was cooled to room temperature and water was added to precipitate the product. Filtration afforded

2.18 as a tan solid (59.5 mg, 81% yield). **Spectral Data.** ^{1}H NMR (700 MHz, DMSO-d_6) δ 11.50 (s, 1H), 9.87 (s, 1H), 8.22 (s, 1H), 7.67 (t, J=5.7 Hz, 1H), 7.61 (d, J=7.6 Hz, 1H), 7.60-7.55 (m, 1H), 7.49-7.46 (m, 1H), 7.45-7.41 (m, 1H), 7.37 (td, J=7.6, 1.6 Hz, 2H), 7.33 (t, J = 7.5 Hz, 1H), 7.29-7.25 (m, 2H), 7.23 (t, J = 7.7 Hz, 1H), 6.05 (s, 1H), 5.02 (d, J=14.0 Hz, 1H), 3.61 (d, J=14.0 Hz, 1H), 3.58-3.44 (m, 9H), 3.12-3.05 (m, 1H), 2.93 (ddt, J=14.0, 8.8, 5.7 Hz, 1H), 2.41 (s, 3H), 2.22 (s, 3H). ^{13}C NMR (176 MHz, dmso) δ 171.64, 170.54, 165.64, 162.97, 162.66, 160.36, 157.40, 151.87, 148.81, 141.27, 139.26, 133.96, 132.88, 130.00, 129.49, 129.41, 128.64, 128.60, 128.46, 128.16, 127.44, 127.24, 126.20, 125.64, 122.91, 121.86, 114.73, 108.53, 83.20, 55.28, 44.49, 43.88, 43.63, 42.67, 41.33, 35.49, 34.64, 30.68, 28.22, 26.02, 25.97, 18.76. MS-ESI (m/z): $[M + H]^+$ calcd for $C_{42}H_{40}ClN_9O_4S$ 802.2685; found 802.2682.

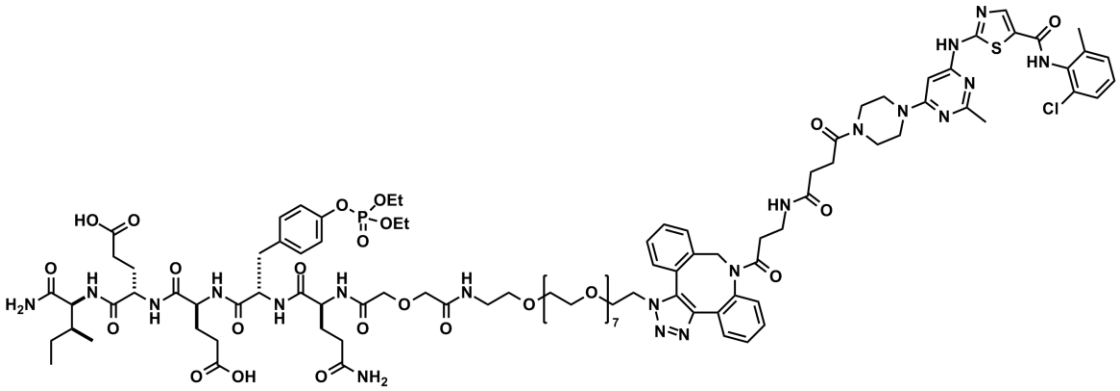

Synthesis of 2.19: **2.18** (59.5 mg, 0.074 mmol) was stirred in DMF (0.30 mL). **2.2** was dissolved in DMF to make a 0.125 M solution. **2.2** in DMF (0.60 mL, 0.075 mmol) was added to **2.18** in DMF. The reaction mixture was stirred overnight. The crude reaction was purified by reverse-phase HPLC using a linear 20→80% acetonitrile + 0.1% TFA in water gradient. Lyophilization afforded **2.19** as a white solid (3.7 mg, 2.3% yield). **Spectral data.** MS-ESI (m/z): $[M - H]^-$ calcd for $C_{98}H_{135}ClN_{20}O_{29}PS$, 2151.8700; found 2151.8681.

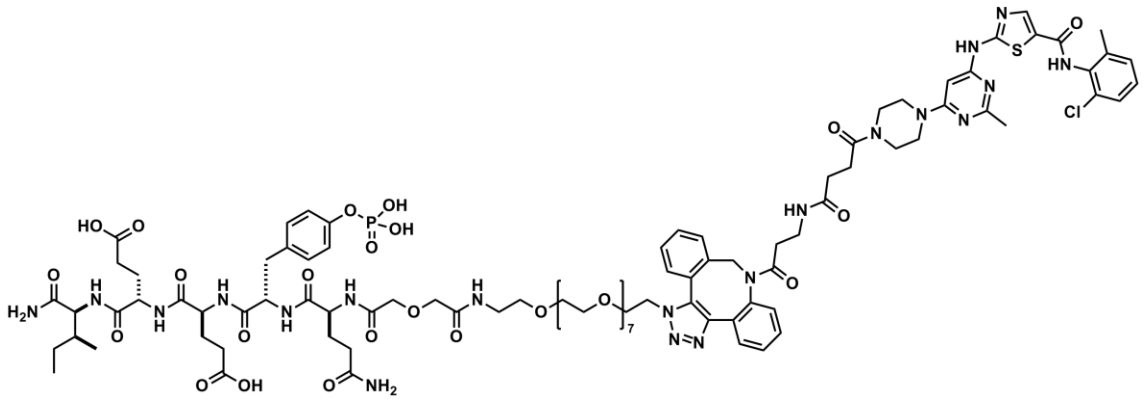

Synthesis of 2.5: **2.19** (3.7 mg, 0.0017 mmol) was added to an oven-dried flask. ACN (0.5 mL) was then added followed by TMS-Br (0.5 mL) and reaction mixture was stirred overnight. Water (0.5 mL) was then added and the reaction was again stirred for an hour. The solvent was then removed under reduced pressure. The reaction was purified by reverse-phase HPLC using a linear 20→80% acetonitrile + 0.1% TFA in water gradient. Lyophilization afforded **2.5** as a white powder (0.9 mg, 24% yield). **Spectral data.** HRMS-ESI (m/z): $[M - H]^-$ calcd for $C_{94}H_{126}ClN_{20}O_{29}PS$, 2095.8007; found 2095.8074.

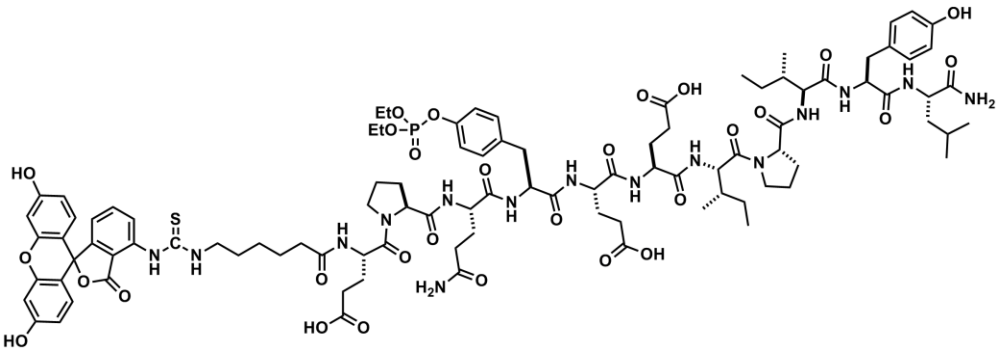

Synthesis of 2.20: Compound **2.20** was synthesized on 0.2 mmol scale on Rink Amide AM resin (0.47 mmol/g) using standard Fmoc solid-phase peptide synthesis. Couplings were performed using DIEA and HBTU in NMP and were allowed to proceed for 30 minutes at room temperature. Fmoc deprotections were performed using piperidine in NMP and were allowed to proceed for 15 min at room temperature. The completeness of each coupling and deprotection was monitored by the Kaiser test. After deprotection of the final amino acid in the sequence, the peptide was capped by coupling on FITC (4 mg, 0.010 mmol) using DIEA in DMF (1 mL). Cleavage of the peptide from the resin with concomitant removal of all side chain-protecting

groups was accomplished with 6 mL of a 95% TFA, 2.5% H_2O, and 2.5% TIPS solution for 45 minutes twice. The TFA was mostly removed under reduced pressure. The product was precipitated in ether and carried forward crude without purification assuming theoretical yield.

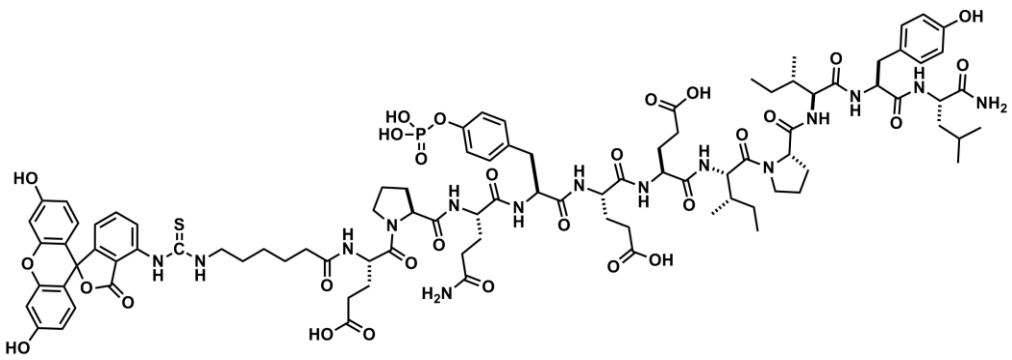

Synthesis of 2.21: **2.20** was added to an oven-dried flask. ACN (0.5 mL) was then added followed by TMS-Br (0.5 mL) and reaction mixture was stirred overnight. Water (0.5 mL) was then added and the reaction was again stirred for an hour. The solvent was then removed under reduced pressure. The reaction was purified by reverse-phase HPLC using a linear 5→80% acetonitrile + 0.1% TFA in water gradient. Lyophilization afforded **2.21** as a white powder (2.2 mg, 0.56% yield). **Spectral data.** HRMS-ESI (m/z): $[M - H]^-$ calcd for $C_{93}H_{120}N_{15}O_{29}PS$ 1972.7762; found 1972.7802.

Spectral Data for Compounds

Spectral data (^1H, ^{13}C NMR) for compounds are shown in **Appendix A**.

General Biochemical Methods

Black, opaque-bottom 96 well plates were purchased from Nunc. All proteins were expressed in *E.coli* using previously published procedures.[28] Data were obtained using Biotek Synergy Mx and Biotek Synergy 4 plate readers. Curve fitting was done using Graphpad Prism 6 software.

Determination of Inhibitor IC_{50} Values against Src Family Kinases.

A continuous fluorescence assay was used to determine IC_{50}.[27] The reaction volume was 100 μL consisting of 85 μL of enzyme in buffer, 2.5 μL of the appropriate inhibitor dilution (typically 10000, 3333.33, 1111.11, 370.37, 123.46, 41.15, 13.72, 4.57, 1.52, and 0 μM in DMSO), and 2.5 μL (1.8 mM in DMSO) of a substrate peptide ("compound 3" as described in Wang et al.)[27]. The reaction was initiated with 10 μL of ATP (1 mM in water), and reaction progress was immediately monitored at 405 nm (ex. 340 nm) for 10 minutes. Reactions had final concentrations of 30 nM enzyme, 45 μM peptide substrate, 100 μM ATP, 100 μM Na_3VO_4, 100 mM Tris buffer (pH 8), 10 mM $MgCl_2$, 0.01% Triton X-100 unless otherwise noted. The initial rate data collected was used for determination of IC_{50} values. For IC_{50} determination, the kinetic values were obtained directly from nonlinear regression of substrate-velocity curves in the presence of various concentrations of the inhibitor. The equation Y=Bottom + (Top-Bottom)/(1+10^((LogEC$_{50}$-X)*HillSlope)), X = log(concentration) and Y = binding; was used in the nonlinear regression unless otherwise noted. An IC_{50} value was determined for each inhibitor using at least three independent experiments. The individual IC_{50} values for the three runs were then averaged. A representative inhibition curve of a single run is shown in **Appendix A**.

Determination of inhibitor IC_{50} Values Against c-Abl.

A continuous fluorescence assay was used to determine IC_{50}.[27] The reaction volume was 100 μL consisting of 85 μL of enzyme in buffer, 2.5 μL of the appropriate inhibitor dilution (typically 10000, 3333.33, 1111.11, 370.37, 123.46, 41.15, 13.72, 4.57, 1.52, and 0 μM in DMSO), and 2.5 μL (2.4 mM in DMSO) of a substrate peptide.[31] The reaction was initiated with 10 μL of ATP (1 mM in water), and reaction progress was immediately monitored at 405 nm (ex. 340 nm) for 10 minutes. Reactions had final concentrations of 30 nM enzyme, 60 μM peptide substrate, 100 μM ATP, 100 μM Na_3VO_4, 100 mM Tris buffer (pH 8), 10 mM $MgCl_2$, 0.01% Triton X-100. The initial rate data collected was used for determination of IC_{50} values. For IC_{50} determination, the kinetic values were obtained directly from nonlinear regression of substrate-velocity curves in the presence of various concentrations of the inhibitor. The equation Y=Bottom + (Top-Bottom)/(1+10^((LogEC$_{50}$-X)*HillSlope)), X = log(concentration) and Y = binding; was used in the nonlinear regression. An IC_{50} value was determined for each inhibitor

using at least three independent experiments. The individual IC_{50} values for the three runs were then averaged. A representative inhibition curve of a single run is shown in **Appendix A**.

Determination of SH2 Peptide (2.21) K_d.

A fluorescence polarization assay was used to determine K_d of peptide **2.21**. The reaction volume was 50 μL consisting of 49 μL of enzyme dilutions in buffer (50 mM Tris buffer (pH 8), 10 mM NaCl, 5% Glycerol, 1 mM DTT) and 1.0 μL of **2.21** (10 mM in DMSO). The protein was plated to provide 2x dilutions. The peptide was then added and the plate was incubated on ice for 1 hr. After 1 hr, fluorescence polarization was monitored at 528 nm (ex. 485 nm). Reactions had final concentrations of 200 nM **2.21**. For K_d determination, the mPolarization values were plotted vs. varying protein concentrations. The equation Y=Bmax*X/(Kd + X), X = Protein concentration and Y = FP response; was used in the nonlinear regression. A single representative inhibition curve with error bars is shown in **Appendix A**.

References

(1) Knight, Z. A.; Shokat, K. M. Features of Selective Kinase Inhibitors. *Chem. Biol.* **2005**, *12* (6), 621–637.

(2) Zhang, J.; Yang, P. L.; Gray, N. S. Targeting Cancer with Small Molecule Kinase Inhibitors. *Nat. Rev. Cancer* **2009**, *9* (1), 28–39.

(3) Brandvold, K. R.; Steffey, M. E.; Fox, C. C.; Soellner, M. B. Development of a Highly Selective c-Src Kinase Inhibitor. *ACS Chem. Biol.* **2012**, *7* (8), 1393–1398.

(4) Manning, G.; Whyte, D. B.; Martinez, R.; Hunter, T.; Sudarsanam, S. The Protein Kinase Complement of the Human Genome. *Science.* **2002**, *298* (5600), 1912–1934.

(5) Anastassiadis, T.; Deacon, S. W.; Devarajan, K.; Ma, H.; Peterson, J. R. Comprehensive Assay of Kinase Catalytic Activity Reveals Features of Kinase Inhibitor Selectivity. *Nat. Biotechnol.* **2011**, *29* (11), 1039–1045.

(6) Fabian, M. A.; Biggs, W. H.; Treiber, D. K.; Atteridge, C. E.; Azimioara, M. D.; Benedetti, M. G.; Carter, T. A.; Ciceri, P.; Edeen, P. T.; Floyd, M.; Ford, J. M.; Galvin, M.; Gerlach, J. L.; Grotzfeld, R. M.; Herrgard, S.; Insko, D. E.; Insko, M. A.; Lai, A. G.; Lélias, J.-M.; Mehta, S. A.; Milanov, Z. V; Velasco, A. M.; Wodicka, L. M.; Patel, H. K.; Zarrinkar, P. P.; Lockhart, D. J. A Small Molecule-Kinase Interaction Map for Clinical Kinase Inhibitors. *Nat. Biotechnol.* **2005**, *23* (3), 329–336.

(7) Breen, M. E.; Steffey, M. E.; Lachacz, E. J.; Kwarcinski, F. E.; Fox, C. C.; Soellner, M. B. Substrate Activity Screening with Kinases: Discovery of Small-Molecule Substrate-Competitive c-Src Inhibitors. *Angew. Chem. Int. Ed.* **2014**, *53* (27), 7010–7013.

(8) Cox, K. J.; Shomin, C. D.; Ghosh, I. Tinkering Outside the Kinase ATP Box: Allosteric (Type IV) and Bivalent (Type V) Inhibitors of Protein Kinases. *Futur. Med. Chem.* **2011**, *3* (1), 29–43.

(9) Lamba, V.; Ghosh, I. New Directions in Targeting Protein Kinases: Focusing upon True

Allosteric and Bivalent Inhibitors. *Curr. Pharm. Des.* **2012**, *18* (20), 2936–2945.
(10) Brandvold, K. R.; Santos, S. M.; Breen, M. E.; Lachacz, E. J.; Steffey, M. E.; Soellner, M. B. Exquisitely Specific Bisubstrate Inhibitors of c-Src Kinase. *ACS Chem. Biol.* **2015**, *10*, 1387–1391.
(11) Kolb, H. C.; Finn, M. G.; Sharpless, K. B. Click Chemistry: Diverse Chemical Function from a Few Good Reactions. *Angew. Chem. Int. Ed.* **2001**, *40* (11), 2004–2021.
(12) Agard, N. J.; Prescher, J. A.; Bertozzi, C. R. A Strain-Promoted [3 + 2] Azide−Alkyne Cycloaddition for Covalent Modification of Biomolecules in Living Systems. *J. Am. Chem. Soc.* **2004**, *126* (46), 15046–15047.
(13) Gower, C. M.; Thomas, J. R.; Harrington, E.; Murphy, J.; Chang, M. E. K.; Cornella-Taracido, I.; Jain, R. K.; Schirle, M.; Maly, D. J. Conversion of a Single Polypharmacological Agent into Selective Bivalent Inhibitors of Intracellular Kinase Activity. *ACS Chem. Biol.* **2016**, *11* (1), 121–131.
(14) Hah, J.-M.; Sharma, V.; Li, H.; Lawrence, D. S. Acquisition of a "Group A"-Selective Src Kinase Inhibitor via a Global Targeting Strategy. *J. Am. Chem. Soc.* **2006**, *128* (18), 5996–5997.
(15) Profit, A.; Lee, T.; Lawrence, D. Bivalent Inhibitors of Protein Tyrosine Kinases. *J. Am. Chem. Soc.* **1999**, *121* (2), 280–283.
(16) Hill, Z. B.; Perera, B. G. K.; Maly, D. J. A Chemical Genetic Method for Generating Bivalent Inhibitors of Protein Kinases. *J. Am. Chem. Soc.* **2009**, *131* (19), 6686–6688.
(17) Wenqing, X.; Harrison, S.; Eck, M. Three-Dimensional Structure of the Tyrosine Kinase c-Src. *Nature* **1997**, *385*, 595–602.
(18) Cowan-Jacob, S. W.; Fendrich, G.; Manley, P. W.; Jahnke, W.; Fabbro, D.; Liebetanz, J.; Meyer, T. The Crystal Structure of a c-Src Complex in an Active Conformation Suggests Possible Steps in c-Src Activation. *Structure* **2005**, *13* (6), 861–871.
(19) Yeatman, T. J. A Renaissance for SRC. *Nat. Rev. Cancer* **2004**, *4* (6), 470–480.
(20) Bernadó, P.; Pérez, Y.; Svergun, D. I.; Pons, M. Structural Characterization of the Active and Inactive States of Src Kinase in Solution by Small-Angle X-Ray Scattering. *J. Mol. Biol.* **2008**, *376* (2), 492–505.
(21) Jung, F. H.; Morgentin, R. R.; Ple, P. Quinoline Derivatives as Platelet-Derived Growth Factor Inhibitors, Their Preparation, Pharmaceutical Compositions, and Use in the Treatment of Cancer. *PCT Int. Appl.* **2007**, No. WO 2007099323, 1–154.
(22) Moussa, I. A.; Banister, S. D.; Beinat, C.; Giboureau, N.; Reynolds, A. J.; Kassiou, M. Design, Synthesis, and Structure-Affinity Relationships of Regioisomeric N-Benzyl Alkyl Ether Piperazine Derivatives as σ-1 Receptor Ligands. *J. Med. Chem.* **2010**, *53*, 6228–6239.
(23) Statsuk, A. V; Maly, D. J.; Seeliger, M. A.; Fabian, M. A.; Biggs, W. H.; Lockhart, D. J.; Zarrinkar, P. P.; Kuriyan, J.; Shokat, K. M. Tuning a Three-Component Reaction for Trapping Kinase Substrate Complexes. *J. Am. Chem. Soc.* **2008**, *130* (51), 17568–17574.
(24) Kwarcinski, F. E.; Fox, C. C.; Steffey, M. E.; Soellner, M. B. Irreversible Inhibitors of c-Src Kinase That Target a Nonconserved Cysteine. *ACS Chem. Biol.* **2012**, *7* (11), 1910–1917.
(25) Zhou, S.; Shoelson, S.; Chaudhuri, M.; Gish, G.; Pawson, T.; Haser, W.; King, F.; Roberts, T.; Ratnofsky, S.; Lechleider, R.; Neel, B.; Birge, R.; Fajardo, J.; Chou, M.; Hanafusa, H.; Schaffhausen, B.; Cantley, L. SH2 Domains Recognize Specific Phosphopeptide Sequences. *Cell* **1993**, *72* (5), 767–778.

(26) Wang, H.; Yang, C.; Wang, L.; Kong, D.; Zhang, Y.; Yang, Z. Self-Assembled Nanospheres as a Novel Delivery System for Taxol: A Molecular Hydrogel with Nanosphere Morphology. *Chem. Commun.* **2011**, *47*, 4439–4441.
(27) Wang, Q.; Cahill, S. M.; Blumenstein, M.; Lawrence, D. S. Self-Reporting Fluorescent Substrates of Protein Tyrosine Kinases. *J. Am. Chem. Soc.* **2006**, *128* (6), 1808–1809.
(28) Seeliger, M. A.; Young, M.; Henderson, M. N.; Pellicena, P.; King, D. S.; Falick, A. M.; Kuriyan, J. High Yield Bacterial Expression of Active c-Abl and c-Src Tyrosine Kinases. *Protein Sci.* **2005**, *14*, 3135–3139.
(29) Cooper, J. A.; Howell, B. The When and How of Src Regulation. *Cell* **1993**, *73* (6), 1051–1054.
(30) Ayrapetov, M. K.; Wang, Y.-H.; Lin, X.; Gu, X.; Parang, K.; Sun, G. Conformational Basis for SH2-Tyr(P)527 Binding in Src Inactivation. *J. Biol. Chem.* **2006**, *281* (33), 23776–23784.
(31) Rabuck, J. N.; Hyung, S.-J.; Ko, K. S.; Fox, C. C.; Soellner, M. B.; Ruotolo, B. T. Activation State-Selective Kinase Inhibitor Assay Based on Ion Mobility-Mass Spectrometry. *Anal. Chem.* **2013**, *85* (15), 6995–7002.
(32) Nagar, B.; Hantschel, O.; Young, M. A.; Scheffzek, K.; Veach, D.; Bornmann, W.; Clarkson, B.; Superti-Furga, G.; Kuriyan, J. Structural Basis for the Autoinhibition of c-Abl Tyrosine Kinase. *Cell* **2003**, *112* (6), 859–871.
(33) Boggon, T. J.; Eck, M. J. Structure and Regulation of Src Family Kinases. *Oncogene* **2004**, *23* (48), 7918–7927.
(34) Liu, B. A.; Jablonowski, K.; Shah, E. E.; Engelmann, B. W.; Jones, R. B.; Nash, P. D. SH2 Domains Recognize Contextual Peptide Sequence Information to Determine Selectivity. *Mol. Cell. Proteomics* **2010**, *9*, 2391–2404.
(35) Krishnamurty, R.; Brigham, J. L.; Leonard, S. E.; Ranjitkar, P.; Larson, E. T.; Dale, E. J.; Merritt, E. A.; Maly, D. J. Active Site Profiling Reveals Coupling between Domains in SRC-Family Kinases. *Nat. Chem. Biol.* **2013**, *9* (1), 43–50.
(36) Porter, M.; Schindler, T.; Kuriyan, J.; Miller, W. T. Reciprocal Regulation of Hck Activity by Phosphorylation of Tyr527 and Tyr416. *J. Biol. Chem.* **2000**, *275* (4), 2721–2726.
(37) Register, A. C.; Leonard, S. E.; Maly, D. J. SH2-Catalytic Domain Linker Heterogeneity Influences Allosteric Coupling across the SFK Family. *Biochemistry* **2014**, *53* (44), 6910–6923.
(38) Azam, M.; Seeliger, M. A.; Gray, N. S.; Kuriyan, J.; Daley, G. Q. Activation of Tyrosine Kinases by Mutation of the Gatekeeper Threonine. *Nat. Struct. Mol. Biol.* **2008**, *15* (10), 1109–1118.
(39) Apsel, B.; Blair, J. A.; Gonzalez, B.; Nazif, T. M.; Feldman, M. E.; Aizenstein, B.; Hoffman, R.; Williams, R. L.; Shokat, K. M.; Knight, Z. A. Targeted Polypharmacology: Discovery of Dual Inhibitors of Tyrosine and Phosphoinositide Kinases. *Nat. Chem. Biol.* **2008**, *4* (11), 691–699.
(40) Getlik, M.; Grütter, C.; Simard, J. R.; Klüter, S.; Rabiller, M.; Rode, H. B.; Robubi, A.; Rauh, D. Hybrid Compound Design To Overcome the Gatekeeper T338M Mutation in cSrc. *J. Med. Chem.* **2009**, *52* (13), 3915–3926.
(41) Chen, B.-C.; Droghini, R.; Lajeunesse, J.; Dimarco, J. D.; Galella, M.; Chidamdaram, R. Process for Preparing 2-Aminothiazole-5-Aromatic Carboxamides as Kinase Inhibitors. WO 2005/077945 A2, 2005.
(42) Jester, B. W.; Cox, K. J.; Gaj, A.; Shomin, C. D.; Porter, J. R.; Ghosh, I. A Coiled-Coil

Enabled Split-Luciferase Three-Hybrid System: Applied Toward Profiling Inhibitors of Protein Kinases. *J. Am. Chem. Soc.* **2010**, *132* (33), 11727–11735.
(43) Jester, B. W.; Gaj, A.; Shomin, C. D.; Cox, K. J.; Ghosh, I. Testing the Promiscuity of Commercial Kinase Inhibitors Against the AGC Kinase Group Using a Split-Luciferase Screen. *J. Med. Chem.* **2012**, *55* (4), 1526–1537.
(44) Jewett, J. C.; Bertozzi, C. R. Cu-Free Click Cycloaddition Reactions in Chemical Biology. *Chem. Soc. Rev.* **2010**, *39* (4), 1272–1279.
(45) Liu, B. A.; Shah, E.; Jablonowski, K.; Stergachis, A.; Engelmann, B.; Nash, P. D. The SH2 Domain–Containing Proteins in 21 Species Establish the Provenance and Scope of Phosphotyrosine Signaling in Eukaryotes. *Sci. Signal.* **2011**, *4* (202), ra83-ra83.

CHAPTER III

An Allosteric Modulator of c-Src Tyrosine Kinase that Alters Global Conformation

Abstract

We have identified a small molecule activator of the tyrosine kinase c-Src. It was identified *via* a screen of 1,000 Maybridge compounds. Importantly, this screen was carried out against three domain c-Src in order to identify compounds that could alter the global conformation of the kinase. After the initial screen, we used a protease accessibility assay to evaluate how the hits from the screen affected c-Src global conformation. Two of the hits were determined to cause an open conformation in c-Src. In turn, one of the inhibitors capable of opening c-Src also activated the enzyme. Furthermore, this activator was selective and improved the potency in HT-29 cells of another kinase inhibitor known to stabilize the open conformation in c-Src.

Introduction

Kinases play a crucial regulatory role in a variety of cell processes. Dysregulation of these important enzymes can lead to a variety of disease states.[1,2] ATP-competitive kinase inhibitors have been highly successful in treating a variety of cancers and a few other diseases.[3] One downfall of most kinase inhibitors, however, is that they almost all bind in the conserved ATP-binding pocket, and are, as a result, often promiscuous.[4,5] In order to truly understand the role a kinase plays *incellulo*, it is important to have selective inhibitors. In **Chapter II**, we detailed the development of a selective bivalent inhibitor of the protein tyrosine kinase c-Src as an attempt to target other sites besides the ATP-binding pockets. Another method to study kinases outside the ATP-binding pocket is through the use of allosteric modulators. There are many allosteric kinase inhibitors; however, until very recently, c-Src did not have a known allosteric inhibitor.[6,7] Furthermore, as we demonstrate in **Chapter II**, inhibitors can be used to explore the global conformation of kinases.

c-Src is a cytosolic protein tyrosine kinase containing the catalytic kinase domain as well as two regulatory domains, SH2 and SH3.[8] The conformation that these three domains adopt in relationship to each other can be referred to as the global conformation. As mentioned in **Chapter II**, c-Src can adopt two known global conformations, open and closed (**Figure 1.1**).[9,10] The phosphorylation state of c-Src is highly connected to global conformation. The autophosphorylation site Tyr416 is important for full activity of c-Src,[11] and the phosphorylation site Tyr527 is responsible for binding the SH2, which closes the kinase.[9] It has been shown that ATP-competitive inhibitors have the ability to modulate the global conformation of protein tyrosine kinases, despite the fact that they bind in the kinase domain.[12] We wanted to identify an inhibitor capable of modulating the global conformation of c-Src *via* binding in an allosteric pocket.

Hit Identification and Assessment of Global Conformation

We tested a library of 1,000 compounds from Maybridge for compounds that would bind three domain c-Src.[a] Using three domain c-Src was crucial as opposed to screens that use only the kinase domain,[5,13] since we desired a compound that would affect global conformation. We used a thermal shift assay to determine compound binding to c-Src. The library consisted of 13 plates, each of which was analyzed separately, with its own set of controls. The positive control was dasatinib and the negative control was 1% DMSO vehicle. A hit was defined as a compound with a Tm that was greater than 3 standard deviations from the negative control. An example of the hits from one plate is shown in **Figure 3.1**. All of the other plates were plotted and analyzed in the same fashion (**Appendix B**). Using our 3 standard deviation cutoff, the screen yielded 37 hits. Structures for the 37 hits are shown in **Table B1**.

[a] Michael P. Agius made several direct contributions to the work in this chapter including: helping to run the screen, establishing the protease accessibility assay, and determining the half-lives of 3 hits using 5 time-point curves.

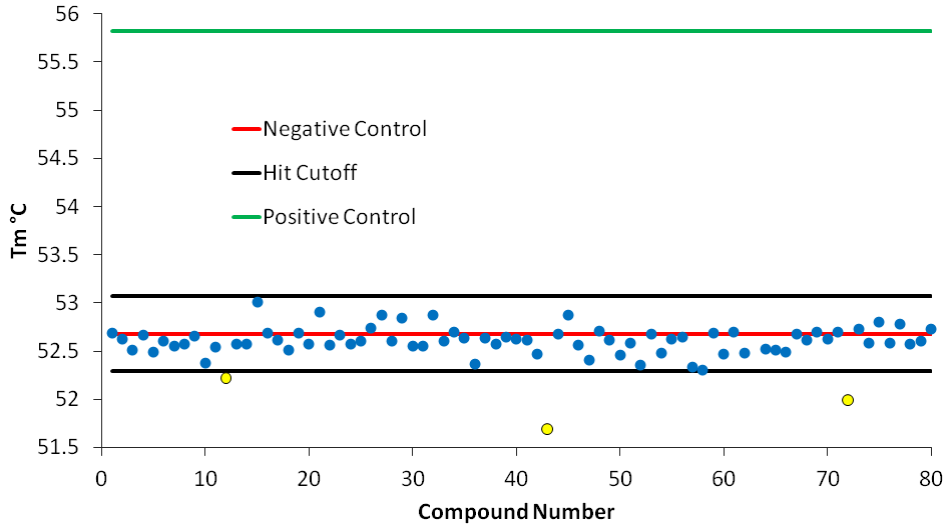

Figure 3.1. Tm for Plate 1 Compounds. Every compound is shown in blue with hits highlighted in yellow. The Tm for the negative control is shown in red, the Tm for the positive control is shown in green, and the 3 standard deviation cutoff for hits is shown in black.

After identification of 37 hits that bound c-Src, we assessed the effect that the hits had on the global conformation of c-Src. We used a protease accessibility assay developed in our lab. It is simple, low cost, and medium throughput. It is based on the accessibility of the linker between the kinase and SH2 domains. The protease thermolysin is known to cleave c-Src at a site on the linker.[14] Cleavage of the kinase over time by thermolysin can be evaluated by measuring the intensity of the full-length protein *via* SDS. The band intensity can then be plotted vs. time to obtain a half-life curve. A construct that is more open will have a more exposed linker, be proteolyzed more quickly by thermolysin, and thus have a shorter half-life (**Figure 3.2**). We used established constructs to validate that thermolysin half-life corresponded to known "openness" of the construct.

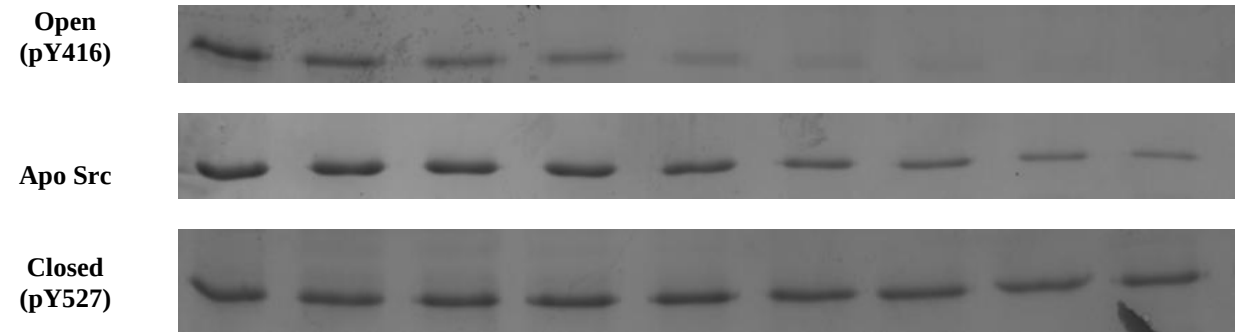

a

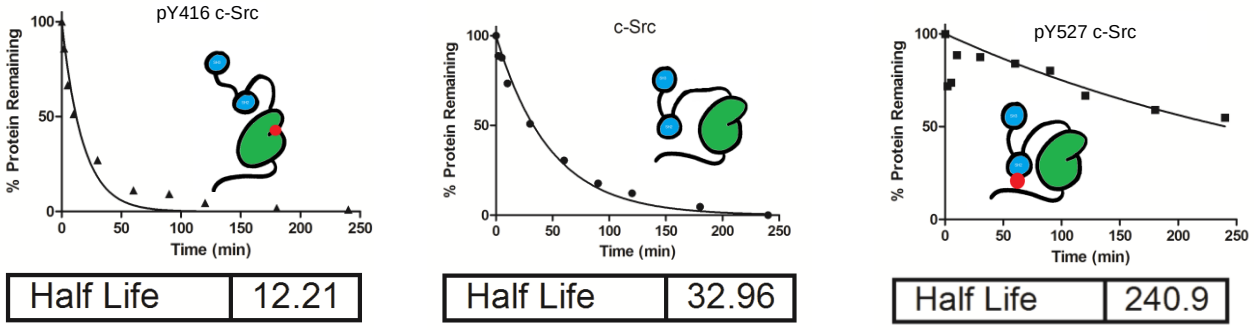

b

Figure 3.2. Controls for thermolysin proteolysis accessibility assay. **a**)The gel showing the disappearance of the protein band for the open, WT, and closed controls for c-Src along with (**b**) the corresponding half live curves and illustrations of the constructs.

For the controls in Figure **3.2**, we assessed the presence of protein at 10 different time points. In order to evaluate our 37 hits more quickly, we assessed the hits using 5 time points. Of the 37 initial hits, 9 compounds were different from apo Src by a standard deviation. These were re-evaluated using the full 10 time point curves previously established. The half-life curves are shown in **Appendix B**. When re-evaluated, we decided to only pursue the two most open hits. The structures are shown below with their half-life curves.

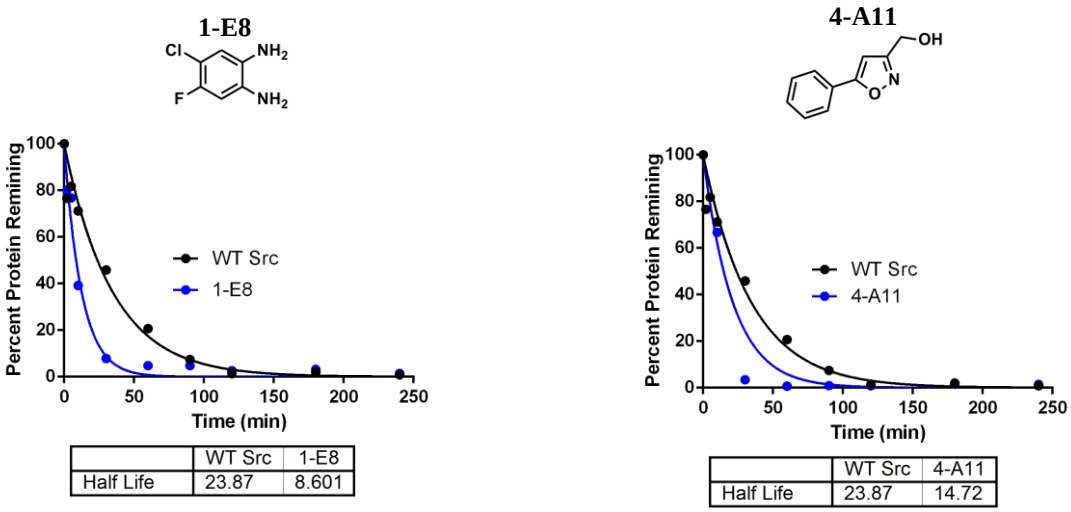

	WT Src	1-E8
Half Life	23.87	8.601

	WT Src	4-A11
Half Life	23.87	14.72

Figure 3.3. Hits capable of altering the global conformation of three domain c-Src. Compounds **1-E8** and **4-A11** that both adopt an open conformation compared to apo c-Src are shown with their half-life curves.

Activity of 1-E8 in 3D Src

Once we had established **1-E8** and **4-A11** as hits capable of stabilizing an open conformation in c-Src, we tested them against three domain c-Src using a continuous activity assay.[15] We did not observe any effect for 4-A11; however, gratifyingly, **1-E8** activated c-Src with EC_{50} = 90 μM. These data confirmed our hypothesis that a compound capable of stabilizing an open conformation in c-Src would activate the kinase. Furthermore, **1-E8** did not seem to be ATP-competitive as a change in the concentration of ATP had no effect upon the EC_{50} (**Appendix B**).

We also looked at the effect of different phosphorylation-states of c-Src. As mentioned earlier, the autoregulation of c-Src is known to be controlled by the phosphorylation-states of c-Src. c-Src is down regulated when Tyr527 is phosphorylated and up-regulated when Tyr416 is phosphorylated.[9,10] We saw that **1-E8** had no effect upon pY527 and it had a very small inhibitory effect upon pY416 (IC_{50} = 930 μM). These data suggest several things about activator **1-E8**. First, knowing that pY419 is open and active, it is reasonable to expect that **1-E8** would not be able to activate the kinase further, exhibiting very little effect. Furthermore, its inability to activate pY527 suggests that **1-E8** may bind somewhere at the interface between the kinase domain and SH2/SH3 domains. The fact that **1-E8** cannot bind the closed conformation of c-Src indicates a binding site inaccessible when the kinase is closed but accessible in the apo kinase.

Identification of Possible Binding Site

Focal adhesion kinase (FAK) is known to be a substrate of c-Src, and is known to activate c-Src.[16] The linker between the FERM domain and kinase domain of FAK contains a binding site for the SH3 domain of c-Src as well as a phosphotyrosine binding site for the SH2 domain of c-Src (Tyr397).[7,17] Once we knew that that **1-E8** cannot bind when c-Src adopts a closed conformation, we hypothesized that it would bind in the same location on c-Src as a pFAK peptide.[7] We again determined the EC_{50} of **1-E8** with a competitive, constant concentration of the pFAK peptide. As shown in Figure **3.4b**, the addition of pFAK peptide eliminates the activator activity of **1-E8**. This suggested to us the possibility that **1-E8** does in fact bind somewhere at the interface between the kinase domain and SH2/SH3 domains. To further establish the binding site of **1-E8**, we determined the EC_{50} of c-Src SH2 peptide **2.21**, with and without a constant concentration of **1-E8**. Without **1-E8**, we determined the EC_{50} of **2.21** to be 100 nM, while it was 1000 nM in the presence of 100 μM **1-E8** (**Appendix B**). This suggests that **1-E8** binds within the SH2 domain, which is consistent with the observation that it cannot bind pY527 c-Src.

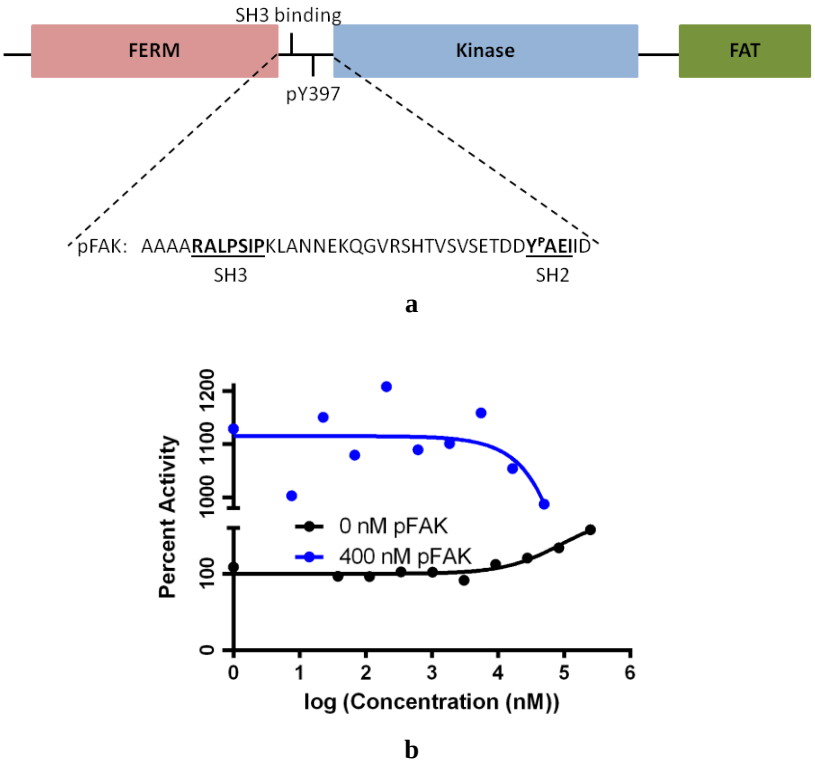

Figure 3.4. FAK and **1-E8** Competition. **a**) Structure of FAK with pFAK Src binding peptide highlighted (**b**) EC_{50} curves for **1-E8** with and without competing pFAK peptide

Selectivity and *In cellulo* Effect

We used two homologous kinases, c-Abl and Hck, to evaluate the selectivity of **1-E8**. As mentioned earlier, selectivity is an important feature for using kinase inhibitors in a cellular environment. As stated in **Chapter II**, both c-Abl and Hck contain SH2 domains that bind phosphotyrosine. Given its small size and the fact that it competes with **2.21**, we hypothesized that **1-E8** would bind in the phosphotyrosine-binding pocket within the SH2 domain of c-Src, and similarly, c-Abl and Hck. We found, however, that **1-E8** had no effect upon c-Abl (**Appendix B**) and a very minimal *inhibitory* effect upon Hck (IC_{50} = 550 ± 100 μM). This suggests that **1-E8** competes with **2.21** binding to the SH2 domain of c-Src through some mechanism other than the phosphotyrosine-binding pocket. Additionally, it further elaborates upon the findings in **Chapter II** that c-Src and Hck have differences in their global conformations. Upon finding that **1-E8** is selective for c-Src over homologous kinases, we wanted to test it in a c-Src dependent cell line.

In HT-29 cells (a c-Src dependent colon cancer cell line)[18], **1-E8** has no observable effect (GI_{50} > 10 μM, **Appendix B**). We proposed, however, they **1-E8** might be able to act cooperatively in cells with other inhibitors. We have shown that Das-DFGO-II[19] developed by our lab as part of a matched inhibitor set causes an open conformation in kinases (**Chapter V**). We determined the GI_{50} of Das-DFGO-II in HT-29 cells and also determined its GI_{50} with the addition of 10 μM **1-E8**. We observed a decrease in the GI_{50} of Das-DFGO-II by three fold from 157 nM to 52 nM with the addition of **1-E8**. What is striking about these data is the fact that at 10 μM **1-E8** has no effect on HT-29 cells. This lends further credence to the ability of **1-E8** to affect the global conformation of c-Src. It seems likely that **1-E8** was able to open and activate c-Src in a way that allowed an inhibitor also known to bind to an open conformation (Das-DGFO-II) to bind better and inhibit the growth of c-Src dependent cells better.

Conclusions

Using a medium throughput screen, we identified a small molecule allosteric activator or the tyrosine kinase c-Src. We screened a 1,000 compound Maybridge against full-length c-Src using Thermofluor. We identified 37 hits that changed the Tm by greater than 3 standard deviations from the negative control. These hits were then analyzed using a protease accessibility assay to determine their effect on the global conformation of full-length c-Src. From the 37 hits,

two were seen to cause an open conformation in c-Src. Only one of them had an effect upon the activity of c-Src. This hit (**1-E8**) activated c-Src with a double-digit micromolar EC_{50}. This was an excellent conformation of results from the protease assay. One would predict that a small molecule that caused the kinase to adopt an open conformation would also activate the kinase. Furthermore, **1-E8** was specific to c-Src, against homologous kinases, in its ability to activate the enzyme. Additionally, it interferes with binding both of a pFAK peptide and a SH2 binding peptide (**2.21**) suggesting a possible binding site. Most exciting was the ability to correlate the global conformation that a small molecule could induce in a kinase with its effect upon kinase activity.

Materials and Methods

General Biochemical Methods

Black, opaque-bottom 96 well plates were purchased from Nunc. Black, 384 well plates for Thermofluor were purchased from Thermoscientific. All proteins were expressed in *E.coli* using previously published procedures.[20] Data were obtained using Biotek Synergy Mx and Biotek Synergy 4 plate readers. Curve fitting was done using Graphpad Prism 6 software.

Determination of Tm for Maybridge Library Against Full-Length c-Src.

A thermal shift assay was used to determine compound Tm. The reaction volume was 5 μL consisting of 4 μL of enzyme/1-anilino-8-naphthalenesulfonate (ANS) mix in buffer plus 1 μL of inhibitor dilution. Stock compound plates of 10 mM compound in 100% DMSO were diluted 1:20 in buffer before being added to the reaction mix. 1.5 μL of silicon oil was added to the top of every well to prevent evaporation and the plate was centrifuged at 1000xg for 1 min. All compounds were tested in quadruplicate in a 384 well plate. Reactions had final concentrations of 0.2 mg/mL enzyme, 0.2 mM ANS, 50 mM Tris buffer (pH 8), 100 mM NaCl, 5% glycerol, and 1 mM DTT unless otherwise noted. Using a Thermofluor instrument (Johnson & Johnson Pharmaceutical Research and Development, L.L.C), plates were heated from 25-80°C with 1 min at each degree with a shutter closed image taken every degree. Tm values were determined using Thermofluor++ ver 1.3.7 software, which plotted fluorescence intensity vs. °C. Hits were defined as compounds that had a Tm that was greater than 3 standard deviations from

the DMSO negative control. Tm values for every plate along with negative and positive controls are shown in **Appendix B**.

Determination of Inhibitor IC_{50} Values against Src Family Kinases.

A continuous fluorescence assay was used to determine IC_{50}.[15] The reaction volume was 100 μL consisting of 85 μL of enzyme in buffer, 2.5 μL of the appropriate inhibitor dilution (typically 10000, 3333.33, 1111.11, 370.37, 123.46, 41.15, 13.72, 4.57, 1.52, and 0 μM in DMSO), and 2.5 μL (1.8 mM in DMSO) of a substrate peptide ("compound 3" as described in Wang et al.).[15] The reaction was initiated with 10 μL of ATP (1 mM in water), and reaction progress was immediately monitored at 405 nm (ex. 340 nm) for 10 minutes. Reactions had final concentrations of 30 nM enzyme, 45 μM peptide substrate, 100 μM ATP, 100 μM Na_3VO_4, 100 mM Tris buffer (pH 8), 10 mM $MgCl_2$, 0.01% Triton X-100 unless otherwise noted. The initial rate data collected was used for determination of IC_{50} values. For IC_{50} determination, the kinetic values were obtained directly from nonlinear regression of substrate-velocity curves in the presence of various concentrations of the inhibitor. The equation Y = Bottom + (Top - Bottom)/(1 + $10^{(X-LogIC50)}$), X = log(concentration) and Y = binding; was used in the nonlinear regression unless otherwise noted. An IC_{50} value was determined for each inhibitor using at least three independent experiments. The individual IC_{50} values for the three runs were then averaged. A representative inhibition curve of a single run is shown in **Appendix B**.

Determination of Inhibitor IC_{50} Values against 3D Abl.

A continuous fluorescence assay was used to determine IC_{50}.[15] The reaction volume was 100 μL consisting of 85 μL of enzyme in buffer, 2.5 μL of the appropriate inhibitor dilution (typically 10000, 3333.33, 1111.11, 370.37, 123.46, 41.15, 13.72, 4.57, 1.52, and 0 μM in DMSO), and 2.5 μL (2.4 mM in DMSO) of a substrate peptide.[21] The reaction was initiated with 10 μL of ATP (1 mM in water), and reaction progress was immediately monitored at 405 nm (ex. 340 nm) for 10 minutes. Reactions had final concentrations of 60 nM enzyme, 60 μM peptide substrate, 100 μM ATP, 100 μM Na_3VO_4, 100 mM Tris buffer (pH 8), 10 mM $MgCl_2$, 0.01% Triton X-100. The initial rate data collected was used for determination of IC_{50} values. For IC_{50} determination, the kinetic values were obtained directly from nonlinear regression of substrate-velocity curves in the presence of various concentrations of the inhibitor. The equation Y =

Bottom + (Top - Bottom)/(1 + $10^{(X-LogIC50)}$), X = log(concentration) and Y = binding; was used in the nonlinear regression. An IC_{50} value was determined for each inhibitor using at least three independent experiments. The individual IC_{50} values for the three runs were then averaged. A representative inhibition curve of a single run is shown in **Appendix B**.

General procedure for BODIPY probe EC_{50} determination.

A fluorescence polarization was used to determine EC_{50} values. Reaction volumes of 50 μL were used in 96-well plates. 34 μL of buffer (50 mM Tris buffer (pH 8), 10 mM NaCl, 5% Glycerol, 1 mM DTT) was added to a single row, followed by 15 μL of enzyme (3.3X concentration) in buffer with 2-fold dilutions (typically 150, 75, 37.5, 18.75, 9.375, 4.69, 2.34, 1.17, 0.586, 0.293, and 0 nM final well concentration). Then, 1 μL of a 500 nM stock of the appropriate dasatinib analog BODIPY probe in DMSO was added (2% DMSO final). Wells were incubated on ice for 30 minutes prior to fluorescence polarization read (ex/em 485/535 nm). After the initial read, 1 μL of 51 μM GNF-2 was added to each well for a final concentration of 1 μM GNF-2. Following another 30 minute incubation on ice, the wells were read again. Reactions had final concentrations of 10 nM BODIPY-probe, 50 mM Tris buffer (pH 8), 10 mM NaCl, 5% Glycerol, 1 mM DTT. For K_d determination, the mPolarization values (normalized to the 0 nM protein control) were plotted vs. varying protein concentrations. The equation Y = (Bmax * X)/(EC_{50} + X), X = Protein concentration and Y = FP response; was used in the nonlinear regression. In two separate runs, the EC_{50} value was determined using at least four independent experiments. The EC_{50} value determined from the two separate runs was averaged. A single representative inhibition curve with error bars is shown in **Appendix B**.

General Procedure for Proteolysis Half-Life Determination

c-Src was diluted in proteolysis buffer (50 mM Tris-HCl pH 8.0, 100 mM NaCl, 0.5 mM $CaCl_2$) to yield a final protein concentration of 2 μM (for 5 point curves this solutions was split in half). This was followed by the addition 1 μL of a 10 mM stock of each compound being tested to give a final concentration of 57 μM compound (113 μM for 5 point curves). 15 μL of the protein/compound solution was added to 5 μL of 50 mM EDTA as the 0 min time point. The proteolysis reaction was initiated by adding Thermolysin (purchased from Promega, catalog number: V4001) from a 3.8 μM stock solution to a final concentration of 50 nM. At various time

points (2, 5, 10, 30, 60, 90, 120, 180, and 240 mins for full curves and 5, 30, 60, 90 mins for 5 point curves), 15 µL of the proteolysis reaction was added to 5 µL of 50 mM EDTA to quench proteolysis. The quenched samples were analyzed by SDS-PAGE (12 % Bis-Tris gel in MES running buffer, staining with coomassie blue). Band intensities were analyzed by ImageJ imaging software. Percent protein remaining was plotted against time and fit to an exponential decay equation using GraphPad Prism software to obtain half-lives of each protein. Each half-life was determined using a single experiment. The half-life curves are shown along with the gel for each apo protein (**Appendix B**).

***General procedure for cellular characterization*.**

1. Cell culture and seeding: HT-29 cells were cultured in McCoy's 5A media with 10% FBS. Media was aspirated and cells were washed with 12.5 mL of DPBS, which was then aspirated. 2 mL of 0.05% trypsin-EDTA was added to the cells and incubated at 37°C and 5% CO_2 until cells detached. 5 mL of prepared media was added to the cells in trypsin-EDTA and an aliquot of the cells was mixed with Trypan Blue solution and the cell number was quantified using a hemocytometer. The cells were plated 100 µL in each well at 30,000 cells/mL so that each well contained 3,000 cells. The cells were plated into sterile, clear bottom 96 well plates and incubated overnight at 37°C and 5% CO_2 overnight for cells to re-adhere. Additionally, 3 wells were created containing 100 µL of media with no cells.

2. Dosing: The compounds were made in 100% DMSO at 1,000X the final concentrations that were desired for the assay generally covering a concentration range of 6 log units. These DMSO stocks were diluted 10X in McCoy's 5A media. 1 µL of the compound diluted in media was added to each well for a final concentration of 0.1% DMSO. The wells containing only media were not dosed. In general, each compound concentration was dosed in triplicate wells. The plates were returned to normal culture conditions (per ATCC) for 72 hours.

3. Assay: After 72 hours, the plates were removed from the incubator, and 10 µL of WST-1 reagent was added to each well. The plates were returned to the incubator and the color change was visually monitored for 0.5 – 2 hours. When sufficient color change had occurred, the plates were shaken on a plate shaker for 30 seconds, and absorbance at 450 and 630 nm was read in a Biotek Synergy 4 plate reader. The absorbance at 630 nm was subtracted from the absorbance at 450 nm.

4. Data Analyses: The average absorbance value from wells containing media without cells was subtracted from the absorbance value for all the wells containing cells. The absorbance values were then taken as a percentage of the absorbance for the vehicle wells (0.1% DMSO - no compound). The percent compared to vehicle was then plotted vs. log[Concentration (M)]. Data analyses and curve fitting were performed using Graphpad Prism 6. In two separate runs, the GI_{50} value was determined using at least three independent experiments. The GI_{50} value determined from the two separate runs was averaged. A single representative inhibition curve with error bars is shown in **Appendix B**.

References

(1) Cohen, P. Protein Kinases--the Major Drug Targets of the Twenty-First Century? *Nat. Rev. Drug Discov.* **2002**, *1* (4), 309–315.

(2) Blume-Jensen, P.; Hunter, T. Oncogenic Kinase Signalling. *Nature* **2001**, *411* (6835), 355–365.

(3) Wu, P.; Nielsen, T. E.; Clausen, M. H. Small-Molecule Kinase Inhibitors: An Analysis of FDA-Approved Drugs. *Drug Discov. Today* **2016**, *21* (1), 5–10.

(4) Anastassiadis, T.; Deacon, S. W.; Devarajan, K.; Ma, H.; Peterson, J. R. Comprehensive Assay of Kinase Catalytic Activity Reveals Features of Kinase Inhibitor Selectivity. *Nat. Biotechnol.* **2011**, *29* (11), 1039–1045.

(5) Fabian, M. A.; Biggs, W. H.; Treiber, D. K.; Atteridge, C. E.; Azimioara, M. D.; Benedetti, M. G.; Carter, T. A.; Ciceri, P.; Edeen, P. T.; Floyd, M.; Ford, J. M.; Galvin, M.; Gerlach, J. L.; Grotzfeld, R. M.; Herrgard, S.; Insko, D. E.; Insko, M. A.; Lai, A. G.; Lélias, J.-M.; Mehta, S. A.; Milanov, Z. V; Velasco, A. M.; Wodicka, L. M.; Patel, H. K.; Zarrinkar, P. P.; Lockhart, D. J. A Small Molecule-Kinase Interaction Map for Clinical Kinase Inhibitors. *Nat. Biotechnol.* **2005**, *23* (3), 329–336.

(6) Wu, P.; Clausen, M. H.; Nielsen, T. E. Allosteric Small-Molecule Kinase Inhibitors. *Pharmacol. Ther.* **2015**, *156*, 59–68.

(7) Moroco, J. A.; Baumgartner, M. P.; Rust, H. L.; Choi, H. G.; Hur, W.; Gray, N. S.; Camacho, C. J.; Smithgall, T. E. A Discovery Strategy for Selective Inhibitors of c-Src in Complex with the Focal Adhesion Kinase SH3/SH2-Binding Region. *Chem. Biol. Drug Des.* **2015**, *86* (2), 144–155.

(8) Yeatman, T. J. A Renaissance for SRC. *Nat. Rev. Cancer* **2004**, *4* (6), 470–480.

(9) Wenqing, X.; Harrison, S.; Eck, M. Three-Dimensional Structure of the Tyrosine Kinase c-Src. *Nature* **1997**, *385*, 595–602.

(10) Cowan-Jacob, S. W.; Fendrich, G.; Manley, P. W.; Jahnke, W.; Fabbro, D.; Liebetanz, J.; Meyer, T. The Crystal Structure of a c-Src Complex in an Active Conformation Suggests Possible Steps in c-Src Activation. *Structure* **2005**, *13* (6), 861–871.

(11) Brown, M. T.; Cooper, J. A. Regulation, Substrates and Functions of Src. *Biochim. Biophys. Acta* **1996**, *1287* (2), 121–149.

(12) Krishnamurty, R.; Brigham, J. L.; Leonard, S. E.; Ranjitkar, P.; Larson, E. T.; Dale, E. J.; Merritt, E. A.; Maly, D. J. Active Site Profiling Reveals Coupling between Domains in

SRC-Family Kinases. *Nat. Chem. Biol.* **2013**, *9* (1), 43–50.
(13) Karaman, M. W.; Herrgard, S.; Treiber, D. K.; Gallant, P.; Atteridge, C. E.; Campbell, B. T.; Chan, K. W.; Ciceri, P.; Davis, M. I.; Edeen, P. T.; Faraoni, R.; Floyd, M.; Hunt, J. P.; Lockhart, D. J.; Milanov, Z. V; Morrison, M. J.; Pallares, G.; Patel, H. K.; Pritchard, S.; Wodicka, L. M.; Zarrinkar, P. P. A Quantitative Analysis of Kinase Inhibitor Selectivity. *Nat. Biotechnol.* **2008**, *26* (1), 127–132.
(14) MacAuley, A.; Cooper, J. A. Structural Differences between Repressed and Derepressed Forms of p60c-Src. *Mol. Cell Biol.* **1989**, *9* (6), 2648–2656.
(15) Wang, Q.; Cahill, S. M.; Blumenstein, M.; Lawrence, D. S. Self-Reporting Fluorescent Substrates of Protein Tyrosine Kinases. *J. Am. Chem. Soc.* **2006**, *128* (6), 1808–1809.
(16) Lietha, D.; Cai, X.; Ceccarelli, D. F. J.; Li, Y.; Schaller, M. D.; Eck, M. J. Structural Basis for the Autoinhibition of Focal Adhesion Kinase. *Cell* **2007**, *129* (6), 1177–1187.
(17) Thomas, J. W.; Ellis, B.; Renee, J.; Knight, W. B.; White, G. C.; Schaller, M. D.; Boerner, R. J.; Ii, C. W. SH2- and SH3-Mediated Interactions between Focal Adhesion Kinase and Src. *J. Biol. Chem.* **1998**, *273* (1), 577–583.
(18) Zheng, X.; Resnick, R. J.; Shalloway, D. Apoptosis of Estrogen-Receptor Negative Breast Cancer and Colon Cancer Cell Lines by PTP Alpha and Src RNAi. *Int. J. Cancer* **2008**, *122* (9), 1999–2007.
(19) Kwarcinski, F. E.; Brandvold, K. R.; Phadke, S.; Beleh, O. M.; Johnson, T. K.; Meagher, J. L.; Seeliger, M. A.; Stuckey, J. A.; Soellner, M. B. Conformation-Selective Analogues of Dasatinib Reveal Insight into Kinase Inhibitor Binding and Selectivity. *ACS Chem. Biol.* **2016**, *11* (5), 1296–1304.
(20) Seeliger, M. A.; Young, M.; Henderson, M. N.; Pellicena, P.; King, D. S.; Falick, A. M.; Kuriyan, J. High Yield Bacterial Expression of Active c-Abl and c-Src Tyrosine Kinases. *Protein Sci.* **2005**, *14*, 3135–3139.
(21) Rabuck, J. N.; Hyung, S.-J.; Ko, K. S.; Fox, C. C.; Soellner, M. B.; Ruotolo, B. T. Activation State-Selective Kinase Inhibitor Assay Based on Ion Mobility-Mass Spectrometry. *Anal. Chem.* **2013**, *85* (15), 6995–7002.

CHAPTER IV

A Bivalent Inhibitor of c-Abl Tyrosine Kinase That Binds the ATP- and Myristate-Binding Pockets

Abstract

We developed a bivalent inhibitor for the protein tyrosine kinase c-Abl that interacts with the myristate and ATP binding pockets. Our approach transformed a dual c-Src/c-Abl ATP-competitive inhibitor into a bivalent inhibitor that was 100X more potent for c-Abl than c-Src. Furthermore, the bivalent inhibitor was 25X more potent for c-Abl than the initial ATP-competitive inhibitor. Finally, and most important for its use as a tool to study c-Abl in cells, this bivalent inhibitor is cell permeable with a cellular therapeutic index of 14.

Introduction

Protein kinases play important roles in both healthy and diseased cell signaling. There is, however, a lack of selective kinase inhibitors, which makes it difficult to pharmacologically study kinase signaling.[1–3] Almost all reported kinase inhibitors bind to the conserved ATP-binding site,[4] which results in most ATP-competitive kinase inhibitors being promiscuous and binding undesired off-targets.[4–6] Interacting with elements outside the conserved ATP pocket has been recognized as an excellent strategy to improve the selectivity of kinase inhibitors.[7–9]

The nonreceptor tyrosine kinase c-Abl plays an important role in many crucial cell processes, and fusion protein BCR-Abl is the causative factor in Chronic Myelogenous Leukemia (CML). ATP-competitive inhibitors imatinib, nilotinib, and dasatinib have been highly successful for the treatment of CML. Conversely, knowing the advantages of binding outside the conserved ATP-pocket, Gray and coworkers identified an allosteric inhibitor, GNF-2, that binds in the myristate pocket of c-Abl.[10–12] The myristate pocket is located within the kinase domain of c-Abl and serves as a means of autoregulation *via* the myristoylated N-terminal tail (a means of autoregulation unique to c-Abl). Crystallographic data have shown that GNF-2 causes a kinking of the I-helix (similar to that caused by the native myristate) when bound (**Figure 4.1**).[12]

In the native system, this action causes the engagement of the SH2 and SH3 domains with the I-helix and inhibition of the kinase domain.[13] These data suggests that GNF-2-bound Abl kinase domain would also engage the SH2 and SH3 domains, inhibiting the kinase domain.

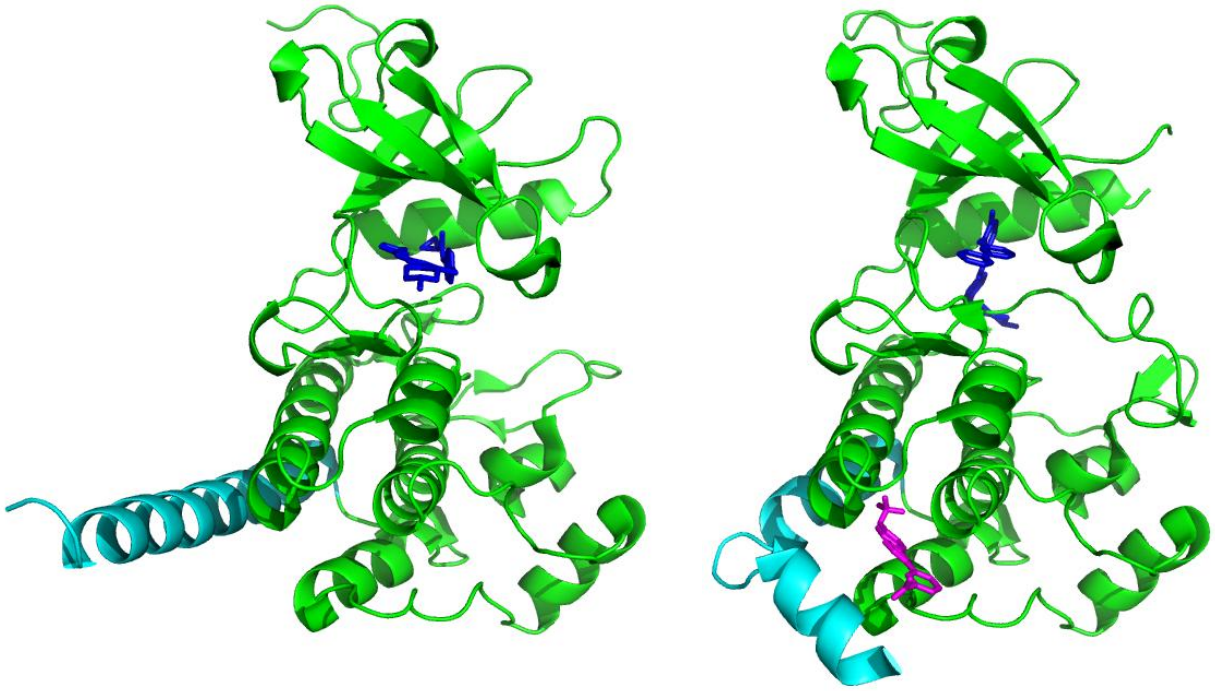

Figure 4.1. Structural effect of GNF-2 binding to c-Abl. Crystal structures showing the kinase domain of c-Abl with ATP-competitive inhibitors (blue) bound demonstrating **a)** an extended I-helix (cyan) when GNF-2 is not bound (PDB: 2F4J) compared to **b)** a kinked I-helix (cyan) when GNF-2 (magenta) is bound (PDB: 3K5V)

Bivalent inhibitors that interact with elements outside the ATP-pocket have proven excellent tools to study kinases.[14–17] There are reported examples of bivalent inhibitors of c-Abl; however these inhibitors have large protein-based linkers,[15,18] and we wanted to create a small-molecule bivalent inhibitor of c-Abl. Our strategy involved a dual c-Src/c-Abl ATP-competitive inhibitor linked to GNF-2. We reasoned that due to the unique selectivity of GNF-2, we could transform a potent yet promiscuous ATP-competitive inhibitor into a highly potent and selective inhibitor of c-Abl. We further hoped to use this inhibitor to inhibit c-Abl in cells.

Bivalent Inhibitor Design

In **Chapter 2**, we designed a bivalent inhibitor of the kinase c-Src that utilized a dasatinib analog with a pendant cyclooctyne (**2.18**).[17] Given that dasatinib is a dual c-Src/c-Abl inhibitor, we decided to use this analog to create a bivalent inhibitor of c-Abl, further demonstrating the

modularity of our previous approach. Additionally, by conjugating **2.18** to GNF-2, we could hopefully impart a great deal of selectivity for c-Abl over c-Src. To enable conjugation to GNF-2, we synthesized **4.1**, a GNF-2 analog with a PEG linker containing a terminal azide (**Scheme 4.1**). Strain-mediated click chemistry made possible by the pendant cyclooctyne of **2.18** was then used to construct bivalent inhibitor **4.2**. We had some concerns that the cyclooctyne functionality of **2.18** might render it too reactive to use in biochemical or cellular assays. To combat this problem, we synthesized analog **4.3** (**Figure 4.2**) where benzyl azide is conjugated to the cyclooctyne creating a benzyl triazole.

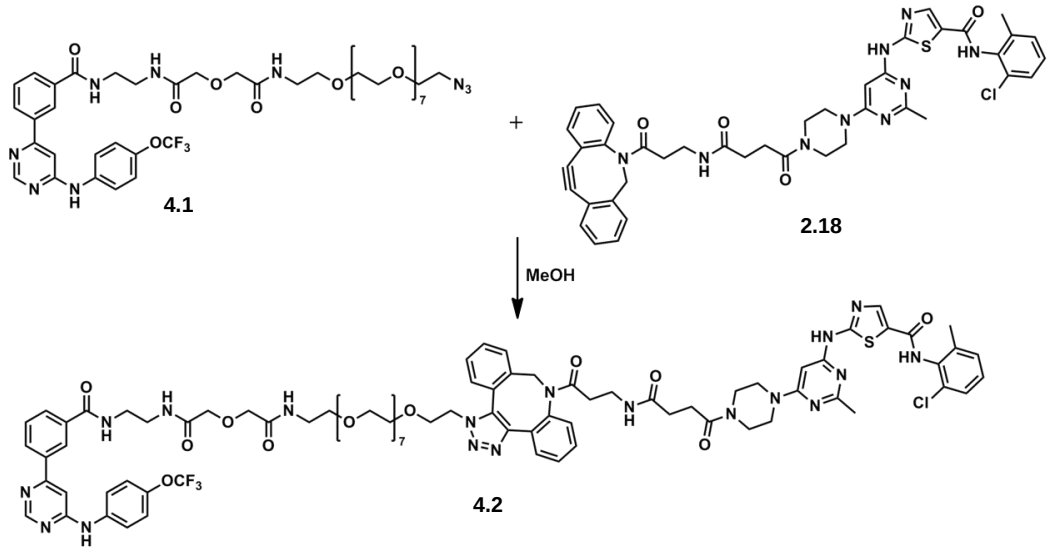

Scheme 4.1. Strain-promoted click cycloaddition of ATP-competitive cyclooctyne **2.18** and azido-GNF-2 **4.1** afford triazole-linked bivalent inhibitor **4.2**.

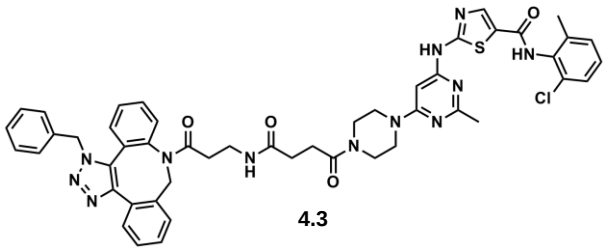

Figure 4.2. Structure of **4.3**, benzyl triazole protected version of cyclooctyne dasatinib analog **2.18**

Biochemical Characterization of Bivalent Inhibitor

GNF-2 only has an inhibitory effect with full-length c-Abl; however, it can bind to the kinase domain construct of c-Abl without inhibiting the activity of the enzyme.[19] Thus, we hypothesized that bivalent inhibitor **4.2** would show an improvement in binding compared to either individual piece against both kinase domain and full-length c-Abl. As such, we tested our

inhibitors **4.1-4.3** against both constructs. Using a continuous activity assay,[20] we observe that bivalent inhibitor **4.2** is approximately 10X more potent than **4.1** and **4.3** in both constructs (**Table 4.1**). Furthermore, we determined the IC_{50} for **4.2** against just the kinase domain of c-Abl but with 8 μM competing GNF-2. As expected (**Table 4.1**), the IC_{50} of **4.2** increased drastically when forced to compete with GNF-2 indicating that the GNF-2 piece is binding in the kinase domain. Additionally, it is known that c-Src is myristoylated similarly to c-Abl, and has a binding pocket for myristate.[21] It is known that GNF-2 cannot inhibit c-Src presumably due to the different mechanisms of autoregulation in c-Src and c-Abl.[13,22] We hypothesized, however, that GNF-2 could possibly bind c-Src without inhibiting activity. Bivalent inhibitor **4.2** gave us the opportunity to test this hypothesis. Given our hypothesis, bivalent inhibitor **4.2** should be at least, if not more, potent than the ATP-competitive inhibitor **4.3** for the kinase domain of c-Src. We did not observe this; **4.2** showed poor inhibition for c-Src (**Table 4.1**). To further illustrate the point that the GNF-2 portion could not bind c-Src, **4.2** did not get any worse when forced to compete with 8 μM free GNF-2.

Table 4.1. IC_{50} values for inhibitors **4.1**-**4.3** against kinase domain (KD) and three domain c-Abl. They are shown with and without competing GNF-2 as well as kinase domain c-Src. DNI = Did not inhibit.

	Abl IC_{50} (nM)			**Src IC_{50} (nM)**	
	Kinase Domain (KD)	Three Domain	KD + 8 μM GNF-2	Kinase Domain	KD + 8 μM GNF-2
4.1	DNI	320			
4.2	26	<30	1,100	1,200	1,700
4.3	150	420		360	

In order to further verify that both portions of the bivalent inhibitor were binding as expected, we performed additional experiments with various mutants of c-Abl in the myrsitate pocket that are known to block GNF-2 binding.[10,12] In full-length mutant c-Abl, we show that when GNF-2 cannot bind, the IC_{50} of **4.2** gets worse and corresponds relatively well to the IC_{50} of **4.3** (**Table 4.2**). In kinase domain c-Abl, the IC_{50} for **4.2** gets markedly worse even compared to **4.3**. This is a little unexpected given that the ATP-competitive portion of **4.2** should still bind; however, the same trend was seen when **4.2** was tested against the kinase domain of c-Abl with competing GNF-2 (**Table 4.1**). A possible explanation could be that when the GNF-2 portion of **4.2** is not able to bind, there is a lot of extra chemical matter present that interferes with the binding of the ATP-competitive portion. This is probably not as significant when using the larger full-length construct of c-Abl.

Table 4.2. IC_{50} values for inhibitors **4.1**-**4.3** against c-Abl mutants. These mutants are known to abrogate GNF-2 binding.

	Abl IC_{50} (nM)					
	Kinase Domain			Three Domain		
	4.3	**4.1**	**4.2**	**4.3**	**4.1**	**4.2**
WT	150	DNI	26	230	320	<30
A337N	270	DNI	1,700	290	240,000	550
P465S	190	700,000	900	220	110,000	830
E505K	230	440,000	700	170	120,000	160

Due to the limits of our activity assay based on protein concentration, we were unable to observe the full effects of our bivalent inhibitor against full-length c-Abl (**Table 4.1**). To resolve this issue, we utilized a commercial binding assay performed in reticulocyte lysate with ~ 5 mM ATP (Luceome Biotechnologies, Tucson, AZ)[23,24] to measure the affinity of bivalent inhibitor **4.2**. In our activity assay, we could only determine the IC_{50} against full-length c-Abl to be less than 30 nM, which was very similar to kinase domain. We hypothesized that **4.2** should be more potent against full-length c-Abl than kinase domain since GNF-2 cannot inhibit kinase domain c-Abl. These data from Luceome Biotechnologies confirm our hypothesis (**Table 4.3**). The IC_{50} for **4.2** in kinase domain was similar to what we had determined using our activity assay, but without the limits of our assay, the IC_{50} for **4.2** against full length c-Abl was 1.2 nM, a 10X improvement. Furthermore, with full length c-Abl, bivalent inhibitor **4.2** is again almost 10X more potent than dasatinib, illustrating the importance of both binding pieces. Additionally, in full length c-Abl, bivalent inhibitor **4.2** is 25X more potent than dasatinib analog **2.18**. To further show the binding importance of the GNF-2 piece of **4.2**, with 20 μM competing GNF-2, the IC_{50} of dasatinib remains relatively the same while the IC_{50} of **4.2** gets 25X worse (**Table 4.3**).

Table 4.3. IC_{50} values for dasatinib and inhibitors **4.2** and **2.18** as determined using Luceome Biotechnologies

	Abl IC_{50} (nM)			**Src IC_{50} (nM)**
	Kinase Domain (KD)	Full Length (FL)	FL + 20 μM GNF-2	Full Length
dasatinib	2.7	9.1	5.0	18
4.2	11.8	1.2	31.1	112
2.18		32		

Selectivity of Bivalent Inhibitor 4.2

We also used the data that we obtained from Luceome to assess the selectivity of **4.2**. dasatinib is known to be a dual c-Src/c-Abl inhibitor. For this reason, we decided to evaluate the selectivity of bivalent inhibitor **4.2** for c-Abl over c-Src. As shown in **Table 4.3**, dasatinib is equipotent for full-length c-Abl and c-Src. Impressively, bivalent inhibitor **4.2** is 100X more

potent for full-length c-Abl than c-Src. By adding the GNF-2 portion, which is highly selective for c-Abl, we were able to make a previously dual c-Src/c-Abl inhibitor much more potent for c-Abl than c-Src.

Cellular Characterization of Bivalent Inhibitor 4.2

Given their large size and often peptidic nature, very few bivalent inhibitors are cell permeable.[16,17] With both binding pieces of bivalent inhibitor **4.2** being small molecules, we believed there was the potential for it to be cell permeable. To test the cell permeability of **4.2**, we utilized a commercial cellular target engagement assay that is performed in HEK 293 cells containing ABL1 (DiscoverX Corporation, San Francisco, CA). We observed an impressive IC_{50} of 15 nM, demonstrating that **4.2** is in fact a cell permeable and effective c-Abl inhibitor. We also tested **4.2** in BCR-Abl Ba/F3 cells, a common cell line to test c-Abl inhibitor. We observed that **4.2** inhibits BCR-Abl Ba/F3 cell growth with a modest GI_{50} value of 700 nM. Additionally, in parental Ba/F3 cells, **4.2** has a $GI_{50} > 10$ μM. This gives it a respectable therapeutic index of >14. We were excited that **4.2** was cell permeable and will continue to explore its cellular effect.

Conclusions

We have developed a bivalent inhibitor of c-Abl that interacts with both the ATP-pocket and the regulatory, myristate pocket. The ATP pocket is conserved across the kinome;[4] however, the autoregulation of c-Abl *via* its myristate pocket is unique. As such, by linking a dual c-Src/c-Abl ATP-competitive inhibitor to GNF-2 we were able to gain a high degree of selectivity for c-Abl. This bivalent inhibitor also showed significant improvement in potency over either binding piece alone. Furthermore, through multiple methods (competition with GNF-2 and site-directed mutagenesis) we validated that both binding pieces were important for the improvement in potency. Additionally, unlike most bivalent inhibitors, our created bivalent inhibitor is cell permeable. It has a modest GI_{50} in BCR/Abl Ba/F3 cells and is entirely ineffective in non-BCR/Abl Ba/F3 cells giving it a respectable therapeutic index.

Materials and Methods

General Synthetic Methods

Unless otherwise noted, all reagents were obtained via commercial sources and used without further purification. All ^{1}H NMR spectra were measured with a Varian MR400 or Inova 500 spectrometer. Mass Spectrometry (HRMS) was carried out by the University of Michigan Mass Spectrometry Facility (J. Windak, director).

Synthetic Protocols

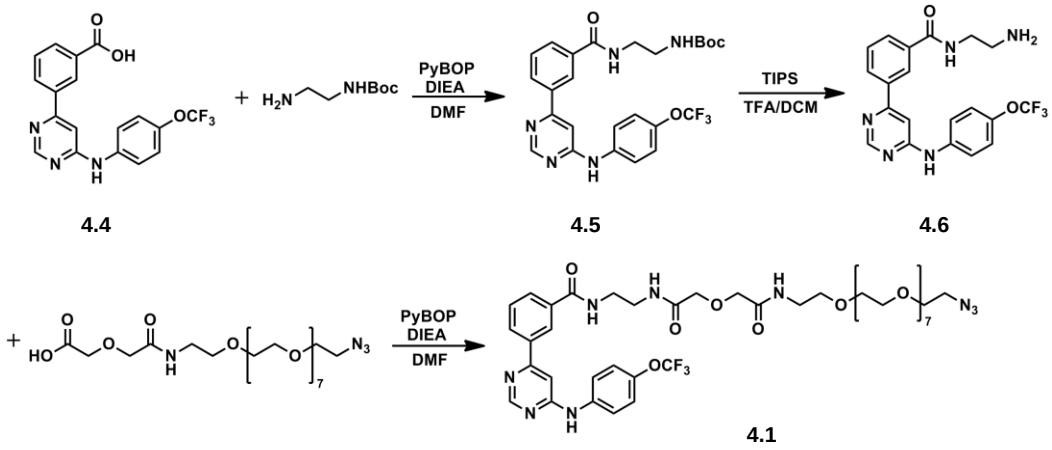

Scheme 4.2. Synthetic Scheme for Compound 4.1

Synthesis of 4.4: This compound was prepared as previously reported.[10]

Synthesis of 4.5: DMF (9.0 mL) was added to a round-bottom flask containing **4.4** (400 mg, 1.07 mmol), 1-boc-ethylenediamine (0.14 mL, 0.89 mmol), and PyBOP (562.4 mg, 1.07 mmol). DIEA (0.31 mL, 1.78 mmol) was then added and the reaction was stirred overnight. The reaction mixure was brought up in 50 mL of ethyl acetate and washed with 10% citrate, sat. bicarb, and brine. After drying over Na_2SO_4, the product was purified by silica gel chromatography using a Biotage Isolera One (linear gradient 30 → 80% ethyl acetate in hexanes). The pure fractions were combined and the solvent was removed under reduced pressure to yield **4.5** as a white solid (190 mg, 41% yield). **Spectral data.** ^{1}H NMR (500 MHz, DMSO-d_6) δ 9.95 (s, 1H), 8.77 (s,

1H), 8.65 (t, *J* = 5.6 Hz, 1H), 8.51 (s, 1H), 8.18 (d, *J* = 7.9 Hz, 1H), 7.97 (d, *J* = 7.8 Hz, 1H), 7.86 (dd, *J* = 9.5, 2.9 Hz, 2H), 7.63 (t, *J* = 7.8 Hz, 1H), 7.43 – 7.29 (m, 3H), 6.94 (t, *J* = 5.9 Hz, 1H), 3.31 (s, 2H), 3.13 (q, *J* = 6.3 Hz, 2H), 1.37 (s, 9H). MS-ESI (m/z): $[M + H]^+$ calcd for $C_{25}H_{26}F_3N_5O_4$ 518.2010; found 518.2009.

Synthesis of 4.6: 4.5 (77.6 mg, 0.15 mmol) was added to an oven-dried flask. DCM (1.0 mL) and TFA (1.0 mL) were added followed by TIPS (20 μL, 0.008 mmol). The resulting solution was stirred for 1 hour. The solvent was then removed under reduced pressure. The resulting residue was carried forward crude without purification assuming theoretical yield.

Synthesis of 4.1: DMF (1.8 mL) was added to a round-bottom flask containing N_3-PEG_7-CO_2H (103.4 mg, 0.18 mmol), **4.6** (62.7 mg, 0.15 mmol), and PyBOP (95.1 mg, 0.18 mmol). DIEA (0.26 mL, 1.5 mmol) was then added and the reaction was stirred overnight. The reaction mixture was purified by reverse-phase HPLC using a linear 20→80% acetonitrile in water gradient. Lyophilization of pure fractions afforded **4.1** as an off-white solid (81.5 mg, 57% yield). **Spectral Data.** ^{1}H NMR (500 MHz, DMSO-d_6) δ 9.94 (s, 1H), 8.83 – 8.74 (m, 2H), 8.52 (t, *J* = 1.8 Hz, 1H), 8.26 (t, *J* = 5.7 Hz, 1H), 8.19 (dt, *J* = 7.9, 1.4 Hz, 1H), 8.07 (t, *J* = 5.9 Hz, 1H), 7.98 (dt, *J* = 7.9, 1.4 Hz, 1H), 7.89 – 7.82 (m, 2H), 7.64 (t, *J* = 7.7 Hz, 1H), 7.40 – 7.30 (m, 3H), 3.95 (d, *J* = 4.2 Hz, 4H), 3.58 (dd, *J* = 5.6, 4.3 Hz, 2H), 3.56 – 3.45 (m, 28H), 3.45 – 3.35 (m, 5H), 3.26 (q, *J* = 6.0 Hz, 2H). MS-ESI (m/z): $[M + H]^+$ calcd for $C_{42}H_{58}F_3N_9O_{13}$ 954.4179; found 954.4176.

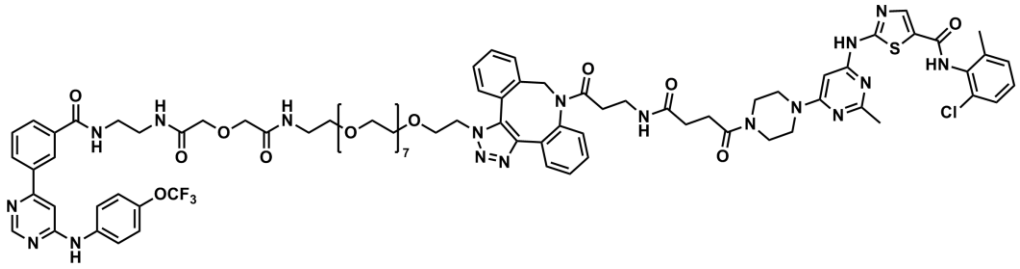

Synthesis of 4.2: 4.1 (1.3 mg, 0.001 mmol) was added to a stirred solution of **2.18** (1.0 mg, 0.001 mmol) in MeOH (0.1 mL). The resulting reaction mixture was stirred overnight. The solvent was then removed under reduced pressure and the resulting residue was brought up in DMSO and purified by reverse-phase HPLC using a linear 30→90% acetonitrile in water

gradient. Lyophilization of pure fractions afforded **4.2** as a white solid (0.63 mg, 36% yield). **Spectral Data.** MS-ESI (m/z): $[M + H]^+$ calcd for $C_{84}H_{98}ClF_3N_{18}O_{17}S$ 1755.6791; found 1755.6751.

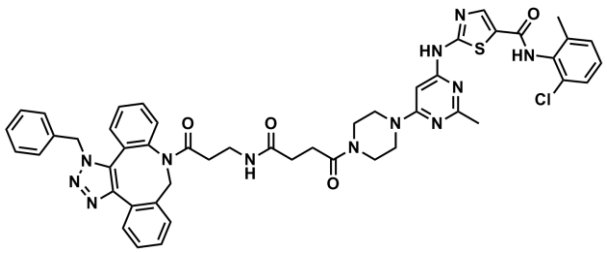

Synthesis of 4.3: Benzyl azide (0.03 mL, 0.24 mmol) was added to a stirred solution of **2.18** (21.1 mg, 0.03 mmol) in MeOH (0.2 mL). The resulting reaction mixture was heated to 70°C overnight. The solvent was then removed under reduced pressure and the resulting residue was brought up in DMSO and purified by C18 silica gel chromatography using a Biotage Isolera One (linear gradient 30 → 90% acetonitrile in water). Lyophilization of the fractions comprising the lone peak were further purified by reverse-phase HPLC using a linear 30→90% acetonitrile + 0.1% TFA in water gradient. Lyophilization of pure fractions afforded **4.3** as a white solid (5.2 mg, 19% yield). **Spectral Data.** ^{1}H NMR (500 MHz, dmso) δ 11.56 (s, 1H), 9.90 (s, 1H), 8.23 (s, 1H), 7.59 (ddt, J = 42.5, 21.8, 6.5, 6.5 Hz, 5H), 7.40 (j, J = 7.7 Hz, 1H), 7.28 (tt, J = 14.3, 14.3, 4.2, 4.2, 7H), 6.95 (d, J = 7.3 Hz, 2H), 6.08 (s, 1H), 5.79 (dd, J = 20.3, 16.5 Hz, 2H), 5.66 (d, J = 16.0 Hz, 1H), 4.40 (d, J = 16.8Hz, 1H), 3.54 (d, J = 14.5 Hz, 8H), 3.07 (dq, J = 13.8, 6.8, 6.7, 6.7 Hz, 1H), 2.92 (dq, J = 14.1, 6.7, 6.6, 6.6 Hz, 1H), 2.42 (s, 3H), 2.23 (s, 2H), 1.87 (dt, J = 15.6, 7.5, 7.5 Hz, 1H), 1.75 (s, 1H), 1.54 (dt, J = 15.8, 7.1, 7.1 Hz, 1H). MS-ESI (m/z): $[M + H]^+$ calcd for $C_{49}H_{47}ClN_{12}O_4S$ 935.3325; found 935.3330.

Spectral Data for Compounds

Spectral data (^{1}H NMR) for compounds are shown in **Appendix C**.

General Biochemical Methods

Black, opaque-bottom 96 well plates were purchased from Nunc. All proteins were expressed in *E.coli* using previously published procedures.[25] Data were obtained using Biotek Synergy Mx and Biotek Synergy 4 plate readers. Curve fitting was done using Graphpad Prism 6 software.

Determination of Inhibitor IC_{50} Values against 3D c-Abl.

A continuous fluorescence assay was used to determine IC_{50}. The reaction volume was 100 μL consisting of 85 μL of enzyme in buffer, 2.5 μL of the appropriate inhibitor dilution (typically 3333.33, 1111.11, 370.37, 123.46, 41.15, 13.72, 4.57, 1.52, 0.507, and 0 μM in DMSO), and 2.5 μL (2.4 mM in DMSO) of a substrate peptide.[26] The reaction was initiated with 10 μL of ATP (50 mM in water unless otherwise noted), and reaction progress was immediately monitored at 405 nm (ex. 340 nm) for 10 minutes. Reactions had final concentrations of 30 nM enzyme (unless otherwise noted), 60 μM peptide substrate, 5 mM ATP, 100 μM Na_3VO_4, 100 mM Tris buffer (pH 8), 10 mM MgCl2, 0.01% Triton X-100. The initial rate data collected was used for determination of IC_{50} values. For IC_{50} determination, the kinetic values were obtained directly from nonlinear regression of substrate-velocity curves in the presence of various concentrations of the inhibitor. The equation Y = Bottom + (Top – Bottom)/(1 + 10^X – LogEC50), X = log(concentration) and Y = binding; was used in the nonlinear regression. An IC_{50} value was determined for each inhibitor using at least two independent experiments (unless otherwise noted). The individual IC_{50} values for the two runs were then averaged. A representative inhibition curve of a single run is shown in **Appendix C**.

***General procedure for cellular characterization*.**

1. Cell culture and seeding: All Ba/F3 cell lines were cultured in RPMI 1640 media with 10% FBS. Parental Ba/F3 cell culture additionally contained 15% WEHI-3 conditioned media. An aliquot of the cells was mixed with Trypan Blue solution and the cell number was quantified using a hemocytometer. The cells were plated 100 μL in each well at 30,000 cells/mL so that each well contained 3,000 cells. The cells were plated into sterile, clear bottom 96 well plates and then immediately dosed with compound. Additionally, 3 wells were created containing 100 μL of media with no cells.

2. Dosing: The compounds were made in 100% DMSO at 1,000X the final concentrations that were desired for the assay generally covering a concentration range of 6 log units. These DMSO stocks were diluted 10X in RPMI 1640 media. 1 μL of the compound diluted in media was added to each well for a final concentration of 0.1% DMSO. The wells containing only media were not

dosed. In general, each compound concentration was dosed in triplicate wells. The plates were returned to normal culture conditions (per ATCC) for 72 hours.

3. Assay: After 72 hours, the plates were removed from the incubator, and 10 μL of WST-1 reagent was added to each well. The plates were returned to the incubator and the color change was visually monitored for 0.5 – 2 hours. When sufficient color change had occurred, the plates were shaken on a plate shaker for 30 seconds, and absorbance at 450 and 630 nm was read in a Biotek Synergy 4 plate reader. The absorbance at 630 nm was subtracted from the absorbance at 450 nm.

4. Data Analyses: The average absorbance value from wells containing media without cells was subtracted from the absorbance value for all the wells containing cells. The absorbance values were then taken as a percentage of the absorbance for the vehicle wells (0.1% DMSO - no compound). The percent compared to vehicle was then plotted vs. log(Concentration). Data analyses and curve fitting were performed using Graphpad Prism 6. For each compound, there were n = 3 data points for each concentration. For curves that did not reach full inhibition, the bottom was set to -10. The curves with error bars are shown in **Appendix C**.

References

(1) Knight, Z. A.; Shokat, K. M. Features of Selective Kinase Inhibitors. *Chem. Biol.* **2005**, *12* (6), 621–637.

(2) Zhang, J.; Yang, P. L.; Gray, N. S. Targeting Cancer with Small Molecule Kinase Inhibitors. *Nat. Rev. Cancer* **2009**, *9* (1), 28–39.

(3) Brandvold, K. R.; Steffey, M. E.; Fox, C. C.; Soellner, M. B. Development of a Highly Selective c-Src Kinase Inhibitor. *ACS Chem. Biol.* **2012**, *7* (8), 1393–1398.

(4) Manning, G.; Whyte, D. B.; Martinez, R.; Hunter, T.; Sudarsanam, S. The Protein Kinase Complement of the Human Genome. *Science (80-.).* **2002**, *298* (5600), 1912–1934.

(5) Anastassiadis, T.; Deacon, S. W.; Devarajan, K.; Ma, H.; Peterson, J. R. Comprehensive Assay of Kinase Catalytic Activity Reveals Features of Kinase Inhibitor Selectivity. *Nat. Biotechnol.* **2011**, *29* (11), 1039–1045.

(6) Fabian, M. A.; Biggs, W. H.; Treiber, D. K.; Atteridge, C. E.; Azimioara, M. D.; Benedetti, M. G.; Carter, T. A.; Ciceri, P.; Edeen, P. T.; Floyd, M.; Ford, J. M.; Galvin, M.; Gerlach, J. L.; Grotzfeld, R. M.; Herrgard, S.; Insko, D. E.; Insko, M. A.; Lai, A. G.; Lélias, J.-M.; Mehta, S. A.; Milanov, Z. V; Velasco, A. M.; Wodicka, L. M.; Patel, H. K.; Zarrinkar, P. P.; Lockhart, D. J. A Small Molecule-Kinase Interaction Map for Clinical Kinase Inhibitors. *Nat. Biotechnol.* **2005**, *23* (3), 329–336.

(7) Breen, M. E.; Steffey, M. E.; Lachacz, E. J.; Kwarcinski, F. E.; Fox, C. C.; Soellner, M. B. Substrate Activity Screening with Kinases: Discovery of Small-Molecule Substrate-Competitive c-Src Inhibitors. *Angew. Chem. Int. Ed.* **2014**, *53* (27), 7010–7013.

(8) Cox, K. J.; Shomin, C. D.; Ghosh, I. Tinkering Outside the Kinase ATP Box: Allosteric

(Type IV) and Bivalent (Type V) Inhibitors of Protein Kinases. *Futur. Med. Chem.* **2011**, *3* (1), 29–43.
(9) Lamba, V.; Ghosh, I. New Directions in Targeting Protein Kinases: Focusing upon True Allosteric and Bivalent Inhibitors. *Curr. Pharm. Des.* **2012**, *18* (20), 2936–2945.
(10) Adrián, F. J.; Ding, Q.; Sim, T.; Velentza, A.; Sloan, C.; Liu, Y.; Zhang, G.; Hur, W.; Ding, S.; Manley, P.; Mestan, J.; Fabbro, D.; Gray, N. S. Allosteric Inhibitors of Bcr-Abl-Dependent Cell Proliferation. *Nat. Chem. Biol.* **2006**, *2* (2), 95–102.
(11) Iacob, R. E.; Zhang, J.; Gray, N. S.; Engen, J. R. Allosteric Interactions between the Myristate- and ATP-Site of the Abl Kinase. *PLoS One* **2011**, *6* (1), e15929.
(12) Zhang, J.; Adrián, F. J.; Jahnke, W.; Cowan-Jacob, S. W.; Li, A. G.; Iacob, R. E.; Sim, T.; Powers, J.; Dierks, C.; Sun, F.; Guo, G.-R.; Ding, Q.; Okram, B.; Choi, Y.; Wojciechowski, A.; Deng, X.; Liu, G.; Fendrich, G.; Strauss, A.; Vajpai, N.; Grzesiek, S.; Tuntland, T.; Liu, Y.; Bursulaya, B.; Azam, M.; Manley, P. W.; Engen, J. R.; Daley, G. Q.; Warmuth, M.; Gray, N. S. Targeting Bcr-Abl by Combining Allosteric with ATP-Binding-Site Inhibitors. *Nature* **2010**, *463* (7280), 501–506.
(13) Nagar, B.; Hantschel, O.; Young, M. A.; Scheffzek, K.; Veach, D.; Bornmann, W.; Clarkson, B.; Superti-Furga, G.; Kuriyan, J. Structural Basis for the Autoinhibition of c-Abl Tyrosine Kinase. *Cell* **2003**, *112* (6), 859–871.
(14) Profit, A.; Lee, T.; Lawrence, D. Bivalent Inhibitors of Protein Tyrosine Kinases. *J. Am. Chem. Soc.* **1999**, *121* (2), 280–283.
(15) Hill, Z. B.; Perera, B. G. K.; Maly, D. J. A Chemical Genetic Method for Generating Bivalent Inhibitors of Protein Kinases. *J. Am. Chem. Soc.* **2009**, *131* (19), 6686–6688.
(16) Brandvold, K. R.; Santos, S. M.; Breen, M. E.; Lachacz, E. J.; Steffey, M. E.; Soellner, M. B. Exquisitely Specific Bisubstrate Inhibitors of c-Src Kinase. *ACS Chem. Biol.* **2015**, *10*, 1387–1391.
(17) Johnson, T. K.; Soellner, M. B. Bivalent Inhibitors of c-Src Tyrosine Kinase That Bind a Regulatory Domain. *Bioconjug. Chem.* **2016**, *27* (7), 1745–1749.
(18) Hill, Z. B.; Perera, B. G. K.; Maly, D. J. Bivalent Inhibitors of the Tyrosine Kinases ABL and SRC: Determinants of Potency and Selectivity. *Mol. BioSyst.* **2011**, *7* (2), 447–456.
(19) Choi, Y.; Seeliger, M. a; Panjarian, S. B.; Kim, H.; Deng, X.; Sim, T.; Couch, B.; Koleske, A. J.; Smithgall, T. E.; Gray, N. S. N-Myristoylated c-Abl Tyrosine Kinase Localizes to the Endoplasmic Reticulum upon Binding to an Allosteric Inhibitor. *J. Biol. Chem.* **2009**, *284* (42), 29005–29014.
(20) Wang, Q.; Cahill, S. M.; Blumenstein, M.; Lawrence, D. S. Self-Reporting Fluorescent Substrates of Protein Tyrosine Kinases. *J. Am. Chem. Soc.* **2006**, *128* (6), 1808–1809.
(21) Patwardhan, P.; Resh, M. D. Myristoylation and Membrane Binding Regulate c-Src Stability and Kinase Activity. *Mol. Cell Biol.* **2010**, *30* (17), 4094–4107.
(22) Wenqing, X.; Harrison, S.; Eck, M. Three-Dimensional Structure of the Tyrosine Kinase c-Src. *Nature* **1997**, *385*, 595–602.
(23) Jester, B. W.; Cox, K. J.; Gaj, A.; Shomin, C. D.; Porter, J. R.; Ghosh, I. A Coiled-Coil Enabled Split-Luciferase Three-Hybrid System: Applied Toward Profiling Inhibitors of Protein Kinases. *J. Am. Chem. Soc.* **2010**, *132* (33), 11727–11735.
(24) Jester, B. W.; Gaj, A.; Shomin, C. D.; Cox, K. J.; Ghosh, I. Testing the Promiscuity of Commercial Kinase Inhibitors Against the AGC Kinase Group Using a Split-Luciferase Screen. *J. Med. Chem.* **2012**, *55* (4), 1526–1537.
(25) Seeliger, M. A.; Young, M.; Henderson, M. N.; Pellicena, P.; King, D. S.; Falick, A. M.;

Kuriyan, J. High Yield Bacterial Expression of Active c-Abl and c-Src Tyrosine Kinases. *Protein Sci.* **2005**, *14*, 3135–3139.

(26) Rabuck, J. N.; Hyung, S.-J.; Ko, K. S.; Fox, C. C.; Soellner, M. B.; Ruotolo, B. T. Activation State-Selective Kinase Inhibitor Assay Based on Ion Mobility-Mass Spectrometry. *Anal. Chem.* **2013**, *85* (15), 6995–7002.

CHAPTER V

Synergy between Allosteric and Active Site Inhibitors of c-Abl Tyrosine Kinase

Abstract

We investigated synergy between ATP-competitive inhibitors of c-Abl and the allosteric inhibitor GNF-2. We have found that inhibitors that bind in different conformations in the ATP-binding site can cause a change in the global conformation of c-Abl. GNF-2, which binds c-Abl in a closed conformation, is only synergistic with ATP-competitive inhibitors that bind the same conformation. Since no approved ATP-competitive inhibitors bind a closed conformation, we turned to an αC-helix-out inhibitor of c-Abl recently developed (Das-CHO-II) in our lab. When combined, GNF-2 and Das-CHO-II were highly synergistic in BCR-Abl Ba/F3 cells as well as K562 cells. Furthermore, this combination resulted in a 1000X improvement in the GI_{50} of Das-CHO-II. Additionally, the synergy seen between GNF-2 and Das-CHO-II was capable of overcoming the common, T315I clinical mutation.

Introduction

Fusion protein BCR-Abl caused by the translocation of chromosomes 19 and 22 is the causative factor in Chronic Myelogenous Leukemia (CML).[1] The ATP-competitive c-Abl inhibitor imatinib is very effective in increasing CML patient survival.[2] Unfortunately, over time, many patients develop resistance to imatinib and several second-generation BCR-Abl inhibitors.[3] This occurs due to a common point mutation, T315I. Third-generation BCR-Abl inhibitor ponatinib is the only approved inhibitor for the T315I mutation of BCR-Abl; however, it carries a black box warning for causing "adverse vascular events" in 48 percent of patients.[4] Since patients who develop CML are typically over 60 years of age often with existing heart conditions,[5] the use of ponatinib is undesirable in these patients. Thus, novel strategies to combat the T315I mutation are critical.

As mentioned in **Chapter IV**, an allosteric inhibitor of c-Abl, GNF-2, was discovered in an attempt to combat resistance.[6] Both NMR and crystallographic data indicate that GNF-2 binds in the myristate pocket of c-Abl.[7,8] The myristate pocket is located within the kinase domain of c-Abl and serves as a means of autoregulation. c-Abl is inactivated when its myristoylated, N-terminal tail tucks itself inside the previously mentioned myristate pocket.[9] This kinks the I-helix in the kinase domain, which provides a docking site for the SH2 domain of c-Abl. The docking of the SH2 domain to the kinase domain of c-Abl causes the linker between the kinase domain and the SH2 domain to coil. The SH3 domain then clamps down on this coiled linker, which reorients the N and C-lobes of the kinase domain rendering it inactive. Crystallographic data has shown that GNF-2 causes a similar kinking of the I-helix when bound in the myristate pocket.[8] This suggests that the binding of GNF-2 engages the SH2 and SH3 domains, inhibiting the kinase domain.

Since its discovery, there has been a strong interest in combining GNF-2 with ATP-competitive inhibitors with the idea that the combination would be synergistic and also slow the development of resistance, including the T315I mutation.[8] Many groups have shown synergy between GNF-2 and various ATP-competitive inhibitors.[7,8,10] There have been, however, contradictory reports suggesting that these combinations are actually not synergistic.[11] Furthermore, it has been shown that both imatinib and GNF-2 affect the global structure of c-Abl; however, they cause c-Abl to adopt slightly different conformations.[12] With these data in mind, we decided to further investigate the relationship between ATP-competitive inhibitors and GNF-2.

Synergy of ATP-Competitive Compounds with GNF-2

As stated, there are several conflicting claims as to whether or not current ATP-competitive inhibitors demonstrate synergy in c-Abl when combined with GNF-2.[8,11] We decided to perform an analysis of combinations between GNF-2 and four approved ATP-competitive inhibitors of c-Abl (dasatinib, imatinib, nilotinib, and ponatinib). Using the Chou-Talalay method, [13,14] we determined the combination indices (CI) for these four combinations in BCR-Abl Ba/F3 cells. The Chou-Talalay method is based upon the median effect principle of the mass action law.[15] To determine a CI value between two drugs, the effect of each drug upon cell growth at varying concentrations is determined. Then, the effect of the two together at varying

concentrations of both is determined. The doses and corresponding cell growth effect data are entered into the CompuSyn computer program, which determines the CI using equation (1) in **Appendix D**.[15] A CI <1 is synergistic, CI = 1 is additive, and CI >1 is antagonistic. As shown in **Table 5.1**, we found that none of the inhibitors tested demonstrated synergy. This was in sharp contrast to several previous reports.[7,8,10] Given their unique binding sites, we hypothesized that both GNF-2 and ATP-competitive inhibitors should be able to bind simultaneously and would thus show synergy. With these results in hand, we decided to investigate why these inhibitors did not show synergy. This led us to a deeper structural investigation of the binding modes of these inhibitors.

Table 5.1. Combination Indices for various ATP-competitive inhibitors with GNF-2

ATP-Competitive Inhibitor	CI_{50}	CI_{75}	CI_{90}	CI_{95}
dasatinib	0.84	0.93	1.04	1.12
imatinib	0.88	0.87	0.87	0.87
nilotinib	0.94	0.94	0.94	0.94
ponatinib	1.02	1.02	1.02	1.02

Evaluating c-Abl Global Conformation

c-Abl activity is carefully regulated in cells by auto-inhibition. In its inactive state, the kinase adopts a compact "closed" conformation in which the SH2 and SH3 domains "clamp down" on the kinase domain, inhibiting activity.[9] When activated, the kinase adopts an "open" conformation where the structure becomes more elongated and the SH2 domain moves to a "top-hat" location on top of the N-lobe of the kinase domain.[16,17] One of the biggest hallmarks of the open vs. closed conformations is whether the linker between the kinase domain and SH2 domain is exposed. WT c-Abl, when not down-regulated, is seen in the "top-hat" conformation where the linker is exposed.[16,17] In SH3 engaged Abl (Abl HAL9), a highly "closed" c-Abl construct, the linker is protected.[18] Mutants, such as A337N, have been shown to be even more active than wild-type, implying a more open conformation.[19]

Our lab has developed a protease accessibility assay to assess these different global conformations of kinases based on the accessibility of the linker between the kinase and SH2 domains. It is simple, low cost, and medium throughput. The protease thermolysin is known to cleave several kinases at a site on the linker (unpublished data by Michael P. Agius). Cleavage of the kinase over time by thermolysin can be evaluated by measuring the intensity of the full-length protein *via* SDS-PAGE. The band intensity can then be plotted vs. time to obtain a half-life curve. A construct that is more open will have a more exposed linker, be proteolyzed more

quickly by thermolysin, and thus have a shorter half-life (**Figure 5.1**). We used the constructs mentioned above to validate that thermolysin half-life corresponded to known conformation of the construct.

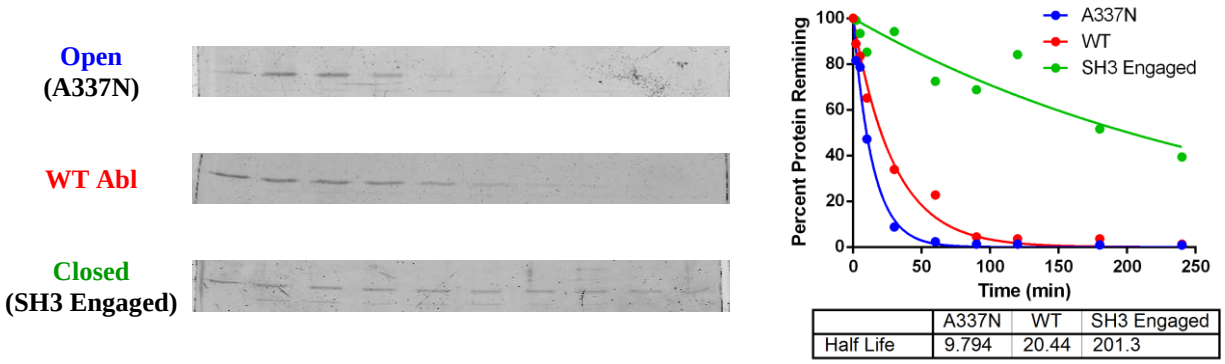

	A337N	WT	SH3 Engaged
Half Life	9.794	20.44	201.3

a **b**

Figure 5.1. Open (A337N Abl), WT, and closed (SH3 Engaged Abl) controls for the protease accessibility assay visualized as (**a**) disappearance of the protein band and (**b**) corresponding half-live decay curves.

Inhibitor Effect on c-Abl Global Conformation

After verifying the proteolysis assay using established c-Abl constructs, we used the assay to analyze each drug tested in combination with GNF-2. To more easily visualize the compounds that stabilized the open *vs*. closed conformation, we represented the data as log($T_{1/2}$ / WT Abl $T_{1/2}$) so that Wild Type Abl would be represented by zero, the closed conformation would be represented by values greater than zero, and the open conformation would be represented by values less than zero. We observed (**Figure 5.2**) that all four ATP-competitive inhibitors stabilized the open conformation of c-Abl, even more so than the A337N mutant. GNF-2 resulted in a closed conformation of c-Abl, similar to SH3 engaged. We contend that the lack of synergy between GNF-2 and the tested ATP-competitive inhibitors was due to the fact that they adopt highly different global conformations.

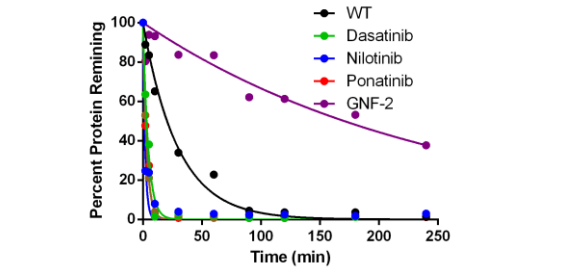

	WT	Dasatinib	Imatinib	Nilotinib	Ponatinib	GNF-2
Half Life	20.44	3.067	2.196	1.274	2.219	170.7

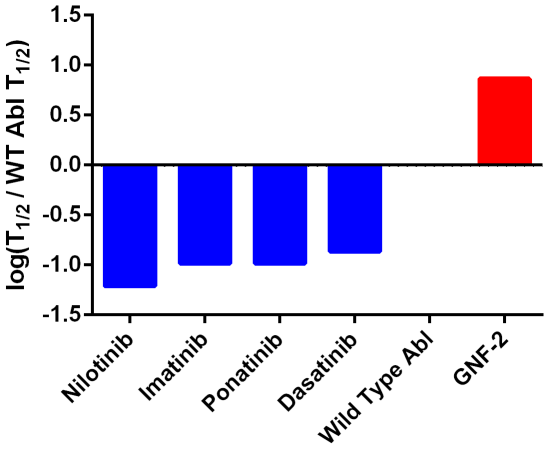

a **b**

Figure 5.2. Effect of ATP-competitive inhibitors and GNF-2 upon WT Abl conformation shown as both (**a**) proteolysis half-lives and (**b**) percent closed

Evaluating αC-helix-out Inhibitors

Once the global conformation for all these inhibitors was determined, we realized that the best inhibitor to potentially combine with GNF-2 would be an ATP-competitive inhibitor that bound a closed conformation of c-Abl. αC-helix-out (CHO) inhibitors are known to bind the closed conformation of kinases. We decided to use a CHO inhibitor developed in our lab as part of a "matched set" of kinase inhibitors created by Kristoffer Brandvold, Sameer Phadke, and Frank Kwarcinski.[20] This set of inhibitors is based on a dasatinib scaffold and contains two CHO inhibitors (Das-CHO-I and Das-CHO-II) and two DFG-out (Type II) inhibitors (Das-DFGO-I and Das-DFGO-II). Since Das-CHO-II is more than ten times more potent than Das-CHO-I, we decided to utilize Das-CHO-II to assess our hypothesis. First, the global conformation that Das-CHO-II adopted was determined. As shown in **Figure 5.3**, compared to apo c-Abl, Das-CHO-II stabilized a more closed conformation. We also tested Das-DFGO-II and were unsurprised to see that it opened c-Abl to the same degree as other Type II c-Abl inhibitors (nilotinib, imatinib, and ponatinib). We also wanted to assess the three known kinase conformation selective inhibitors in combination with GNF-2 to see how those combinations may affect global conformation. We found that the combination of a Das-DFGO-II and GNF-2 was still more open than apo c-Abl indicating an ineffective combination. The combination of dasatinib (a Type-I inhibitor) and GNF-2 was slightly closed but overall, similar to the apo enzyme. Gratifyingly, though, the

combination of Das-CHO-II and GNF-2 was closed, even more so than the highly closed SH3 engaged c-Abl. These data were encouraging, and we hypothesized that Das-CHO-II and GNF-2 would show strong synergy.

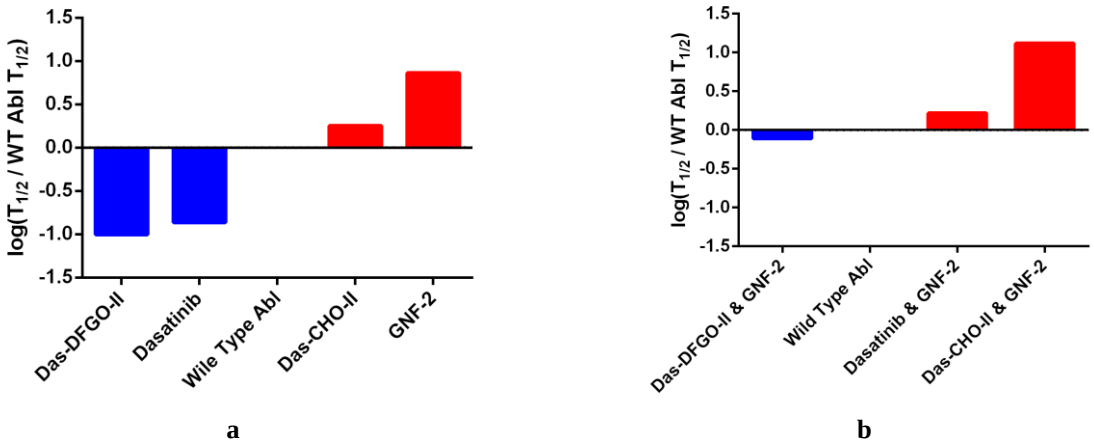

Figure 5.3. Conformation of WT Abl with (**a**) the conformation selective inhibitors and (**b**) combinations of the conformation selective inhibitors with GNF-2

Combining Das-CHO-II and GNF-2

We decided to further evaluate the combination of Das-CHO-II with GNF-2. We evaluated synergy as before, and in conformation of our hypothesis, the combination was observed to be highly synergistic with a CI_{50} of 0.23. An analog of GNF-2[21] was also determined to be synergistic with a CI_{50} of 0.66 (**Appendix D**). GNF-2 and Das-CHO-II are not exceptionally potent in cells compared to other c-Abl inhibitors (GI_{50} (both) ≈ 500nM); however, we wanted to see how the synergy between the two could be used to leverage potency against BCR-Abl Ba/F3 cells. First, we evaluated the GI_{50} of GNF-2 with the addition of a constant, sub-GI_{50} concentration (100 nM) of Das-CHO-II. This lead to a dramatic decrease in the GI_{50} of GNF-2 to 17nM (**Figure 5.4**). The results for Das-CHO-II were even more striking. When combined with 200 nM of GNF-2, we observed a 1,000 fold improvement in the GI_{50} of Das-CHO-II from 550 nM to 0.55 nM (**Table 5.2**).

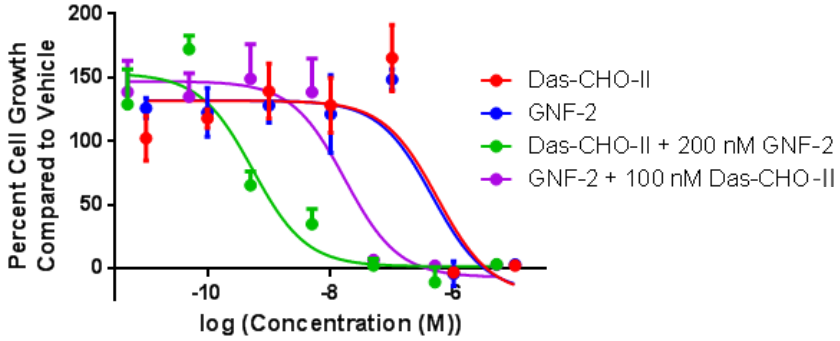

Figure 5.4. GI_{50} curves for GNF-2, Das-CHO-II, GNF-2 + 100 nM Das-CHO-II, and Das-CHO-II + 200 nM GNF-2 in BCR-Abl Ba/F3 cells illustrating the magnitude of improvement realized by the combination of Das-CHO-II and GNF-2

The comparison of a compound's GI_{50} in BCR-Abl Ba/F3 and Parental Ba/F3 cells that do not overexpress BCR-Abl is a common measure of the therapeutic index. By combining the two agents, we were able to significantly increase the therapeutic index. In Parental Ba/F3 cells, GNF-2 did not inhibit cell growth up to 10 μM, and Das-CHO-II had a GI_{50} of 2.8 μM, giving them therapeutic indices of >22 and 5.2, respectively (**Table 5.2**). Combining the two agents did very little to change the GI_{50} values in Parental Ba/F3 cells. The combination of GNF-2 with 100 nM Das-CHO-II still did not inhibit cell growth up to 10 μM, and the combination of Das-CHO-II with 200 nM GNF-2 had a GI_{50} of 1.5 μM. These combinations now gave respective therapeutic indices of >590 and 2,800 (**Table 5.2**).

Table 5.2. GI_{50} values for GNF-2, Das-CHO-II, GNF-2 + 100 nM Das-CHO-II, and Das-CHO-II + 200 nM GNF-2 in both BCR-Abl Ba/F3 and Parental Ba/F3 cells demonstrating improvements in potency and therapeutic index

	BCR-Abl Ba/F3 GI_{50} (nM)	**Improvement in Potency**	**Parental Ba/F3 GI_{50} (nM)**	**Therapeutic Index**
GNF-2	450		>10,000	>22
Das-CHO-II	550		2,800	5
GNF-2 + 100 nM Das-CHO-II	17	26X	>10,000	>590
Das-CHO-II + 200 nM GNF-2	0.55	1000X	1,500	2,700

These data are exciting; however, Ba/F3 cell lines are stably transfected, murine cells, so we wanted to test the combination of GNF-2 and Das-CHO-II in a human CML cell line. We tested for synergy between the two in K562 cells along with constant concentration combinations. Gratifyingly, we observed both synergy and an improvement in potency. In K562, the CI_{50} was 0.47 and the GI_{50} of both GNF-2 and Das-CHO-II increased approximately 4 fold when combined with a constant concentration (GI_{50}) of the other (**Table 5.3**). Finally, using

previously synthesized BODIPY-labeled analogs of our Type II and CHO inhibitors, termed Das-DFGO-II-BODIPY and Das-CHO-II-BODIPY,[20] respectively, we investigated the effect of GNF-2 on the EC_{50} of the two probes. As expected, the EC_{50} of Das-CHO-II-BODIPY improved with 1 μM GNF-2 while the EC_{50} of Das-DFGO-II-BODIPY remained relatively unchanged (**Appendix D**).

Table 5.3. GI_{50} Values of GNF-2, Das-CHO-II, GNF-2 + 65 nM Das-CHO-II, and Das-CHO-II + 800 nM GNF-2 in K562 cells demonstrating an improvement in potency when combined.

	GI_{50} (nM)	**Improvement in Potency**
GNF-2	808	
Das-CHO-II	64	
GNF-2 + 65 nM Das-CHO-II	215	4X
Das-CHO-I + 800 nM GNF-2	16	4X

Overcoming GNF-2 Resistance Mutants

We sought to understand why GNF-2 cannot bind to mutant forms of Abl where the mutation is at a site distinct from the myristate-binding site. We first evaluated several mutants reported in the literature that are not present in the myristate pocket but are resistant to GNF-2 inhibition: P112S, S229P, and the clinical mutation T315I.[8] We evaluated GNF-2 in a continuous activity assay[22] with each mutant and found that GNF-2 could not inhibit any of them (**Appendix D**). Since they do not cause GNF-2 resistance due to steric occlusion, we hypothesized that these mutants cause c-Abl to adopt an open conformation, while GNF-2 binds a closed conformation. We first evaluated each mutant using the protease assay. Gratifyingly, every mutant caused the kinase to adopt an open conformation (**Figure 5.5**). A separate report has validated our finding that T315I Abl adopted a more open conformation than wild-type.[23] Our findings now provided a rationale as to why GNF-2 cannot bind other mutations that occur well away from the binding site.

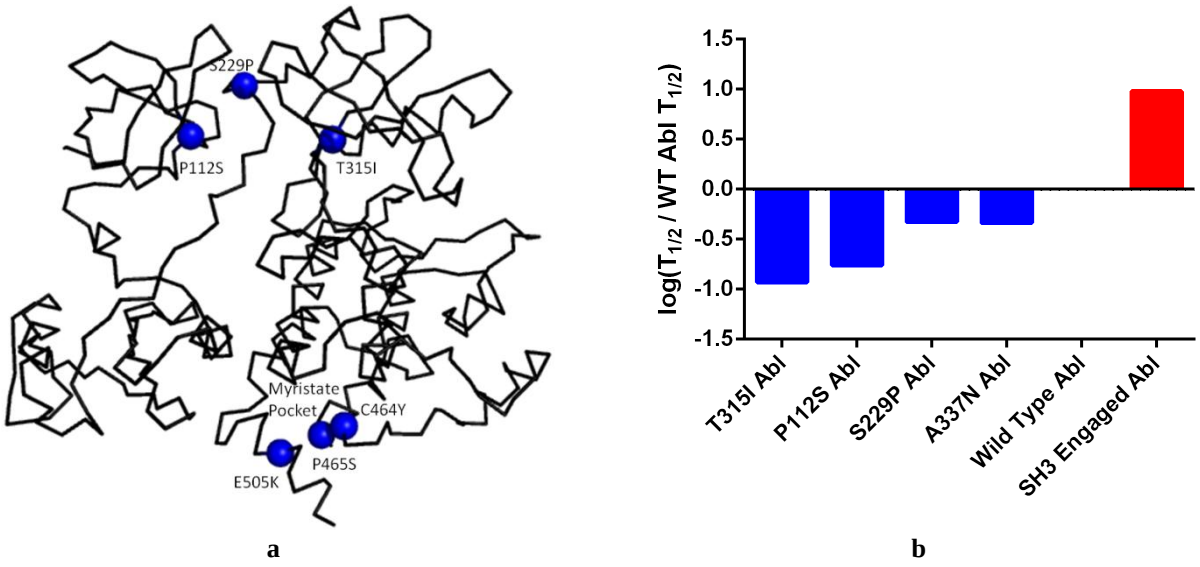

Figure 5.5. GNF-2 resistant mutants. (**a**) Mutants that show resistance to GNF-2 both in the myristate pocket (lower right) and distal sites[8] (**b**) The open conformation of the distal mutants shown in comparison to the A337N open conformation, apo c-Abl, and SH3 engaged closed conformation controls.

Given its clinical importance, we decided to focus the rest of our efforts on T315I Abl. We wanted to investigate whether the combination of GNF-2 and Das-CHO might affect the global conformation of T315I. We found that both inhibitors alone closed T315I slightly; however, they were still more open than wild-type Abl. The combination of the two, however, was capable of closing T315I to a level more closed than wild-type c-Abl. We then hypothesized that the combination of the GNF-2 and Das-CHO-II would be capable of overcoming T315I resistance in T315I Abl Ba/F3 cells.

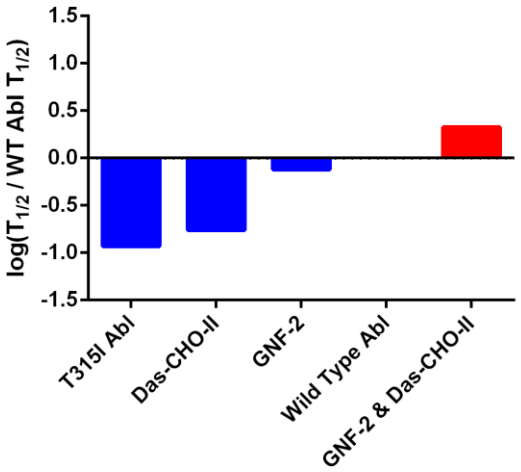

Figure 5.6. Global conformation of GNF-2, Das-CHO-II, and a combination of the two in T315I Abl demonstrating that the combination changes the conformation of the T315I mutation while neither compound alone can.

Alone, both compounds poorly inhibit T315I Abl Ba/F3 growth; GI_{50}(GNF-2) > 10 μM and GI_{50}(Das-CHO-II) = 3.2 μM (**Table 5.4**). Combining them, however, was far more effective. When added at a constant concentration below the GI_{50} (2 μM), the GI_{50} values for GNF-2 and Das-CHO-II improved remarkably, 1.8 μM and 127.9 nM, respectively. This 25 fold improvement for Das-CHO-II improved the therapeutic index against T315I Ba/F3 cells over Parental Ba/F3 cells from 0.9 to 22. Furthermore, when combined with GNF-2, the GI_{50} of Das-CHO-II in T315I Abl Ba/F3 cells was even better than Das-CHO-II alone in BCR-Abl Ba/F3 cells, which is truly remarkable.

Table 5.4. GI_{50} Values for GNF-2, Das-CHO-II, GNF-2 + 2 μM Das-CHO-II, and Das-CHO-II + 2 μM GNF-2 in T315I Abl Ba/F3 cells that show the improvement in potency achieved when Das-CHO-II and GNF-2 are combined

	GI_{50} (μM)	**Improvement in Potency**
GNF-2	>10	
Das-CHO-II	3.2	
GNF-2 + 2 μM Das-CHO-II	1.8	>5.6X
Das-CHO-II + 2 μM GNF-2	0.13	25X

Conclusions

This chapter describes a better understanding of the interaction between allosteric and ATP-competitive inhibitors of c-Abl. Since the discovery of imatinib to treat CML, there has been a huge interest in the development of c-Abl inhibitors. There is a wealth of ATP-competitive approved Abl inhibitors as well as a highly selective allosteric inhibitor, GNF-2. Using a newly developed protease accessibility assay, we evaluated the global conformation that these different inhibitors cause c-Abl to adopt. GNF-2 causes c-Abl to adopt a closed conformation, unlike any approved ATP-competitive inhibitors, which all cause an open conformation. We then turned to recently developed conformation selective inhibitors of c-Abl. Das-CHO-II binds c-Abl in an αC-helix-out conformation, which should close the kinase. We validated this using our protease assay. Gratifyingly, the conformation an inhibitor caused c-Abl to adopt, as determined using the protease assay, was directly related to synergy. GNF-2 did not show synergy with inhibitors that opened c-Abl and showed very strong synergy with inhibitors that closed it. We then evaluated how this synergy would play out in terms of cellular efficiency. The GI_{50} values for both GNF-2 and Das-CHO-II were determined in BCR-Abl Ba/F3 cells. Most remarkable was the fact that Das-CHO-II had a sub-nanomolar GI_{50} when combined with a constant, sub-GI_{50} concentration of GNF-2. This was incredibly exciting result. Furthermore, the

combination of Das-CHO-II and GNF-2 was able to overcome the common, clinical T315I mutation in cells even though both inhibitors were >2 μM inhibitors in T315I expressing Ba/F3 cells alone. Not only did we discover a highly synergistic combination between an ATP-competitive inhibitor and the allosteric c-Abl inhibitor GNF-2, we were also able to directly predict if a combination would show synergy based on the global conformation the inhibitor caused c-Abl to adopt, as determined by a protease accessibility assay.

Materials and Methods

General Biochemical Methods

Black, opaque-bottom 96 well plates were purchased from Nunc. All proteins were expressed in *E.coli* using previously published procedures.[24] Data were obtained using Biotek Synergy Mx and Biotek Synergy 4 plate readers. Curve fitting was done using Graphpad Prism 6 software.

Determination of Inhibitor IC_{50} Values against 3D Abl.

A continuous fluorescence assay was used to determine IC_{50}. The reaction volume was 100 μL consisting of 85 μL of enzyme in buffer, 2.5 μL of the appropriate inhibitor dilution (typically 10000, 3333.33, 1111.11, 370.37, 123.46, 41.15, 13.72, 4.57, 1.52, and 0 μM in DMSO), and 2.5 μL (2.4 mM in DMSO) of a substrate peptide.[25] The reaction was initiated with 10 μL of ATP (50 mM in water unless otherwise noted), and reaction progress was immediately monitored at 405 nm (ex. 340 nm) for 10 minutes. Reactions had final concentrations of 30 nM enzyme (unless otherwise noted), 60 μM peptide substrate, 5 mM ATP, 100 μM Na_3VO_4, 100 mM Tris buffer (pH 8), 10 mM $MgCl_2$, 0.01% Triton X-100. The initial rate data collected was used for determination of IC_{50} values. For IC_{50} determination, the kinetic values were obtained directly from nonlinear regression of substrate-velocity curves in the presence of various concentrations of the inhibitor. The equation Y = Bottom + (Top – Bottom)/(1 + 10^X – $LogEC_{50}$), X = log(concentration) and Y = binding; was used in the nonlinear regression. An IC_{50} value was determined for each inhibitor using at least three independent experiments (unless otherwise noted). The individual IC_{50} values for the three runs were then averaged. A representative inhibition curve of a single run is shown in **Appendix D**.

General procedure for BODIPY probe EC_{50} determination.

A fluorescence polarization was used to determine EC_{50} values. Reaction volumes of 50 µL were used in 96-well plates. 34 µL of buffer (50 mM Tris buffer (pH 8), 10 mM NaCl, 5% Glycerol, 1 mM DTT) was added to a single row, followed by 15 µL of enzyme (3.3X concentration) in buffer with 2-fold dilutions (typically 150, 75, 37.5, 18.75, 9.375, 4.69, 2.34, 1.17, 0.586, 0.293, and 0 nM final well concentration). Then, 1 µL of a 500 nM stock of the appropriate dasatinib analog BODIPY probe in DMSO was added (2% DMSO final). Wells were incubated on ice for 30 minutes prior to fluorescence polarization read (ex/em 485/535 nm). After the initial read, 1 µL of 51 µM GNF-2 was added to each well for a final concentration of 1 µM GNF-2. Following another 30 minute incubation on ice, the wells were read again. Reactions had final concentrations of 10 nM BODIPY-probe, 50 mM Tris buffer (pH 8), 10 mM NaCl, 5% Glycerol, 1 mM DTT. For K_d determination, the mPolarization values (normalized to the 0 nM protein control) were plotted vs. varying protein concentrations. The equation Y = (Bmax * X)/(EC_{50} + X), X = Protein concentration and Y = FP response; was used in the nonlinear regression. In two separate runs, the EC_{50} value was determined using at least four independent experiments. The EC_{50} value determined from the two separate runs was averaged. A single representative inhibition curve with error bars is shown in **Appendix D**.

General Procedure for Proteolysis Half-Life Determination

c-Abl was diluted in proteolysis buffer (50 mM Tris-HCl pH 8.0, 100 mM NaCl, 0.5 mM $CaCl_2$) to yield a final protein concentration of 2 µM. This was followed by the addition 1 µL of a 10 mM stock of each compound being tested to give a final concentration of 57 µM compound. 15 µL of the protein/compound solution was added to 5 µL of 50 mM EDTA as the 0 min time point. The proteolysis reaction was initiated by adding Thermolysin (purchased from Promega, catalog number: V4001) from a 3.8 µM stock solution to a final concentration of 50 nM. At various time points (2, 5, 10, 30, 60, 90, 120, 180, and 240 mins), 15 µL of the proteolysis reaction was added to 5 µL of 50 mM EDTA to quench proteolysis. The quenched samples were analyzed by SDS-PAGE (12 % Bis-Tris gel in MES running buffer, staining with coomassie blue). Band intensities were analyzed by ImageJ imaging software. Percent protein remaining was plotted against time and fit to an exponential decay equation using GraphPad Prism software

to obtain half-lives of each protein. Each half-life was determined using a single experiment, with the exception of WT Abl in order to demonstrate assay reproducibility. The half-life curves are shown along with the gel for each apo protein (**Appendix D**).

***General procedure for cellular characterization*.**

1. Cell culture and seeding: All Ba/F3 and K562 cell lines were cultured in RPMI 1640 media with 10% FBS. Parental Ba/F3 cell culture additionally contained 15% WEHI-3 conditioned media. An aliquot of the cells was mixed with Trypan Blue solution and the cell number was quantified using a hemocytometer. The cells were plated 100 μL in each well at 30,000 cells/mL so that each well contained 3,000 cells. The cells were plated into sterile, clear bottom 96 well plates and then immediately dosed with compound. Additionally, 3 wells were created containing 100 μL of media with no cells.

2. Dosing: The compounds were made in 100% DMSO at 1,000X the final concentrations that were desired for the assay generally covering a concentration range of 6 log units. These DMSO stocks were diluted 10X in RPMI 1640 media. 1 μL of the compound diluted in media was added to each well for a final concentration of 0.1% DMSO. The wells containing only media were not dosed. In general, each compound concentration was dosed in triplicate wells. The plates were returned to normal culture conditions (per ATCC) for 72 hours.

3. Assay: After 72 hours, the plates were removed from the incubator, and 10 μL of WST-1 reagent was added to each well. The plates were returned to the incubator and the color change was visually monitored for 0.5 – 2 hours. When sufficient color change had occurred, the plates were shaken on a plate shaker for 30 seconds, and absorbance at 450 and 630 nm was read in a Biotek Synergy 4 plate reader. The absorbance at 630 nm was subtracted from the absorbance at 450 nm.

4. Data Analyses: The average absorbance value from wells containing media without cells was subtracted from the absorbance value for all the wells containing cells. The absorbance values were then taken as a percentage of the absorbance for the vehicle wells (0.1% DMSO - no compound). The percent compared to vehicle was then plotted vs. log(Concentration). Data analyses and curve fitting were performed using Graphpad Prism 6. For each compound, there were n = 3 data points for each concentration. For curves that did not reach full inhibition, the bottom was set to -10. The curves with error bars are shown in **Appendix D**.

General procedure for cellular synergy.

1. Cell culture and seeding: All Ba/F3 and K562 cell lines were cultured in RPMI 1640 media with 10% FBS. Parental Ba/F3 cell culture additionally contained 15% WEHI-3 conditioned media. An aliquot of the cells was mixed with trypan blue solution and the cell number was quantified using a hemacytometer. The cells were plated 100 μL in each well at 30,000 cells/mL so that each well contained 3,000 cells. The cells were plated into sterile, clear bottom 96 well plates and then immediately dosed with compound.

2. Dosing: The compounds dilutions (2X) and combinations were made in 100% DMSO at 1,000X the final concentrations that were desired for the assay. These DMSO stocks were diluted 10X in RPMI 1640 media. 1 μL of the compound diluted in media was added to each well for a final concentration of 0.1% DMSO. The wells containing only media were not dosed. In general, each compound concentration was dosed in triplicate wells. The plates were returned to normal culture conditions (per ATCC) for 72 hours.

3. Assay: After 72 hours, the plates were removed from the incubator and 10 μL of WST-1 reagent was added to each well. The plates were returned to the incubator and the color change was visually monitored for 0.5 – 2 hours. When sufficient color change had occurred, the plates were shaken on a plate shaker for 60 seconds and read in a Biotek Synergy 4 plate reader.

4. Data Analyses: The average absorbance value from wells containing media without cells was subtracted from the absorbance value for all the wells containing cells. The data were then calculated as a fraction of the vehicle well (1% DMSO) and subtracted from 1 in order to represent the data as the fraction of population affected by the treatment at each given dose. The data were then analyzed using Compusyn to determine the combination indices. The curves and isobolograms are shown in **Appendix D**.

References

(1) Kurzrock, R.; Gutterman, J. U.; Talpaz, M. The Molecular Genetics of Philadelphia Chromosome–Positive Leukemias. *N. Engl. J. Med.* **1988**, *319* (15), 990–998.

(2) Druker, B. J.; Guilhot, F.; O'Brien, S. G.; Gathmann, I.; Kantarjian, H.; Gattermann, N.; Deininger, M. W. N.; Silver, R. T.; Goldman, J. M.; Stone, R. M.; Cervantes, F.; Hochhaus, A.; Powell, B. L.; Gabrilove, J. L.; Rousselot, P.; Reiffers, J.; Cornelissen, J. J.; Hughes, T.; Agis, H.; Fischer, T.; Verhoef, G.; Shepherd, J.; Saglio, G.; Gratwohl, A.; Nielsen, J. L.; Radich, J. P.; Simonsson, B.; Taylor, K.; Baccarani, M.; So, C.; Letvak, L.;

Larson, R. A. Five-Year Follow-up of Patients Receiving Imatinib for Chronic Myeloid Leukemia. *N. Engl. J. Med.* **2006**, *355* (23), 2408–2417.

(3) O'Hare, T.; Eide, C. A.; Deininger, M. W. Bcr-Abl Kinase Domain Mutations and the Unsettled Problem of Bcr-AblT315I: Looking into the Future of Controlling Drug Resistance in Chronic Myeloid Leukemia. *Clin. Lymphoma Myeloma Leuk.* **2016**, *7*, S120–S130.

(4) Prasad, V.; Mailankody, S. The Accelerated Approval of Oncologic Drugs: Lessons from Ponatinib. *JAMA* **2014**, *311* (4), 353–354.

(5) Cortes, J. E.; Kim, D.-W.; Pinilla-Ibarz, J.; le Coutre, P.; Paquette, R.; Chuah, C.; Nicolini, F. E.; Apperley, J. F.; Khoury, H. J.; Talpaz, M.; DiPersio, J.; DeAngelo, D. J.; Abruzzese, E.; Rea, D.; Baccarani, M.; Müller, M. C.; Gambacorti-Passerini, C.; Wong, S.; Lustgarten, S.; Rivera, V. M.; Clackson, T.; Turner, C. D.; Haluska, F. G.; Guilhot, F.; Deininger, M. W.; Hochhaus, A.; Hughes, T.; Goldman, J. M.; Shah, N. P.; Kantarjian, H. A Phase 2 Trial of Ponatinib in Philadelphia Chromosome–Positive Leukemias. *N. Engl. J. Med.* **2013**, *369* (19), 1783–1796.

(6) Adrián, F. J.; Ding, Q.; Sim, T.; Velentza, A.; Sloan, C.; Liu, Y.; Zhang, G.; Hur, W.; Ding, S.; Manley, P.; Mestan, J.; Fabbro, D.; Gray, N. S. Allosteric Inhibitors of Bcr-Abl-Dependent Cell Proliferation. *Nat. Chem. Biol.* **2006**, *2* (2), 95–102.

(7) Iacob, R. E.; Zhang, J.; Gray, N. S.; Engen, J. R. Allosteric Interactions between the Myristate- and ATP-Site of the Abl Kinase. *PLoS One* **2011**, *6* (1), e15929.

(8) Zhang, J.; Adrián, F. J.; Jahnke, W.; Cowan-Jacob, S. W.; Li, A. G.; Iacob, R. E.; Sim, T.; Powers, J.; Dierks, C.; Sun, F.; Guo, G.-R.; Ding, Q.; Okram, B.; Choi, Y.; Wojciechowski, A.; Deng, X.; Liu, G.; Fendrich, G.; Strauss, A.; Vajpai, N.; Grzesiek, S.; Tuntland, T.; Liu, Y.; Bursulaya, B.; Azam, M.; Manley, P. W.; Engen, J. R.; Daley, G. Q.; Warmuth, M.; Gray, N. S. Targeting Bcr-Abl by Combining Allosteric with ATP-Binding-Site Inhibitors. *Nature* **2010**, *463* (7280), 501–506.

(9) Nagar, B.; Hantschel, O.; Young, M. A.; Scheffzek, K.; Veach, D.; Bornmann, W.; Clarkson, B.; Superti-Furga, G.; Kuriyan, J. Structural Basis for the Autoinhibition of c-Abl Tyrosine Kinase. *Cell* **2003**, *112* (6), 859–871.

(10) Khateb, M.; Ruimi, N.; Khamisie, H.; Najajreh, Y.; Mian, A.; Metodieva, A.; Ruthardt, M.; Mahajna, J. Overcoming Bcr-Abl T315I Mutation by Combination of GNF-2 and ATP Competitors in an Abl-Independent Mechanism. *BMC Cancer* **2012**, *12* (1), 563–572.

(11) Fabbro, D.; Manley, P. W.; Jahnke, W.; Liebetanz, J.; Szyttenholm, A.; Fendrich, G.; Strauss, A.; Zhang, J.; Gray, N. S.; Adrian, F.; Warmuth, M.; Pelle, X.; Grotzfeld, R.; Berst, F.; Marzinzik, A.; Cowan-Jacob, S. W.; Furet, P.; Mestan, J. Inhibitors of the Abl Kinase Directed at Either the ATP- or Myristate-Binding Site. *Biochim. Biophys. Acta* **2010**, *1804* (3), 454–462.

(12) Skora, L.; Mestan, J.; Fabbro, D.; Jahnke, W.; Grzesiek, S. NMR Reveals the Allosteric Opening and Closing of Abelson Tyrosine Kinase by ATP-Site and Myristoyl Pocket Inhibitors. *Proc. Natl. Acad. Sci.* **2013**, *110* (47), E4437–E4445.

(13) Chou, T.-C. Theoretical Basis , Experimental Design , and Computerized Simulation of Synergism and Antagonism in Drug Combination Studies. *Pharmacol. Rev.* **2007**, *58* (3), 621–681.

(14) Chou, T.-C. Drug Combination Studies and Their Synergy Quantification Using the Chou-Talalay Method. *Cancer Res.* **2010**, *70* (2), 440–446.

(15) Chou, T.-C.; Talalay, P. Quantitative Analysis of Dose-Effect Relationships: The Combined Effects of Multiple Drugs or Enzyme Inhibitors. *Adv. Enzym. Regul.* **1984**, *22*, 27–55.
(16) Filippakopoulos, P.; Kofler, M.; Hantschel, O.; Gish, G. D.; Grebien, F.; Salah, E.; Neudecker, P.; Kay, L. E.; Turk, B. E.; Superti-Furga, G.; Pawson, T.; Knapp, S. Structural Coupling of SH2-Kinase Domains Links Fes and Abl Substrate Recognition and Kinase Activation. *Cell* **2016**, *134* (5), 793–803.
(17) Grebien, F.; Hantschel, O.; Wojcik, J.; Kaupe, I.; Kovacic, B.; Wyrzucki, A. M.; Gish, G. D.; Cerny-Reiterer, S.; Koide, A.; Beug, H.; Pawson, T.; Valent, P.; Koide, S.; Superti-Furga, G. Targeting the SH2-Kinase Interface in Bcr-Abl Inhibits Leukemogenesis. *Cell* **2011**, *147* (2), 306–319.
(18) Panjarian, S.; Iacob, R. E.; Chen, S.; Wales, T. E.; Engen, J. R.; Smithgall, T. E. Enhanced SH3/Linker Interaction Overcomes Abl Kinase Activation by Gatekeeper and Myristic Acid Binding Pocket Mutations and Increases Sensitivity to Small Molecule Inhibitors. *J. Biol. Chem.* **2013**, *288* (9), 6116–6129.
(19) Hantschel, O.; Nagar, B.; Guettler, S.; Kretzschmar, J.; Dorey, K.; Kuriyan, J.; Superti-Furga, G. A Myristoyl/Phosphotyrosine Switch Regulates c-Abl. *Cell* **2003**, *112* (6), 845–857.
(20) Kwarcinski, F. E.; Brandvold, K. R.; Phadke, S.; Beleh, O. M.; Johnson, T. K.; Meagher, J. L.; Seeliger, M. A.; Stuckey, J. A.; Soellner, M. B. Conformation-Selective Analogues of Dasatinib Reveal Insight into Kinase Inhibitor Binding and Selectivity. *ACS Chem. Biol.* **2016**, *11* (5), 1296–1304.
(21) Furet, P.; Grotzfeld, R. M.; Jones, D. B.; Manley, P.; Marzinzik, A.; Pelle, X. F. A.; Salem, B.; Schoepfer, J. Preparation of Benzamide Derivatives for Inhibiting the Activity of ABL1, ABL2 and BCR-ABL1 for Treating Cancer and Viral Infections. WO 2013/171642 A1, 2013.
(22) Wang, Q.; Cahill, S. M.; Blumenstein, M.; Lawrence, D. S. Self-Reporting Fluorescent Substrates of Protein Tyrosine Kinases. *J. Am. Chem. Soc.* **2006**, *128* (6), 1808–1809.
(23) Badger, J.; Grover, P.; Shi, H.; Panjarian, S. B.; Engen, J. R.; Smithgall, T. E.; Makowski, L. C-Abl Tyrosine Kinase Adopts Multiple Active Conformational States in Solution. *Biochemistry* **2016**, *55* (23), 3251–3260.
(24) Seeliger, M. A.; Young, M.; Henderson, M. N.; Pellicena, P.; King, D. S.; Falick, A. M.; Kuriyan, J. High Yield Bacterial Expression of Active c-Abl and c-Src Tyrosine Kinases. *Protein Sci.* **2005**, *14*, 3135–3139.
(25) Rabuck, J. N.; Hyung, S.-J.; Ko, K. S.; Fox, C. C.; Soellner, M. B.; Ruotolo, B. T. Activation State-Selective Kinase Inhibitor Assay Based on Ion Mobility-Mass Spectrometry. *Anal. Chem.* **2013**, *85* (15), 6995–7002.

CHAPTER VI

Conclusions and Future Directions

Abstract

Kinases are a important enzymes for transmitting cellular signals. Kinase inhibitors have worked successfully as drugs and tools to understand kinase signaling in cells. Most kinase inhibitors, however, bind in the conserved ATP-binding pocket often rendering them promiscuous. To create more selective inhibitors, we explored kinase inhibitors that interacted with other sites of the kinase. This was a successful strategy for creating selective kinase inhibitors. Most importantly, though, we learned about the important role that the global conformation of a kinase plays. Furthermore, some inhibitors, even ones that only bind in the conserved ATP-binding pocket, are capable of modulating kinase global conformation. This has important implications involving potential synergy between inhibitors, especially in cells.

Bivalent Inhibitors of Protein Tyrosine Kinases

Bivalent inhibitors are inhibitors capable of binding two sites of a protein simultaneously. They have the advantage of being more potent and selective than a single binding site inhibitor. In **Chapters II** and **IV**, we created bivalent inhibitors of the protein tyrosine kinases c-Src and c-Abl, respectively. We used a modular strategy where the two binding pieces were conjugated using azide-alkyne click chemistry. We synthesized several ATP-competitive inhibitors with pendant alkynes that could be conjugated to several non-ATP-binding pocket molecules with pendant azides. In this way, we could mix the pieces accordingly to create several different bivalent inhibitors with different properties.

In c-Src, we began by conjugating a promiscuous amino-pyrazole to an optimal c-Src SH2 peptide to create bivalent inhibitor **2.3**. The bivalent inhibitor was designed such that the linker would be too short to reach between the two binding sites when the kinase was in a closed, autoinhibited state. The linker was only long enough when the kinase was in an open, more

flexible conformation. Bivalent inhibitor **2.3** was 18X more potent than either binding portion alone in full length c-Src and 25X more potent for c-Src than a homologous kinase c-Abl, which optimally binds a different SH2 peptide than c-Src. Most interesting, however, was the fact that bivalent inhibitor **2.3** was also selective for c-Src over other Src family kinases (SKFs) which bind the same optimal SH2 peptide.[1,2] This further verified the idea that the global conformation of the kinase plays a role in inhibitor binding. Our bivalent inhibitor was specifically designed to bind the open, flexible conformation of c-Src. Not surprisingly then, the only SFK that bound bivalent inhibitor **2.3** with less than micromolar affinity was Fyn1, which other research has shown to be more flexible than other SFKs.[3]

For the bivalent inhibitor of c-Abl, we used the dasatinib-cyclooctyne as the ATP-binding portion of our bivalent inhibitor. We chose dasatinib-cyclooctyne because it is a dual c-Src/c-Abl inhibitor, and we wanted to demonstrate how a bivalent strategy could turn a dual inhibitor into one specific for a single target. GNF-2, an allosteric inhibitor that is uniquely selective to c-Abl, was conjugated to create bivalent inhibitor **4.2**. This inhibitor was too potent to be fully evaluated using our continuous activity assay.[4] We then used the services provided by Luceome Biotechnologies to determine IC_{50} values for **4.2** in full-length and kinase domain c-Abl, as well of full-length c-Src. We found that **4.2** was 10X more potent for full-length c-Abl, which further shows the effect that kinase global conformation has on inhibitor binding. It was also 25X more potent for c-Abl than c-Src validating our hypothesis that we could transform a dual c-Src/c-Abl inhibitor into an inhibitor specific for c-Abl. Furthermore, this bivalent inhibitor was cell permeable, and can be used as a selective inhibitor for c-Abl in cells.

Both bivalent inhibitors should be further investigated in cells. Inhibitor **4.2** is cell permeable so we could immediately begin more in-depth cellular assays; however, we would have to create a cell permeable version of **2.3**. Bivalent inhibitor **2.3** is likely not cell permeable due to the anionic nature of peptide **2.2**. This could be rectified by appending a cell-permeabilizing peptide to **2.2**. Our lab has successfully used a nona-arginine tail to create cell permeable, bivalent inhibitors.[5,6] Since our bivalent inhibitors interact with sites outside the ATP-binding pocket (where most kinase inhibitors bind), it would be interesting to see how the down-stream signaling effects are different from ATP-competitive inhibitors. For example, the SH2 domain in c-Src is important for substrate recognition and scaffolding. As such, by binding the SH2 domain as well as the ATP-binding pocket, I think we would observe different

downstream effects. For example, c-Src inhibits prolactin (PLR) induced mitogenesis by inhibiting Jak2 phosphorylation; however, pharmacological inhibition of c-Src does not affect Jak2 signaling.[7] Furthermore, a construct of c-Src without the kinase domain containing only the SH2 and SH3 domains was still capable of inhibiting PLR-induced Jak2 phosphorylation suggesting that the scaffolding functions, not the catalytic function of c-Src, were the driving force in this interaction.[8] I hypothesize that a cell permeable version of **2.3** would pharmacologically validate these findings. As such, more in-depth cellular studies with **2.3** and **4.2** should be performed.

Allosteric Modulator of c-Src Kinase

Chapter III highlights our work to identify an allosteric modulator of c-Src capable of altering the global conformation of the kinase. Using a thermal shift assay, we screened a 1,000 compound library from Maybridge for binding to full-length c-Src. It was very important to use full-length c-Src since we desired a compound that would affect global conformation. We defined hits as compounds that changed the Tm of c-Src by greater than three standard deviations from the negative control. Using these parameters, we identified 37 hits (~4% hit rate). We then used a protease accessibility assay to determine how these compounds affected the global conformation of c-Src. Of the 37 hits, we decided to only pursue the two that caused the greatest change in c-Src global conformation (both adopted a more open conformation). We then tested the effect of these hits upon c-Src activity using a continuous activity assay.[4] One had no effect upon c-Src activity; however, the other (**1-E8**) proved to be an activator of c-Src. This confirmed our hypothesis that the global conformation a small molecule stabilized in a kinase would affect catalytic activity correspondingly.

We then wanted to establish a general binding site for activator **1-E8**. We first determined that **1-E8** has no activity against pY527 (the phosphotyrosine responsible for the closed, autoinhibited conformation of c-Src). This suggested that **1-E8** binds somewhere inaccessible in the closed conformation of c-Src, possibly the linker region. We also found that **1-E8** has no activity when competing with a pFAK peptide.[9] Furthermore, it causes a significant increase in the EC_{50} of Src SH2 peptide **2.21**. Taken together, these data suggest that **1-E8** binds in or near the SH2 domain of c-Src.

We established that activator **1-E8** was selective for c-Src compared to two homologous kinases, c-Abl and Hck. **1-E8** has essentially no effect upon the activity of either. Since both possess an SH2 domain and Hck recognizes the same optimal peptide sequence as c-Src, it seems likely that the effect of **1-E8** is unique to the global conformation of c-Src. This continues to demonstrate the importance global conformation plays in inhibitor binding. With a selective c-Src modulator, we wanted to see what effect we would observe in c-Src dependent cells. In HT-29 cells, **1-E8** did not inhibit cell growth at concentrations up to 10 μM. When added to an inhibitor also known to bind an open conformation, however, the GI_{50} of that inhibitor improved twofold. We believe that **1-E8** was able to stabilize an open conformation of c-Src that allowed the other inhibitor to bind more easily and better inhibit the growth of c-Src dependent cells.

Since our data demonstrate that **1-E8** decreases the binding affinity of c-Src SH2 domain peptide **2.21**, there is a possibility that it binds in the same location as **2.21**. If that were the case, it would be interesting to create an analog of c-Src bivalent inhibitor **2.3** using **1-E8** instead of **2.2**. This would create a non-peptidic, bivalent inhibitor of c-Src. Given that bivalent inhibitor **4.2**, which utilizes the same linker, is cell permeable, it would feasible that a bivalent inhibitor composed of **1-E8** and **2.1** would also be cell permeable. This would eliminate the need for the cell-permeabilizing peptides described above. As such, this proposed, small molecule bivalent inhibitor could be utilized in cells in the same manner described above.

Synergy between Allosteric and Orthosteric Inhibitors

Our work in **Chapter V** provides an in-depth investigation into the interplay between allosteric and active-site inhibitors and how the global conformation that a kinase adopts greatly affects this interaction. Specifically, we focused on the allosteric inhibitor of c-Abl, GNF-2, and various approved and non-approved ATP-competitive inhibitors. We started by using the Chou-Talalay method in BCR-Abl Ba/F3 cells to evaluate synergy between GNF-2 and dasatinib, nilotinib, imatinib, and ponatinib.[10,11] Contrary to reported results,[12] none of these inhibitors showed synergy with GNF-2. Using the same protease accessibility assay mentioned previously, we then assessed the conformation that each of these inhibitors stabilized in c-Abl. GNF-2 bound a closed conformation in c-Abl while every ATP-competitive inhibitor bound a very open conformation. We then hypothesized that only an ATP-competitive inhibitor that bound a closed conformation in c-Abl would show synergy with GNF-2.

We then demonstrated that a αC-helix-out inhibitor developed in our lab (Das-CHO-II),[13] stabilized a closed c-Abl conformation. As expected, it was the only ATP-competitive inhibitor to show synergy with GNF-2. Furthermore, combining the two agents caused drastic improvements in their cellular GI_{50} values. The GI_{50} for Das-CHO-II in BCR-Abl Ba/F3 cells improved 1000X when a constant, sub-GI_{50} concentration of GNF-2 was added. This combination virtually no effect in Parental Ba/F3 cells giving a therapeutic index of 2,700. In a patient derived CML cell line, K562, we saw that adding a constant concentration (the GI_{50}) of one compound (GNF-2 or Das-CHO-II) to the GI_{50} curve of the other resulted in a fourfold improvement in potency.

Additionally, GNF-2 has been combined with nilotinib in order to overcome the common and difficult to treat T315I clinical mutation.[12,14,15] We did not observe synergy between the two inhibitors, so we wanted to see if a synergistic combination of would also overcome the T315I mutation. First, we evaluated the global conformation of T315I c-Abl and observed that it was much more open conformation than WT c-Abl, which would explain why GNF-2 cannot bind the T315I mutation despite the fact that the mutation occurs well away from the binding site of GNF-2. Next, we observed that the combination of GNF-2 and Das-CHO-II caused the T315I mutation to adopt a closed conformation when neither agent could alone. This was encouraging and prompted us to try combining Das-CHO-II and GNF-2 in T315I Abl Ba/F3 cells. Alone, GNF-2 showed no growth inhibition up to 10 μM and the GI_{50} for Das-CHO-II was 3.2 μM. When 2 μM of GNF-2 was added to the GI_{50} curve of Das-CHO-II, however, we observed a 25X improvement in growth inhibition. Through these experiments, we demonstrated the importance of the global conformation that a kinase inhibitor stabilizes.

This project has very important implications for drug combination therapy. Currently, Novartis is developing a combination therapy for CML using nilotinib and a GNF-2 analog.[16,17] We have shown, however, that nilotinib is not synergistic with GNF-2, and an αC-helix-out inhibitor was the only ATP-competitive inhibitor to show synergy with GNF-2. As such, a combination therapy between Das-CHO-II and GNF-2 has the potential to be even more successful. To move forward, the combination of Das-CHO-II and GNF-2 should be carried forward into animals. Besides its use in cells, the Chou-Talalay method can be utilized in animals to determine a synergistic combination, which would further validate the synergy seen in cells.[18] In this case, we may want to investigate more analogs of Das-CHO-II and GNF-2. GNF-2

is already known to not have favorable PK properties; however, analogs are being developed.[12,17] Additionally, our lab is moving forward to develop more αC-helix-out inhibitors of c-Abl.

Conclusions

We have demonstrated several strategies for targeting kinases outside of the ATP-binding pocket. We created bivalent inhibitors and discovered allosteric modulators. Both the bivalent and allosteric small molecules exploited the global conformation of the kinase they bound. Furthermore, we investigated the interplay between allosteric and active-site inhibitors. Knowing that inhibitor binding relies so heavily on kinase global conformation, we surprised that very little thought had previously been given to the global conformations inhibitors caused when trying to find synergistic combinations. We used a protease accessibility to determine kinase global conformation stabilized by small molecules and used it to predict combinations that would be synergistic. So often, kinase inhibitor discovery focuses on the kinase domain since that is where the catalytic action takes place, but we have shown that considerations about the global conformation are crucial.

References

(1) Zhou, S.; Shoelson, S.; Chaudhuri, M.; Gish, G.; Pawson, T.; Haser, W.; King, F.; Roberts, T.; Ratnofsky, S.; Lechleider, R.; Neel, B.; Birge, R.; Fajardo, J.; Chou, M.; Hanafusa, H.; Schaffhausen, B.; Cantley, L. SH2 Domains Recognize Specific Phosphopeptide Sequences. *Cell* **1993**, *72* (5), 767–778.

(2) Liu, B. A.; Jablonowski, K.; Shah, E. E.; Engelmann, B. W.; Jones, R. B.; Nash, P. D. SH2 Domains Recognize Contextual Peptide Sequence Information to Determine Selectivity. *Mol. Cell. Proteomics* **2010**, *9*, 2391–2404.

(3) Register, A. C.; Leonard, S. E.; Maly, D. J. SH2-Catalytic Domain Linker Heterogeneity Influences Allosteric Coupling across the SFK Family. *Biochemistry* **2014**, *53* (44), 6910–6923.

(4) Wang, Q.; Cahill, S. M.; Blumenstein, M.; Lawrence, D. S. Self-Reporting Fluorescent Substrates of Protein Tyrosine Kinases. *J. Am. Chem. Soc.* **2006**, *128* (6), 1808–1809.

(5) Brandvold, K. R.; Santos, S. M.; Breen, M. E.; Lachacz, E. J.; Steffey, M. E.; Soellner, M. B. Exquisitely Specific Bisubstrate Inhibitors of c-Src Kinase. *ACS Chem. Biol.* **2015**, *10*, 1387–1391.

(6) Wender, P. A.; Mitchell, D. J.; Pattabiraman, K.; Pelkey, E. T.; Steinman, L.; Rothbard, J. B. The Design, Synthesis, and Evaluation of Molecules That Enable or Enhance Cellular Uptake: Peptoid Molecular Transporters. *Proc. Natl. Acad. Sci.* **2000**, *97* (24), 13003–13008.

(7) Acosta, J. J.; Muñoz, R. M.; González, L.; Subtil-Rodríguez, A.; Dominguez-Caceres, M. A.; García-Martínez, J. M.; Calcabrini, A.; Lazaro-Trueba, I.; Martín-Pérez, J. Src

Mediates Prolactin-Dependent Proliferation of T47D and MCF7 Cells via the Activation of Focal Adhesion kinase/Erk1/2 and Phosphatidylinositol 3-Kinase Pathways. *Mol. Endocrinol.* **2003**, *17* (11), 2268–2282.

(8) García-Martínez, J. M.; Calcabrini, A.; González, L.; Martín-Forero, E.; Agulló-Ortuño, M. T.; Simon, V.; Watkin, H.; Anderson, S. M.; Roche, S.; Martín-Pérez, J. A Non-Catalytic Function of the Src Family Tyrosine Kinases Controls Prolactin-Induced Jak2 Signaling. *Cell. Signal.* **2010**, *22* (3), 415–426.

(9) Moroco, J. A.; Baumgartner, M. P.; Rust, H. L.; Choi, H. G.; Hur, W.; Gray, N. S.; Camacho, C. J.; Smithgall, T. E. A Discovery Strategy for Selective Inhibitors of c-Src in Complex with the Focal Adhesion Kinase SH3/SH2-Binding Region. *Chem. Biol. Drug Des.* **2015**, *86* (2), 144–155.

(10) Chou, T.-C. Drug Combination Studies and Their Synergy Quantification Using the Chou-Talalay Method. *Cancer Res.* **2010**, *70* (2), 440–446.

(11) Warmuth, M.; Kim, S.; Gu, X.; Xia, G.; Adrián, F. Ba/F3 Cells and Their Use in Kinase Drug Discovery. *Curr. Opin. Oncol.* **2007**, *19* (1), 55–60.

(12) Zhang, J.; Adrián, F. J.; Jahnke, W.; Cowan-Jacob, S. W.; Li, A. G.; Iacob, R. E.; Sim, T.; Powers, J.; Dierks, C.; Sun, F.; Guo, G.-R.; Ding, Q.; Okram, B.; Choi, Y.; Wojciechowski, A.; Deng, X.; Liu, G.; Fendrich, G.; Strauss, A.; Vajpai, N.; Grzesiek, S.; Tuntland, T.; Liu, Y.; Bursulaya, B.; Azam, M.; Manley, P. W.; Engen, J. R.; Daley, G. Q.; Warmuth, M.; Gray, N. S. Targeting Bcr-Abl by Combining Allosteric with ATP-Binding-Site Inhibitors. *Nature* **2010**, *463* (7280), 501–506.

(13) Kwarcinski, F. E.; Brandvold, K. R.; Phadke, S.; Beleh, O. M.; Johnson, T. K.; Meagher, J. L.; Seeliger, M. A.; Stuckey, J. A.; Soellner, M. B. Conformation-Selective Analogues of Dasatinib Reveal Insight into Kinase Inhibitor Binding and Selectivity. *ACS Chem. Biol.* **2016**, *11* (5), 1296–1304.

(14) O'Hare, T.; Eide, C. A.; Deininger, M. W. Bcr-Abl Kinase Domain Mutations and the Unsettled Problem of Bcr-AblT315I: Looking into the Future of Controlling Drug Resistance in Chronic Myeloid Leukemia. *Clin. Lymphoma Myeloma Leuk.* **2016**, *7*, S120–S130.

(15) Prasad, V.; Mailankody, S. The Accelerated Approval of Oncologic Drugs: Lessons from Ponatinib. *JAMA* **2014**, *311* (4), 353–354.

(16) Wylie, A.; Schoepfer, J.; Berellini, G.; Cai, H.; Caravatti, G.; Cotesta, S.; Dodd, S.; Donovan, J.; Erb, B.; Furet, P.; Gangal, G.; Grotzfeld, R.; Hassan, Q.; Hood, T.; Iyer, V.; Jacob, S.; Jahnke, W.; Lombardo, F.; Loo, A.; Manley, P. W.; Marzinzik, A.; Palmer, M.; Pelle, X.; Salem, B.; Sharma, S.; Thohan, S.; Zhu, S.; Keen, N.; Petruzzelli, L.; Vanasse, K. G.; Sellers, W. R. ABL001, a Potent Allosteric Inhibitor of BCR-ABL, Prevents Emergence of Resistant Disease When Administered in Combination with Nilotinib in an *in Vivo* Murine Model of Chronic Myeloid Leukemia. *Blood* **2014**, *124* (21), 398.

(17) Furet, P.; Grotzfeld, R. M.; Jones, D. B.; Manley, P.; Marzinzik, A.; Pelle, X. F. A.; Salem, B.; Schoepfer, J. Preparation of Benzamide Derivatives for Inhibiting the Activity of ABL1, ABL2 and BCR-ABL1 for Treating Cancer and Viral Infections. WO 2013/171642 A1, 2013.

(18) Chou, T.-C. Theoretical Basis , Experimental Design , and Computerized Simulation of Synergism and Antagonism in Drug Combination Studies. *Pharmacol. Rev.* **2007**, *58* (3), 621–681.

APPENDIX A

Analytical Data for Chapter II

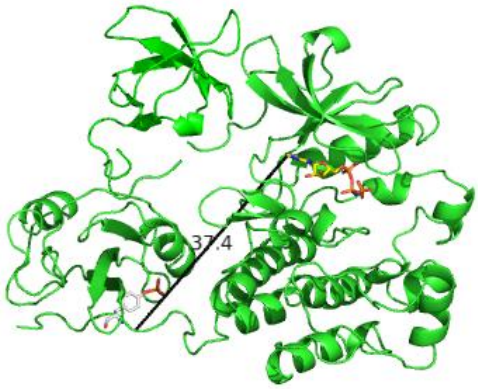

A

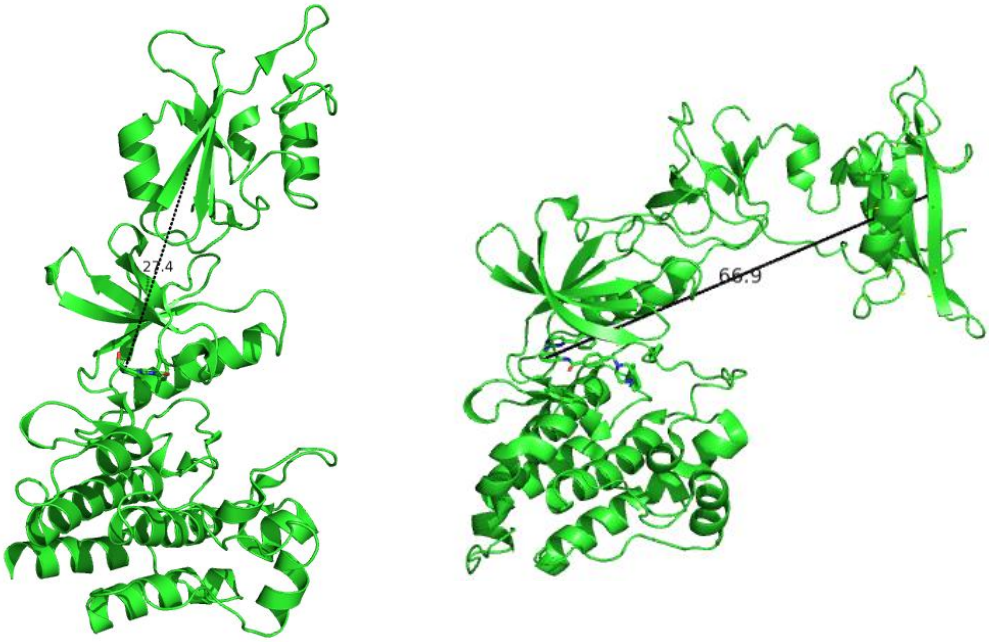

B

Figure A.1: Crystal structures showing measurements between the ATP-pocket and SH2 domain of protein tyrosine kinases in various conformations. **A)** Closed/inactive conformation (1.5 Å, PDB code: 2SRC) **B)** Open/active conformations exhibiting a variety of distances between the kinase domain and SH2 domain ranging from 27 Å (3.42 Å, PDB code: 1OPL) to 67 Å (1.91 Å, PDB code: 1Y57).

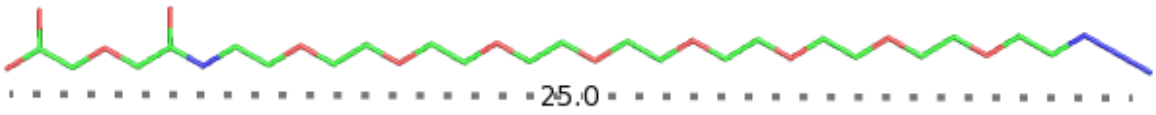

Figure A.2: PyMOL measurement in Angstroms of the PEG linker used to create **2.2** and bivalent inhibitors **2.3**, **2.4**, and **2.5**.

Spectral Data for Compounds 2.1-2.18.

2.7:

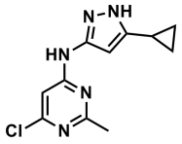

^{1}H:

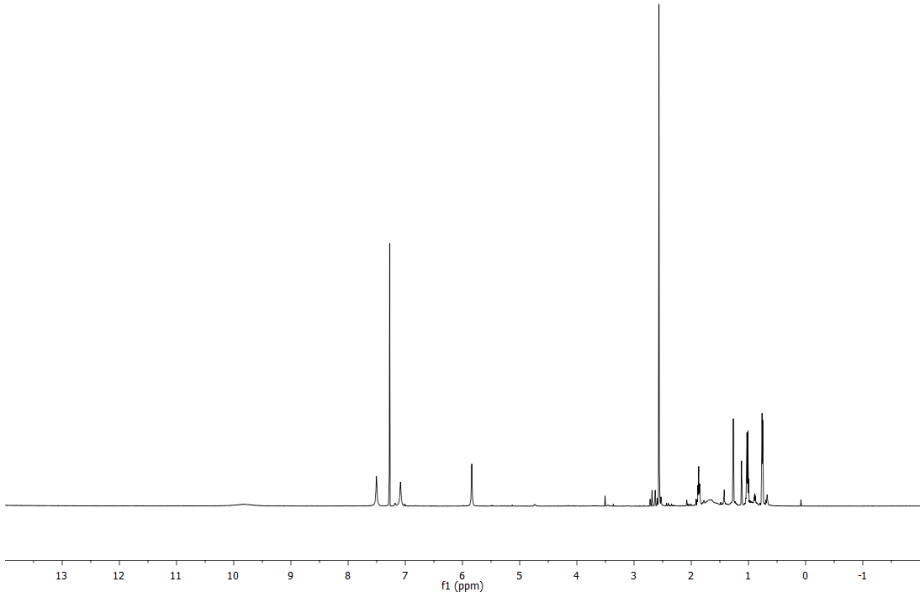

^{13}C:

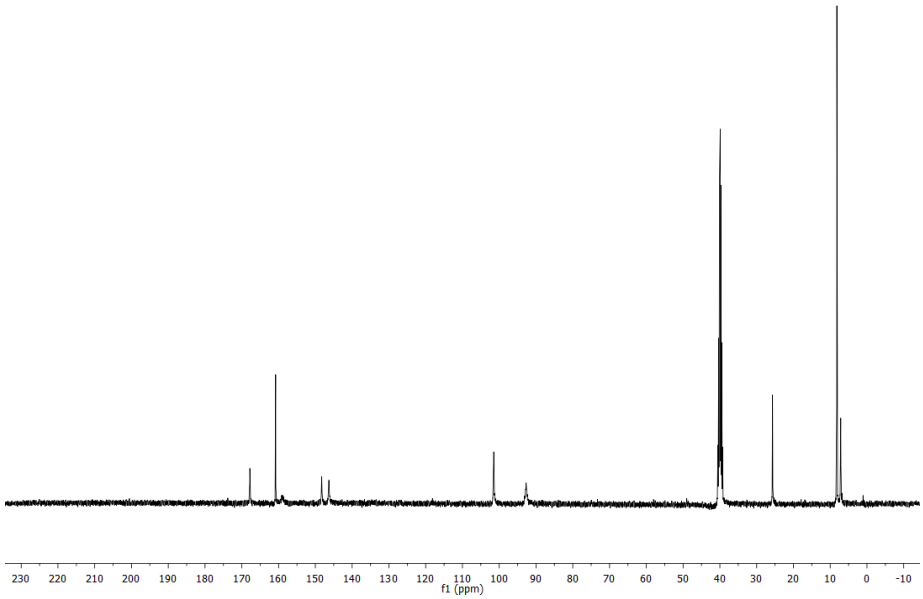

2.9:

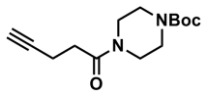
NBoc
N
O

^{1}H:

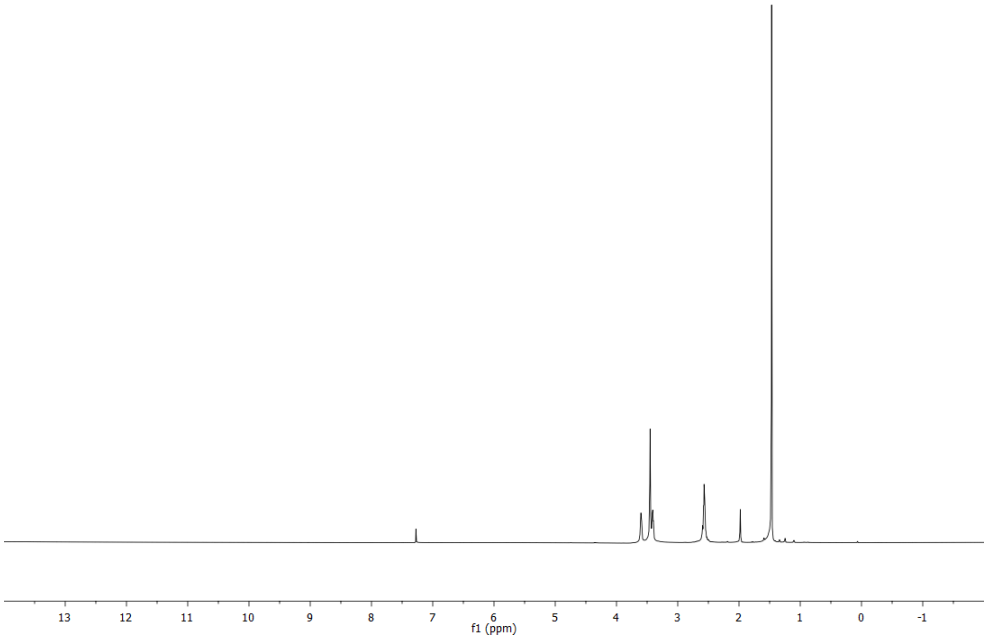
13 12 11 10 9 8 7 6 5 4 3 2 1 0 -1
f1 (ppm)

^{13}C:

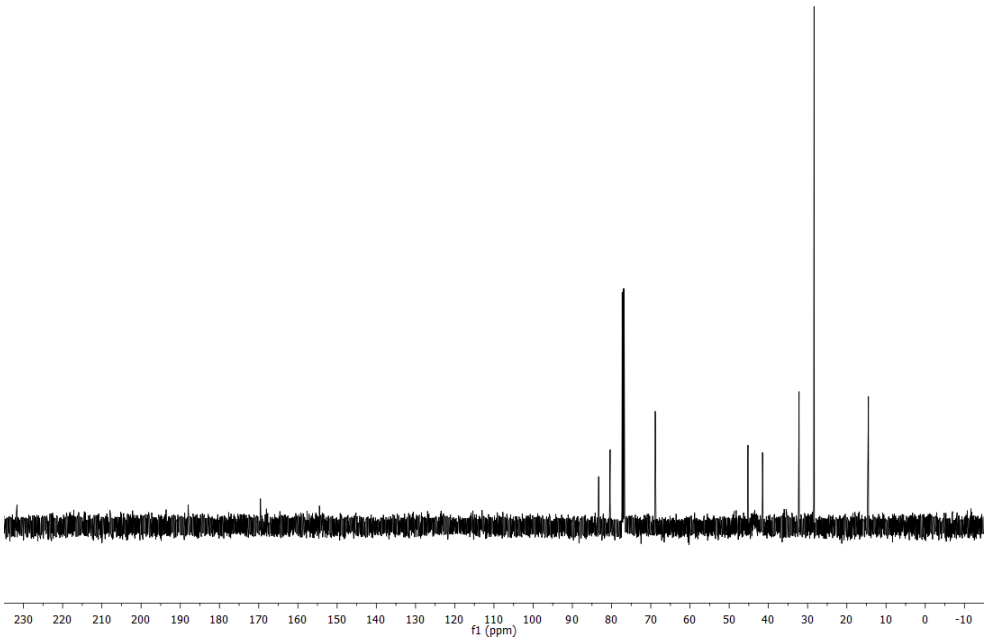
230 220 210 200 190 180 170 160 150 140 130 120 110 100 90 80 70 60 50 40 30 20 10 0 -10
f1 (ppm)

2.1:

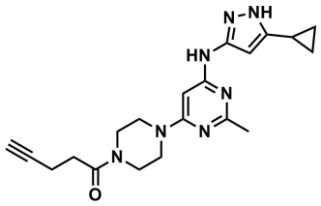

^{1}H:

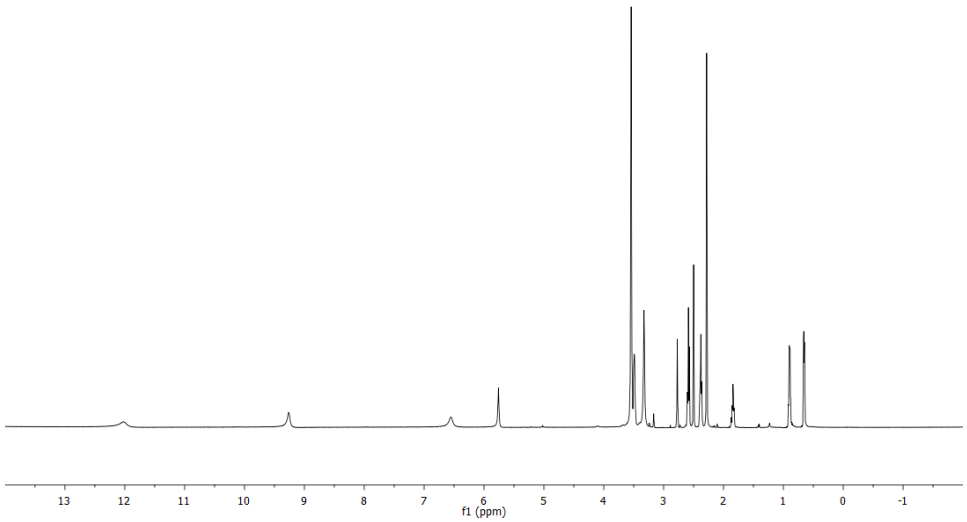
13
12
11
10
9
8
7
6
5
4
3
2
1
0
-1
f1 (ppm)

^{13}C:

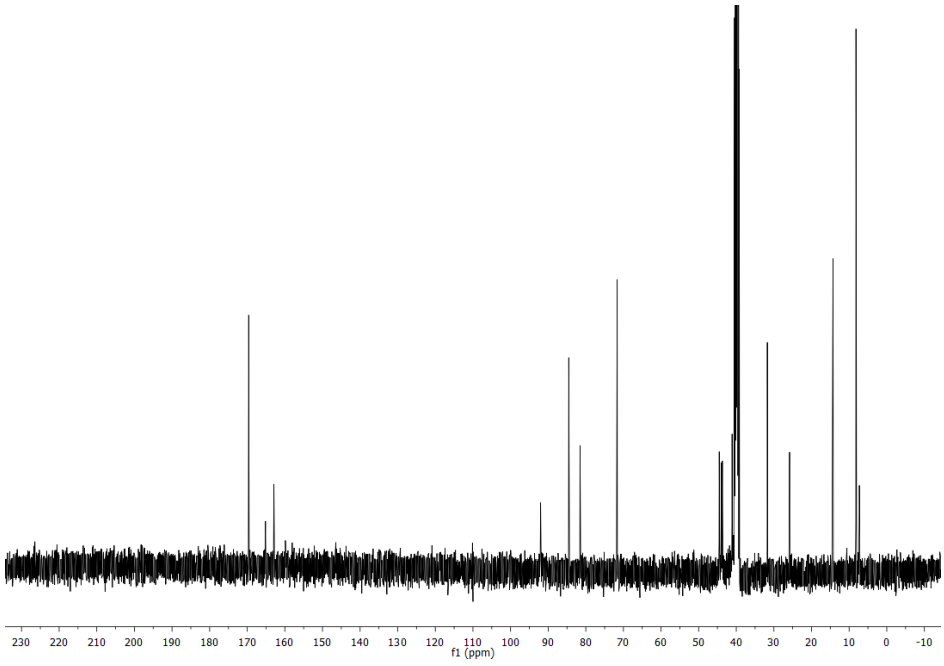
230
220
210
200
190
180
170
160
150
140
130
120
110
100
90
80
70
60
50
40
30
20
10
0
-10
f1 (ppm)

2.15:

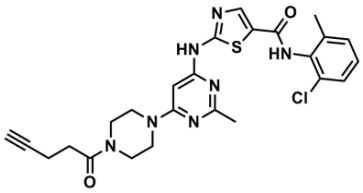

^{1}H:

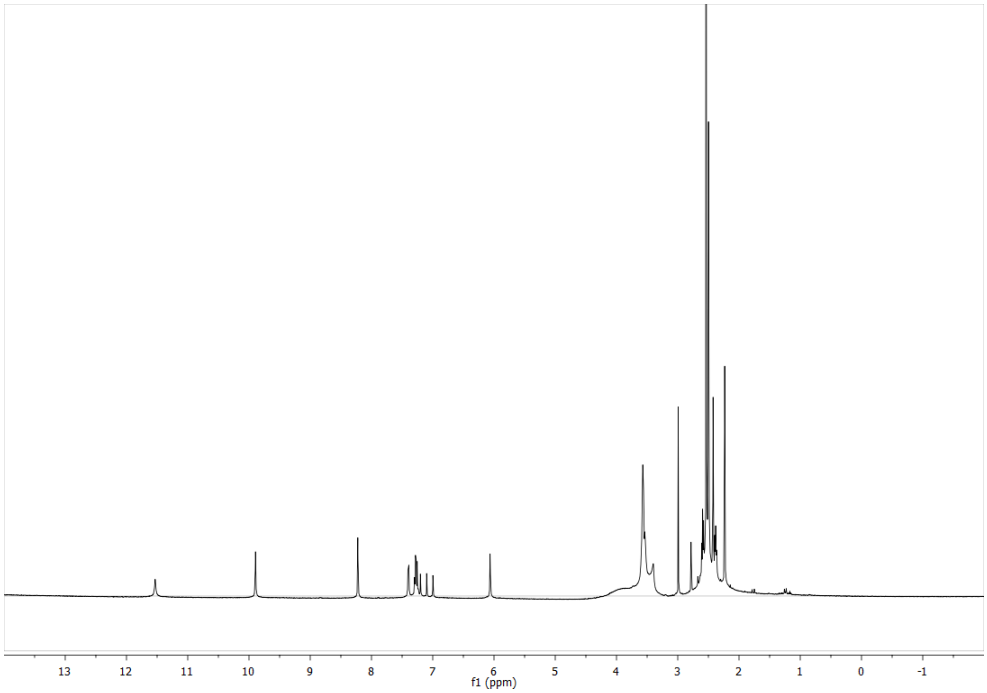
13
12
11
10
9
8
7
6
5
4
3
2
1
0
-1
f1 (ppm)

^{13}C:

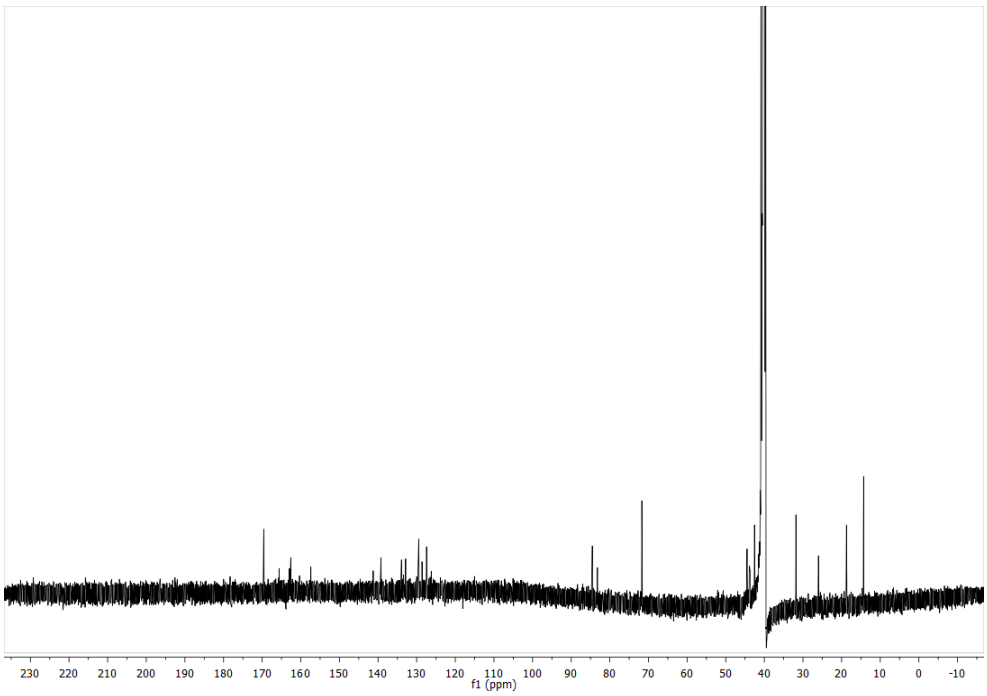
230
220
210
200
190
180
170
160
150
140
130
120
110
100
90
80
70
60
50
40
30
20
10
0
-10
f1 (ppm)

2.17:

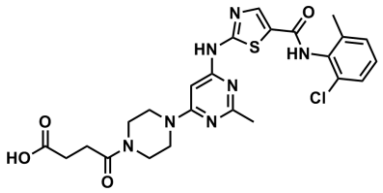

^{1}H:

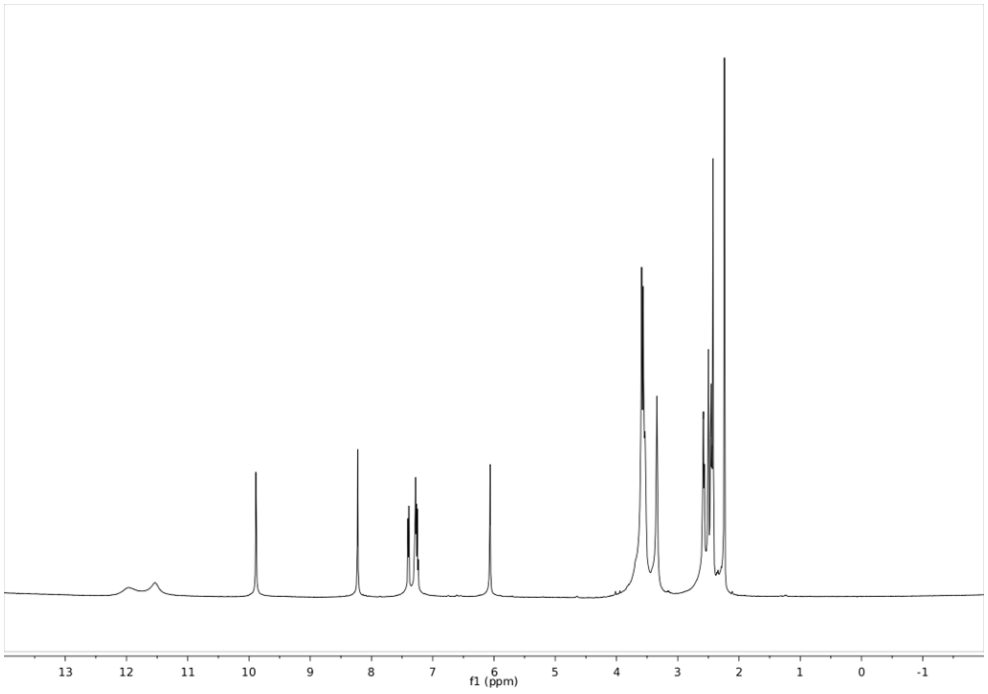
13 12 11 10 9 8 7 6 5 4 3 2 1 0 -1
f1 (ppm)

^{13}C:

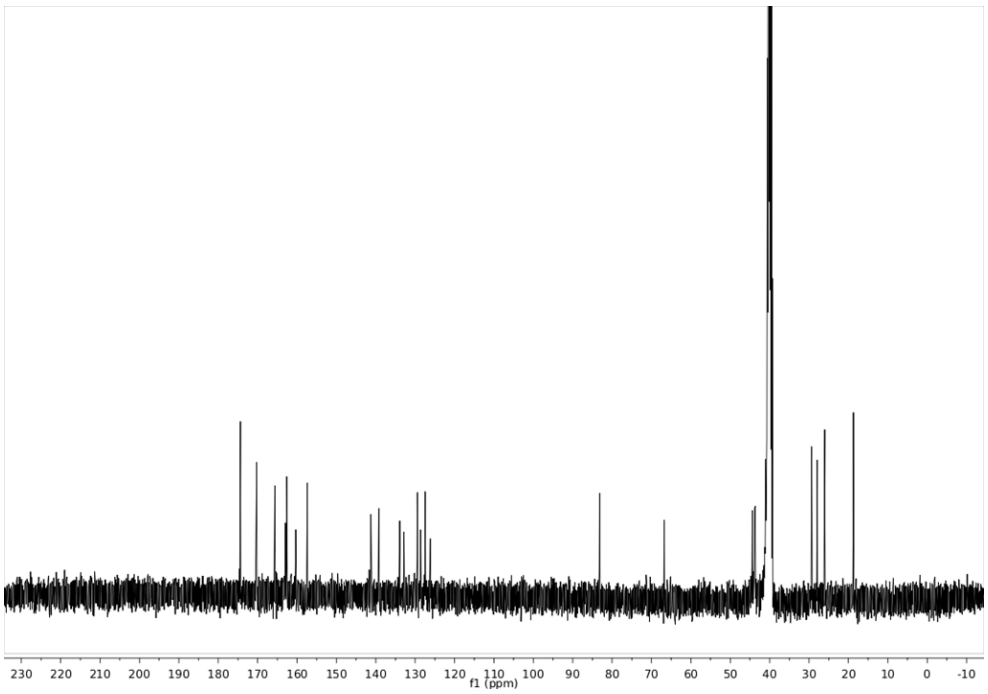
230 220 210 200 190 180 170 160 150 140 130 120 110 100 90 80 70 60 50 40 30 20 10 0 -10
f1 (ppm)

2.18:

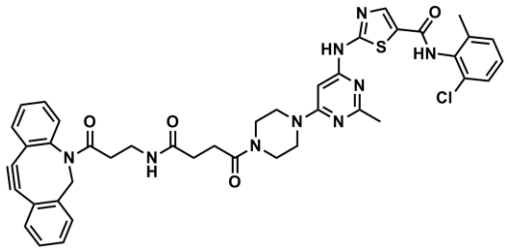

^{1}H:

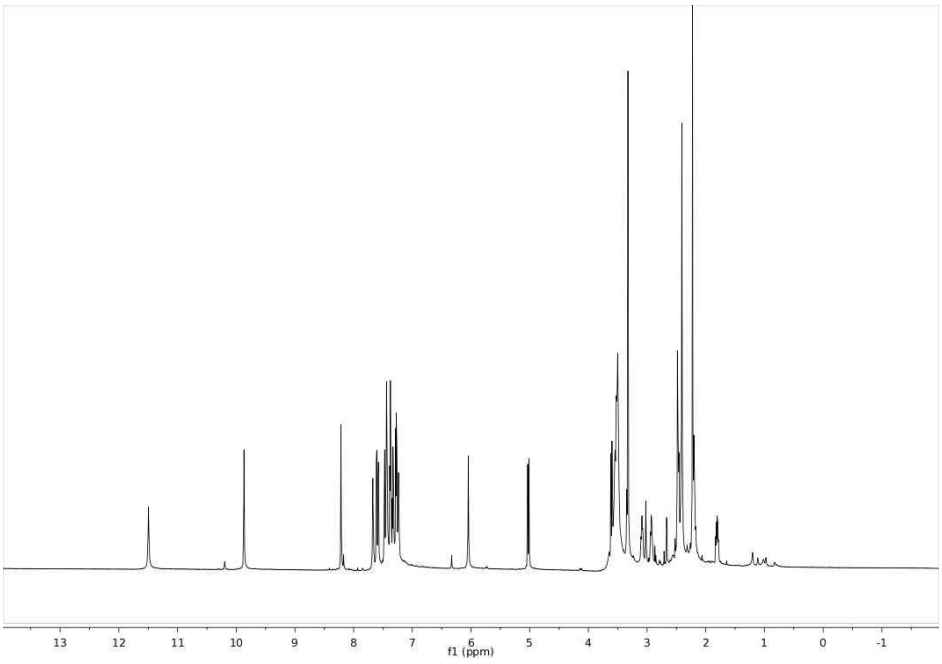
13 12 11 10 9 8 7 6 5 4 3 2 1 0 -1
f1 (ppm)

^{13}C:

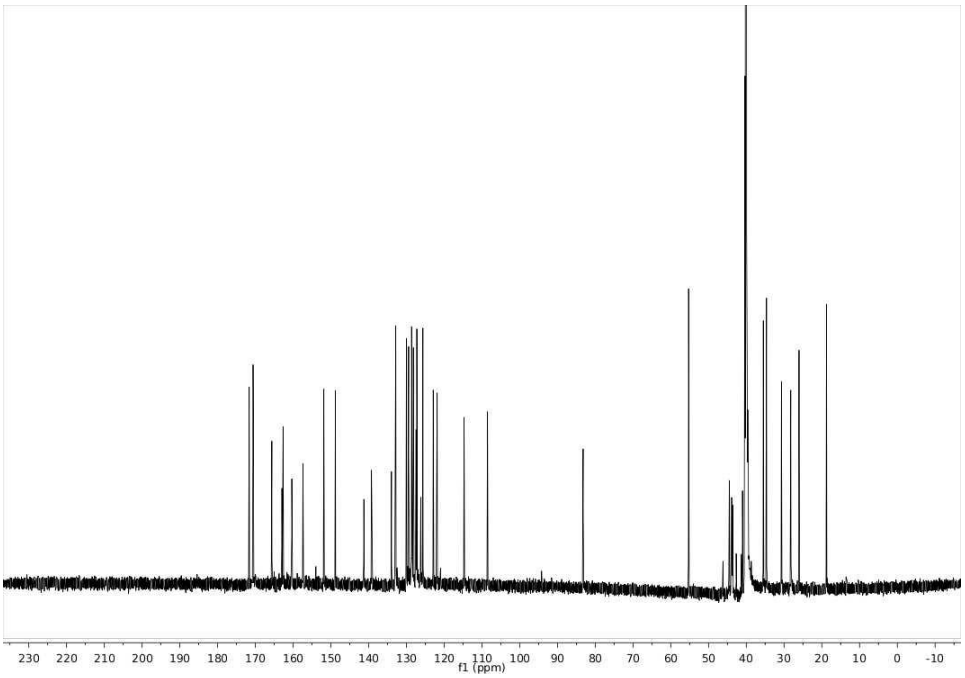
230 220 210 200 190 180 170 160 150 140 130 120 110 100 90 80 70 60 50 40 30 20 10 0 -10
f1 (ppm)

Analytical Data for IC_{50} Values against c-Src KD.

2.1:

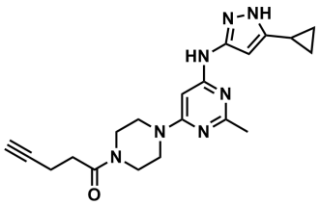

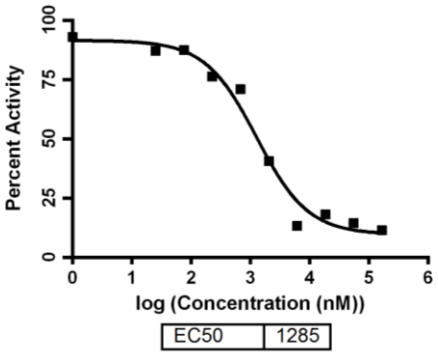

Avg IC_{50} = 1.3 ± 0.5 μM

2.3:

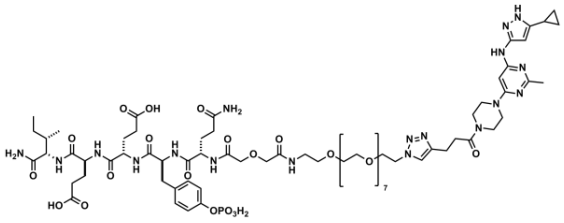

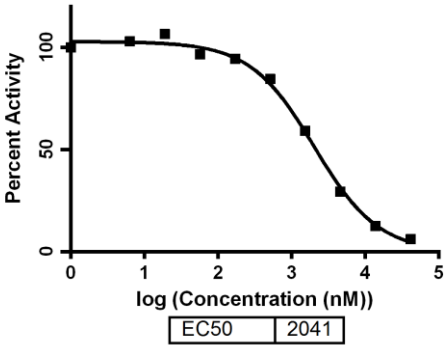

Avg IC_{50} = 2.1 ± 0.3 μM

2.15:

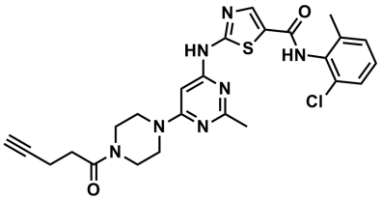

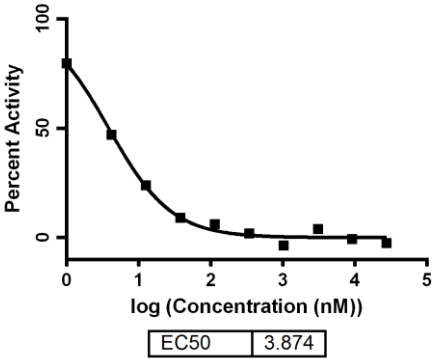

Avg IC_{50} < 10 nM

[ATP] = 5 mM

[Src] = 10 nM

2.4:

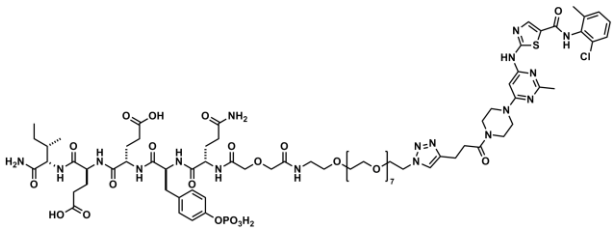

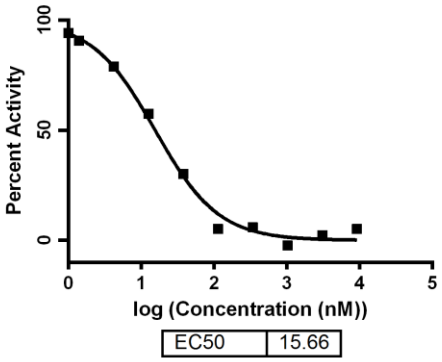

Avg IC_{50} < 10 nM

[ATP] = 5 mM

[Src] = 10 nM

Analytical Data for IC_{50} Values against 3D c-Src.

2.1:

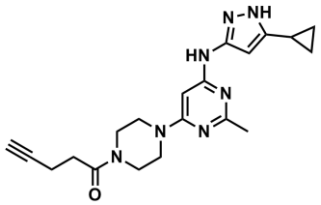

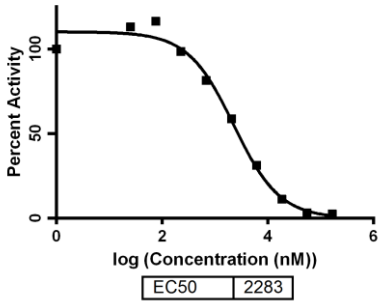

Avg IC_{50} = 2.9 ± 0.6 μM

2.3:

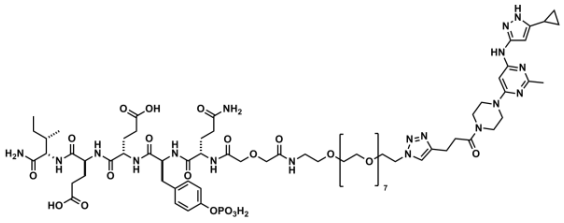

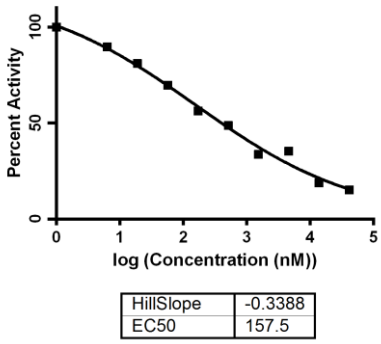

Avg IC_{50} = 160 ± 4 nM

2.15:

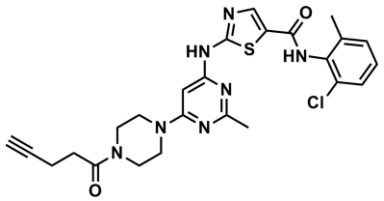

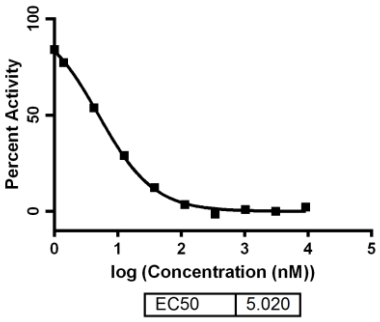

Avg IC_{50} < 10 nM

[ATP] = 5 mM

[Src] = 10 nM

2.4:

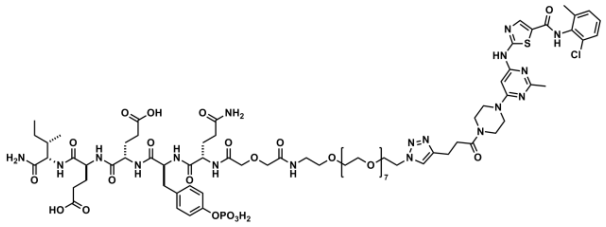

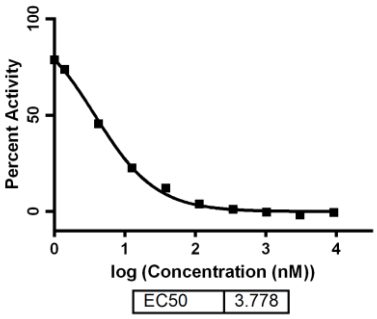

Avg IC_{50} < 10 nM

[ATP] = 5 mM

[Src] = 10 nM

2.5:

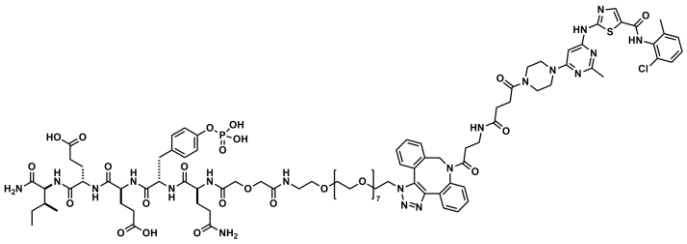

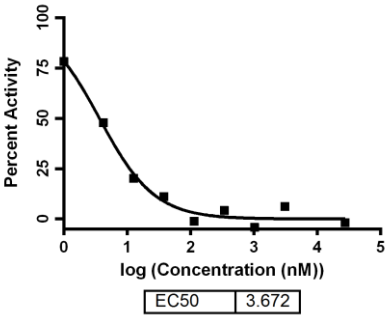

Avg IC_{50} < 10 nM

[ATP] = 5 mM

[Src] = 10 nM

2.21:

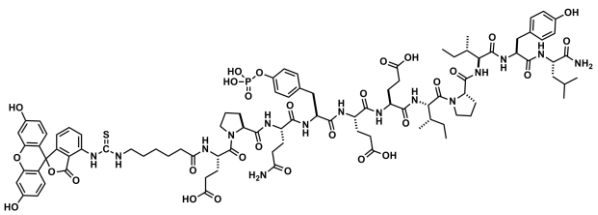

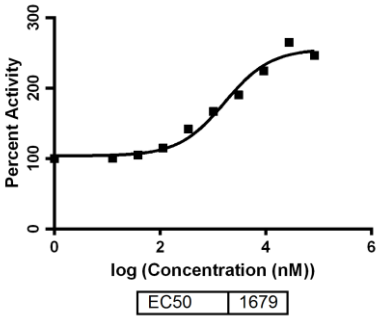

Avg EC_{50} (activation) = 1.6 ± 0.3 μM

Analytical data IC_{50} Values against Hck KD.

2.1:

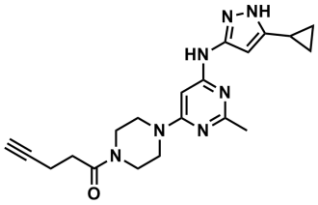

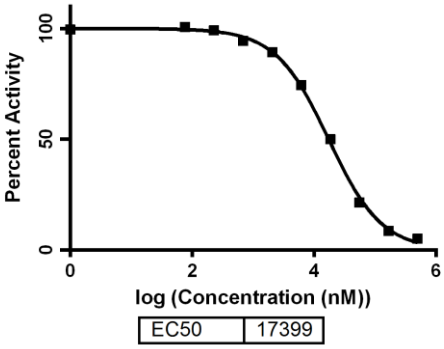

Avg IC_{50} = 20 ± 3 μM

2.3:

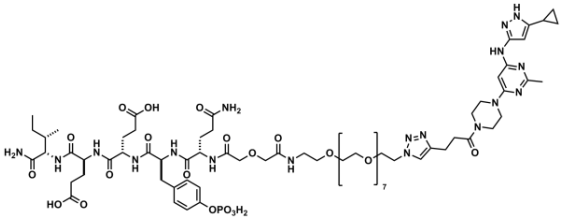

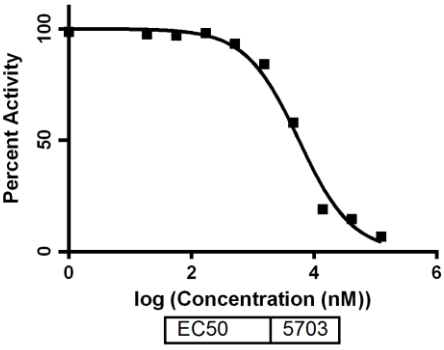

Avg IC_{50} = 6 ± 1 μM

Analytical Data for IC_{50} Values against 3D Hck.

2.1:

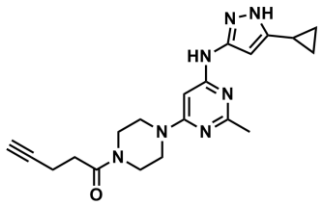

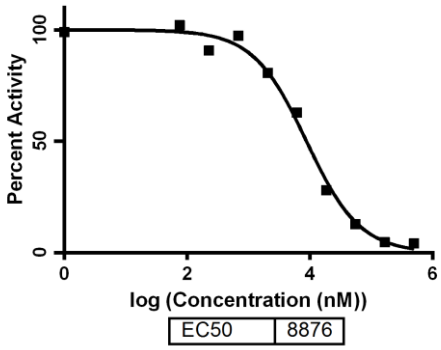

Avg IC_{50} = 8.9 ± 0.5 μM

2.3:

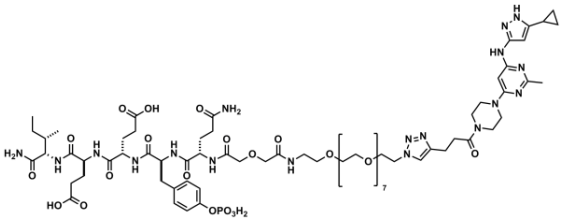

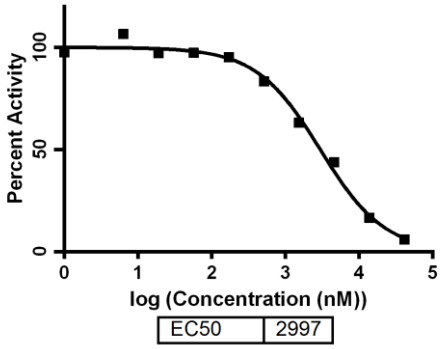

Avg IC_{50} = 2.8 ± 0.7 μM

Analytical Data for IC_{50} Values against T338M 3D c-Src.

2.1:

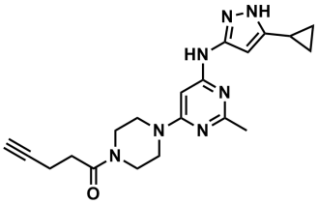

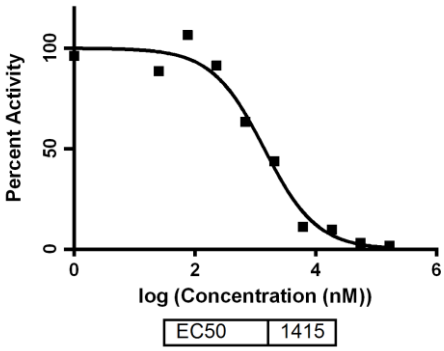

Avg IC_{50} = 1.2 ± 0.3 μM

2.3:

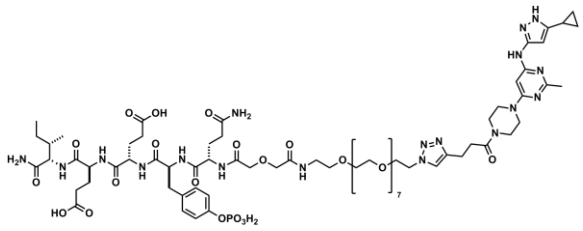

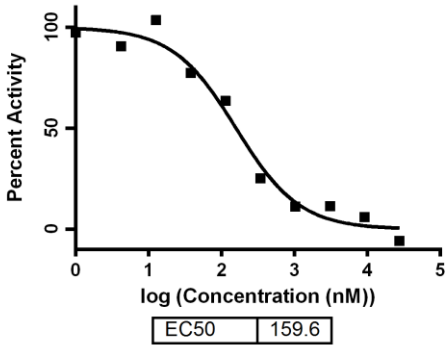

Avg IC_{50} = 189 ± 8 nM

Analytical Data for IC_{50} Values against pY416 3D c-Src.

2.1:

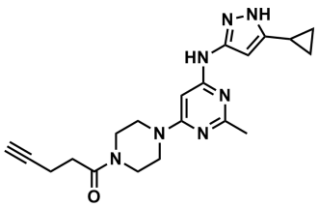

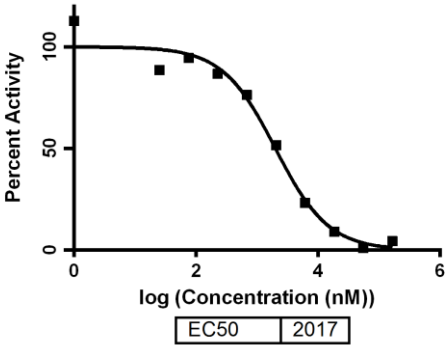

Avg IC_{50} = 2.4 ± 0.6 μM

2.3:

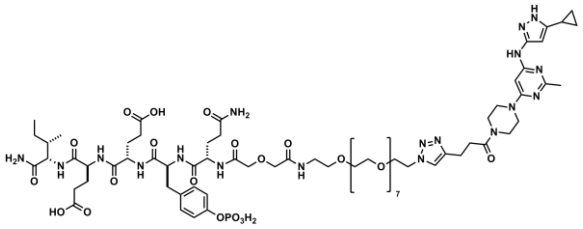

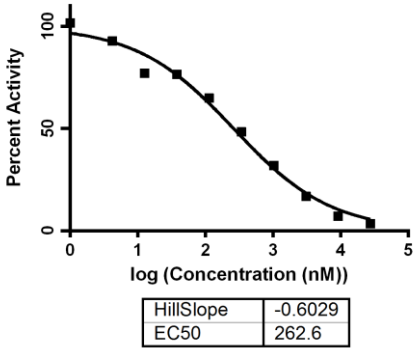

Avg IC_{50} = 240 ± 100 nM

Analytical Data for IC_{50} Values against pY527 3D c-Src.

2.1:

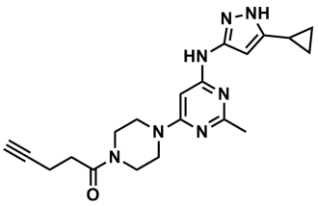

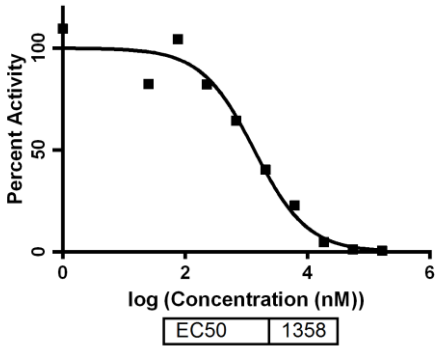

Avg IC_{50} = 1.38 ± 0.08 μM

2.3:

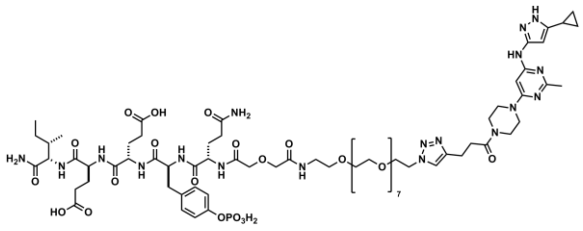

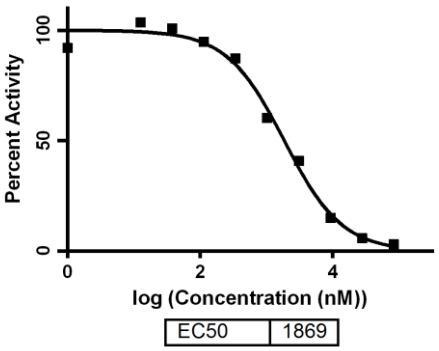

Avg IC_{50} = 1.8 ± 0.1 μM

Analytical Data for IC_{50} Values against a Panel of 3D Src Family Kinases.

Src Family Kinase	**2.1:**	**2.3:**
	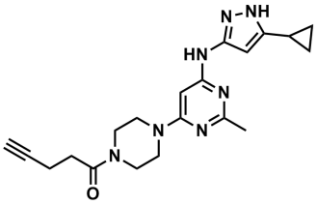	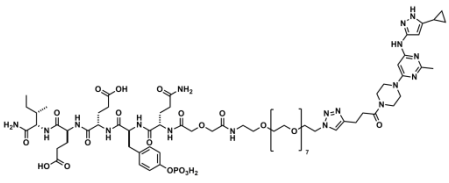

Lck

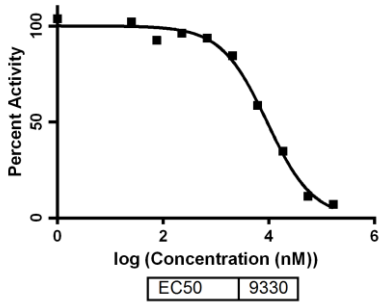

IC_{50} = 9.3 μM

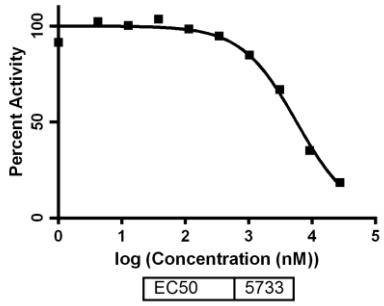

Avg IC_{50} = 5.3 ± 0.6 μM

Blk

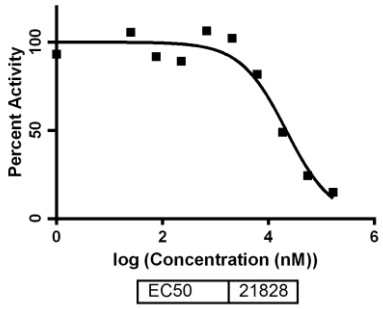

IC_{50} = 21.8 μM

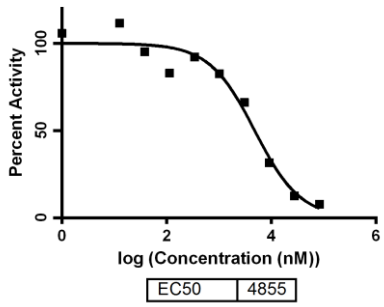

Avg IC_{50} = 5.3 ± 0.7 μM

Frk

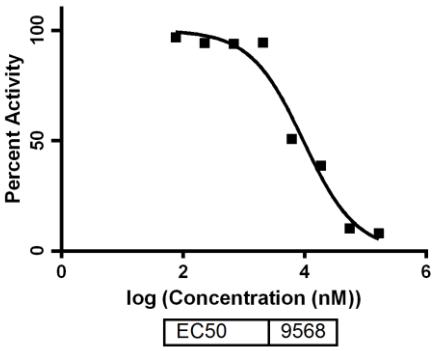

IC_{50} = 9.6 μM

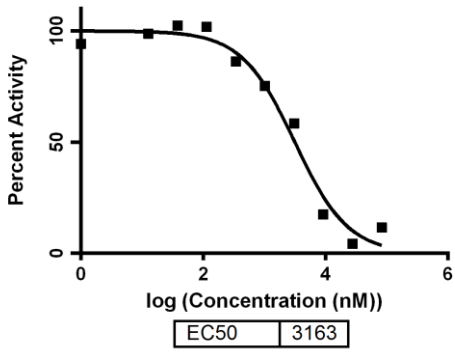

Avg IC_{50} = 5.6 ± 3.4 μM

Fyn

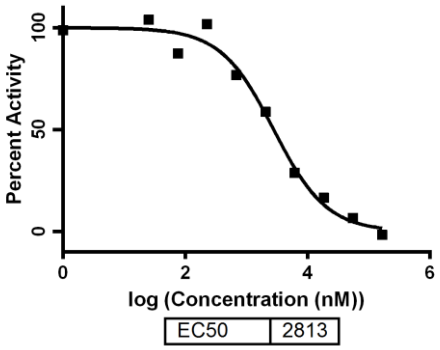

IC_{50} = 2.8 μM

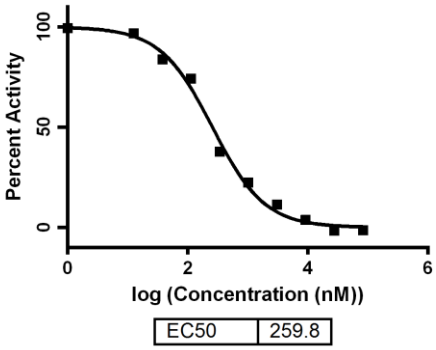

Avg IC_{50} = 0.27 ± 0.02 μM

Fgr

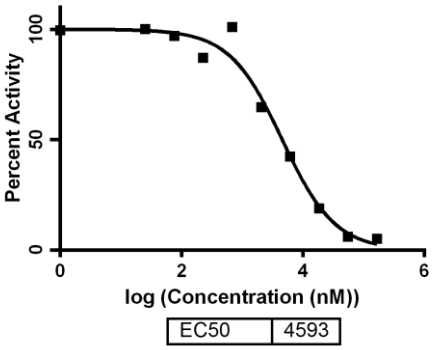

IC_{50} =4.6 μM

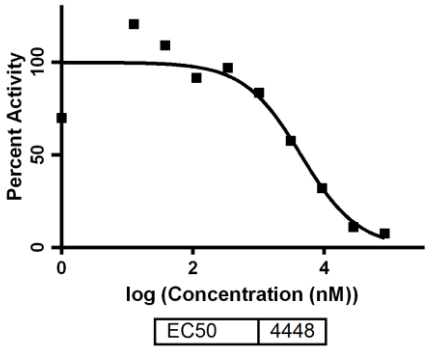

Avg IC_{50} = 3.1 ± 1.9 μM

Lyn

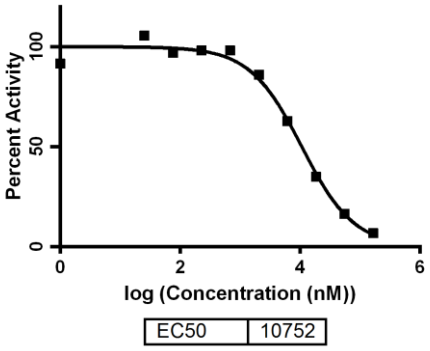

IC_{50} = 10.8 μM

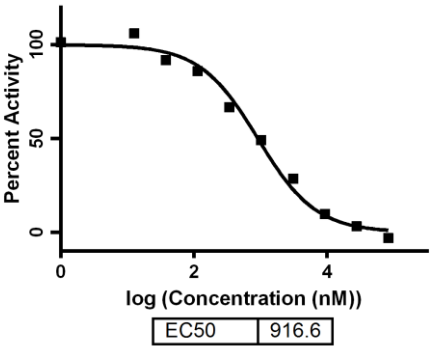

Avg IC_{50} = 2.5 ± 2.2 μM

Analytical Data for IC_{50} Values against 3D SH2-engaged Src.

2.1:

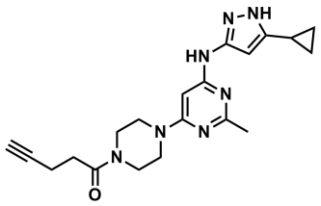

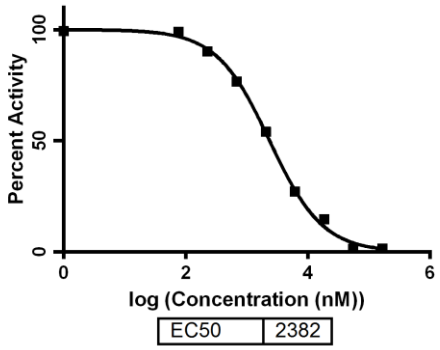

Avg IC_{50} = 2.7 ± 0.6 μM

2.3:

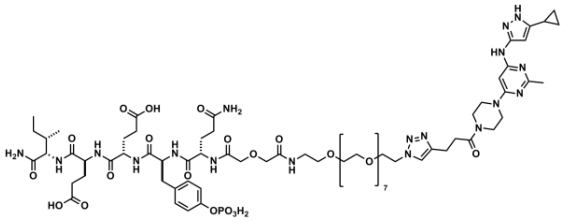

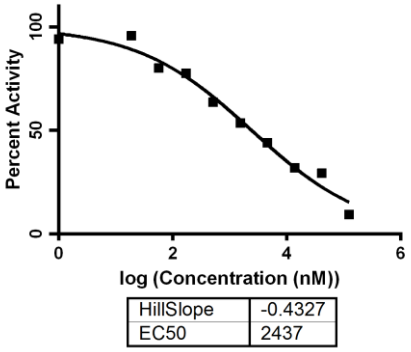

Avg IC_{50} = 2.2 ± 0.8 μM

Analytical Data for IC_{50} Values against 3D SH2-enagaged Hck.

2.1:

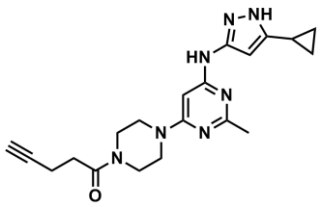

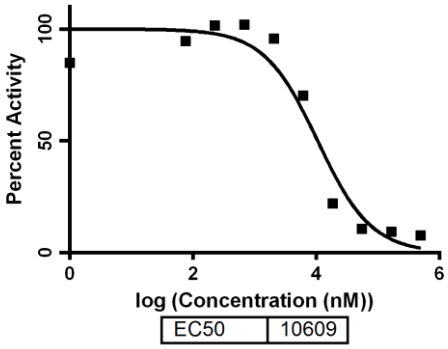

Avg IC_{50} = 9 ± 2 μM

(n=2)

2.3:

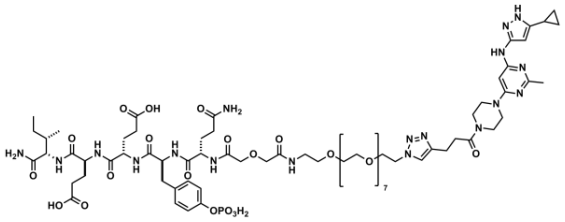

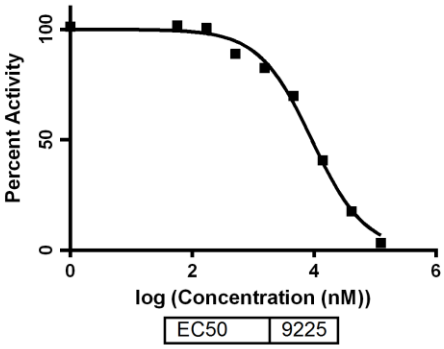

Avg IC_{50} = 10 ± 3 μM

Analytical Data for IC_{50} Values against 3D SH3-engaged Hck.

2.1:

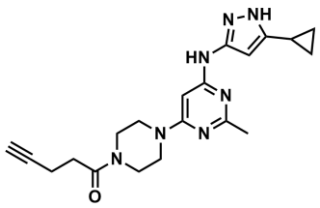

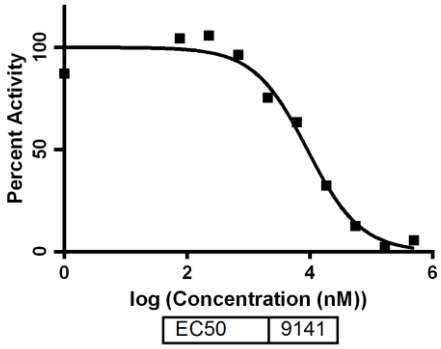

Avg IC_{50} = 9.3 ± 0.3 μM

2.3:

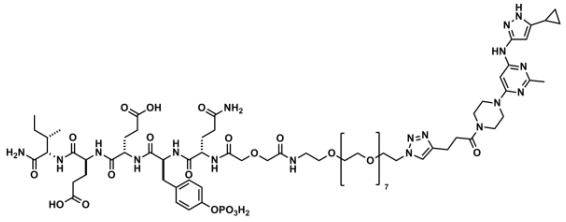

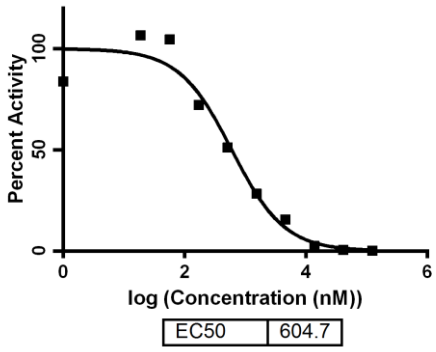

Avg IC_{50} = 609 ± 62 nM

Analytical Data for IC_{50} Values against c-Abl KD.

2.1:

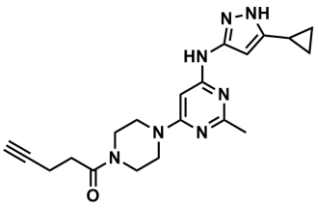

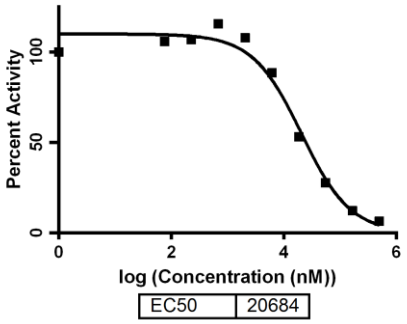

Avg IC_{50} = 20 ± 2 μM

2.3:

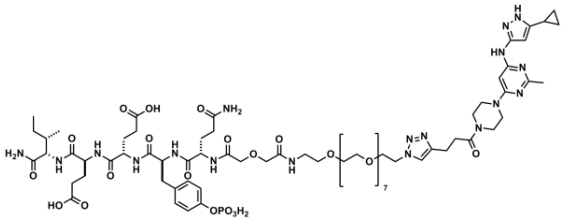

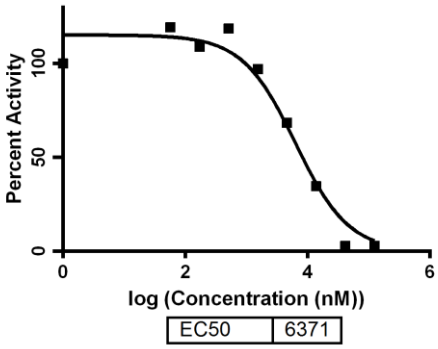

Avg IC_{50} = 6.1 ± 0.7 μM

Analytical Data for IC_{50} Values against 3D c-Abl.

2.1:

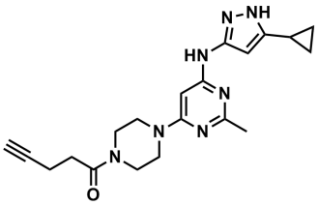

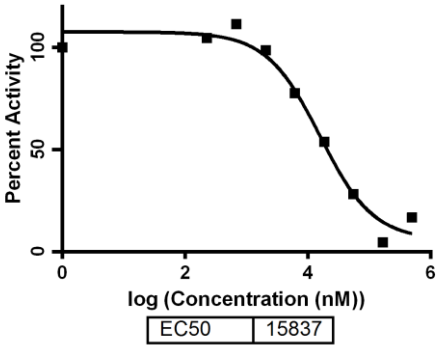

Avg IC_{50} = 15 ± 4 μM

2.3:

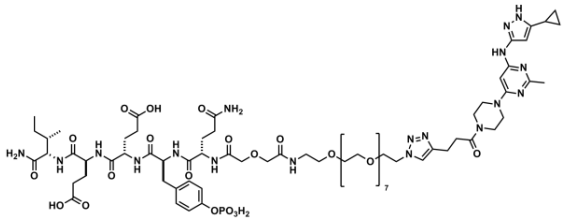

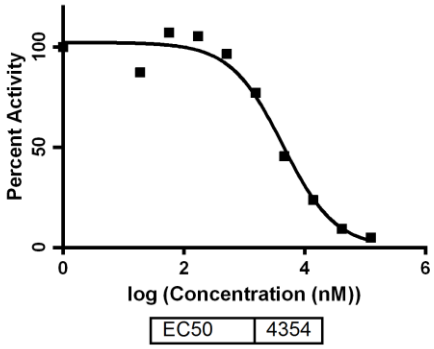

Avg IC_{50} = 4.1 ± 0.4 μM

Analytical Data for EC_{50} Value of SH2 Peptide 2.21.

3D Src

Avg EC_{50} = 0.73 ± 0.1 μM

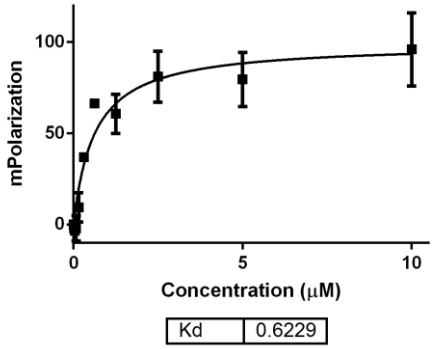

3D Hck

Avg EC_{50} = 1.0 ± 0.3 μM

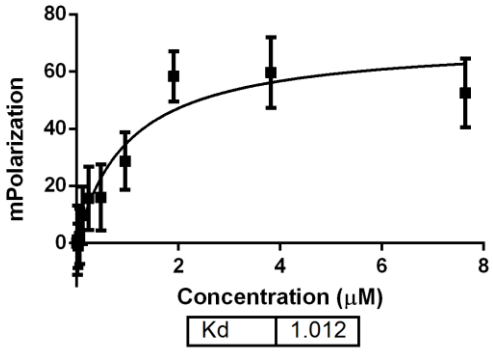

Analytical Data for IC_{50} Values against Src Using Kinase Seeker, Luceome Biotechnologies

Dasatinib:

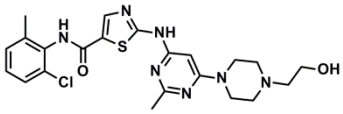

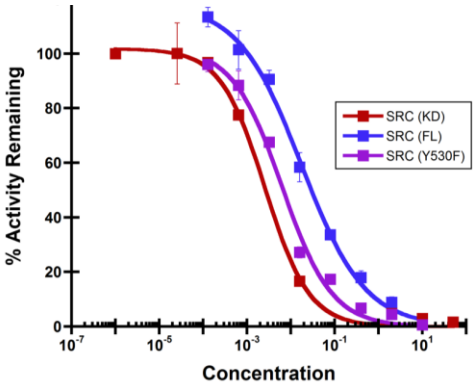

IC_{50} = 18 ± 5 nM

2.4:

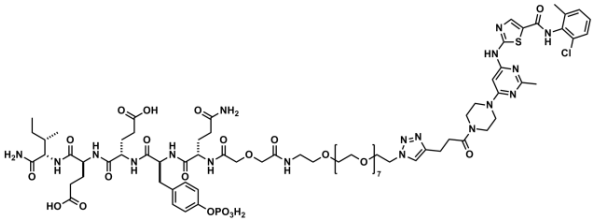

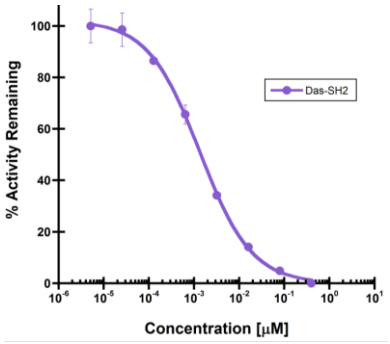

IC_{50} = 1.34 ± 0.07 nM

Appendix B

Analytical Data for Chapter III

Analytical data for compound Tm from Thermofluor screen

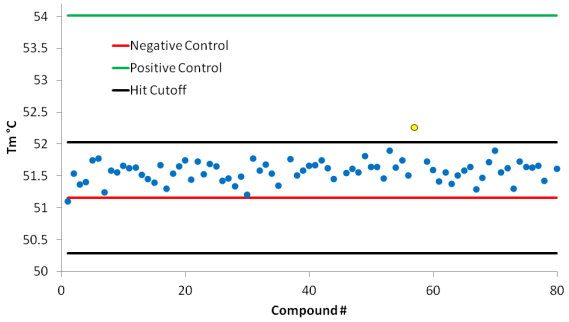

Plate 2

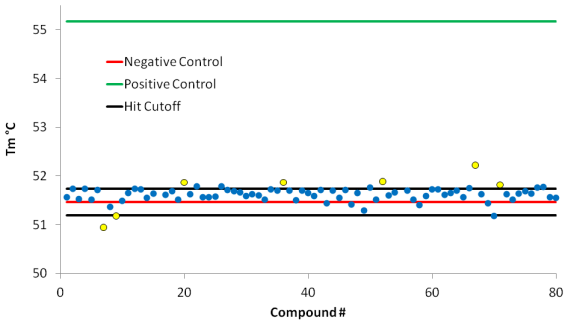

Plate 4

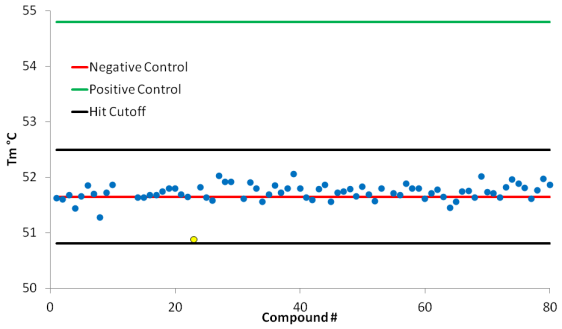

Plate 5

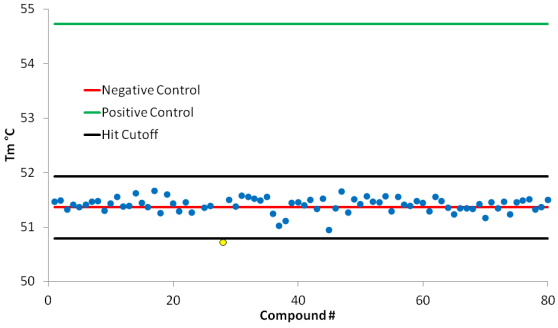

Plate 6

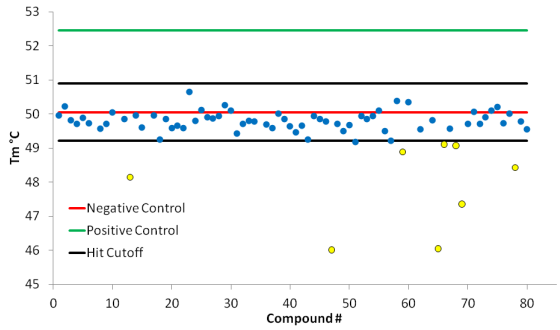

Plate 7

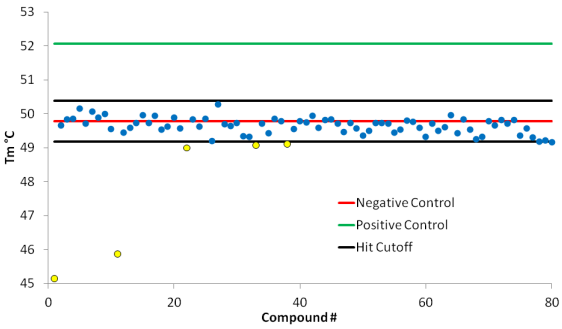

Plate 9

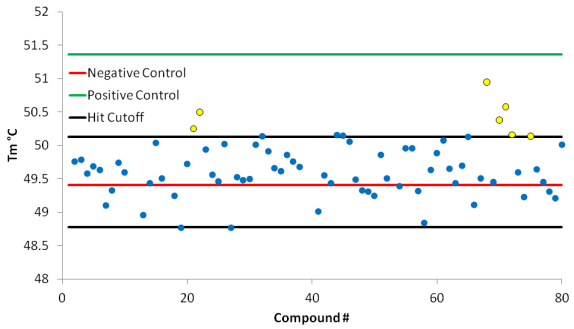

Plate 10

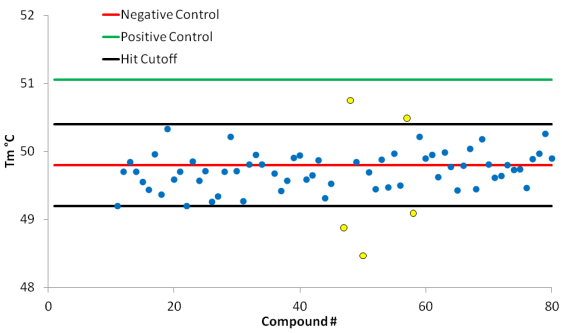

Plate 11

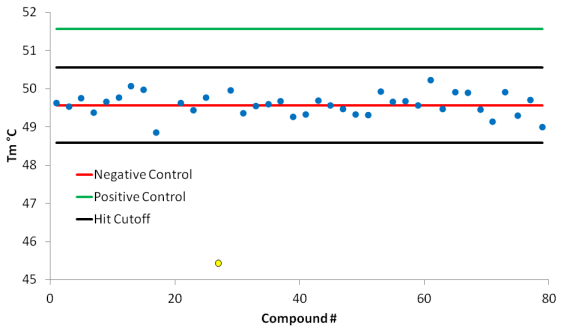

Plate 13

Plates 3, 8, 12 had no hits

Structure of 37 Thermofluor Hits

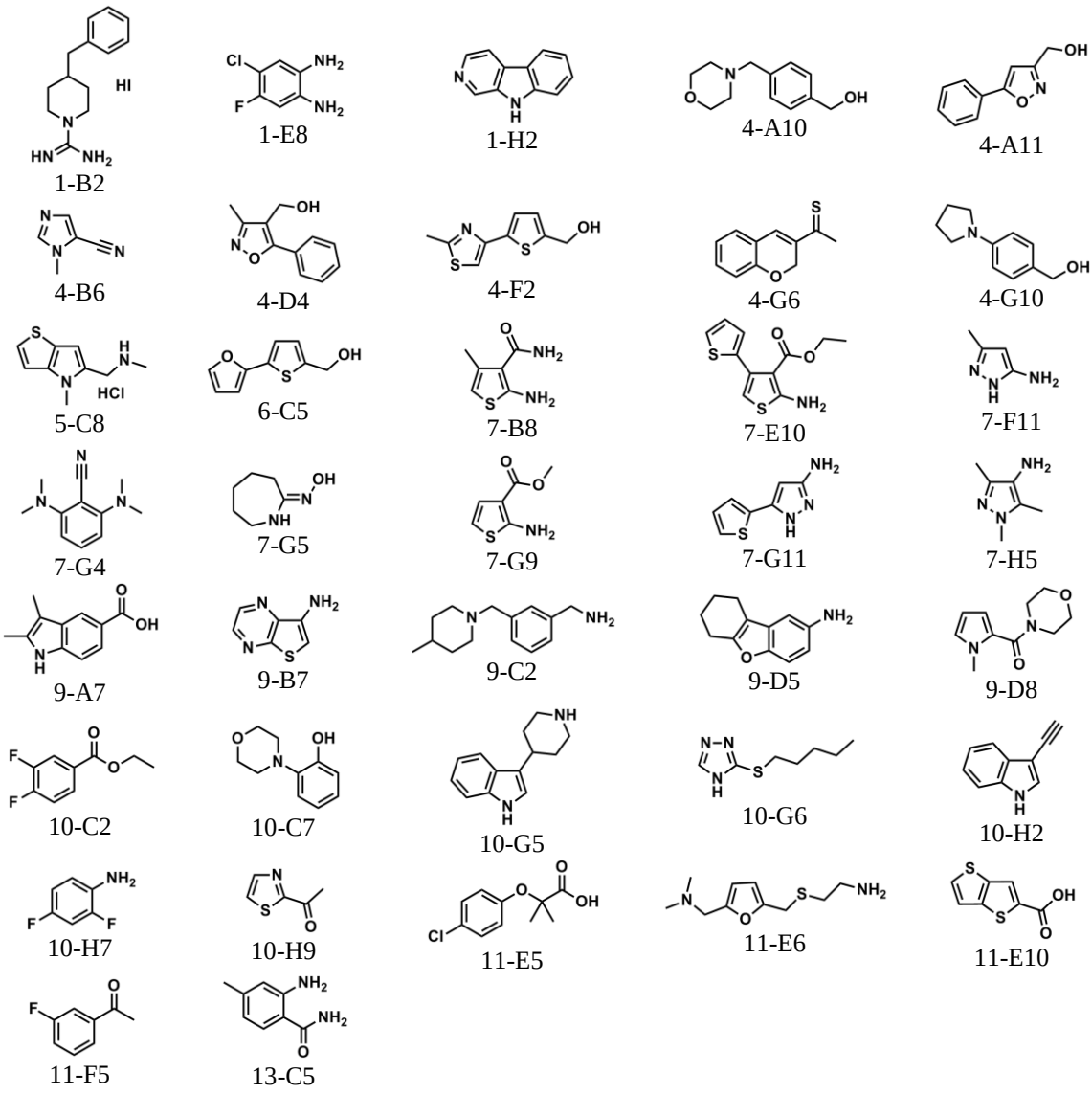

Analytical data for Protein Half Lives as Determined *via* 5 Time Point Proteolysis Assay

	5-Point Half Life (min)
Apo c-Src	29 ± 12 (n=10)
4-D4	63
4-A11	58
1-E8	53.52
4-B6	51
4-F2	34.47
4-G6	33.91
1-B2	33.05
7-G9	32.88
7-E10	31.2
1-H2	31.1
4-G10	30.15
10-H2	29.24
7-G5	27.82
7-F11	26.26
10-C2	25.96
10-G6	25.35
10-C7	24.44
7-G11	24.21
9-B7	23.08
7-G4	22.96
10-H9	22.61
11-F5	21.92
11-E10	21.78
5-C8	21.33
9-A7	21.21
10-G5	21.12
10-H7	20.52
7-B8	20.1
7-H5	19.81
11-E5	19.78
13-C5	17.43
11-E6	17.05
9-D5	16.86
9-C2	15.05
6-C5	8.999
9-D8	8.69

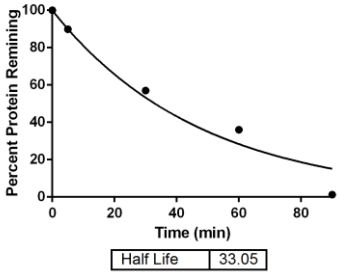

1-B2

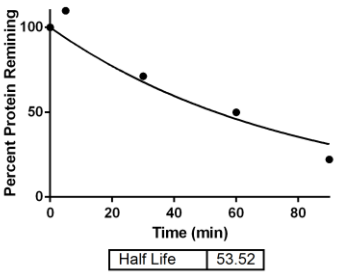

1-E8

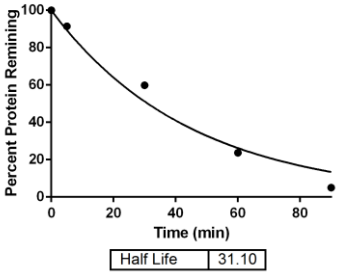

1-H2

See 10 point curve below
4-A10

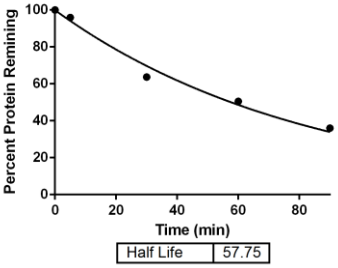

4-A11

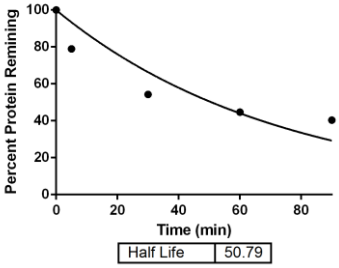

4-B6

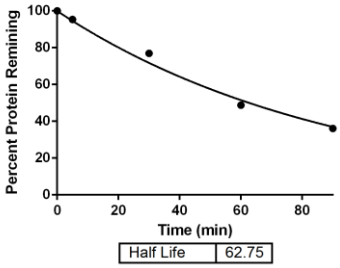

4-D4

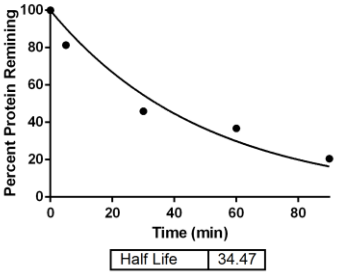

4-F2

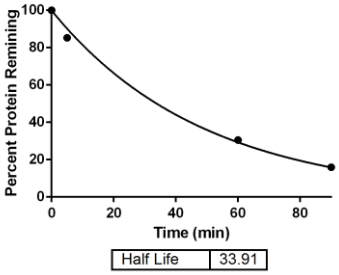

4-G6

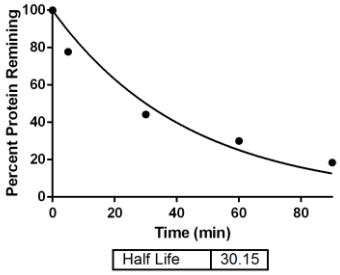

4-G10

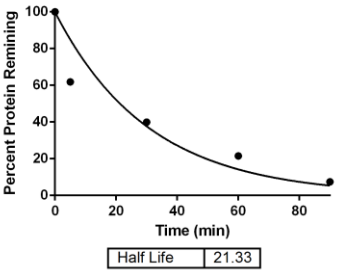

5-C8

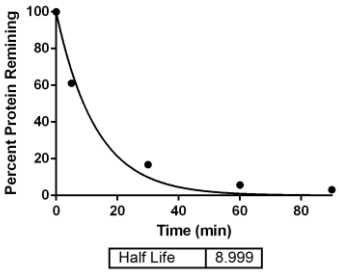

6-C5

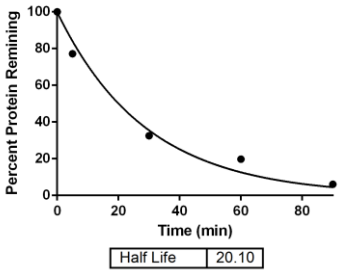

7-B8

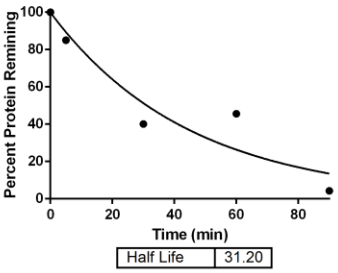

7-E10

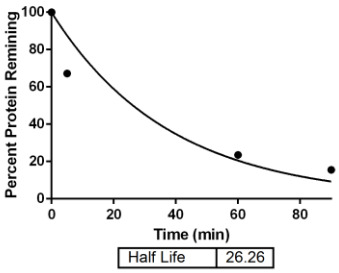

7-F11

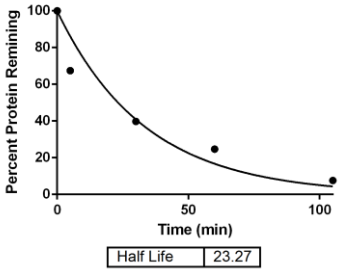

7-G4

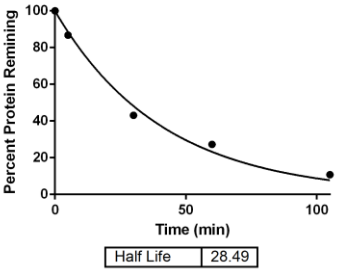

7-G5

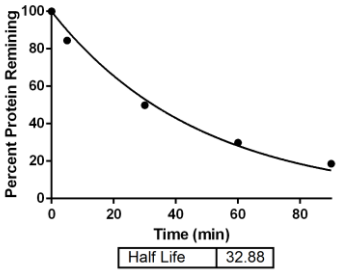

7-G9

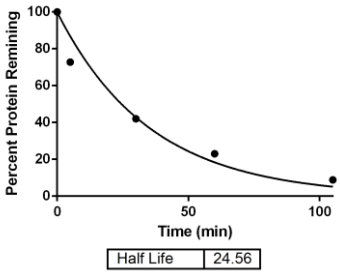

7-G11

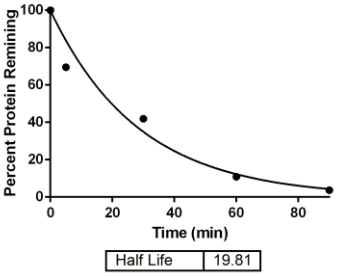

7-H5

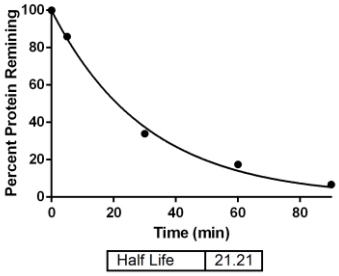

9-A7

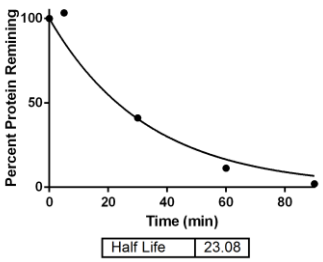

9-B7

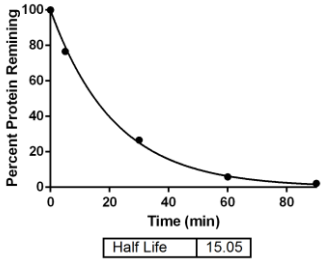

9-C2

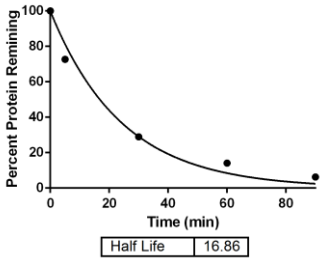

9-D5

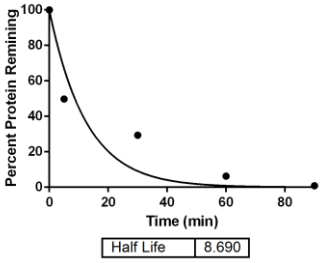

9-D8

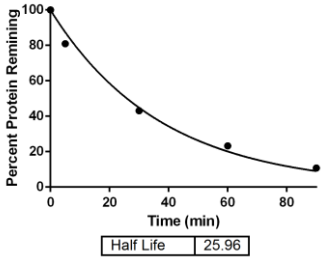

10-C2

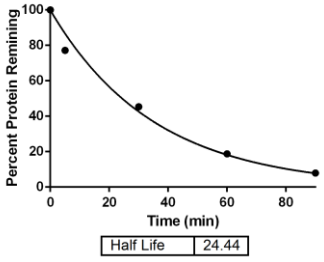

10-C7

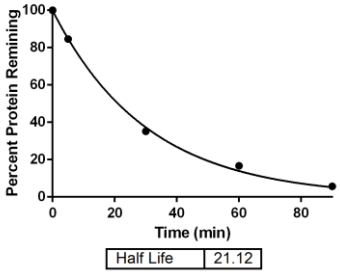

10-G5

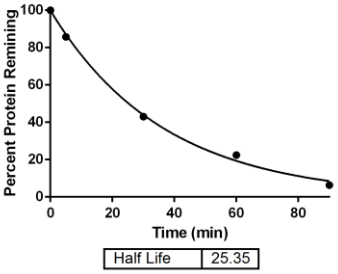

10-G6

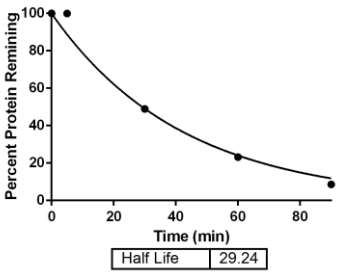

10-H2

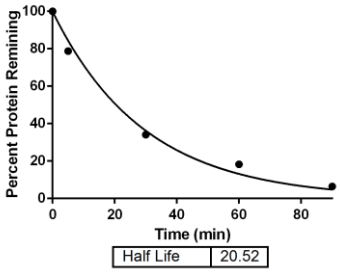

10-H7

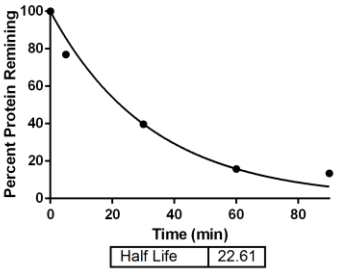

10-H9

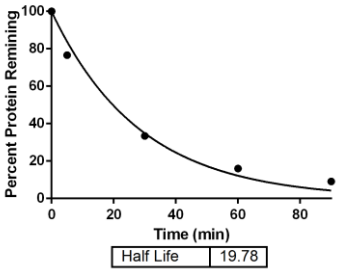

11-E5

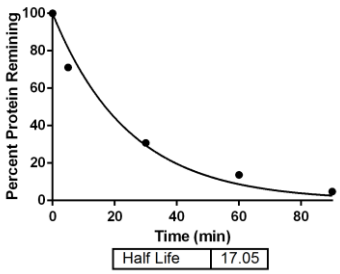

11-E6

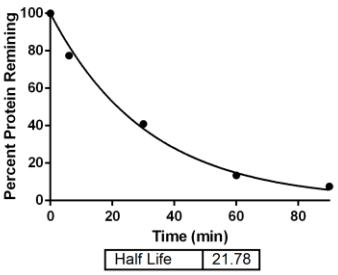

11-E10

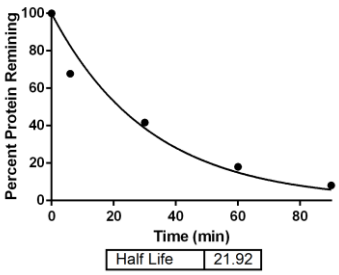

11-F5

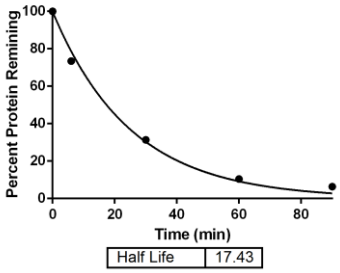

13-C5

Apo c-Src

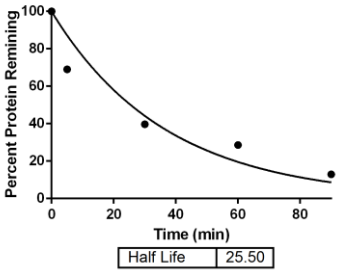

Apo c-Src

Analytical data for Protein Half Lives as Determined *via* 10 Time Point Proteolysis Assay

	10-Point Half Life (min)
Apo c-Src	32 ± 12 (n=2)
9-C2	39.49
9-D8	33.27
11-E6	25.16
9-D5	25.04
1-A10	22.27
4-D4	16.27
4-B6	15.55
4-A11	14.72
1-E8	8.601

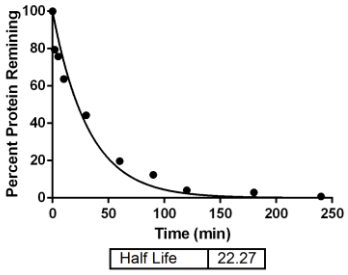

1-A10

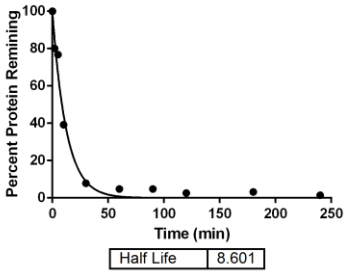

1-E8

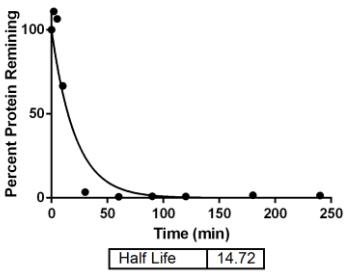

4-A11

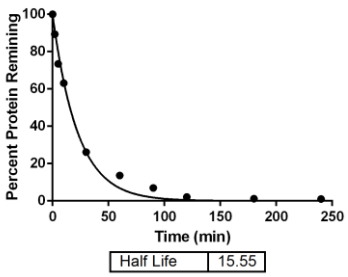

4-B6

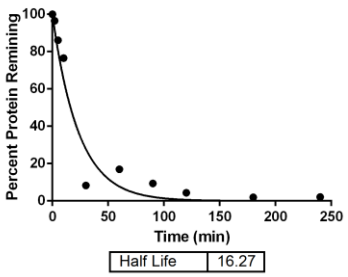

4-D4

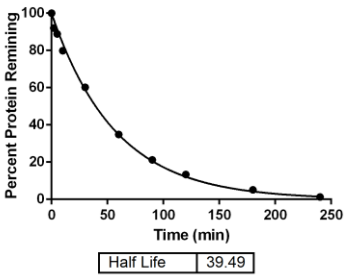

9-C2

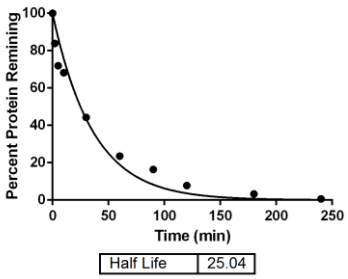

9-D5

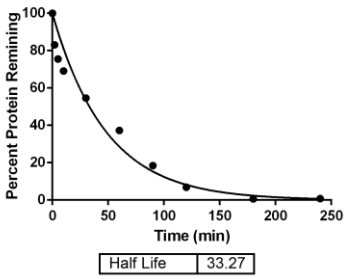

9-D8

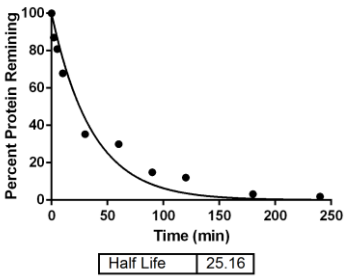

11-E6

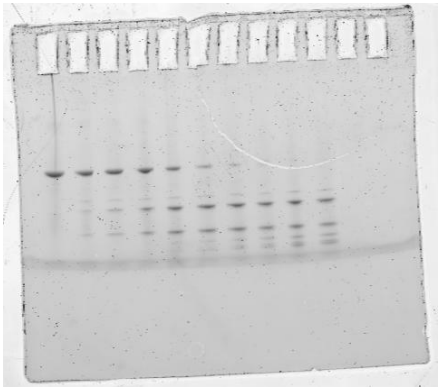

Apo c-Src

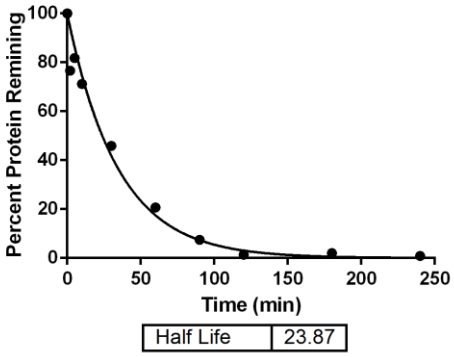

Apo c-Src

Analytical data for 3D Src EC_{50} determination.

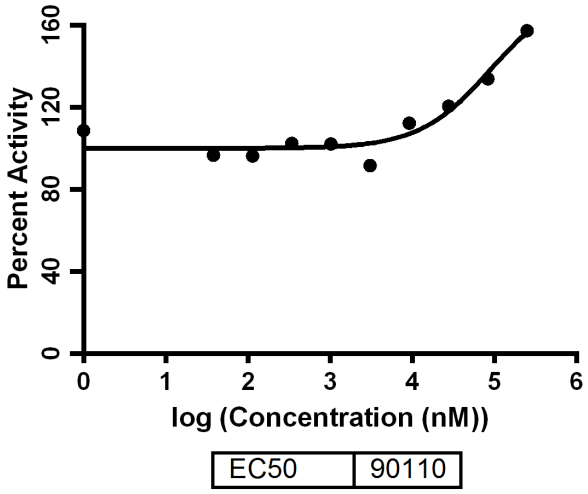

Avg EC_{50} (activation) = 84 ± 21 μM
[ATP] = 100 μM

1-E8:

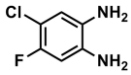

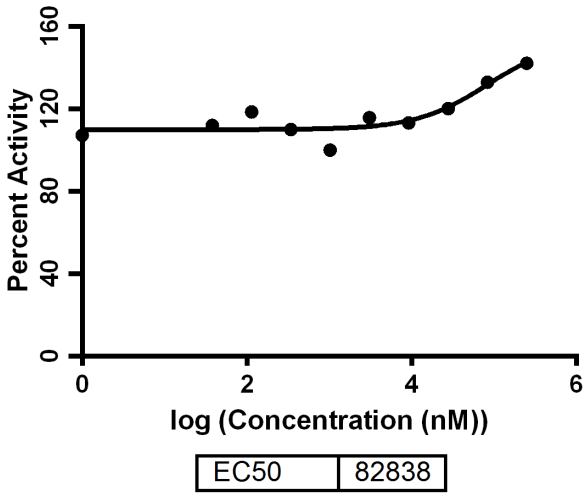

Avg EC_{50} (activation) = 83 μM
[ATP] = 1 mM

1-E8 + 400 nM pFAK

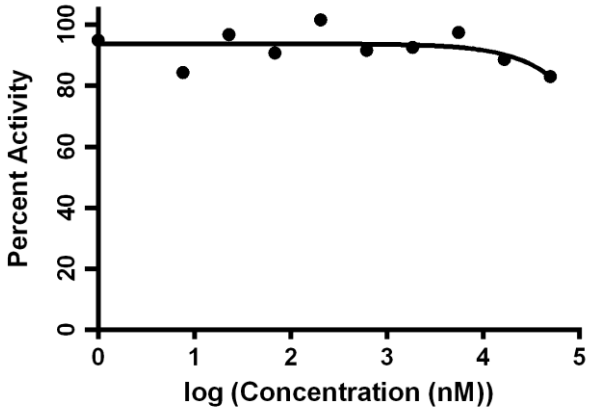

No effect

4-A11:

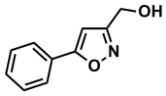

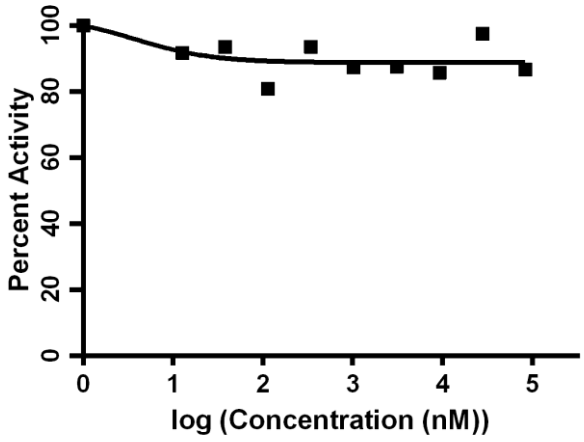

No Effect

Analytical data for pY416 3D c-Src IC_{50} determination.

1-E8:

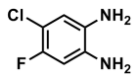

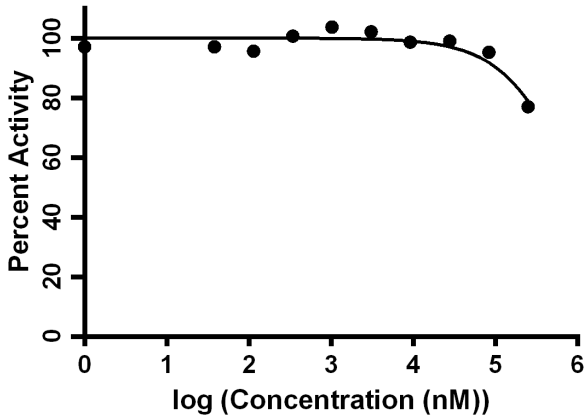

EC50	936588

Avg IC_{50} = 930 ± 70 μM

Analytical data for pY527 3D c-Src IC_{50} determination.

1-E8:

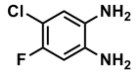

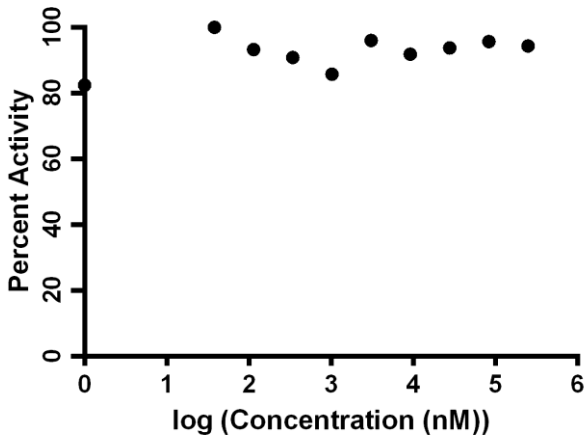

No Effect

Analytical data for 3D Hck IC_{50} determination.

1-E8:

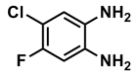

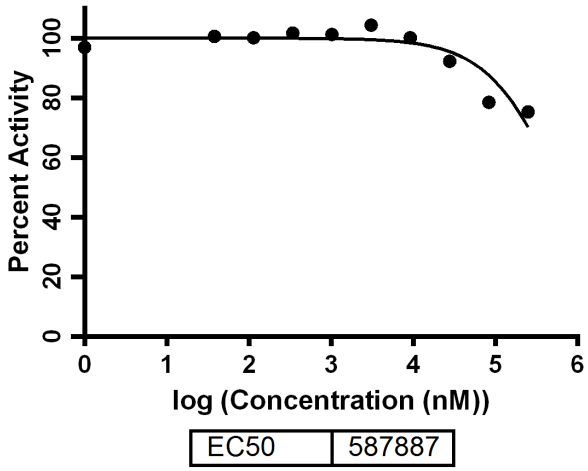

EC50	587887

Avg IC_{50} = 550 ± 100 μM

Analytical data for 3D Abl IC_{50} determination.

1-E8:

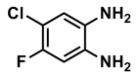

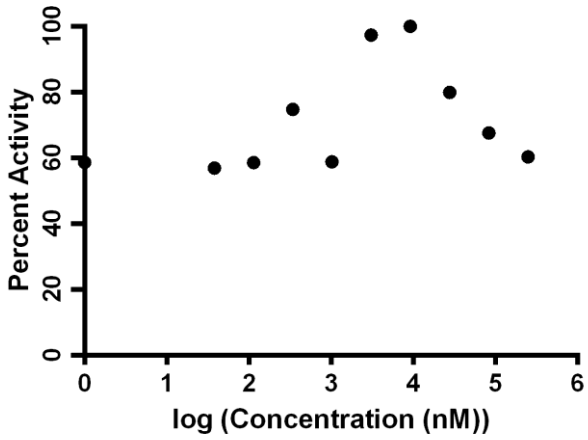

No Effect

Analytical data for EC_{50} value of SH2 Peptide 2.21.

2.21

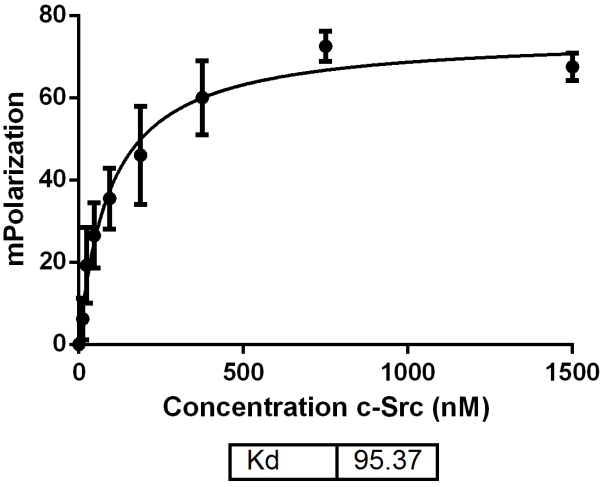

EC_{50} = 100 ± 7 nM

2.21 + 100 μM **1-E8**

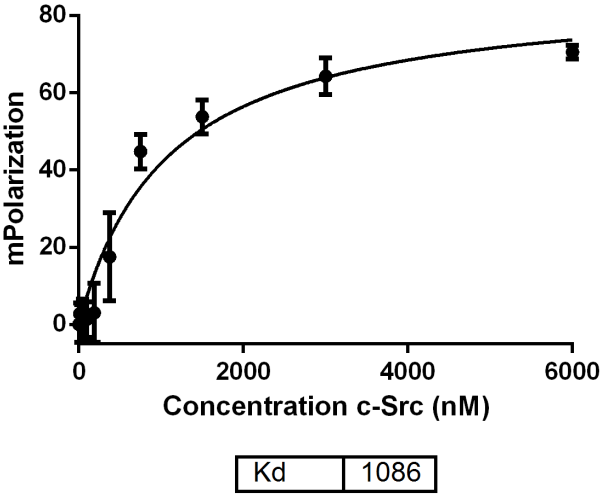

EC_{50} = 1043 ± 61 nM

Analytical data for HT-29 GI_{50} determination.

1-E8:

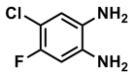

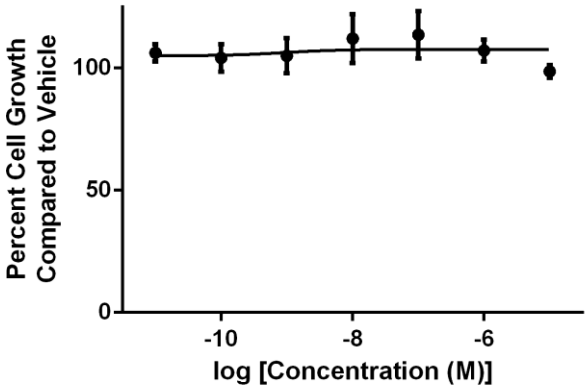

GI_{50} > 10 μM

Das-DFGO-II

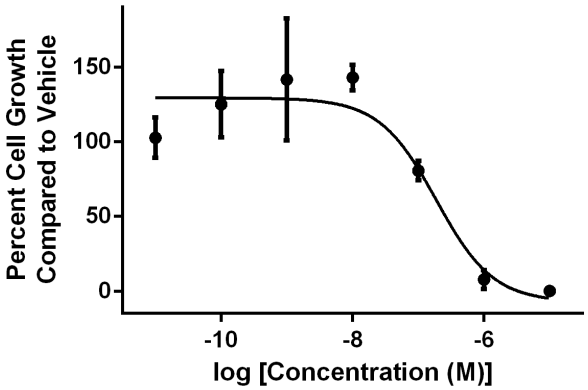

EC50	1.878e-007

Avg GI_{50} = 157 ± 44 nM

Das-DFGO-II + 10 μM 1-E8

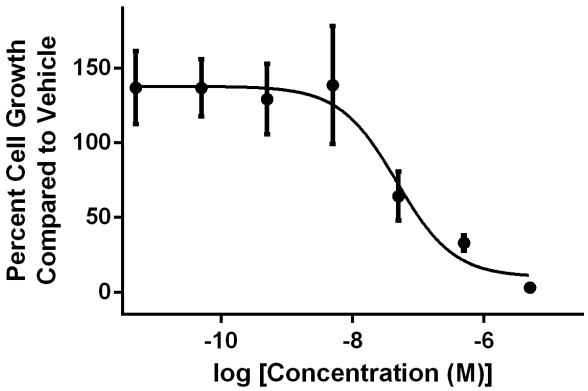

EC50	4.702e-008

Avg GI_{50} = 52 ± 7 nM

Appendix C

Analytical Data for Chapter IV

Spectral Data for Compounds 4.2-4.6.

4.5:

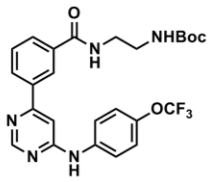

^{1}H:

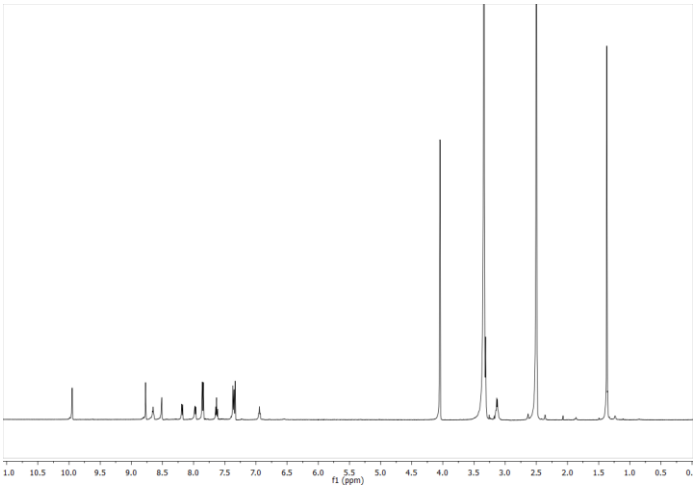

4.1:

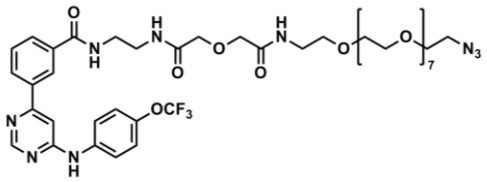

^{1}H:

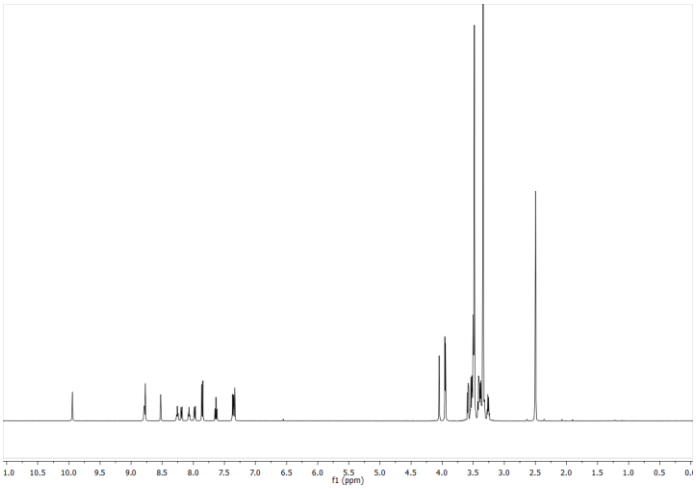

4.3:

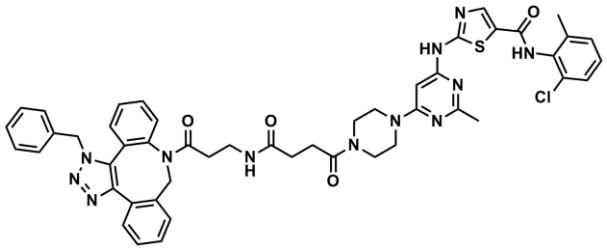

^{1}H:

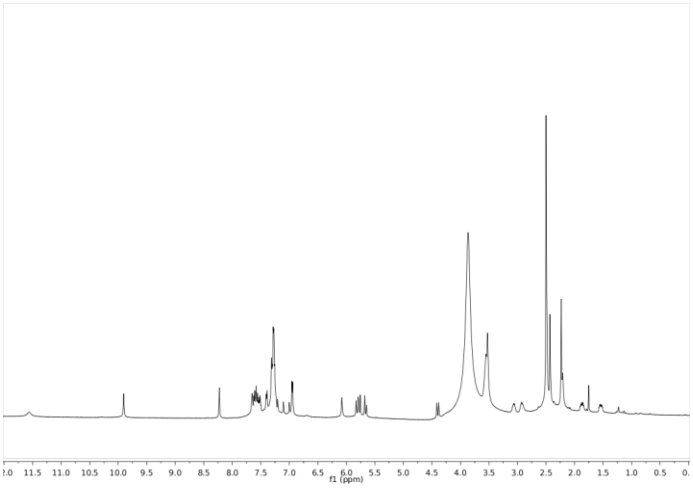

Analytical data for IC_{50} Values against c-Abl kinase domain.

4.1:

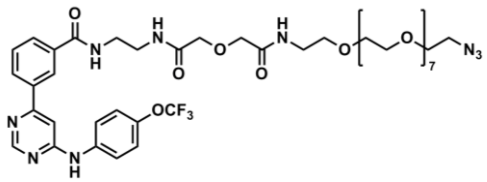

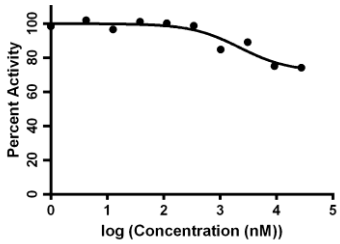

Avg IC_{50} > 83 µM

4.2:

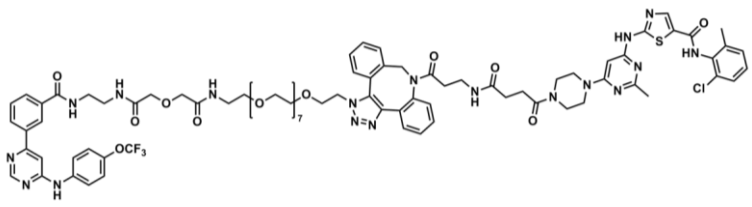

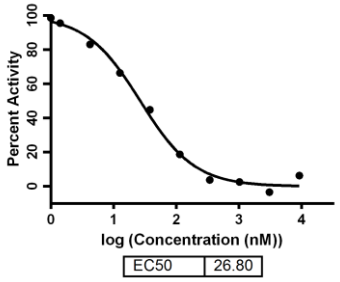

Avg IC_{50} = 26 ± 1 nM

4.2 + 8 µM GNF-2

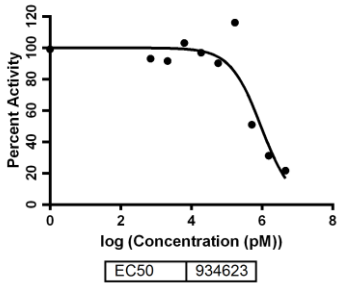

Avg IC_{50} = 1.1 ± 0.4 µM

4.3:

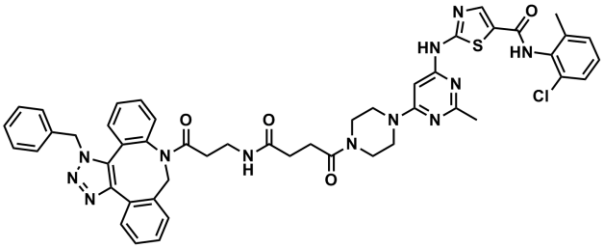

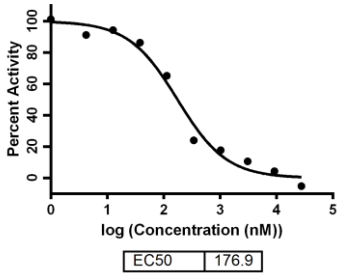

Avg IC_{50} = 149 ± 47 nM

Analytical data for IC_{50} Values against A337N c-Abl kinase domain.

4.1:

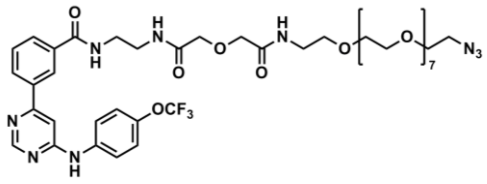

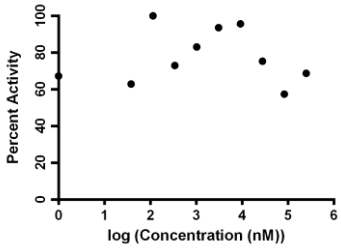

Avg IC_{50} > 250 µM

4.2:

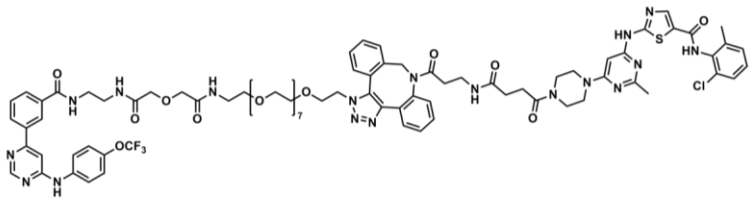

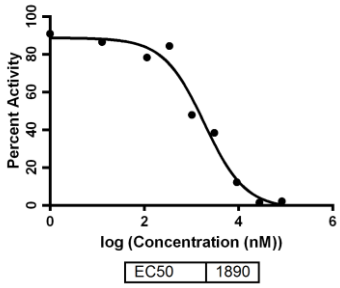

Avg IC_{50} = 2.0 ± 0.2 µM

4.3:

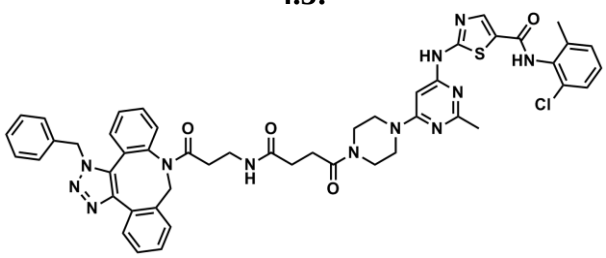

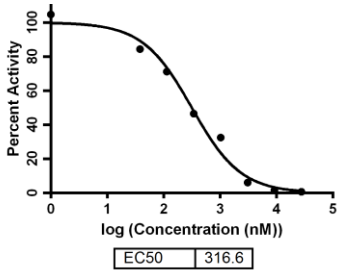

Avg IC_{50} = 270 ± 59 nM

Analytical data for IC_{50} Values against P465S c-Abl kinase domain.

4.1:

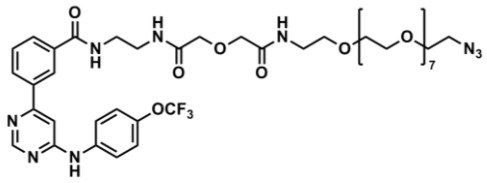

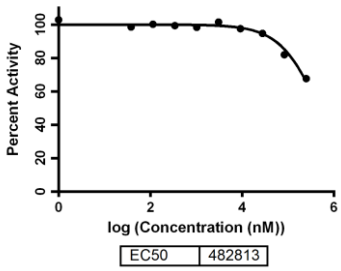

Avg IC_{50} = 700 ± 400 μM

4.2:

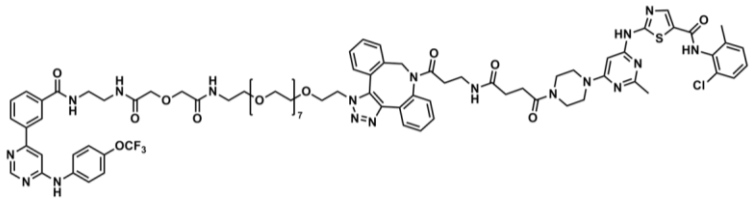

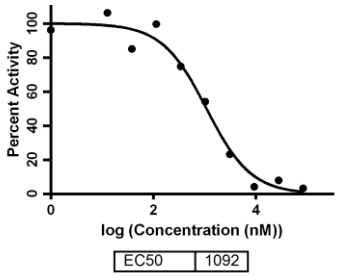

Avg IC_{50} = 900 ± 400 nM

4.3:

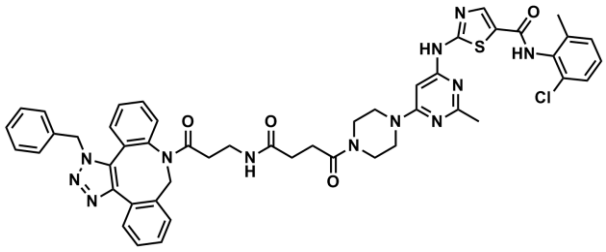

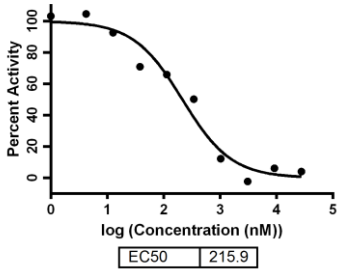

Avg IC_{50} = 190 ± 50 nM

Analytical data for IC_{50} Values against E505K c-Abl kinase domain.

4.1:

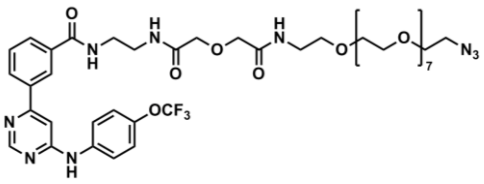

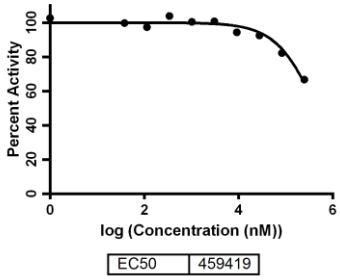

Avg IC_{50} = 440 ± 50 μM

4.2:

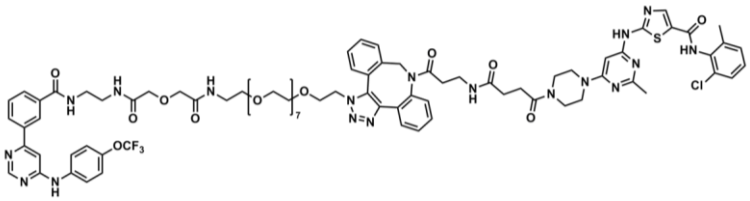

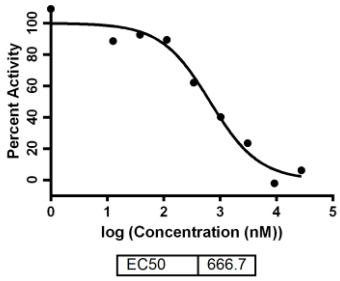

Avg IC_{50} = 700 ± 170 nM

4.3:

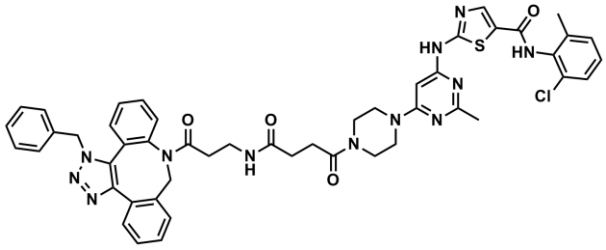

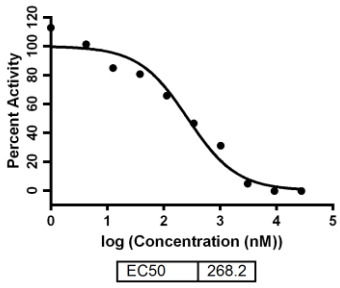

Avg IC_{50} = 230 ± 90 nM

Analytical data for IC_{50} Values against 3D c-Abl.

4.1:

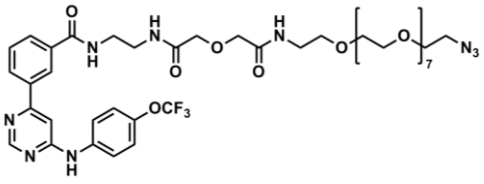

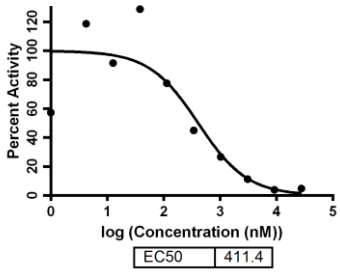

Avg IC_{50} = 320 ± 130 nM

4.2:

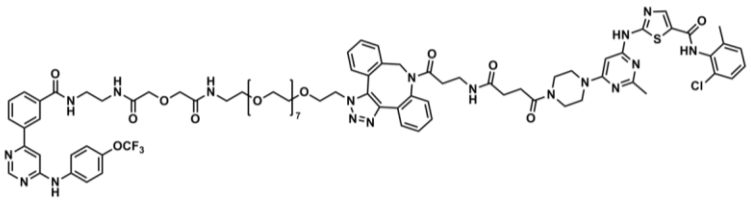

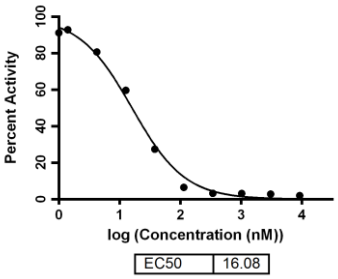

Avg IC_{50} < 30 nM

4.3:

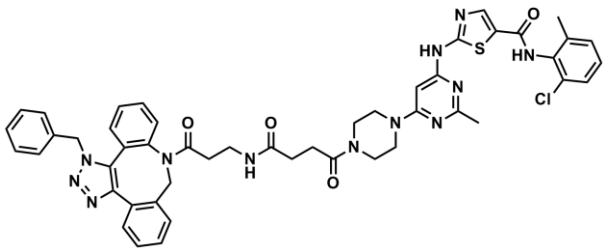

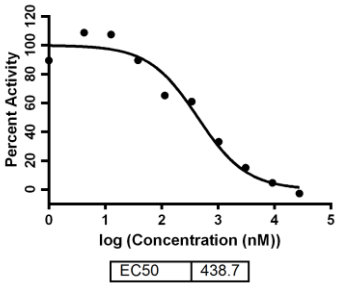

Avg IC_{50} = 418 ± 23 nM

Analytical data for IC_{50} Values against A337N 3D c-Abl.

4.1:

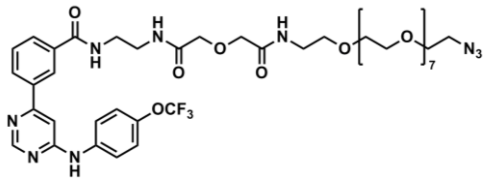

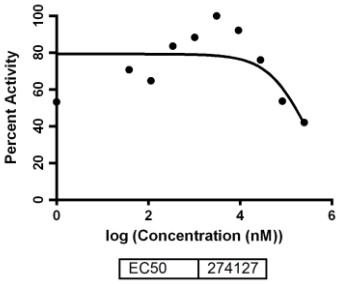

Avg IC_{50} = 240 ± 90 μM

4.2:

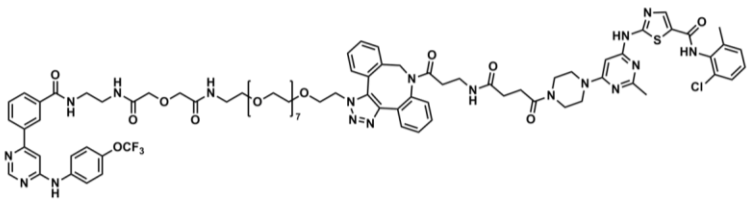

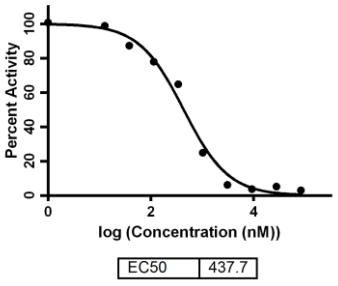

Avg IC_{50} = 550 ± 220 nM

4.3:

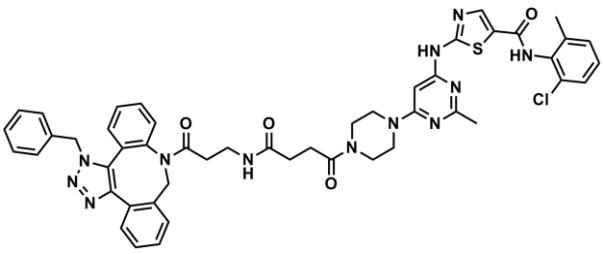

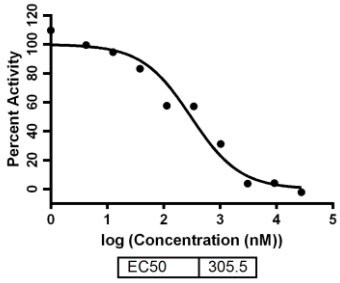

Avg IC_{50} = 290 ± 40 nM

Analytical data for IC_{50} Values against P465S 3D c-Abl.

4.1:

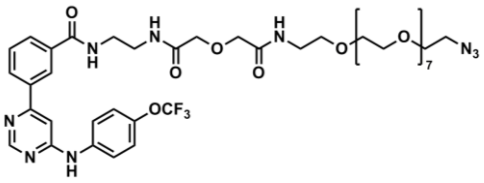

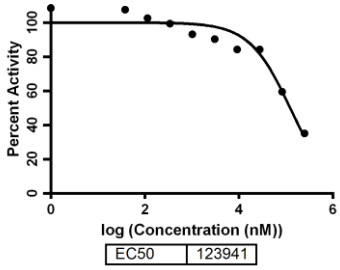

Avg IC_{50} = 110 ± 30 μM

4.2:

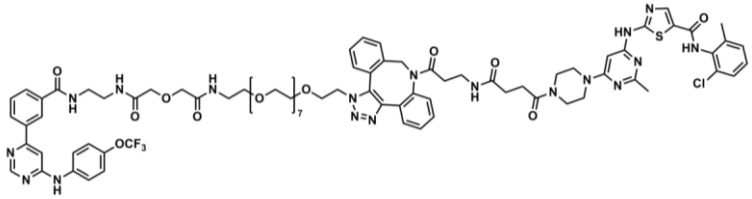

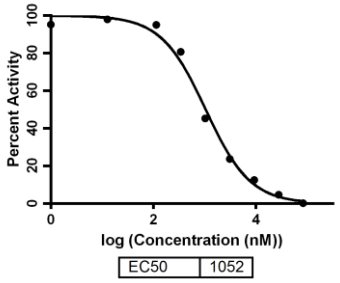

Avg IC_{50} = 830 ± 250 nM

4.3:

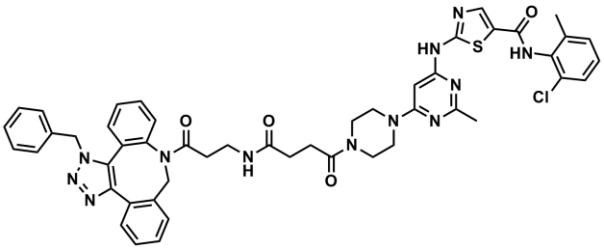

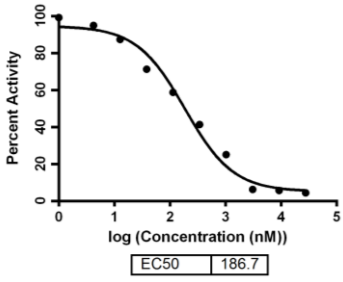

Avg IC_{50} = 220 ± 65 nM

Analytical data for IC_{50} Values against E505K 3D c-Abl.

4.1:

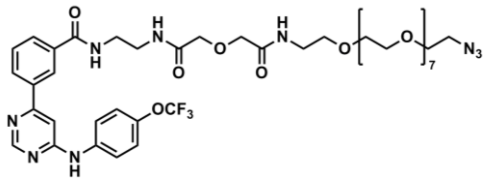

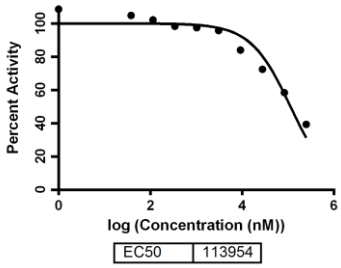

Avg IC_{50} = 120 ± 13 μM

4.2:

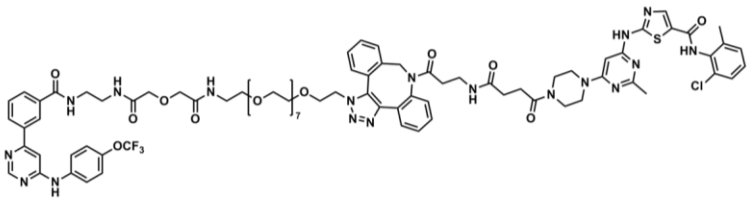

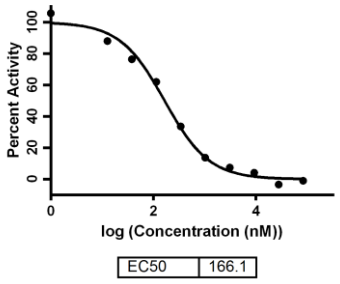

Avg IC_{50} = 160 ± 40 nM

4.3:

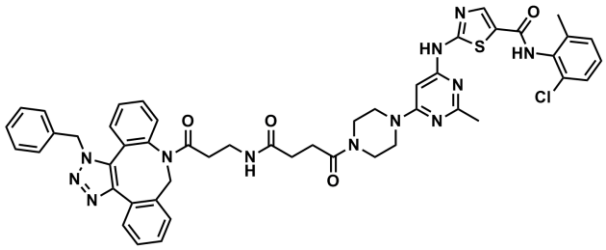

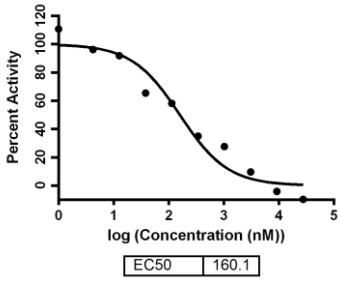

Avg IC_{50} = 170 ± 60 nM

Analytical data for IC_{50} Values against c-Src kinase domain.

4.2:

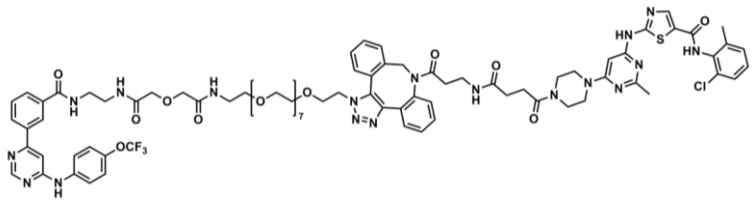

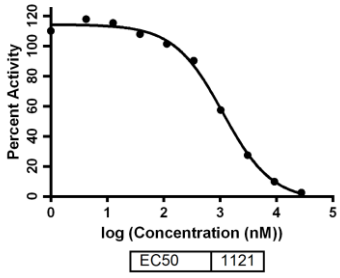

Avg IC_{50} = 1.2 ± 0.4 μM

4.2 + 8 μM GNF-2

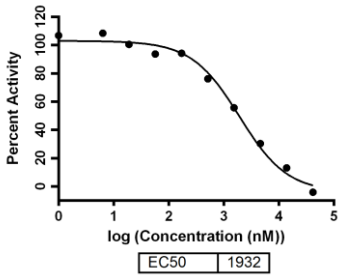

Avg IC_{50} = 1.7 ± 0.2 μM

4.3:

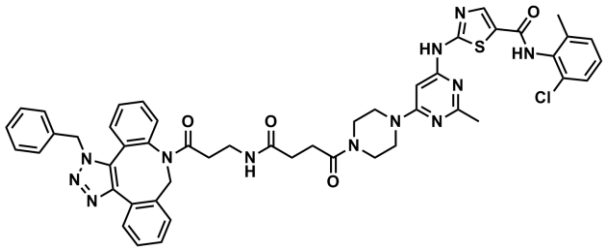

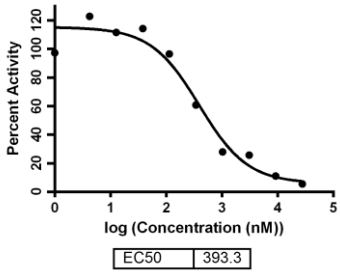

Avg IC_{50} = 360 ± 90 nM

Analytical Data for IC_{50} Values against Abl Using Kinase Seeker, Luceome Biotechnologies.

Dasatinib:

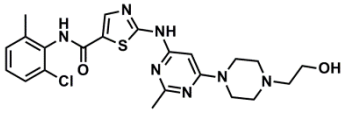

4.2:

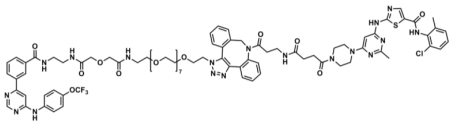

Abl Kinase Domain	Full-Length Abl
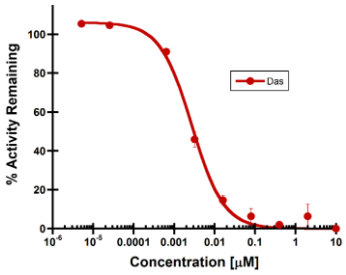	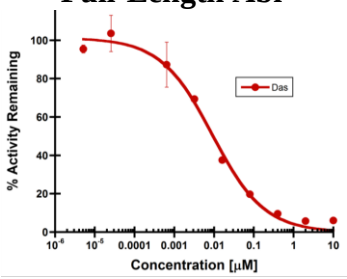
IC_{50} = 0.0027 ± 0.0003 μM	IC_{50} = 0.0091 ± 0.0019 μM
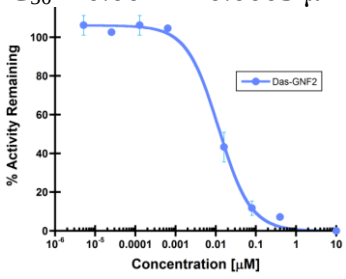	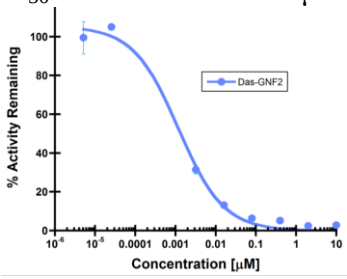
IC_{50} = 0.0118 ± 0.0014 μM	IC_{50} = 0.0012 ± 0.0005 μM

Dasatinib + 20 μM GNF-2

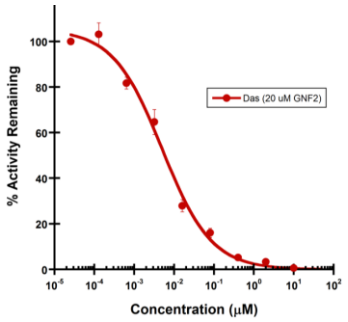

IC_{50} = 0.0050 ± 0.0010 μM

4.2 + 20 μM GNF-2

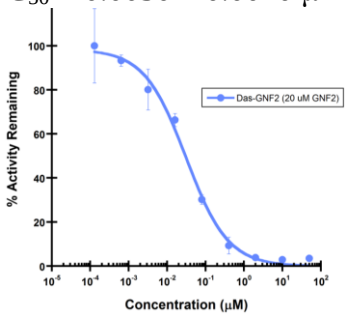

IC_{50} = 0.0311 ± 0.0051 μM

2.18:

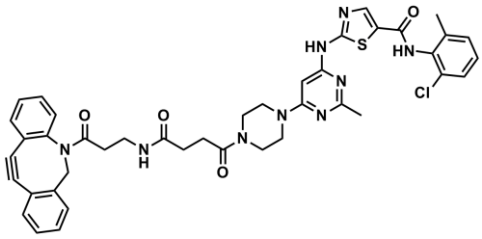

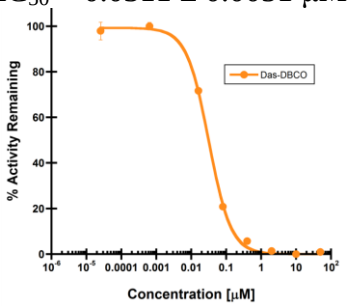

IC_{50} = 0.032 ± 0.002 μM

Analytical Data for IC_{50} Values against 3D Src Using Kinase Seeker, Luceome Biotechnologies.

4.2:

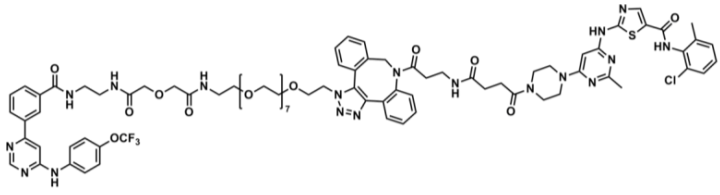

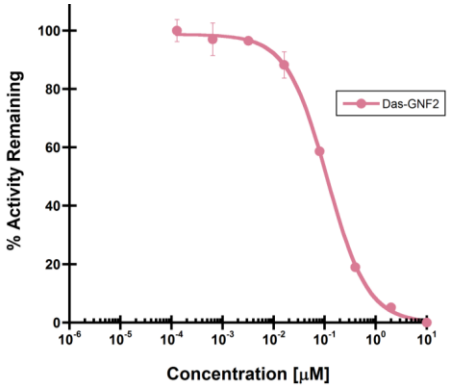

IC_{50} = 0.112 ± 0.004 μM

Analytical data for Bivalent Inhibitor 4.2 in Ba/F3 cells.

4.2:

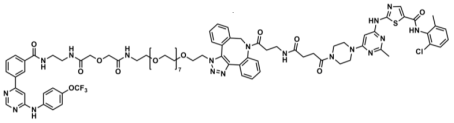

BCR/Abl Ba/F3

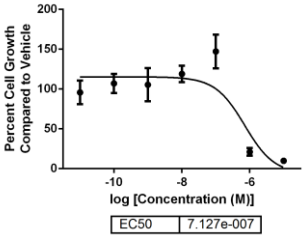

Avg GI_{50} = 713 nM

Parental Ba/F3

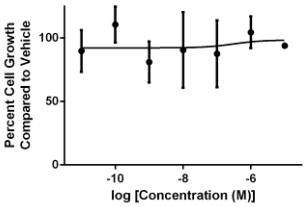

Avg GI_{50} > 10 μM

Analytical data for Bivalent Inhibitor 4.2 using InCELL Pulse, DiscoverX Corporation.

4.2:

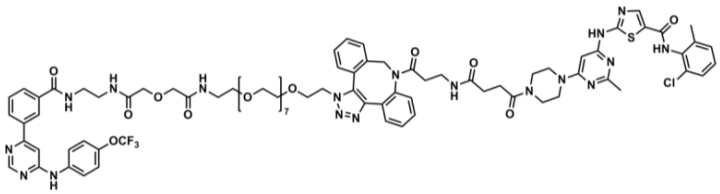

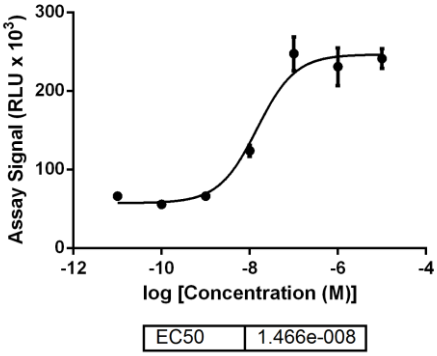

Avg GI_{50} = 15 nM

Appendix D

Analytical Data for Chapter V

Equation for Determination of Combination Index (CI)

$$CI = \frac{(D)_1}{(D_x)_1} + \frac{(D)_2}{(D_x)_2} = \frac{(D)_1}{(D_m)_1\left[fa/(1-f_a)\right]^{1/m_1}} + \frac{(D)_2}{(D_m)_2\left[fa/(1-f_a)\right]^{1/m_2}} \quad (1)^1$$

where $(D)_1$ and $(D)_2$ are the doses of drugs 1 and 2, D_m is the dose required to produce the median effect (analogous to IC_{50}, ED_{50}, or LD_{50} values), m is a Hill-type coefficient signifying the sigmoidicity of the dose-effect curve, and f_a is fraction affected[1]

Analytical Data for IC_{50} Values against 3D c-Abl

Imatinib
Avg IC_{50} = 270 ± 50 nM
Avg K_i = 5.4 ± 0.9 nM

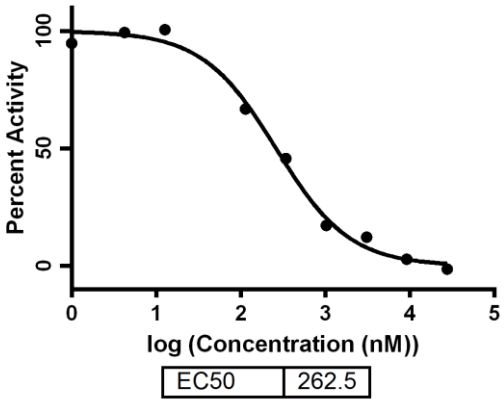

GNF-2
IC_{50} = 114.7 nM
n = 1

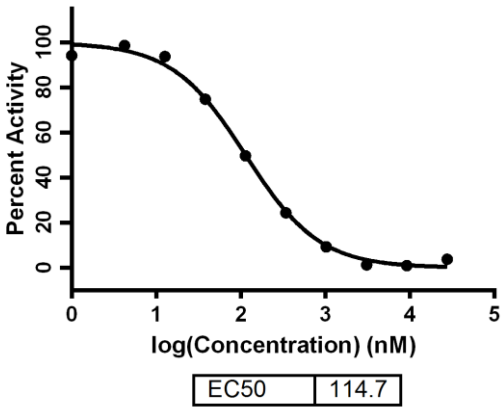

Analytical data for IC_{50} Values against 3D T315I Abl.

GNF-2
Avg IC_{50} > 83 μM
Avg K_i > 42 μM
[ATP] = 100 μM
[Abl] = 60 nM

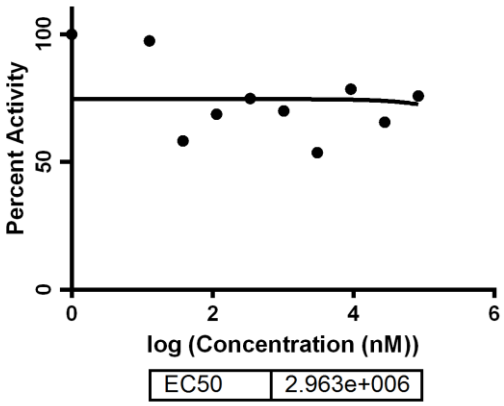

Das-CHO-II
Avg IC_{50} = 141 ± 100 μM
Avg K_i = 70 ± 50 μM
[ATP] = 100 μM
[Abl] = 60 nM

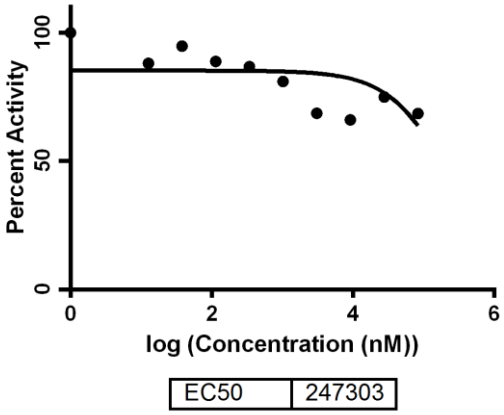

Analytical data for IC_{50} Values against 3D P112S Abl.

GNF-2
Avg IC_{50} > 83 μM
Avg K_i > 42 μM
[ATP] = 100 μM
[Abl] = 60 nM

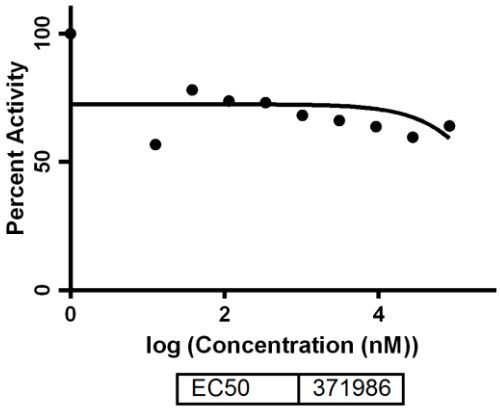

Das-CHO-II
Avg IC_{50} < 60 nM
K_i < 1.2 nM
[Abl] = 60 nM

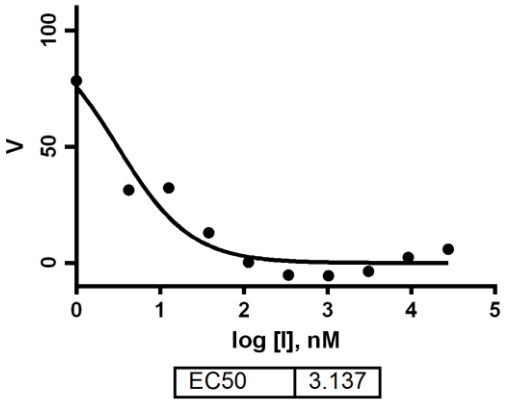

Imatinib
Avg IC_{50} = 113 ± 27 nM
Avg K_i = 2.2 ± 0.5 nM

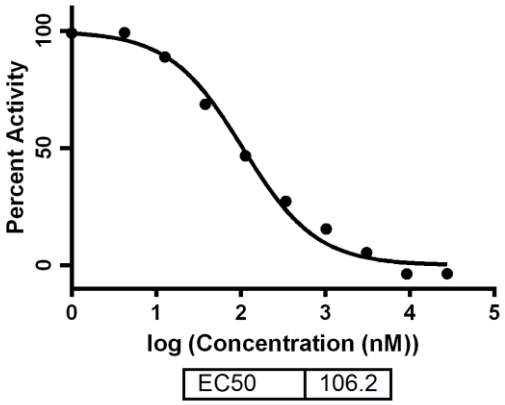

Analytical data for IC_{50} Values against 3D S229P Abl.

GNF-2
Avg IC_{50} > 83 μM
Avg K_i > 42 μM
[ATP] = 100 μM
[Abl] = 60 nM

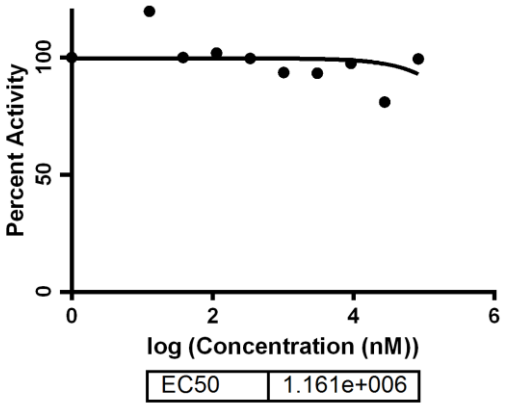

Das-CHO-II
Avg IC_{50} < 30 nM
Avg K_i < 0.6 nM

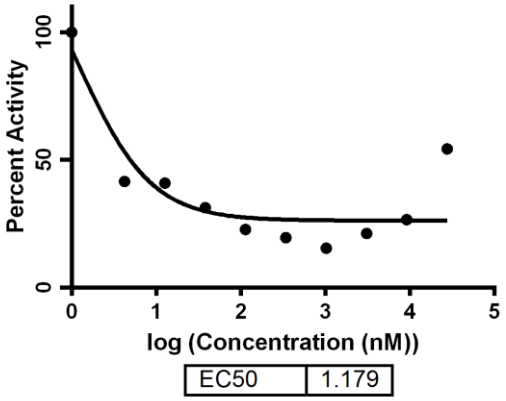

Imatinib
Avg IC_{50} < 30 nM
Avg K_i < 0.6 nM

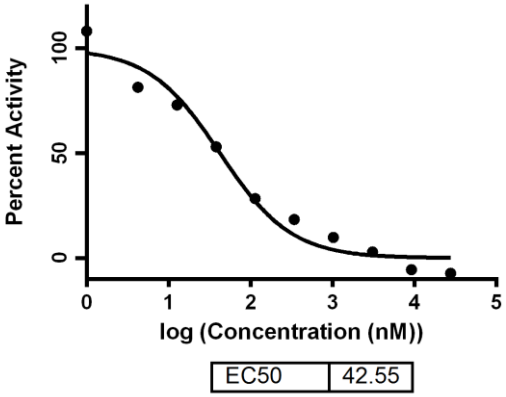

Analytical data for BODIPY probe EC_{50} determination.

	EC_{50} (nM)	
	Without GNF-2	**With 1 µM GNF-2**
Das-DFGO-II	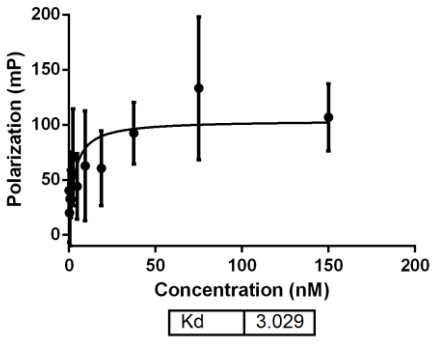	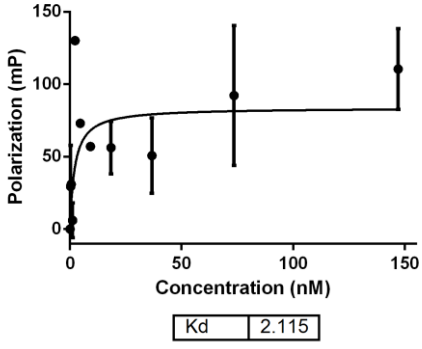
	Avg EC_{50} = 3.4 ± 0.4	Avg EC_{50} = 1.9 ± 0.2

Das-CHO-II

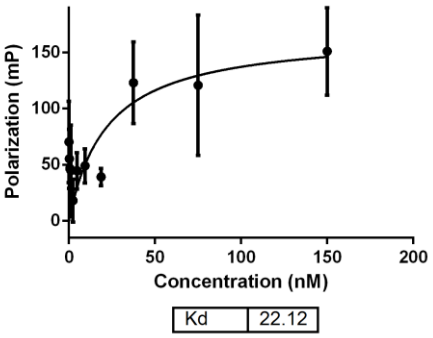

Avg EC_{50} = 21 ± 1

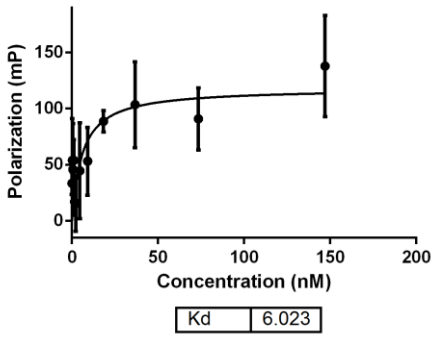

Avg EC_{50} = 5.2 ± 1.1

Analytical data for Protein Half Lives as Determined *via* Proteolysis Assay.

	Half Life (min)	$\frac{\mathbf{T_{1/2}}}{\mathbf{WT\ Abl\ T_{1/2}}}$	**log(Relative Half Life)**
WT Abl (n = 5)	21.2 ± 3.3	1	0
SH3 Engaged Abl	202.0	9.53	0.979
A337N Abl	9.8	0.46	-0.337
WT Abl + Dasatinib	2.9	0.14	-0.854
WT Abl + Imatinib	2.2	0.10	-1
WT Abl + Nilotinib	1.3	0.06	-1.222
WT Abl + Ponatinib	2.2	0.10	-1
WT Abl + Das-DFGO-II	2.1	0.10	-1
WT Abl + Das-CHO-II	37.7	1.78	0.250
WT Abl + GNF-2	154.6	7.29	0.863
WT Abl + Dasatinib & GNF-2	35.0	1.65	0.217
WT Abl + Das-DFGO-II & GNF-2	16.5	0.78	-0.108
WT Abl + Das-CHO-II & GNF-2	279.4	13.18	1.120
WT Abl + "ABL001"	83.2	3.92	0.593
T315I Abl	2.5	0.12	-0.921
T315I Abl + GNF-2	16.1	0.76	-0.119
T315I Abl + Das-CHO-II	3.7	0.17	-0.770
T315I Abl + GNF-2 & Das-CHO-II	44.9	2.12	0.326
P112S Abl	3.7	0.17	-0.770
P112S Abl + GNF-2	16.4	0.77	-0.114
P112S Abl + Das-CHO-II	4.0	0.19	-0.721
S229P Abl	10.0	0.47	-0.328
S229P Abl + GNF-2	48.1	2.27	0.356
S229P Abl + Das-CHO-II	29.3	1.38	0.140

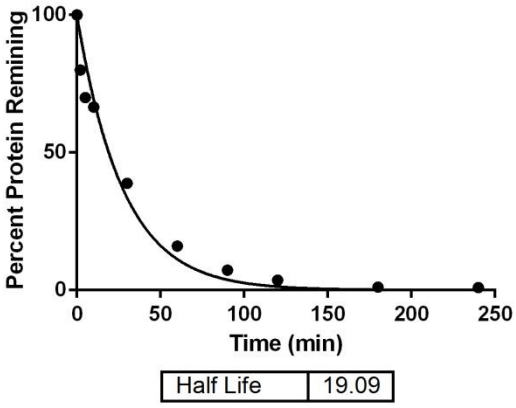

WT Abl

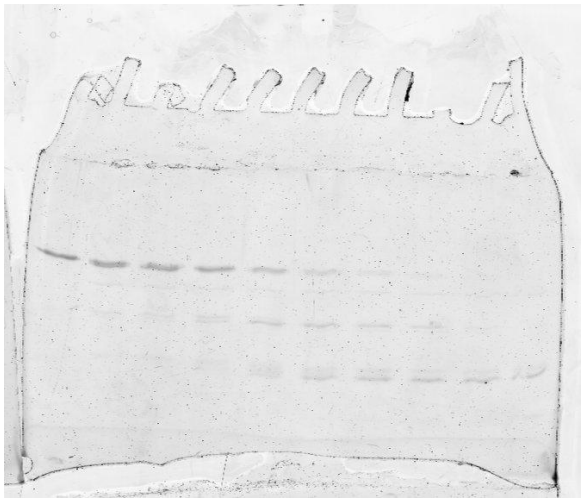

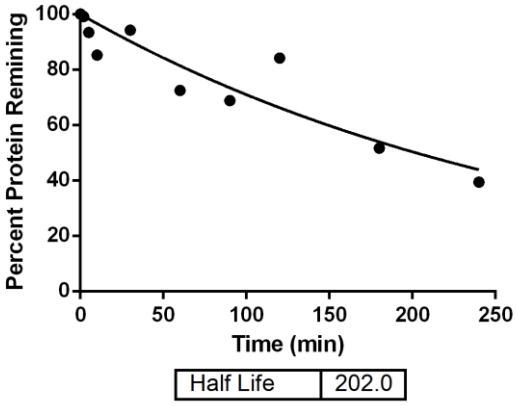

SH3 Engaged Abl

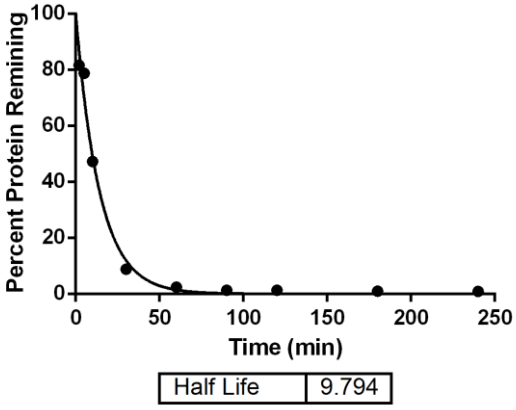

A337N Abl

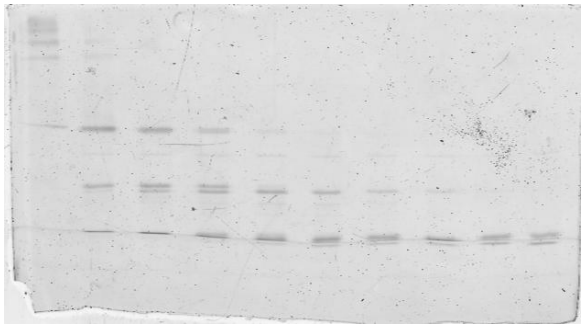

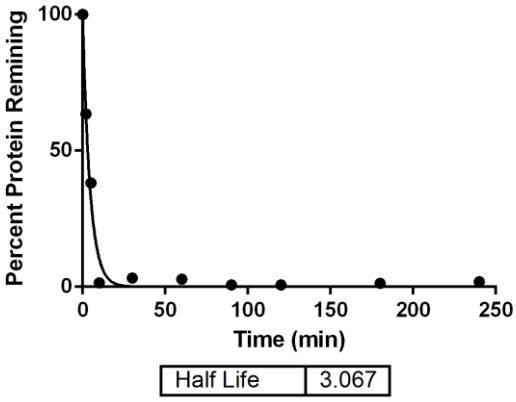

WT Abl + Dasatinib

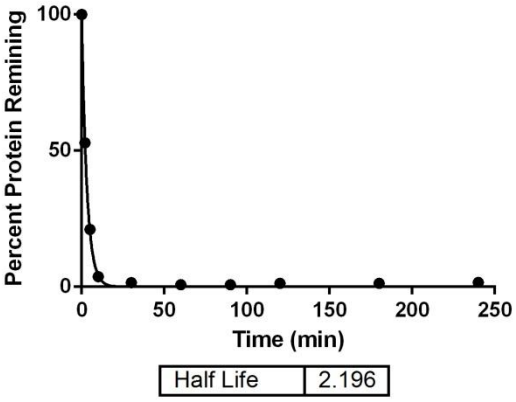

WT Abl + Imatinib

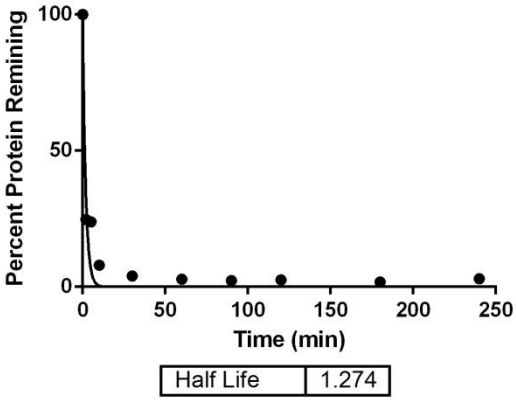

WT Abl + Nilotinib

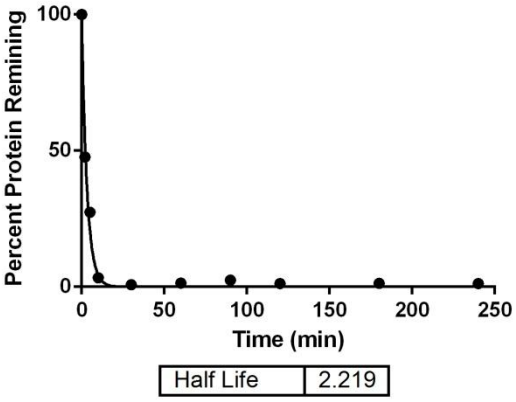

WT Abl + Ponatinib

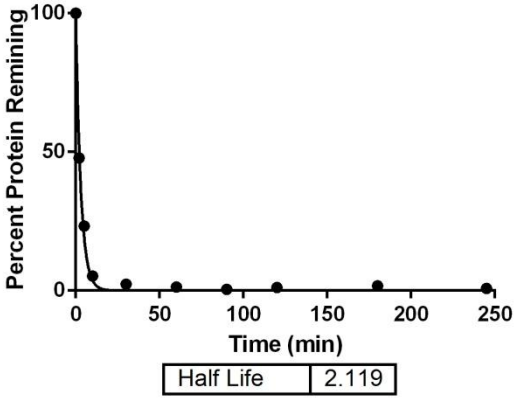

WT Abl + Das-DFGO-II

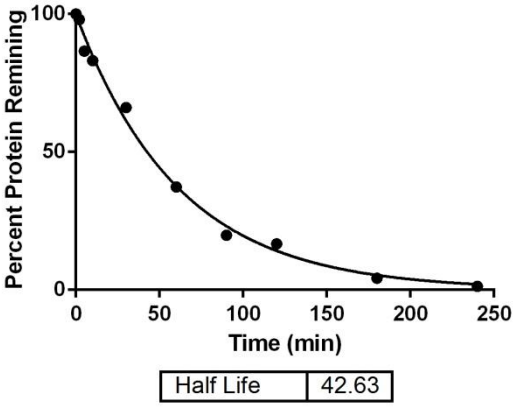

WT Abl + Das-CHO-II

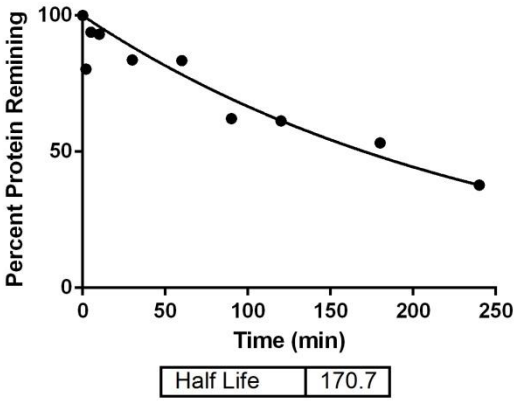

WT Abl + GNF-2

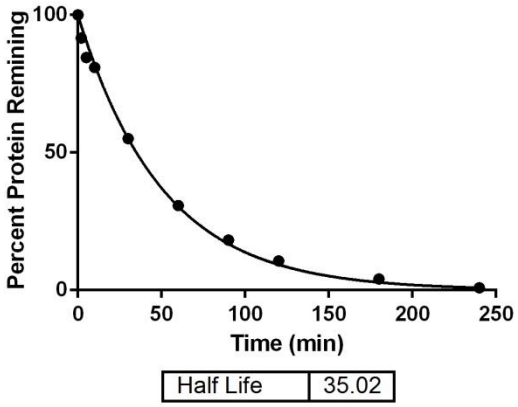

WT Abl + Dasatinib & GNF-2

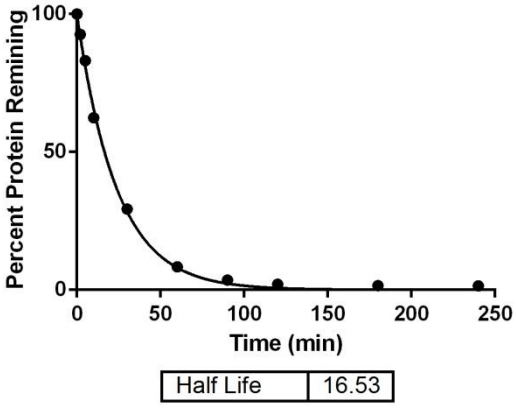

WT Abl + Das-DFGO-II & GNF-2

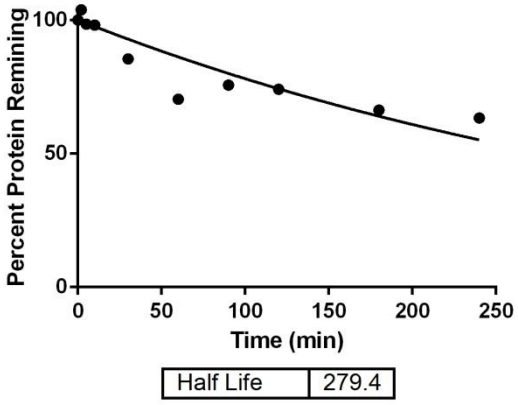

WT Abl + Das-CHO-II & GNF-2

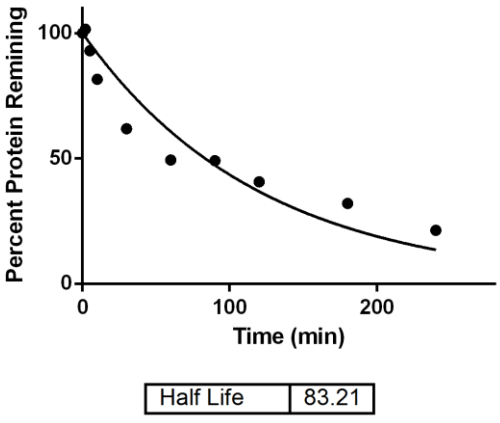

WT Abl + "ABL001"

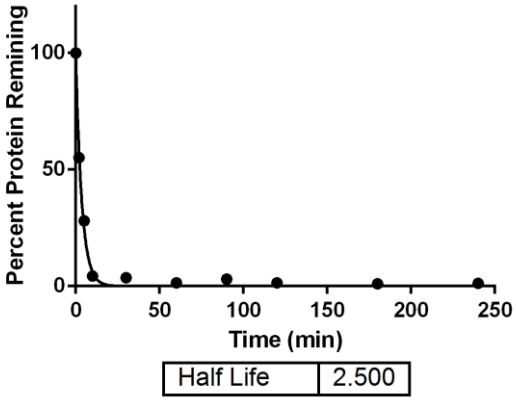

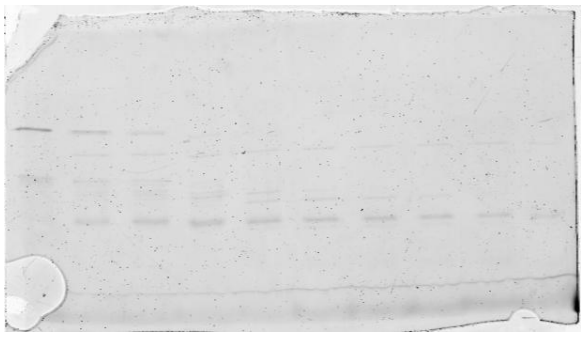

T315I Abl

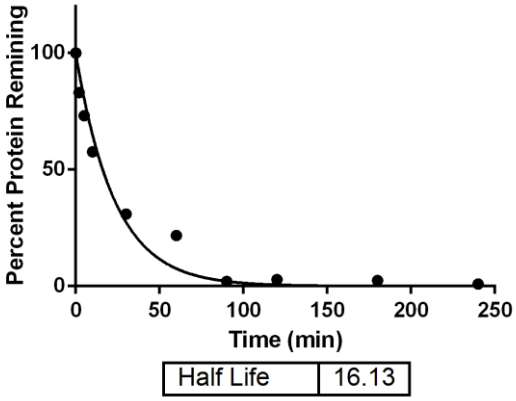

T315I Abl + GNF-2

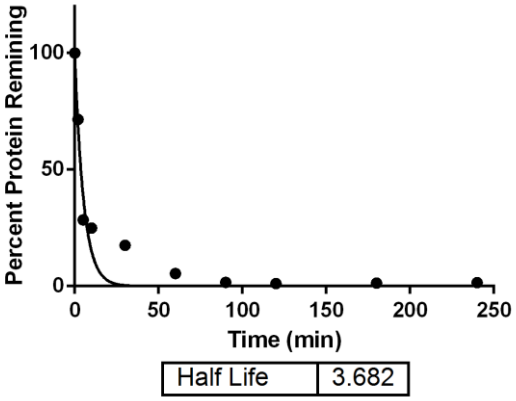

T315I Abl + Das-CHO-II

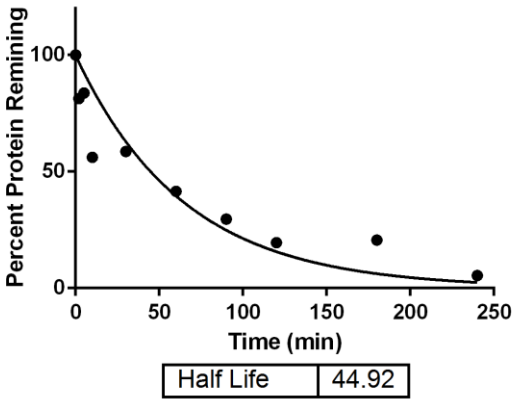

T315I Abl + GNF-2 & Das-CHO-II

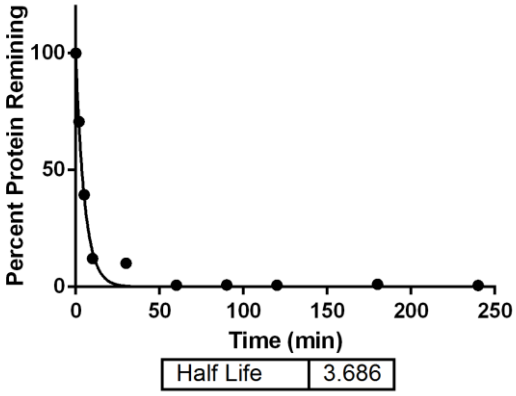

P112S Abl

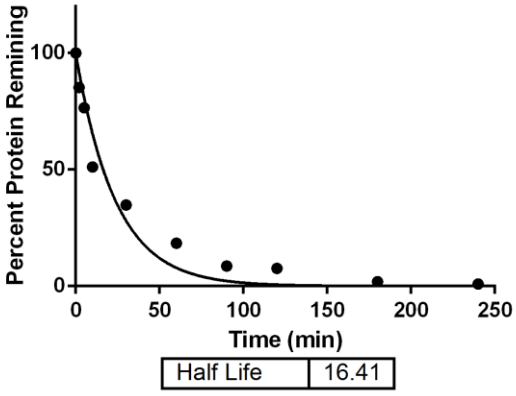

P112S Abl + GNF-2

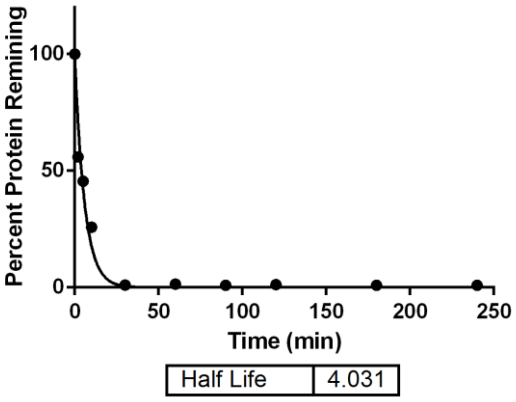

P112S Abl + Das-CHO-II

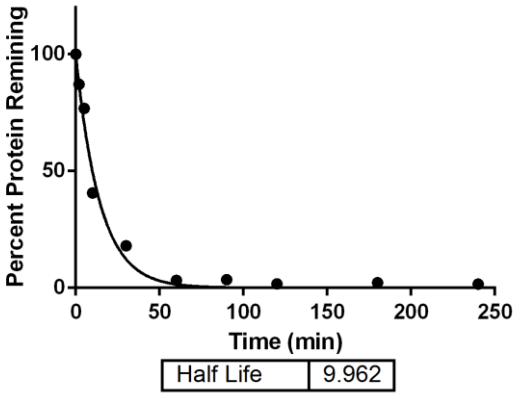

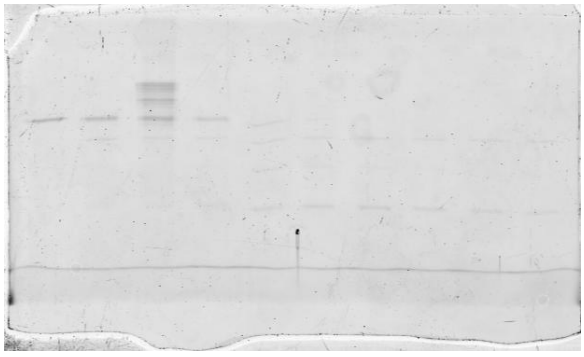

S229P Abl

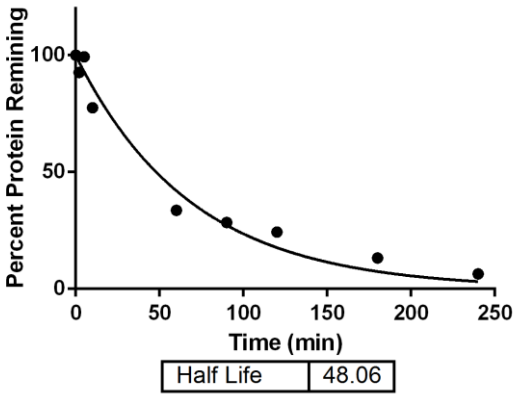

S229P Abl + GNF-2

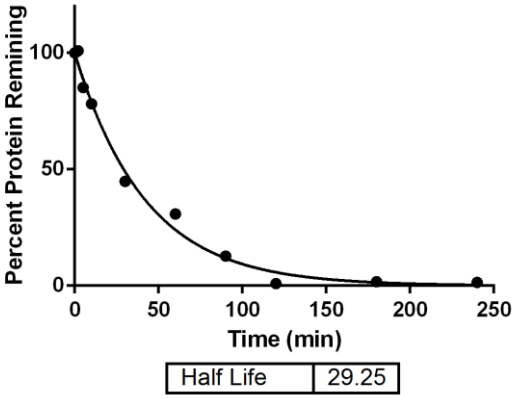

S229P Abl + Das-CHO-II

Analytical data for GI_{50} Values in BCR-Abl Ba/F3 cells.

Das-CHO-II
GI_{50} = 546.0 nM

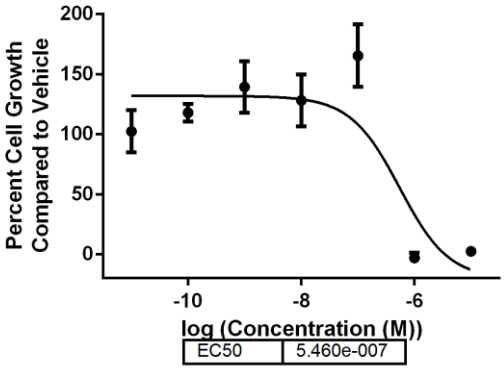

GNF-2
GI_{50} = 452.3 nM

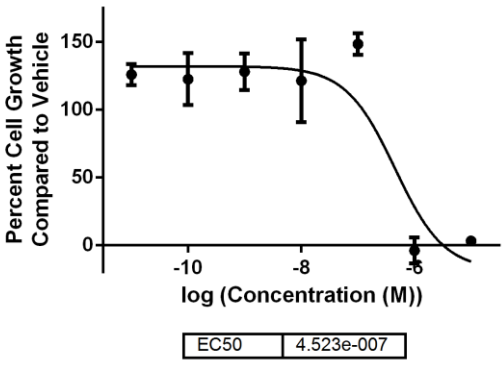

Das-CHO-II + 200 nM GNF-2
GI_{50} = 0.545 nM

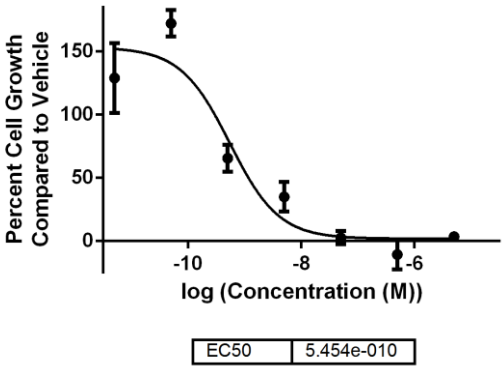

GNF-2 + 100 nM Das-CHO-II
GI_{50} = 17.2 nM

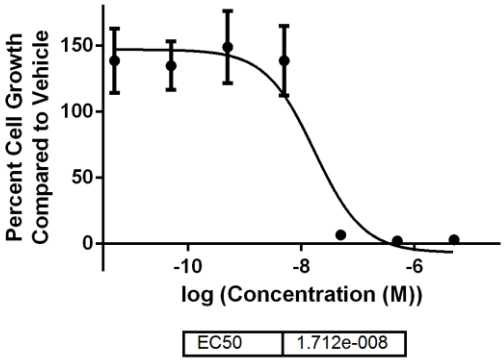

Analytical data for GI_{50} Values in T315I Abl Ba/F3 cells.

Das-CHO-II
GI_{50} = 3.2 μM

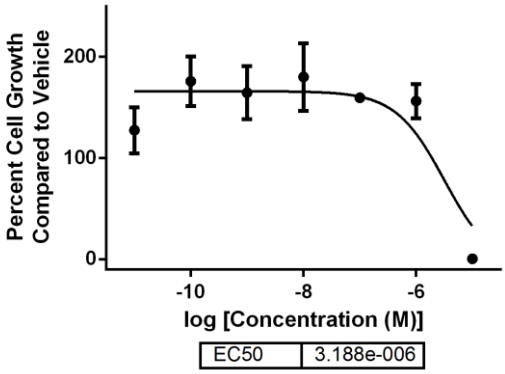

GNF-2
GI_{50} > 10 μM

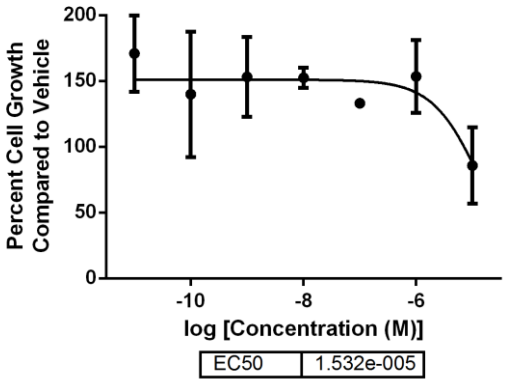

Das-CHO-II + 2 μM GNF-2
GI_{50} = 127.9 nM

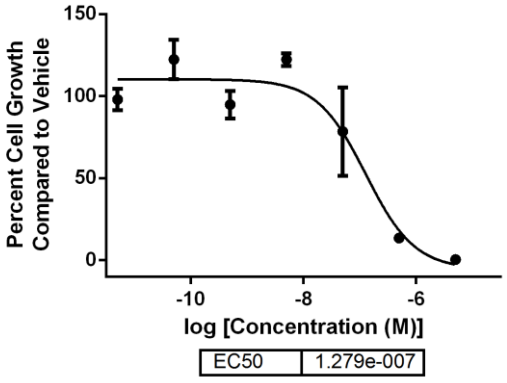

GNF-2 + 2 μM Das-CHO-II
GI_{50} = 1.8 μM

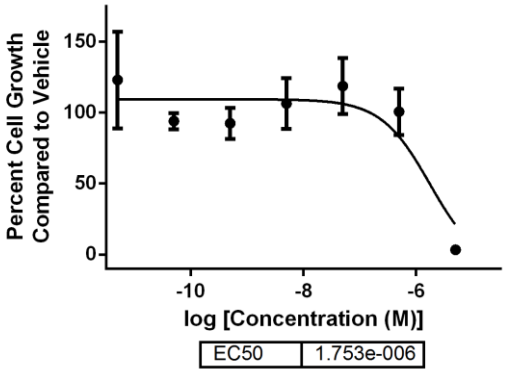

Analytical data for GI_{50} Values in Parental Ba/F3 cells.

Das-CHO-II
GI_{50} = 2.8 μM

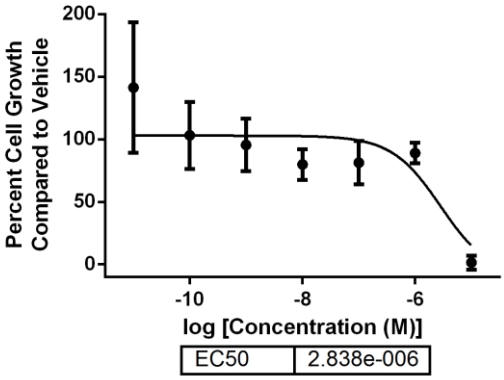

GNF-2
GI_{50} > 10 μM

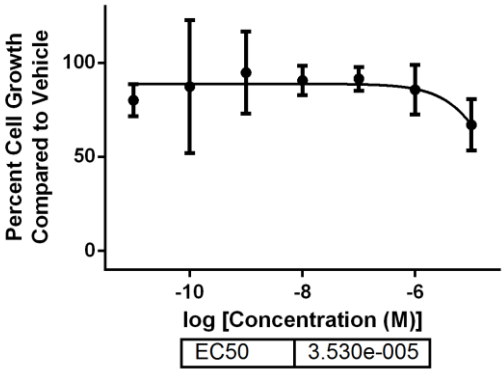

Das-CHO-II + 200 nM GNF-2
GI_{50} = 1.5 μM

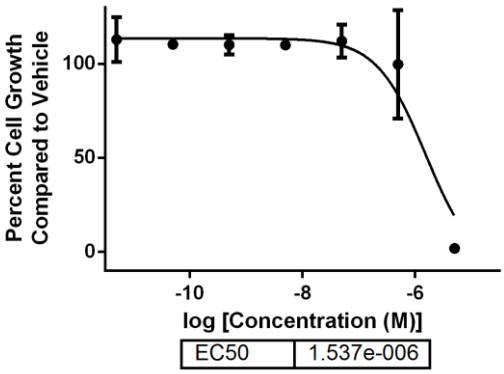

GNF-2 + 100 nM Das-CHO-II
GI_{50} > 5 μM

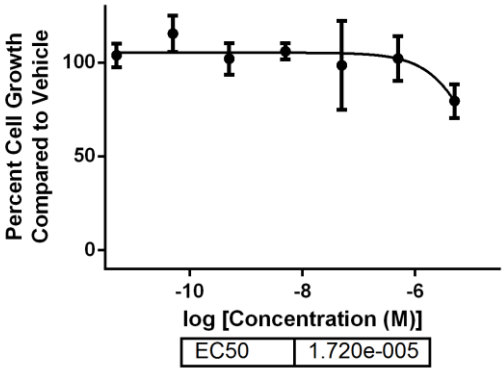

Analytical data for GI_{50} Values in K562 cells.

Das-CHO-II
GI_{50} = 64.4 nM

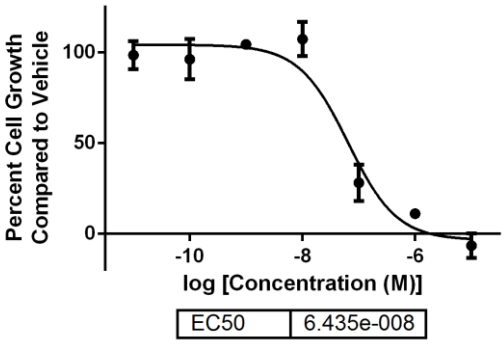

GNF-2
GI_{50} = 807.7 nM

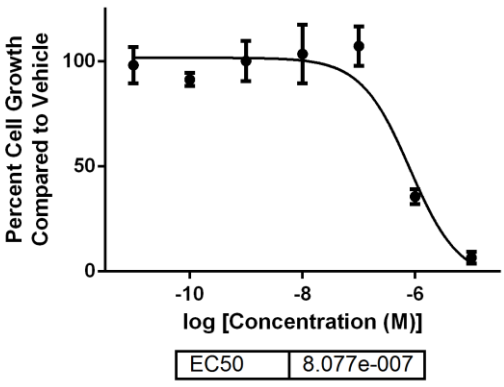

Das-CHO-II + 800 nM GNF-2
GI_{50} = 16.5 nM

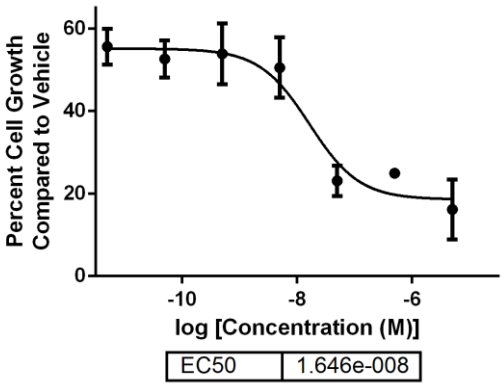

GNF-2 + 65 nM Das-CHO-II
GI_{50} = 215.3 nM

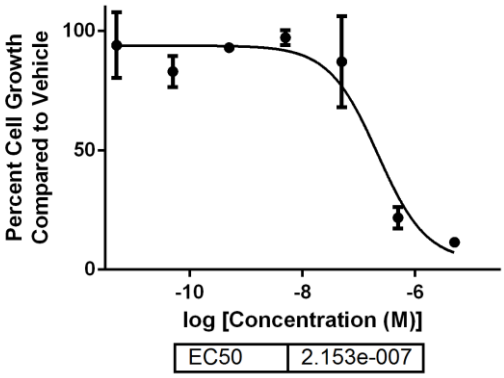

Analytical Data for Cellular Synergy.

Cell Line	Combinations	CI_{50}	CI_{75}	CI_{90}	CI_{95}
	Dasatinib + GNF-2	0.84	0.93	1.04	1.12
	Imatinib + GNF-2	0.88	0.87	0.87	0.87
	Nilotinib + GNF-2	0.94	0.94	0.94	0.94
WT Abl Ba/F3	Ponatinib + GNF-2	1.02	1.02	1.02	1.02
	Das-DFGO-II + GNF-2	0.74	0.70	0.66	0.64
	Das-CHO-II + GNF-2	0.23	0.23	0.23	0.23
	Das-CHO-II + "ABL001"	0.66	0.66	0.66	0.66
K652	Das-CHO-II + GNF-2	0.47	0.64	0.88	1.09

Cell Line	Combinations	Dose Effect Curves	Isobolograms
WT Abl Ba/F3	Dasatinib + GNF-2	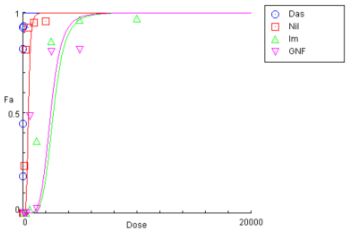 Single Agent 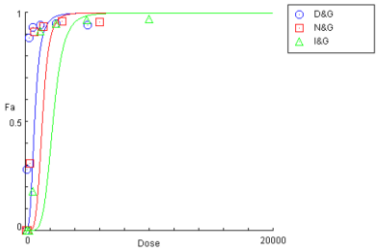 Combination	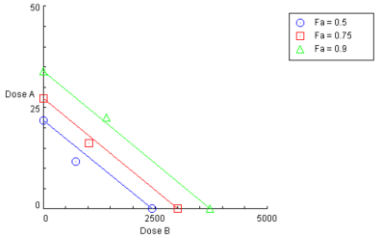
WT Abl Ba/F3	Imatinib + GNF-2	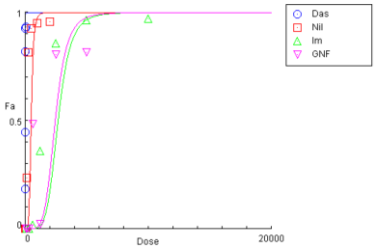 Single Agent 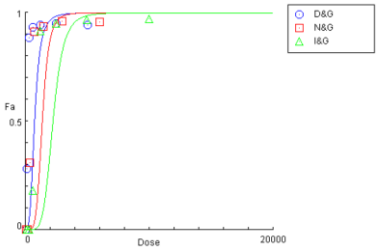 Combination	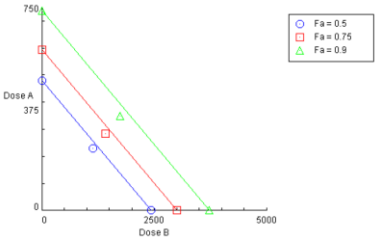

WT Abl Ba/F3	Nilotinib + GNF-2	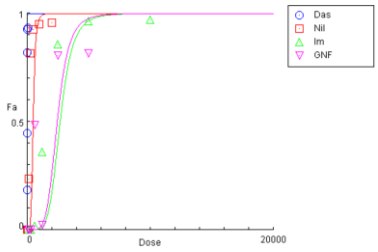 Single Agent 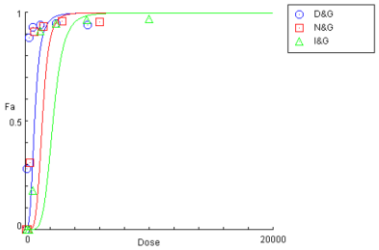 Combination	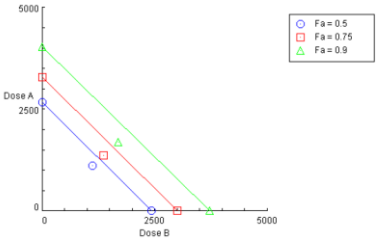
WT Abl Ba/F3	Ponatinib + GNF-2	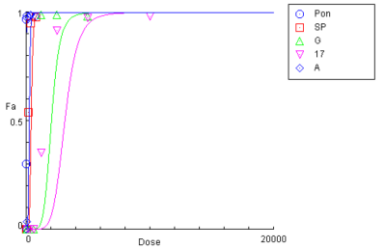 Single Agent 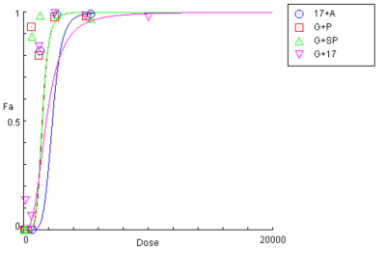 Combination	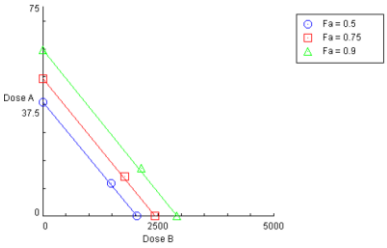

WT Abl Ba/F3	Das-DFGO-II + GNF-2	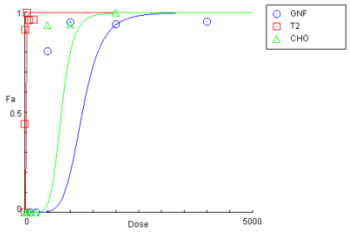 Single Agent 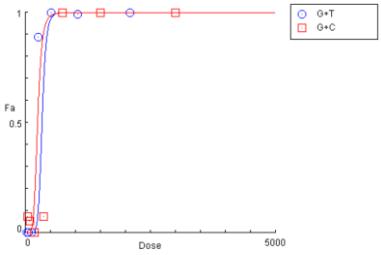 Combination	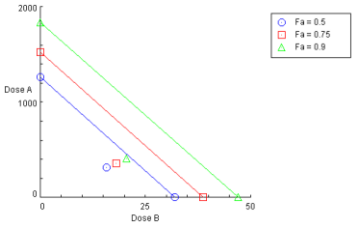
WT Abl Ba/F3	Das-CHO-II + GNF-2	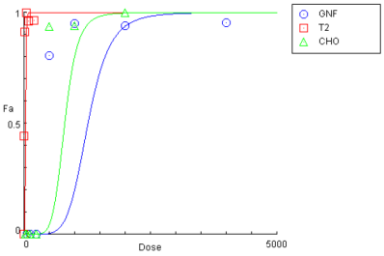 Single Agent 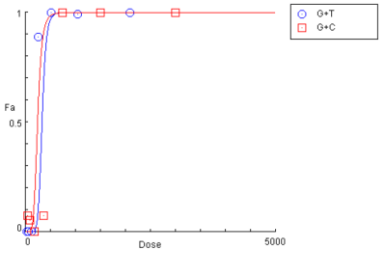 Combination	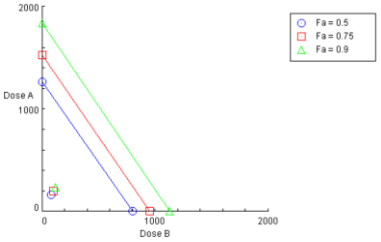

WT Abl Ba/F3	Das-CHO-II + "ABL001"	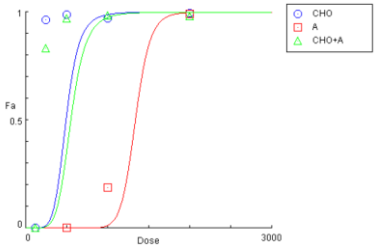	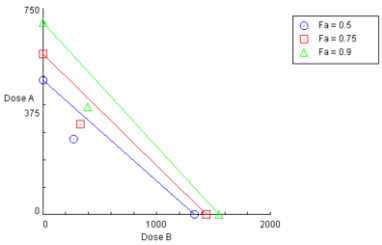
K562	Das-CHO-II + GNF-2	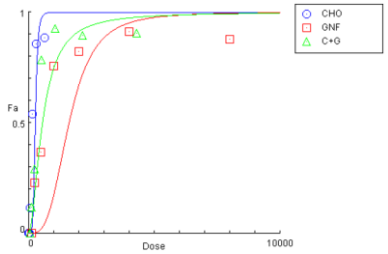	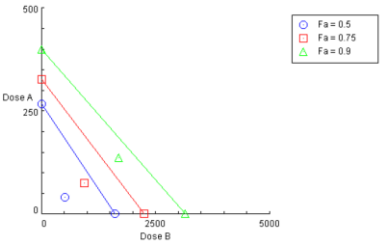

References

(1) Chou, T.-C.; Talalay, P. Quantitative Analysis of Dose-Effect Relationships: The Combined Effects of Multiple Drugs or Enzyme Inhibitors. *Adv. Enzym. Regul.* **1984**, *22*, 27–55.